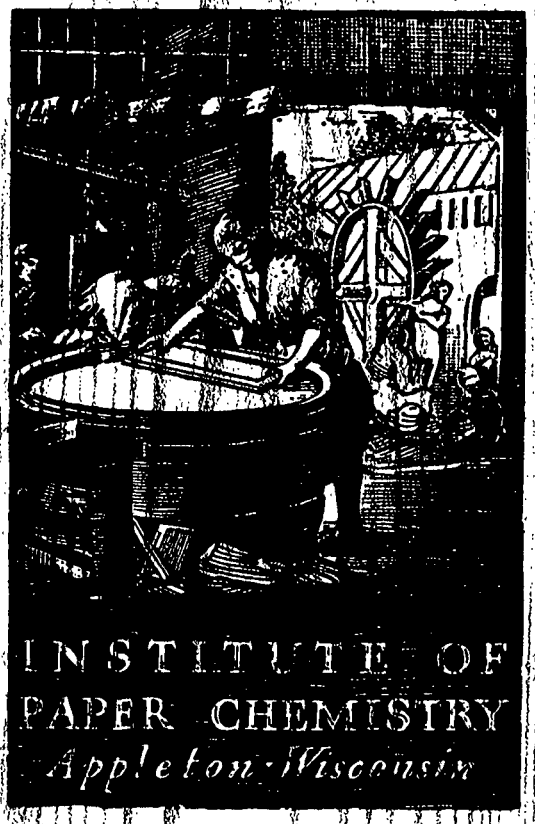

THE STATUS OF THE SHEET-FORMING PROCESS

A CRITICAL REVIEW

✓ Project 2549

December 31, 1965

℄ Project 2348, 2570

The Institute of Paper Chemistry
Appleton, Wisconsin

The Status of the Sheet-Forming Process

A Critical Review

December 31, 1965

TABLE OF CONTENTS

I. GENERAL INTRODUCTION AND BRIEF SUMMARY

More than a century ago the ancient art of papermaking was adapted to continuous operation, its essential principles remaining unchanged. Thanks to the successive mechanical improvements, the modern paper machine has vastly increased capacity with only moderate gain in efficiency and at some sacrifice of quality. Witnessing such a massive machine in so delicate an operation, one can but feel impressed. However, when one proceeds to probe beneath the surface and beyond the apparent, one begins to wonder if there could not be better means for achieving the same purpose. The inventive man immediately directs his mind to possible innovations while the research man becomes thoughtfully intrigued with the complex problem. Both will contribute to the technology, though in different ways.

Concerted research of the sheet-forming process was initiated some two decades ago and became ever more intensified in recent years. Early findings available in the literature have not yet been fully assessed, while improved theories and new results are being rapidly accumulated. It appears to be timely to initiate a unified treatment of the subject. As the Institute has done much work in various aspects of the general problem, we deem it appropriate to take up this ambitious task. The present review is the result of our effort in this direction, and will be subject to further refinements and extensions as research proceeds.

OUTLINE OF CONTENTS

The review is divided into three parts. Part One deals with theories and laws. We have always treated the sheet-forming process as filtration of a compressible material. Only recently, we succeeded in constructing a broad

mathematical model for the macroscopic description of the filtration process, incorporating the essential features of fiber retention, flow resistance, mat compressibility, and particle distribution. Fiber dispersion has remained the missing link. An outline of these aspects and their interconnections is presented in the diagram of Fig. I-1.

Theoretical treatment is necessarily an abstraction of a real system. Its validity must be tested for its power of prediction. The empirical laws founded on experiments need at least partial theoretical justification for intellectual satisfaction. In both respects we have strived to present such indications.

In Part One we begin with elementary concepts, appropriate definitions, and basic relations concerning unsteady filtration. Next are introduced useful expressions for fluid permeation, mat compression, particle attenuation, and fiber retention. Each of these topics is subsequently treated in proper detail and with some rigor, depending on our present understanding. We then proceed to obtain solutions for simple filtrations, some of which are well known in the field and others quite new and interesting. The analysis of high-consistency filtration is mathematically involved, but conceptually important for development of new types of formers. At this point we attempt to show possible further generalization to the case of incomplete fiber retention in a rigorous manner for future reference.

Our past work has been criticized for its alleged failure to account for the sheet structure. We are of the opinion that structure and drainage are interrelated in the sheet-forming process. In an appropriate description of flow through a fiber mat, the porous properties of the mat are necessarily taken into consideration in the dynamic sense. It is, however, also possible to describe a

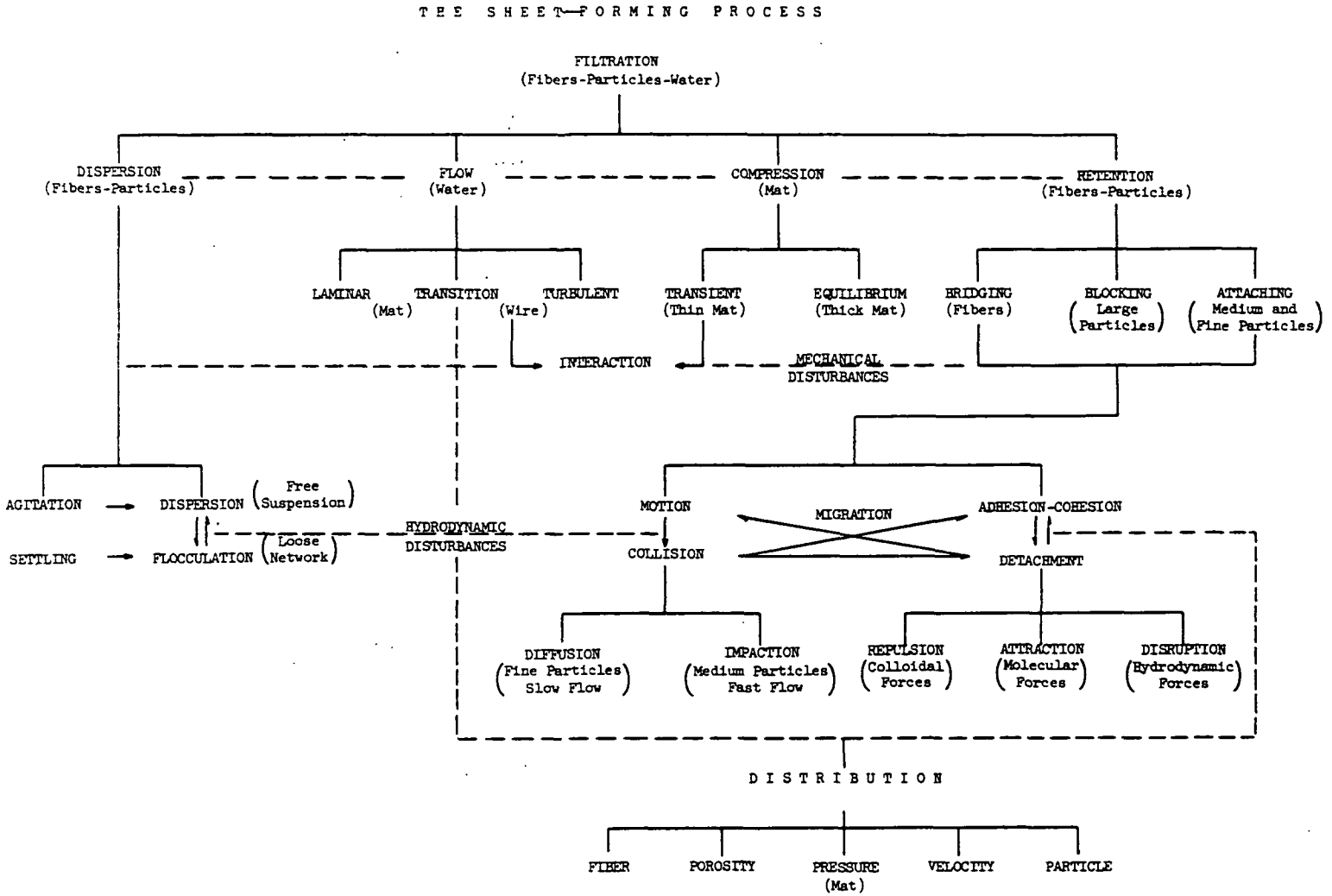

Figure I-1. An Outline of the Sheet-Forming Process

static porous structure statistically and proceed to predict its dynamic behavior. Accordingly, we present a review of some noted work in other fields with this approach and point out its limitation. Several workers in the paper field prefer dealing with the solid structure for the obvious reason that it is the object of the sheet-forming process. In this sense the bonded structure of paper is conceived in the orientation and contact of wet fibers. We also offer a rigorous version of such a description, from which mat compressibility, as well as fiber retention, may be deduced.

In the course of drainage studies, it was soon found that the fiber-wire interaction should not be neglected in forming thin sheets. An approximate analysis is presented to account for the effect of mat penetration into a wire structure on drainage. This is a debatable treatment, though amenable to further improvement. Because of its apparent importance, fiber flocculation has received much attention, but the progress has been rather slow. From the previous work we have tried to construct a consistent picture of the important factors governing flocculation. It appears to us that a strictly hydrodynamic approach to this critical problem will not be adequate for its eventual solution. Based on our study of particle retention, the dynamic concept of fiber interactions due to molecular, colloidal, and hydrodynamic forces is reviewed with the hope that this broad approach may lead to more fruitful research.

As a technological review, it would be incomplete if it did not deal with the operating principles of paper machines. The theory of table-roll suction is critically examined. An analysis of two-wire forming is added to demonstrate the use of the filtration theory in development of new types of formers.

Part Two is concerned with experiments, results, and interpretations. It naturally starts with compressibility tests. With the guidance of theory the meaning of the compressibility constants are clarified to a larger extent than previously. The limitation of the simple power function and the comparison of more refined expressions are demonstrated. In concluding the chapter a comprehensive set of compressibility data accumulated over the years is presented with a new analysis.

The chapter on permeation dealing with cylindrical fibers summarizes how the flow expression covering a wide range of porosity and velocity is established. These experimental facts should settle a large part of the persistent controversy over whether drainage on a paper machine is controlled by viscous or by turbulent flow through a fiber web. It should be mentioned that the porosity function so established with the support of theory has begun to be accepted by most workers in the paper field.

The results with cylindrical fibers are then utilized for evaluation of two important cellulosic fiber properties, specific surface and volume. The historical development of such work is recast in the new light, and the latest refinement is incorporated. From here we proceed to examine dynamic effects in rapid filtrations. Along the way our attention is temporarily diverted to the phenomenon of fiber-wire interaction in forming thin sheets, which is a more thorny problem than it may appear to be. We do offer some way of dealing with it, but not yet to our own satisfaction.

The problem of fine particle retention in the filtration process has commanded our effort for some time. We deem it legitimate to devote two chapters to this topic, one dealing with verification of the theory and the other with

analysis of collection mechanisms, both from the hydrodynamic standpoint. The retention of fiber, however, has received a quite different treatment. It is based largely on the probability theory. The experimental support of the predicted initial retention is one of the satisfying experiences in research. In the more complex case of subsequent retention, we have partially resolved the problem by empiricism with the aid of theory. The final chapter is a brief summary of the hydrodynamic behavior of fiber suspensions. Regretfully, space requirements have permitted only minor considerations of a number of excellent references on this subject.

By the end of Part Two the review has already become lengthy, and from the research viewpoint, we may rightfully conclude it at this point. However, we are conscious of the often-heard opinion that some illustrations of possible applications could be a more effective way of communicating research findings to practicing engineers. In this light we have made a deliberate attempt to prepare Part Three within the extent of our contact with commercial operations. Most applications are naturally in developing, designing, and operating paper machines. As our knowledge of the sheet-forming process is far from being complete, the methods of application necessarily entail approximations. In some cases we are able to demonstrate that such methods are superior to accumulated experience or pure intuition, but in others our results may not be very convincing.

In this final part we begin with a discussion of pressure-suction formers which have proven advantageous for certain grades of paper. Our treatment of the fourdrinier machine leaves much to be desired. Nevertheless, some limited uses of the suggested method are demonstrable. The chapter on two-wire forming is timely in view of its recent rapid development. The cylinder machine is excluded not only because of our inability to do much about it but also based on the

evidence of its being obsolescent both in principle and in practice. As an addendum we use the final chapter to relate some actual case histories of application. Needless to reiterate, the review contains more new information that will sooner or later be utilized in dealing with practical problems than our limited experience can show at the present time.

SUMMARY OF RESULTS

The most precise way of summarizing quantitative information is by means of mathematical expressions. The following provides, at a glance, the major findings to date about the sheet-forming process.

Mat Compression

The static compressibility of a fiber mat is expressed in mat density c as a function of compacting pressure p_f with three parameters c_o, M, and N in the following form:

$$c - c_o = Mp_f^N .$$

The value of c_o is estimated to be 10^{-2} g./cc. For first compression of freshly formed mats in the range $c_o \ll c$, the simple power function applies to mats as thin as 14 g./sq. m. in basis weight. Both M and N are related to the modulus of elasticity E:

$$\log \left[\frac{MN^N c_o^{5N-1}}{\rho_f^{5N}} \right] = N \log \left[\frac{M'}{E} \right] .$$

For cellulosic and synthetic fibers above their critical axis ratios, N varies from 0.22 to 0.45, and M'/E is constant at 10^{-16} sq. cm./dynes, M' being a positive number. The critical axis ratio L_f/d_f is itself dependent on E,

its value for glass fibers being about 500, for nylon fibers about 100, and for most cellulosic fibers less than 100. The simple power function is also applicable to mechanically conditioned mats after several compression-recovery cycles, but with smaller N and larger M than first compression. Recovery is never complete. Creep under constant load in both compression and recovery follows

$$c - c_o = (M_1 + M_2 \log t)p_f^N .$$

This expression is applicable to time t as short as 10^{-1} sec. With some reservations the static compressibility function may be used for dynamic conditions by replacing p_f with pressure drop.

Fluid Flow

Fluid flow through compressible fiber mats involves both viscous and inertial resistances. The pressure drop Δp across the mat of basis weight W is related to the velocity U in terms of mat porosity ϵ, specific volume v, surface S_v, fluid density ρ, and viscosity μ:

$$\frac{\Delta p}{W} = \frac{\bar{k}(1 - \bar{\epsilon})\, S_v^2 v}{\bar{\epsilon}^3}\mu U + \frac{b'\sqrt{\bar{k}}\, S_v v}{\bar{\epsilon}^3}\rho U^2 .$$

The average Kozeny factor $\bar{k}$, which is equivalent to the viscous resistance coefficient, is expressed by the porosity function:

$$\bar{k} = k_1 \frac{\bar{\epsilon}^3}{(1 - \bar{\epsilon})^{1/2}}\left[1 + k_2(1 - \bar{\epsilon})^3\right] .$$

The values of k_1 and k_2 are 3.5 and 57, respectively. The average porosity is defined by

$$\bar{\epsilon} = 1 - (1 - N/2)^2 vM(\Delta p)^N$$

in which v is the fiber specific swollen volume. The value of the inertial resistance coefficient b' is 0.1. This flow expression based on cylindrical fibers covers a velocity range of 1-400 cm./sec. and a porosity range of 0.75-0.95. For $\epsilon < 0.75$, k is practically constant at 5.5. The same expression is also applicable to wire screens with k equal to 5.15 and b' slightly dependent on velocity in turbulent flow.

Constant-Rate Filtration

The flow expression without the inertial term is used for the evaluation of specific surface and volume of cellulosic fibers in constant-rate filtration, forming a thick mat from a dilute suspension of consistency s at a low velocity. The simple filtration expression is

$$\frac{\Delta p}{\sqrt{c}\, t} = \frac{k_1 S_w^2}{s\rho\mu U_0^2 \sqrt{v}} [1 + k_2 v^3 c^{-3}] ,$$

where U_0 is the filtrate velocity, and $S_w = vS_v$. Both S_w and v are pressure dependent and may be represented by power functions in a limited range. The average specific surface is about 5×10^3 sq. cm./g. and swollen volume about 2 g./cc. for a classified unrefined pulp. With conventional refining the surface may increase to as much as 3×10^4 and volume to 3, again for classified fibers. Using high-consistency refining the corresponding values are 2×10^4 and 3.2. When fines are included, the apparent surface can be as large as 8×10^4, while the specific volume remains practically unchanged.

In rapid drainage the flow expression is used in its complete form. There appears to be no discernible dynamic effects. In forming thin sheets

the pressure drop is higher due to fiber-wire interaction than would be predicted by adding the pressure drops across the sheet and the wire at the same drainage The discrepancy may be corrected by

$$\bar{\varepsilon} = 1 - Ivc ,$$

$\underline{I}$ being an experimentally determined factor which approaches exponentially the value of $(1 - \underline{N}/2)^2$ with increasing basis weight. At a basis weight of 10 g. per sq. m., the wire, viscous, and inertial resistances are about equally divided in terms of pressure drops. With increasing basis weights viscous resistance becomes controlling.

High-consistency filtrations involve appreciable relative water-fiber motion. The filtration equation becomes dependent on both $\underline{z}$ and $\underline{t}$ co-ordinates:

$$\frac{\partial c}{\partial t} + U_0 \frac{\partial c}{\partial z} - \frac{\gamma}{M_0} \frac{\partial}{\partial z} \left(\frac{c^\gamma}{a} \frac{\partial c}{\partial z}\right) = 0 ,$$

which utilizes the compressibility function:

$$c^\gamma - c_0^\gamma = M_0 p_f$$

and the slow flow expression:

$$a = k_1 \mu S_v^2 v^{3/2} c^{3/2} [1 + k_2 v^3 c^3] .$$

This high-consistency filtration equation can be solved numerically with specified initial and boundary conditions. By solving the more general equation graphically for constant-rate filtration in transition flow, it is shown that the filtration resistance for 1% consistency is only 80% of that for 0.1% consistency at the same

basis weight. The average mat moisture $\bar{m}$ is about 30% higher at the same pressure drop, indicating a more diffuse structure from high-consistency forming.

Particle Distribution

When fine particles are collected in a fiber mat formed by filtration, their distribution is exponential:

$$-\ln\left(1 - \frac{m' - m'_s}{m_s}\right) = \frac{EA_f W}{V_f \rho_f}\left(1 - \frac{w}{W}\right) ;$$

m and m' are the free and bound particle-fiber mass ratios, respectively, the subscript s referring to the suspension. A_f, V_f, and ρ_f are the projected area, volume, and density of the fibers in the mat of basis weight W. E is the collection efficiency taken to be constant from $w = 0$ to $w = W$. This expression has been experimentally confirmed for both incompressible and compressible mats formed from simple filtrations with titanium dioxide-dacron and fines-sulfite systems, respectively.

The collection efficiency is dependent on three major mechanisms:

$$\text{Diffusion} \qquad E = \alpha\left(\frac{\mu}{\rho D}\right)^{-1/2}\left(\frac{\rho d_f U}{\mu}\right)^{-1/2} ,$$

$$\text{Impaction} \qquad E = \beta\left(\frac{d_p^2 \rho_p}{18 d_f^2 \rho}\right)\left(\frac{\rho d_f U}{\mu}\right)^{3/2} ,$$

and

$$\text{Interception} \qquad E = \gamma\left(\frac{d_p}{d_f} - 0.085\right) ;$$

d is diameter and D is diffusivity. The subscripts p and f are for particle and fibers, respectively. The coefficients α, β, and γ are representative of particle-fiber adhesion which is governed by the natural molecular attraction and the imposed ionic repulsion. They are, in turn, strongly dependent on the nature of the particle and fiber surfaces.

The removal of bound particles from a formed mat with uniform particle distribution is also expressed as an exponential function with three parameters m_o, A_o, and t_o:

$$m' - m_o' = A_o \exp(-t/t_o) .$$

From this evidence the specific rate of particle detachment is deduced to be constant at slow velocities.

Fiber Retention

The initial fiber retention R_o in mass fraction on a wire screen as deduced from the probability theory has been experimentally verified under idealized conditions. The subsequent retention for mat build-up is expressed by

$$W_s - W = \frac{1}{k_o} \ln \frac{1 - (1 - R_o) \exp(-k_o W)}{R_o} ,$$

or in terms of filtrate consistency s_o and suspension consistency s:

$$s_o = s(1 - R_o) \exp(-k_o W) ,$$

k_o is the retention coefficient which varies from 5×10^2 to 2×10^3 sq. cm./g. according to the known data.

Constant-Pressure Filtration

In the case of slow filtration at constant pressure with incomplete fiber retention, the filtration equation is

$$\frac{(k_0 W)d(k_0 W)}{1 - (1 - R_0)\exp(-k_0 W)} = \frac{k_0^2 s\rho(\Delta p)dt}{k_1 \mu S_v^2 v(1 - \bar{\epsilon})^{1/2}[1 + k_2(1 - \bar{\epsilon})^3](1 - s\bar{m})}$$

which can be integrated numerically. For small fiber losses the solution is approximated by

$$t = \frac{k_1 \mu S_v^2 v(1 - \bar{\epsilon})^{1/2}[1 + k_2(1 - \bar{\epsilon})^3](1 - s\bar{m})w^2}{2(s - \bar{s}_0)\rho(\Delta p)} .$$

This equation has been used for design of pressure-suction formers.

Conclusion

Possible applications of the findings just summarized are illustrated in Fig. I-2, which is a diagram of various types of formers in use or development with indication of their main operating features. From the review of the status of the sheet-forming process, we have arrived at a set of criteria for paper machines. These are (1) high consistency, (2) uniform dispersion, (3) symmetrical drainage, (4) complete retention, and (5) preferred orientation. While they are obviously desirable features, the means of achieving them may not be easy. In this review we offer a feasible method of analysis for design and operation of two-wire formers, which may largely meet the prescribed criteria, except the key problem of fiber flocculation. In this respect will the major breakthrough come through research, we hope, to the sheet-forming technology.

CONTINUOUS SHEET FORMERS

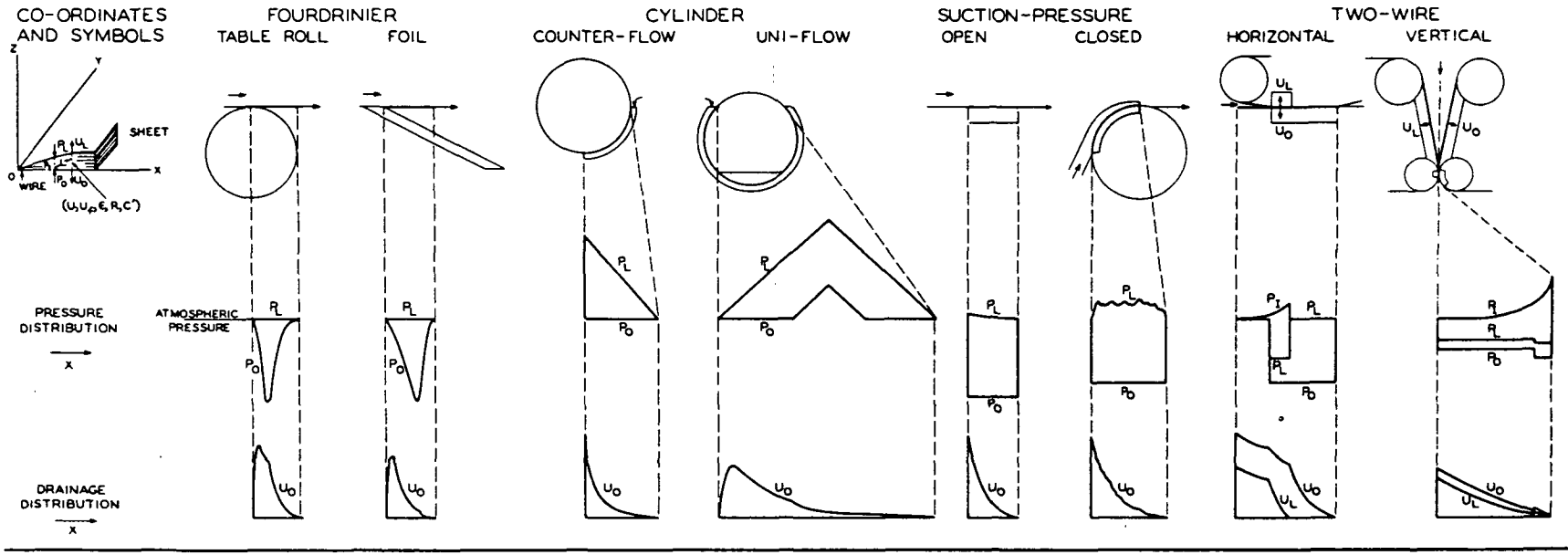

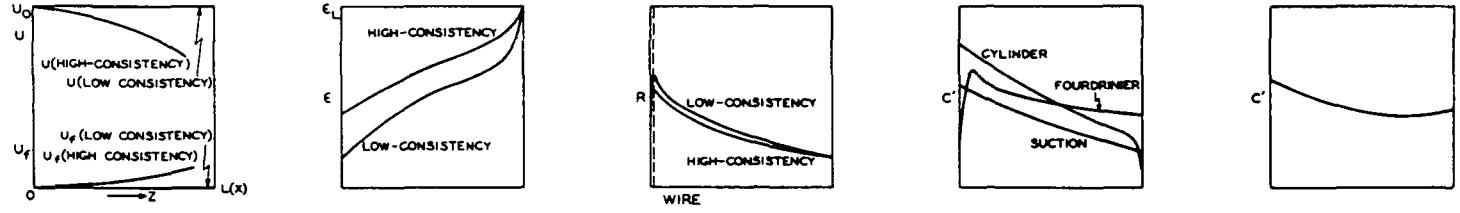

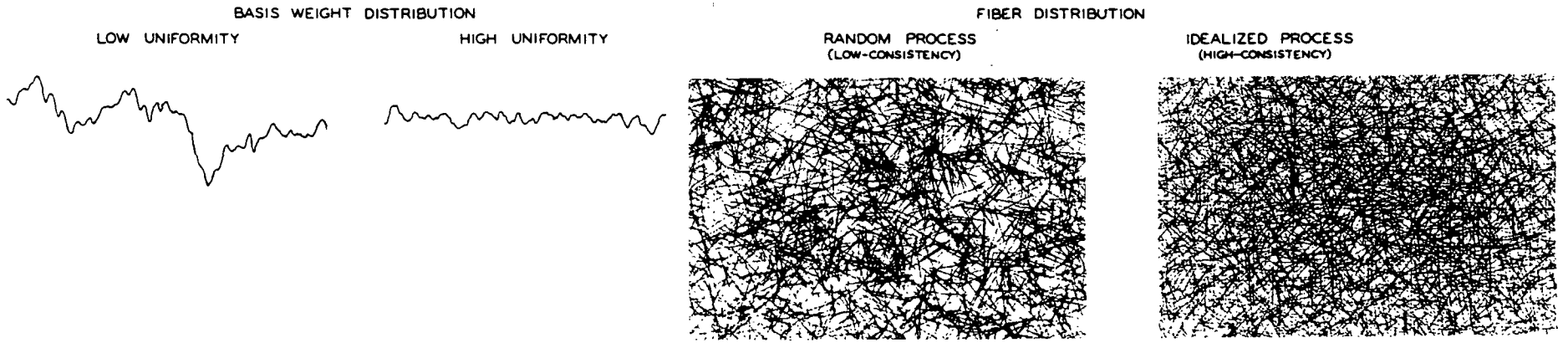

PART ONE

THEORIES AND LAWS

II. ELEMENTARY CONSIDERATIONS OF UNSTEADY FILTRATION

The system under general consideration consists of a porous medium composed of solid structural elements and a fluid. The process to be analyzed is the consolidation of the solids suspended in a fluid into a porous structure by removal of the excess fluid. Specifically, we are dealing with the sheet-forming process, in which a suspension of fibers and fine particles in water is drained through a wire screen to form a thick mat or a thin sheet containing retained particles.

This analysis was recently presented in three separate but related papers by Nelson (II-1), Ingmanson (II-2), and Han (II-3). Earlier work of Hisey (II-4) and Meyer (II-5) has also been consulted. For specific details the reader is referred to these publications.

CO-ORDINATE FRAME

For the purpose of analysis, a rectangular co-ordinate frame will be chosen for a mat in contact with a screen in the x-y plane and the positive z axis directed upward, its origin being located at the contact. The screen is considered as one boundary of the system, and for the time being, is assumed merely to support the mat and to exert no influence whatsoever on the process. The other boundary is usually the mat-suspension interface which consists physically of nothing more than discontinuities in some of the quantities serving to describe the system. Thus, the system to be analyzed is confined by a stationary boundary at $z = 0$ and a moving boundary at $z = L(t)$, z and t being the independent variables. Other initial and boundary conditions will be specified at the appropriate points of analysis.

In a preliminary analysis the fibers are considered as solid cylinders distributed uniformly on the supporting screen, with their axes oriented randomly in the $\underline{x}$-$\underline{y}$ plane. Swollen fibers with complicated structures will be dealt with in Part Two. Fine particles, if present, are supposed to occupy an insignificant volume of the system and to be all alike in their behavior, statistically.

Two essential features of the system, however, are to be preserved. It is readily compressible and highly porous.

MACROSCOPIC VARIABLES

The dependent variables of practical concern are all "macroscopic" quantities in the very nature of a porous medium. These are the averages of the corresponding "microscopic" quantities over small volumes of the system so that fluctuations in the resulting quantities are not appreciable. It is essential to the adequacy of the treatment that the distancestypical of such volumes should not greatly exceed the distances within which the resulting averages undergo significar change. It is further understood that the microscopic quantities themselves are the averages of molecular fluctuations.

One macroscopic property of a porous structure is obviously its porosity or void fraction. In any small portion of the system, the fluid is thought of as occupying the fraction ϵ of the total volume concerned in the averaging process, the solid fraction being accordingly $(1 - \epsilon)$.

The flow takes place downward, opposite to the $\underline{z}$ direction. The superficial velocity $\underline{U}$ of the fluid is defined as the volume of fluid which flows, per unit time, across a surface in the $\underline{x}$-$\underline{y}$ plane, per unit area of the surface. Follo ing the macroscopic concept and provided that it varies only with $\underline{z}$,

$$U = \frac{1}{A}\int_{\epsilon A} u dA = \epsilon \bar{u} \qquad \text{(II-1)},$$

where $\bar{u}$ is the average of the microscopic velocity u over the fluid area, and A the total area of the surface. By convention, these velocities are negative with respect to the z direction. Treating the solid phase also as a continuum, we define similarly the superficial velocity of the fibers as

$$U_f = \frac{1}{A}\int_{(1-\epsilon)A} u_f dA = (1 - \epsilon)\bar{u}_f \qquad \text{(II-2)},$$

where $\bar{u}_f$ is averaged over the solid area. The superficial mass fluxes of the fluid and the fibers are then ρU and $\rho_f U_f$, respectively, ρ being the fluid density and ρ_f the fiber density.

To describe the transport of fine particles in the system we make a distinction between free and bound particles. Free particles are suspended in the fluid and bound particles are attached to the fibers. We express the free particle concentration C as the number of particles per unit volume of fluid and the bound particle concentration C' as the number of particles per unit volume of fibers. The respective fluxes are taken to be UC and $U_f C'$, each expressed as the number of particles carried across the x-y plane per unit time and per unit area. The justification of these definitions was discussed in (II-1).

CONTINUITY CONDITIONS

By the principle of mass conservation, the rate of accumulation of each component (water, fibers, and particles) per unit volume of system must be equal to the net influx of that component. Thus, the three continuity conditions are

$$\frac{\partial}{\partial t}[\rho\epsilon] = -\frac{\partial}{\partial z}[\rho U] \qquad \text{(II-3)},$$

$$\frac{\partial}{\partial t}[\rho_f(1-\epsilon)] = -\frac{\partial}{\partial z}[\rho_f U_f] \qquad \text{(II-4)},$$

and

$$\frac{\partial}{\partial t}[\epsilon C + (1-\epsilon)C'] = -\frac{\partial}{\partial z}[UC + U_f C'] \qquad \text{(II-5)}.$$

In the sheet-forming process the fluid, water, is incompressible. Equation (II-3) thereby, at constant temperature, reduces to

$$\frac{\partial \epsilon}{\partial t} = -\frac{\partial U}{\partial z} \qquad \text{(II-6)}.$$

While the mat is deformable, the fiber itself may be taken to be incompressible, i.e., ρ_f being constant. By this assumption Equation (II-4) becomes

$$\frac{\partial \epsilon}{\partial t} = \frac{\partial U_f}{\partial z} \qquad \text{(II-7)}.$$

Hence,

$$\frac{\partial U}{\partial z} = -\frac{\partial U_f}{\partial z} \qquad \text{(II-8)},$$

which, upon integration with respect to z at constant A, with the boundary condition $U_f = 0$ at $z = 0$, yields

$$U + U_f = U_0 \qquad \text{(II-9)},$$

indicating that the sum of the instantaneous superficial water and fiber velocities at any plane in the system must always equal the filtrate velocity which is necessarily the same as the approach velocity of the suspension or slurry. This conclusion is illustrated in Fig. II-1.

RELATIVE VELOCITY

Since water and fiber are in relative motion, there is invariably dissipation of energy, as revealed by the loss of pressure. On the microscopic scale, the relative velocity of concern is $(\underline{u} - \underline{u_f})$. Averaging it over the fluid area as before, we define the relative superficial velocity as a macroscopic quantity to be

$$U_r = \epsilon(\bar{u} - \bar{u}_f) = U - \frac{\epsilon}{1 - \epsilon} U_f \qquad \text{(II-10)},$$

in which it will be assumed that the fibers move as a "layer" at the same velocity $\underline{\bar{u}_f}$. The change of $\underline{U_r}$ is depicted in the previous figure. Its magnitude increases rapidly from zero at the mat face to a maximum at the screen.

The concept of relative velocity is important in dealing with filtration of high-consistency suspensions because in such cases the amount of water being squeezed out of the mat due to the reduction of porosity constitutes a sizable fraction of the drainage. If the suspension is dilute, the water velocity through the mat is so large, compared with the fiber velocity, that the relative velocity is practically the velocity of the water itself. In the simplest case of forming an incompressible mat, the fibers, once deposited, are no longer in motion. Then the instantaneous flow is constant in the mat. From this discussion it will be shown later that for the same drainage the smaller the relative velocity, the less is the energy dissipation.

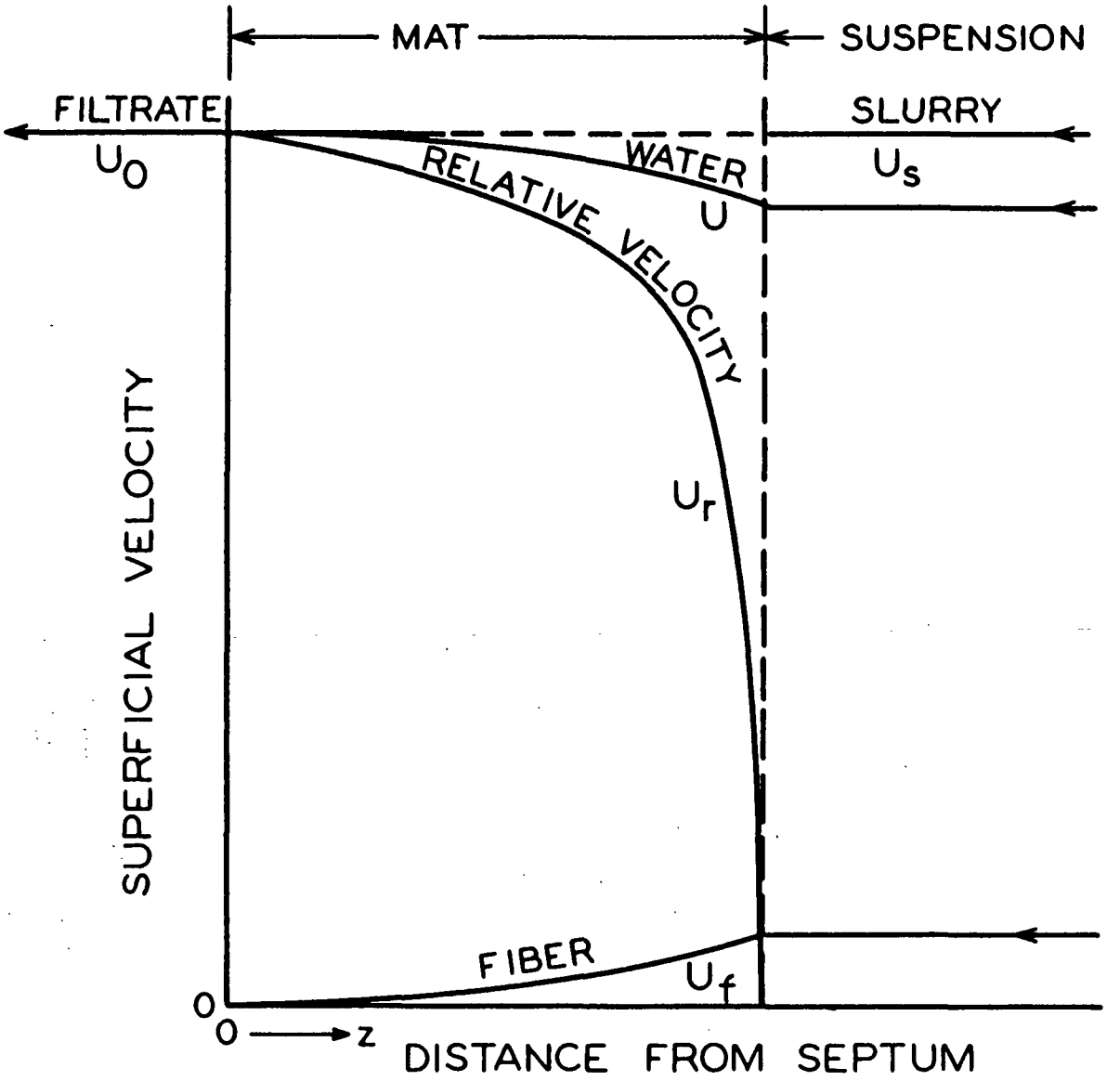

Figure II-1. Superficial Velocity Distributions in a Fiber Mat

FORCE RELATIONSHIPS

If the force required to produce acceleration in the flow direction, in either water or fiber, can be ignored, a simple relation exists, connecting the hydrostatic pressure, $\underline{p}$, and the compacting pressure, $\underline{p_f}$:

$$\frac{\partial p}{\partial z} = - \frac{\partial p_f}{\partial z} \qquad \text{(II-11)} .$$

$\underline{p_f}$ is the total force per unit area sustained by the system, corrected for the hydrostatic pressure. Upon integration we obtain

$$p - p_0 = p_{f,0} - p_f \qquad \text{(II-12)}$$

and

$$p - p_L = p_{f,L} - p_f \qquad \text{(II-13)} .$$

For greater generality the force required for acceleration in the $\underline{z}$ direction, as well as the gravitational effect, should be taken into account. A force balance for each phase per unit volume results in

$$\rho\epsilon\left[\frac{\partial \bar{u}}{\partial t} + \bar{u}\frac{\partial \bar{u}}{\partial z}\right] = - \frac{\partial p}{\partial z} - \rho g + \frac{\partial p'}{\partial z} \qquad \text{(II-14)}$$

and

$$\rho_f(1 - \epsilon)\left[\frac{\partial \bar{u}_f}{\partial t} + \bar{u}_f\frac{\partial \bar{u}_f}{\partial z}\right] = - \frac{\partial p_f}{\partial z} - (1 - \epsilon)(\rho_f - \rho)g - \frac{\partial p'}{\partial z} \qquad \text{(II-15)} .$$

The last term in each equation accounts for the average shear stress arising from the water-fiber interaction due to their relative motion, $\underline{p'}$ being the pressure exerted by the water on the fiber.

Since the fiber velocity is generally small compared with the water velocity, the inertial forces of the fibers may be neglected, and the two equatio reduce to a single one in terms of the fluid superficial velocity:

$$\frac{\partial p'}{\partial z} = -\frac{\partial}{\partial z}\left[p_f + (1-\epsilon)(\rho_f - \rho)gz\right]$$

$$= \frac{\partial}{\partial z}(p + \rho gz) + \rho\epsilon\left[\frac{\partial(U/\epsilon)}{\partial t} + \frac{U}{\epsilon}\frac{\partial(U/\epsilon)}{\partial z}\right] \qquad \text{(II-16)}$$

This may be called the equation of motion. If the fluid acceleration can also b neglected, as will be the usual case, the three pressure gradients are equal, neglecting the gravitational force:

$$\frac{\partial p'}{\partial z} = \frac{\partial p}{\partial z} = -\frac{\partial p_f}{\partial z} \qquad \text{(II-17)},$$

which reverts to Equation (II-11).

III. PRELIMINARY INTRODUCTION OF EMPIRICAL EXPRESSIONS

Further development of the macroscopic equations of continuity and motion requires appropriate expressions for describing the rate of the process and the state of the system. Such relationships have been established experimentally under simplified conditions and subsequently generalized or refined. The pertinent ones with accepted validity or utility will be reviewed here. These are concerned with fluid permeation, mat compression, particle attenuation, and fiber retention.

FLUID PERMEATION

Steady isothermal slow flow of an incompressible viscous fluid through a homogeneous undeformable porous medium in one direction obeys the well-known Darcy law (III-1):

$$U = \frac{K_o}{L}(p_0 - p_L - \rho g L) \qquad \text{(III-1)},$$

where p_L and p_0 are the fluid pressures at the upper and lower boundaries of the medium, respectively, and $\rho g L$ accounts for the gravitational pressure. The coefficient K_o is often called Darcy's permeability. It is inversely proportional to the viscosity μ of the fluid and dependent on at least two geometric properties of the medium: void fraction ϵ and specific surface S_o, both based on the volume of the medium. For low to medium porosities the Kozeny-Carman (III-2) expression of Darcy's permeability applies:

$$K_o = \frac{\epsilon^3}{k\mu S_o^2} = \frac{\epsilon^3}{k\mu S_v^2 (1 - \epsilon)^2} \qquad \text{(III-2)},$$

in which the Kozeny factor k is practically constant, and S_v is the specific surface based on the volume of the solid element.

However, at higher porosities it was soon found that the Kozeny factor itself is porosity dependent. For fiber structures Davis (III-3) correlated the variation of k with ϵ in the following form:

$$k = k_1 \frac{\epsilon^3}{(1-\epsilon)^2} [1 + k_2 (1-\epsilon)^3] \qquad \text{(III-3)},$$

where k_1 and k_2 are two constants. Carroll (III-4) recently proposed another correlation which has the advantage of covering a wide porosity range:

$$k = k_3 + \exp[k_4 (\epsilon - \epsilon^0)] \qquad \text{(III-4)}.$$

For flow beyond Darcy's region the Forchheimer (III-5) formula is often used:

$$\frac{|p_0 - p_L - \rho g L|}{L} = a|U| + bU^2 \qquad \text{(III-5)},$$

where a and b are flow resistances. a is equivalent to the reciprocal of Darcy's permeability K_0.

When the flow is slow, the viscous effect predominates, and Forchheimer's formula reduces to Darcy's law. In transition flow the inertial effect represented by the quadratic velocity term becomes significant. For turbulent flow the Darcy term is inappreciable, and only the quadratic term is retained. In this sense a and b are the viscous and inertial resistances, respectively. According to Equation (III-2), the viscous resistance may be expressed as

$$a = \alpha' \frac{(1-\epsilon)^2}{\epsilon^3} S_v^2 \mu \qquad \text{(III-6)},$$

where α' is the viscous resistance coefficient at moderate porosities.

Ergun (III-6) proposed the correlation for the inertial resistance as

$$b = \beta' \frac{1 - \epsilon}{\epsilon^3} S_v \rho \qquad \text{(III-7)},$$

where β' is the inertial resistance coefficient, also at medium porosities.

MAT COMPRESSION

The compressibility of a homogeneous fiber mat, subject to a uniform compacting load in quasi equilibrium, was first described by Qviller (III-7), followed by Campbell (III-8), and lately modified by Ingmanson and Whitney (III-9). The Ingmanson form is

$$c - c_o = M p_f^N \qquad \text{(III-8)},$$

where c is the mat density (mass of fibers per unit mat volume) at the applied pressure p_f, and c_o that at zero p_f. M and N are the compressibility constants.

By his analysis Wilder (III-10) suggested an alternate compressibility function:

$$c^\gamma - c_o^\gamma = M_b p_f \qquad \text{(III-9)}.$$

If $c_o \ll c$, either function reduces to Campbell's simple form:

$$c = M p_f^N \qquad \text{(III-10)}.$$

PARTICLE ATTENUATION

The attenuation of fine particles suspended in a fluid in steady permeation of an incompressible homogeneous fiber mat was originally described,

in connection with aerosol filtration, by

$$C_0 = C_L e^{-KL} \qquad \text{(III-11)},$$

where K is the attenuation coefficient. For flow downward, C_L and C_0 are the particle concentrations at the upper and lower boundaries of the mat, respectively.

The attenuation coefficient may be further resolved into the geometric factors of the fiber mat by

$$K = E \frac{A_f}{V_f} (1 - \varepsilon) \qquad \text{(III-12)},$$

in which A_f/V_f is the cross-sectional area of the fibers projected in the direction of flow per unit volume of the fibers and E represents the collection efficiency of the mat.

FIBER RETENTION

The retention of fibers on a screen may be expressed in the following form as suggested by Estridge (III-11):

$$W_s = W + \frac{1}{k_0} \ln \frac{1 - (1 - R_0)e^{-k_0 W}}{R_0} \qquad \text{(III-13)},$$

where W is the mass of fibers retained and W_s that approaching the screen, per unit area. R_0 is the initial retention in mass fraction and k_0 the retention coefficient. In terms of fiber consistencies an equivalent expression was earlier presented by Han (III-12):

$$s_0 = s(1 - R_0)e^{-k_0 W} \qquad \text{(III-14)},$$

which relates the fiber consistency $\underline{s}_0$ in the filtrate to the basis weight, $\underline{W}$, $\underline{s}$ being the fiber consistency in the suspension. Consistency is expressed in the mass of fibers per unit mass of the suspension or filtrate.

IV. PARTIAL JUSTIFICATION OF PERMEATION LAWS

The laws of permeation have been introduced on the empirical basis. Because of the complexity of flow in porous media these laws cannot be rigorously derived from the fundamental hydrodynamic equations. It is, however, possible to demonstrate their macroscopic validity by the space average of the microscopic flow which obeys the Navier-Stokes equation. The following treatment is modified from the original paper of Irmay (IV-1).

MICROSCOPIC FLOW

The Navier-Stokes equation in vectorial notation for steady imcompressibl isothermal flow of a viscous fluid is

$$\rho\vec{u} \cdot \nabla\vec{u} = -\nabla p + \rho\vec{g} + \mu\nabla^2\vec{u} \qquad \text{(IV-1)},$$

which may also be written as

$$\nabla E = \nabla(p + \rho g z + \rho|\vec{u}|^2/2) = \rho\vec{u} \times (\nabla \times \vec{u}) + \mu\nabla^2\vec{u} \qquad \text{(IV-2)},$$

where

$$|\vec{u}|^2 = u_x^2 + u_y^2 + u_z^2 \qquad \text{(IV-3)}.$$

E is Bernoulli's energy per unit volume. The first term on the right side of Equation (IV-2) involves vorticity $(\nabla \times \vec{u})$ and the second term viscous dissipation.

Taking the divergence of Equation (IV-2), we have

$$\nabla \cdot \nabla(p + \rho g z + \rho|\vec{u}|^2/2) = \nabla \cdot [\rho\vec{u} \times (\nabla \times \vec{u})] + \nabla \cdot \mu\nabla^2\vec{u} \qquad \text{(IV-4)}.$$

For slow flow the inertia terms which are of the second order in $\vec{u}$ may be neglected, and the last term is zero by virtue of the equation of continuity:

$$\nabla \cdot \vec{u} = 0 \qquad \text{(IV-5)} .$$

Hence,

$$\nabla^2 (p + \rho g z) = 0 \qquad \text{(IV-6)} .$$

This is the Laplace equation for creeping flow, which formally resembles that for irrotational or potential flow. As pointed out by Rouse (IV-2): "...these systems (potential flow) are distinguished by initial absence of vorticity and negligible viscous influence. Paradoxically, however, potential theory is also highly useful in analyzing the percolation of fluids through permeable media, provided that viscous action dominates--i.e., that the flow is laminar."

At any point in the pore space the flow obeys Equation (IV-2). Whereas we have treated the macroscopic flow through a porous medium as one dimensional, the microscopic flow in the void space is obviously three dimensional. The z component of the flow gives

$$\frac{\partial E}{\partial z} = \frac{\rho}{2} \frac{\partial}{\partial z}(u_x^2 + u_y^2) - \rho\left(u_x \frac{\partial u_z}{\partial x} + u_y \frac{\partial u_z}{\partial y}\right)$$

$$+ \mu\left(\frac{\partial^2 u_z}{\partial x^2} + \frac{\partial^2 u_z}{\partial y^2} + \frac{\partial^2 u_z}{\partial z^2}\right) \qquad \text{(IV-7)} ,$$

from which both Darcy's law and Forchheimer's formula may be approximately deduced as follows.

SPACE AVERAGE

Consider a volume sufficiently large so as to include a great number of the solid elements of the porous medium, yet sufficiently small so that its macroscopic properties do not change appreciably. By averaging the velocity components over such a space occupied by the fluid, we may say

$$\bar{u}_x = \bar{u}_y = 0 \qquad \text{(IV-8)} .$$

Furthermore, if the average of one factor is zero, and there is no correlation between two factors, then the following equation is correct:

$$\overline{u_x \frac{\partial u_z}{\partial x}} = \overline{u_y \frac{\partial u_z}{\partial y}} = 0 \qquad \text{(IV-9)} .$$

Thus, by the process of space average, Equation (IV-7) becomes

$$\overline{\frac{\partial E}{\partial z}} = \frac{\rho}{2} \overline{\frac{\partial}{\partial z}(u_x^2 + u_y^2)} + \mu \overline{\left(\frac{\partial^2 u_z}{\partial x^2} + \frac{\partial^2 u_z}{\partial y^2} + \frac{\partial^2 u_z}{\partial z^2}\right)} \qquad \text{(IV-10)} .$$

MACROSCOPIC SIMILITUDE

Let d_o be the smallest distance of separation between the solid-elemer surfaces. As an approximation the space average of the second derivatives of u_z may be expressed in terms of $\bar{u}_z$ and d_o ,

$$\overline{\frac{\partial^2 u_z}{\partial x^2} + \frac{\partial^2 u_z}{\partial y^2} + \frac{\partial^2 u_z}{\partial z^2}} = -\alpha \frac{\bar{u}_z}{d_o^2} \qquad \text{(IV-11)} ,$$

where α serves as a pore shape function. The minus sign is incorporated because these second derivatives can be shown to be always negative.

If $\underline{d}$ is a representative diameter of the solid elements composing an isotropic medium, then

$$\frac{d_o}{d} = \frac{\epsilon}{1 - \epsilon} \qquad \text{(IV-12)} .$$

Furthermore, by the definition of superficial velocity,

$$\bar{u}_z = \bar{u} = \frac{U}{\epsilon} \qquad \text{(IV-13)} ,$$

in which the velocities are understood here to be positive.

Therefore, if all the quadratic terms may be neglected, Equation (IV-10) is simplified to

$$- \frac{\partial}{\partial z}(\bar{p} + \rho g z) = \frac{\alpha \mu}{d^2} \frac{(1 - \epsilon)^2}{\epsilon^3} U \qquad \text{(IV-14)} ,$$

which is the differential form of Darcy's equation. Recognizing that the specific surface $\underline{S_V}$ is inversely proportional to $\underline{d}$, we have

$$K_o = \frac{\epsilon^3}{\alpha' \mu S_V^2 (1 - \epsilon)^2} \qquad \text{(IV-15)} ,$$

in which the viscous resistance coefficient α' may be interpreted as the Kozeny factor $\underline{k}$ in the Kozeny-Carman form of Darcy's law.

If the quadratic terms are significant, we can, in the first place, still eliminate the dynamic pressure term in $\underline{E}$ because by virtue of Equations (IV-5) and (IV-8)

$$\overline{\frac{\partial}{\partial z} |\vec{u}|^2} = \overline{\frac{\partial}{\partial z}(u_x^2 + u_y^2 + u_z^2)} = 0 \qquad \text{(IV-16)} .$$

In the second place, since the quantity $(\underline{u}_{\underline{x}}^2 + \underline{u}_{\underline{y}}^2)$ is always zero at the greatest contraction $\underline{d}_o$ and always positive in the converging zone, its derivative with respect to $\underline{z}$ is always negative. In the diverging zone there often occurs flow separation. Here the derivative is either zero or mildly positive. Hence, by averaging this derivative over both converging and diverging zones, the result is

$$\overline{\frac{\partial}{\partial z}(u_x^2 + u_y^2)} < 0 \qquad \text{(IV-17)} .$$

By these deductions the macroscopic similitude calls for

$$\overline{\frac{\partial}{\partial z}(u_x^2 + u_y^2)} = -\beta \frac{\bar{u}_z^2}{d_o} = -\frac{\beta}{d} \frac{(1 - \epsilon)}{\epsilon^3} U^2 \qquad \text{(IV-18)} ;$$

thereby Equation (IV-10) reduces to the differential form of Forchheimer's formula:

$$-\frac{\partial}{\partial z}(\bar{p} + \rho g z) = \alpha' \frac{(1 - \epsilon)^2}{\epsilon^3} S_v^2 \mu U + \beta' \frac{(1 - \epsilon)}{\epsilon^3} S_v \rho U^2 \qquad \text{(IV-19)} ,$$

with the resistances $\underline{a}$ and $\underline{b}$ expressed in the same way as before:

$$a = \alpha' \frac{(1 - \epsilon)^2}{\epsilon^3} S_v^2 \mu \qquad \text{(III-6)}$$

and

$$b = \beta' \frac{(1 - \epsilon)}{\epsilon^3} S_v \rho \qquad \text{(III-7)} .$$

V. FURTHER ELABORATION OF RESISTANCE COEFFICIENTS

The expression for steady flow through homogeneous undeformable porous media with negligible gravitational effects has been shown to be

$$\frac{|\Delta p|}{L} = \alpha' \frac{(1-\epsilon)^2}{\epsilon^3} S_v^2 \mu |U| + \beta' \frac{(1-\epsilon)}{\epsilon^3} S_v \rho U^2 \qquad (V\text{-}1) .$$

It remains to clarify the two resistance coefficients α' and β', and their possible connection, especially with regard to fiber mats.

VISCOUS FLOW

It has been mentioned that α', or the Kozeny factor k, is porosity dependent in the high-porosity range. This point was early analyzed by Emersleben (V-1). Lately, Happel (V-2) proposed a free-surface model to arrive at a similar conclusion. His solution for the case of creeping flow through a regular assemblage of cylinders is reviewed here in view of its particular pertinence to the permeability of fiber mats.

In Happel's model each cylinder in the assemblage is considered to be surrounded by a concentric envelope of fluid with a free surface, constituting a unit cell. The cylinder is supposed to be moving in the direction perpendicular to its axis at a uniform velocity U (positive) in a stationary fluid. The radius of the cylinder is r_i and that of the fluid envelope is r_o.

The equation of continuity and the Navier-Stokes equations for steady incompressible two-dimensional creeping flow in cylindrical co-ordinates (r and θ) are

$$\frac{\partial}{\partial r}(ru_r) + \frac{\partial u_\theta}{\partial \theta} = 0 \qquad \text{(V-2)},$$

$$\frac{1}{\mu}\frac{\partial p}{\partial r} = \frac{\partial}{\partial r}\left[\frac{1}{r}\frac{\partial}{\partial r}(ru_r)\right] + \frac{1}{r^2}\frac{\partial^2 u_r}{\partial \theta^2} - \frac{2}{r^2}\frac{\partial u_\theta}{\partial \theta} \qquad \text{(V-3)},$$

and

$$\frac{1}{\mu r}\frac{\partial p}{\partial \theta} = \frac{\partial}{\partial r}\left[\frac{1}{r}\frac{\partial}{\partial r}(ru_\theta)\right] + \frac{1}{r^2}\frac{\partial^2 u_\theta}{\partial \theta^2} + \frac{2}{r^2}\frac{\partial u_r}{\partial \theta} \qquad \text{(V-4)}.$$

The boundary conditions are specified to be

$$r = r_i\,, \quad u_r = U\cos\theta\,, \quad u_\theta = -U\sin\theta \qquad \text{(V-5)}$$

and $$r = r_o\,, \quad u_r = 0\,, \quad \frac{\partial u_\theta}{\partial r} + \frac{1}{r}\frac{\partial u_r}{\partial \theta} - \frac{u_\theta}{r} = 0 \qquad \text{(V-6)}.$$

Without giving the details of his solution for velocity and pressure distributions, Happel presented the drag force per unit length of the cylinder as

$$F = \frac{4\pi\mu U}{\ln\frac{r_o}{r_i} - \frac{1}{2}\left[\frac{r_o^4 - r_i^4}{r_o^4 + r_i^4}\right]} \qquad \text{(V-7)}.$$

Since the porosity of a unit cell is related to its radii by

$$\epsilon = 1 - \left(\frac{r_i}{r_o}\right)^2 \qquad \text{(V-8)},$$

the drag force may also be expressed in terms of porosity,

$$F = \frac{4\pi\mu U}{\frac{1}{2}\left[\ln\frac{1}{1-\epsilon} - \frac{1-(1-\epsilon)^2}{1+(1-\epsilon)^2}\right]} \qquad \text{(V-9)}.$$

Now the pressure drop across the assemblage of cylinders of diameter d_f is related to the drag force by

$$|\Delta p| = \frac{4L(1-\epsilon)|F|}{\pi d_f^2} \qquad \text{(V-10)}.$$

Hence, Darcy's permeability, according to the free-surface model, is

$$K_o = \frac{d_f^2}{32\mu(1-\epsilon)}\left[\ln\frac{1}{1-\epsilon} - \frac{1-(1-\epsilon)^2}{1+(1-\epsilon)^2}\right] \qquad \text{(V-11)}.$$

Since the specific surface S_v for a cylinder is $4/d_f$, the Kozeny factor is seen to be

$$k = \frac{2\epsilon^3}{(1-\epsilon)\left[\ln\frac{1}{1-\epsilon} - \frac{1-(1-\epsilon)^2}{1+(1-\epsilon)^2}\right]} \qquad \text{(V-12)}.$$

Happel's solution may be compared with the previously introduced empirical correlations (III-3) and (III-4). For further treatment of permeation, Davis' equation is more realistic and convenient than Happel's. Accordingly, we shall use the Davis porosity function for the viscous resistance in accordance with Equation (III-6):

$$a = k_1(1-\epsilon)^{3/2}[1 + k_2(1-\epsilon)^3]S_v^2\mu \qquad \text{(V-13)}.$$

TRANSITION FLOW

The pattern of flow may be characterized by the Reynolds number which represents the ratio of inertial to viscous forces. The Reynolds number is the product of a characteristic velocity and a characteristic linear dimension of the flow system, divided by the kinematic viscosity (μ/ρ) of the fluid. From the previous analysis (Chapter IV) if we may, as suggested by Han (V-3), choose $\bar{u}_z$

as the characteristic velocity and $\sqrt{d_o^2/\alpha}$ as the characteristic dimension which includes the effect of pore shape on the flow, then the Reynolds number for porous media is defined as

$$Re' = \frac{d_o \rho \bar{u}_z}{\sqrt{\alpha}\mu} = \frac{\rho|U|}{\sqrt{\alpha'}\,(1-\epsilon)S_v\mu} \qquad (V\text{-}14)\ .$$

Since in the flow expression (V-1) the second resistance term represents the inertial effect and the first the viscous effect, their ratio should be proportional to the Reynolds number,

$$\frac{\beta'\rho|U|}{\alpha'(1-\epsilon)S_v\mu} \propto Re' \qquad (V\text{-}15)\ .$$

Accordingly, we obtain, in combination with the Davis porosity function (III-3),

$$\beta' = b'\sqrt{\alpha'} = b'\left[k_1 \frac{\epsilon^3}{(1-\epsilon)^{1/2}}\right]^{1/2} [1 + k_2(1-\epsilon)^3]^{1/2} \qquad (V\text{-}16)\ ,$$

and finally, substituting this into Equation (III-7),

$$b = b' k_1^{1/2} \epsilon^{-3/2} (1-\epsilon)^{3/4} [1 + k_2(1-\epsilon)^3]^{1/2} S_v \rho \qquad (V\text{-}17)\ .$$

It is seen that the flow expression contains three empirical constants, k_1 , k_2 , and b' , which are to be experimentally determined.

The steady flow expression may also be put in a dimensionless form:

$$\frac{\epsilon^3 |\Delta p|}{\sqrt{\alpha'}(1-\epsilon)S_v \rho U^2 L} = \frac{\sqrt{\alpha'}(1-\epsilon)S_v\mu}{\rho|U|} + b' \qquad (V\text{-}18)\ ,$$

or simply

$$f' = \frac{1}{Re'} + b' \qquad \text{(V-19)},$$

where $\underline{f}'$ is the friction factor defined by the term containing the over-all pressure gradient in Equation (V-18).

GENERALIZED EXPRESSION

In filtration of a high-consistency suspension to form a compressible mat at a rapid rate, the solid phase consisting of fibers is in appreciable motion, as previously explained. Consequently, it is the relative superficial velocity to be related to the fluid pressure gradient in the macroscopic description of flow:

$$-\frac{\partial(p + \rho g z)}{\partial z} = aU_r + bU_r^2 \operatorname{sgn}(U_r) \qquad \text{(V-20)},$$

where the viscous and inertial resistances, $\underline{a}$ and $\underline{b}$, have the same respective meanings as before, and $\operatorname{sgn}(\underline{U_r})$ has the value $+1$ if $\underline{U_r}$ is positive and the value -1 if $\underline{U_r}$ is negative.

VI. APPROXIMATE FORMULATION OF COMPRESSIBILITY FUNCTIONS

Fiber mats are more or less compressible. The static compressibility of a fiber mat may be represented empirically by several functions, among which three similar ones have been introduced in Chapter III, and are commonly used in dealing with filtration of compressible materials. These functions cannot yet be derived rigorously because of complexity of fiber structures. In the following the approximate development of Wilder's function based on the bending of elastic fibers is reviewed from his work (III-10).

FIBER CONTACTS

Consider a uniform mat composed of a large number of cylindrical fibers oriented randomly in the x-y plane with negligible orientations with the z axis. As will be shown later (Chapter XII), the number of apparent contact points, N_c, per unit area of the mat, when all the fibers are projected on the x-y plane, can be calculated from

$$N_c = N_f^2 L_f^2 / \pi \qquad \text{(VI-1)},$$

where N_f is the number of fibers per unit area and L_f the length of a fiber. The basis weight of the mat is simply

$$W = N_f (\pi d_f^2 / 4) L_f \rho_f \qquad \text{(VI-2)}.$$

If we imagine that the mat consists of a number of similar layers, each one-fiber diameter thick, then the mat density without an applied load is

$$c_o = \frac{W}{n d_f} \qquad \text{(VI-3)},$$

where n is the number of such layers. The projected intersections in one layer between two adjacent layers may be considered to represent the virtual contact points for that layer. Since two adjacent layers contain $2N_f/n$ fibers, the number of virtual contacts per unit area per layer is, according to (VI-1),

$$n_{c,o} = 2\left(\frac{2N_f}{n}\right)^2\left(\frac{L_f^2}{\pi}\right) \qquad \text{(VI-4)},$$

where the first factor 2 accounts for the fact that there is an adjacent layer on each side of any layer concerned. Utilizing Equations (VI-2) and (VI-3), we arrive at

$$n_{c,o} = \frac{128c_o^2}{\pi^3 d_f^2 \rho_f^2} \qquad \text{(VI-5)}.$$

The average distance between two virtual contact points is called the segment length, L_s. Since the total fiber length per unit area per layer is $N_f L_f/n$, the segment length under no applied load may be calculated from

$$L_{s,o} = \frac{\pi^2 d_f \rho_f}{32c_o} \qquad \text{(VI-6)},$$

in which the possible complication of fiber ends is ignored. If we consider that, as an average, the virtual contacts are distributed alternately above and below a fiber, the segment length, $L_{s,o}$, between two points supported from below will be twice the value indicated in (VI-6). This mat density-segment length relationship was first derived by Onogi and Sasaguri (VI-1).

BENDING ASSUMPTION

As a uniform compacting load is applied to the mat described above, deformation will occur by virtue of several possible mechanisms. If mat

compressibility is due entirely to elastic bending between frictionless supports (ρ_f remaining unchanged), the segment length will decrease from the initial value $L_{s,o}$ to some value L_s as proportionately more contacts are formed under the applied load. Lacking precise knowledge of the bending mechanism, we assume a power function between L_s and c, such that

$$\frac{L_s}{L_{s,o}} = \left(\frac{c_o}{c}\right)^{\gamma_o} \qquad \text{(VI-7)},$$

where γ_o is of the order of unity. Then the number of virtual contacts per unit area per layer is

$$n_c = \frac{N_f L_f}{n L_s} \qquad \text{(VI-8)}.$$

Upon application of an infinitesimal load per unit area, dp_f, the incremental force sustained by each contact in the layer is dp_f/n_c. Using the simple beam theory, the reduction in thickness of the layer is

$$-\frac{dL}{n} = \frac{L_s^3}{N'EI}\frac{dp_f}{n_c} \qquad \text{(VI-9)},$$

where N' is a number dependent on the distribution of load and support, E the modulus of elasticity, and I the moment of inertia. Expressing L as W/c and utilizing Equation (VI-3), we have

$$\frac{dc}{c^2} = \left(\frac{1}{N'EId_f c_o}\right)\frac{L_s^3}{n_c}\,dp_f \qquad \text{(VI-10)}.$$

Since by the previous assumptions, L_s and n_c are related to c by

$$L_s = \frac{\pi^2 \rho_f d_f c_o^{\gamma_o - 1}}{16 c^{\gamma_o}} \qquad \text{(VI-11)}$$

and

$$n_c = \frac{64 c_o^{2-\gamma_o} c^{\gamma_o}}{\pi^3 \rho_f^2 d_f^2} \qquad \text{(VI-12)},$$

and the moment of inertia of the beam so supported is

$$I = \frac{\pi d_f^4}{64} \qquad \text{(VI-13)},$$

the differential equation for mat compression due to fiber bending alone becomes

$$c^{4\gamma_o - 2}\, dc = \frac{\pi^8 \rho_f^5}{16^3 N' E c_o^{6-4\gamma_o}}\, dp_f \qquad \text{(VI-13)}.$$

Integrating for the whole mat between the limits: c_o at zero p_f and c at p_f, the resulting compressibility expression is

$$c^{4\gamma_o - 1} - c_o^{4\gamma_o - 1} = \frac{M'(4\gamma_o - 1)\rho_f^5}{E c_o^{6-4\gamma_o}}\, p_f \qquad \text{(VI-14)},$$

where M' has absorbed all the numerical values.

Onogi and Sasaguri (VI-1) further stated that if a distribution of z orientations is introduced by the compression process, Equation (VI-6) will no longer hold. Assuming the distribution function to be proportional to $\sin^6\theta$, where θ is the angle that a fiber makes with the z axis, they developed the relationship:

$$\frac{c}{\rho_f} = \left[\frac{1}{k_1'(L_s/d_f) + k_2'}\right]^2 \left[\frac{1}{k_3'(L_s/d_f) + k_4'}\right]\left(\frac{L_s}{d_f}\right) \qquad \text{(VI-15)},$$

where k's are constants. This would indicate that the effect of z orientations could be equivalent to reducing the value of γ_o to less than unity which is strictly true for the case of random orientation in the x-y plane only. In Wilder's development this effect has been included in the assumption that the value of γ_o is of the order of unity.

SIMPLIFIED FORMS

Wilder's static compressibility function (VI-14) has been simplified to

$$c^{\gamma} - c_o^{\gamma} = M_b p_f \qquad \text{(III-9)},$$

where M_b implies its dependence on c_o. If the value of γ is 3, Wilder's equation agrees in form with the function developed earlier by Van Wyk (VI-2). When $c_o \ll c$, it reduces to Campbell's form:

$$c = M p_f^N \qquad \text{(III-10)}.$$

By this analysis Wilder's form is more tenable than Ingmanson's form:

$$c - c_o = M p_f^N \qquad \text{(III-8)}.$$

VII. ANALYTICAL TREATMENT OF PARTICLE COLLECTION

The collection of fine particles by a fiber mat during permeation, as governed by the attenuation law, will be explained in some detail with clarification of the meaning of collection efficiency. The same law will then be extended to the filtration process for the analysis of particle distribution in fiber mats (II-1, II-3).

ATTENUATION LAW

Consider a suspension of fine particles in a fluid permeating steadily through a stationary fiber mat of a fixed thickness L. By virtue of their motion, some particles will collide with the fibers and others will penetrate through the mat. For a large number of particles the chances of their capture are statistically determinable. It is reasonable to assume that the more particles there are approaching an infinitesimal layer of fibers, the more will be captured. With this contention the rate of particle attenuation in the flow direction may be said to be directly proportional to the particle concentration. Thus, as the flow is opposite the z direction,

$$-\frac{dC}{d(L - z)} = KC \qquad \text{(VII-1)}.$$

If all factors influencing particle collection remain constant throughout the mat, K will be independent of z. By integration from 0 to L, we arrive at the previously introduced attenuation expression:

$$C_0 = C_L e^{-KL} \qquad \text{(III-11)}.$$

In this derivation it is implied that the concentration is uniform as the particles approach a "layer" of fibers. After attenuation some sort of mixing process presumably takes place so that the concentration is uniform again. The mixing process is probably very effective at the intersections of a large number of interconnected pores.

COLLECTION EFFICIENCY

The term "collection efficiency" was conceived in the field of aerosol filtration, and has since been widely accepted as a rational basis for evaluation of fiber filters. The original concept was based on the idealized case of a single cylinder placed in a fluid stream moving in the direction perpendicular to the axis of the cylinder. The collection efficiency of the cylinder was defined as the ratio of the number of particles collected by the cylinder to the total number of particles in the fluid stream approaching the cross-sectional area of the cylinder. This definition of collection efficiency may be generalized for application to fiber mats.

In an infinitesimal layer of a mat, the total cross-sectional area of the fibers projected in the direction of flow is $(\underline{A_f}/\underline{V_f})(1 - \epsilon)d(\underline{L} - \underline{z})$. The fraction of the approaching particles collected by this layer will be $\underline{E}(\underline{A_f}/\underline{V_f})(1 - \epsilon)d(\underline{L} - \underline{z})$, $\underline{E}$ being the collection efficiency of the fibers in a collective sense. Across this layer the free particle concentration is attenuated from $\underline{C}$ by $-d\underline{C}$. It then becomes apparent that

$$-\frac{dC}{C} = E\,\frac{A_f}{V_f}(1 - \epsilon)d(L - z) \qquad \text{(VII-2)} .$$

Comparing with Equation (VII-1), it is seen that

$$K = E \frac{A_f}{V_f} (1 - \epsilon) \qquad \text{(III-12)} .$$

For cylindrical fibers the relation becomes

$$K = E \frac{4(1 - \epsilon)}{\pi d_f} \qquad \text{(VII-3)} .$$

PARTICLE FILTRATION

In a filtration process, as fibers are deposited on a screen, the excess water with free particles permeates through the mat already formed. During the passage of the fluid, some free particles become attached to the fibers. However, the deposited fibers may also be in motion. Therefore, again, the relative velocity must be taken into account. Suppose an observer is moving along with a layer of fibers at the same velocity; then the rate of particle retention will be described by the observer as

$$(1 - \epsilon) \frac{\partial C'}{\partial t} = K|U_r|C \qquad \text{(VII-4)} .$$

Now, if the observer looks at a stationary frame of the system, he also sees the motion of the fibers carrying bound particles. As a consequence the rate of increase of bound particles in the layer will be described as

$$(1 - \epsilon) \frac{\partial C'}{\partial t} + U_f \frac{\partial C'}{\partial z} = K|U_r|C \qquad \text{(VII-5)} .$$

Recalling the equations of particle and fiber continuity:

$$\frac{\partial}{\partial t}\left[\epsilon C + (1 - \epsilon)C'\right] = -\frac{\partial}{\partial z}\left[UC + U_f C'\right] \qquad \text{(II-5)}$$

and

$$\frac{\partial \epsilon}{\partial t} = \frac{\partial U_f}{\partial z} \qquad \text{(II-7)},$$

we may utilize these equations in conjunction with the retention equation (VII-5) to yield the attenuation equation:

$$\epsilon \frac{\partial C}{\partial t} + U \frac{\partial C}{\partial z} = -K|U_r|C \qquad \text{(VII-6)}.$$

For steady penetration $(\partial \underline{C}/\partial \underline{t} = 0)$ through an incompressible mat $(\underline{U_f} = 0)$ opposite to the $\underline{z}$ direction $(|\underline{U_r}| = |\underline{U}|)$, the last equation reduces to Equation (VII-1) since $\underline{L}$ is constant and $\underline{U}$ is negative.

INCOMPRESSIBLE MAT

In forming an incompressible mat of uniform porosity, the decrease of free particles in the flow direction through the mat already formed follows the attenuation law (VII-1). Integrating from $\underline{z}$ to $\underline{L}$ and setting the free particle concentration in the suspension as $\underline{C_s}$, the result is

$$C = C_s e^{-K(L-z)} \qquad \text{(VII-7)}.$$

Meanwhile more fibers are deposited on the mat. Suppose the mat face moves at a constant velocity $\underline{U'}$. Then, taking partial differentiation of Equation (VII-7) with respect to the independent variables $\underline{t}$ and $\underline{z}$, we have

$$\frac{\partial C}{\partial t} = -KU'C_s e^{-K(U't-z)} \qquad \text{(VII-8)}$$

and

$$\frac{\partial C}{\partial z} = KC_s e^{-K(U't-z)} \qquad \text{(VII-9)} .$$

Under the prescribed conditions (ϵ = constant, $\underline{U}$ = constant, and $\underline{U_f} = 0$), the equation of particle continuity (II-5) reduces to

$$\epsilon \frac{\partial C}{\partial t} + (1 - \epsilon) \frac{\partial C'}{\partial t} = -U \frac{\partial C}{\partial z} \qquad \text{(VII-10)} .$$

Combining the above three equations, we obtain a single partial differential equation to describe the retention process:

$$\frac{\partial C'}{\partial t} = KC_s \frac{\epsilon U' - U}{1 - \epsilon} e^{-K(U't-z)} \qquad \text{(VII-11)} ,$$

which may be integrated with respect to $\underline{t}$ to yield

$$C' = -C_s \frac{\epsilon U' - U}{U'(1 - \epsilon)} e^{-K(U't-z)} + f(z) \qquad \text{(VII-12)} .$$

If the bound particle concentration in the suspension is $\underline{C_s'}$, the integration constant is evaluated to be

$$f(z) = C_s' + C_s \frac{\epsilon U' - U}{U'(1 - \epsilon)} \qquad \text{(VII-13)} ,$$

and the solution is

$$C' - C_s' = C_s \frac{U - \epsilon U'}{U'(1 - \epsilon)} [e^{-K(L-z)} - 1] \qquad \text{(VII-14)} .$$

If it is desired to express all quantities in mass units, the following relations apply:

$$z = \frac{\rho_f(1 - \epsilon)}{w} \qquad \text{(VII-15)},$$

$$L = \frac{\rho_f(1 - \epsilon)}{W} \qquad \text{(VII-16)},$$

$$C = \frac{m\rho_f(1 - \epsilon)}{w_p\epsilon} \qquad \text{(VII-17)},$$

$$C_s = \frac{m_s\rho_f(1 - \epsilon_s)}{w_p\epsilon_s} \qquad \text{(VII-18)},$$

$$C' = \frac{m'\rho_f}{w_p} \qquad \text{(VII-19)},$$

and

$$C'_s = \frac{m'_s\rho_f}{w_p} \qquad \text{(VII-20)},$$

where $\underline{m}$ and $\underline{m}'$ are the masses of free and bound particles per unit mass of the fluid and fibers, respectively, with the subscript $\underline{s}$, if present, referring to the suspension. $\underline{w_p}$ is the mass per particle and $\epsilon_{\underline{s}}$ the void fraction of the suspension.

The relation between the superficial fluid velocity and the mat face velocity may be established by a fiber balance:

$$-\frac{1 - \epsilon_s}{\epsilon_s} U = (1 - \epsilon)U' \qquad \text{(VII-21)}.$$

Since for a dilute suspension, $|\underline{U}'| \ll |\underline{U}|$,

$$\frac{U - \epsilon U'}{U'(1 - \epsilon)} = \frac{U}{U'(1 - \epsilon)} = -\frac{\epsilon_s}{1 - \epsilon_s} \qquad \text{(VII-22)}.$$

Substituting these relations into Equation (VII-14), the solution for the bound particle distribution becomes

$$\frac{m' - m'_s}{m_s} = 1 - \exp\left[-\frac{KW}{\rho_f(1-\epsilon)}\left(1 - \frac{w}{W}\right)\right] \qquad \text{(VII-23)} .$$

COMPRESSIBLE MAT

Beginning with the partial differential retention and attenuation equations:

$$(1-\epsilon)\frac{\partial C'}{\partial t} + U_f \frac{\partial C'}{dz} = K|U_r|C \qquad \text{(VII-5)}$$

and

$$\epsilon \frac{\partial C}{\partial t} + U \frac{\partial C}{\partial z} = -K|U_r|C \qquad \text{(VII-6)} ,$$

it is seen at once that the first equation reduces to Equation (VII-11) for the incompressible case under the condition: $|\underline{U}'| \ll |\underline{U}|$.

To solve for the compressible case under simplified conditions and in mass quantities, we proceed with conversion of these equations into suitable forms. Introducing two new independent variables as

$$w' = W(t) - w = W - \rho_f \int_o^z (1-\epsilon)dz \qquad \text{(VII-24)} ,$$

and

$$t' = t \qquad \text{(VII-25)} ,$$

the original variables are related to the new ones, respectively, by

$$\frac{\partial}{\partial z} = -\rho_f(1-\epsilon)\frac{\partial}{\partial w'} \qquad \text{(VII-26)}$$

and

$$\frac{\partial}{\partial t} = \frac{\partial w}{\partial t}\frac{\partial}{\partial w} + \frac{dW}{dt'}\frac{\partial}{\partial w'} + \frac{\partial}{\partial t'} \qquad \text{(VII-27)} .$$

Since

$$\frac{\partial w}{\partial t} = -\rho_f \int_o^z \frac{\partial \epsilon}{\partial t}\, dz \qquad \text{(VII-28)} ,$$

and from the equation of fiber continuity (II-7),

$$\int_o^z \frac{\partial \epsilon}{\partial t}\, dz = U_f \qquad \text{(VII-29)} ,$$

Equation (VII-27) becomes

$$\frac{\partial}{\partial t} = \rho_f U_f \frac{\partial}{\partial w'} + \frac{dW}{dt'}\frac{\partial}{\partial w'} + \frac{\partial}{\partial t'} \qquad \text{(VII-30)} .$$

Now the retention and attenuation equations may be expressed in terms of the new independent variables, respectively, as

$$(1 - \epsilon)\frac{\partial C'}{\partial t'} + (1 - \epsilon)\frac{dW}{dt'}\frac{\partial C'}{\partial w'} = K|U_r|C \qquad \text{(VII-31)}$$

and

$$\epsilon \frac{\partial C}{\partial t'} - \left[\rho_f (1 - \epsilon) U_r - \epsilon \frac{dW}{dt'}\right]\frac{\partial C}{\partial w'} = -K|U_r|C \qquad \text{(VII-32)} .$$

Under the previous prescribed conditions of slow filtration of a dilute suspension, the mat could be considered to be in successive equilibrium states, and the transition of particles from the free to bound state would be nearly independent of time at the same relative position of the growing mat. Thus, Equations (VII-31) and (VII-32) are simplified, respectively, to

$$\frac{\partial C'}{\partial w'} = - \frac{KUC}{(1 - \epsilon)(dW/dt')} \qquad \text{(VII-33)}$$

and

$$\frac{\partial C}{\partial w'} = - \frac{KUC}{\rho_f(1 - \epsilon)U - \epsilon(dW/dt')} \qquad \text{(VII-34)} .$$

The rate of accumulation of fibers in the mat for constant-rate filtration may be calculated by a fiber balance:

$$\frac{dW}{dt'} = - \frac{1 - \epsilon_s}{\epsilon_s} \rho_f U \qquad \text{(VII-35)} .$$

For a dilute suspension its magnitude is negligible compared with $\rho_f(1 - \epsilon)U$ in Equation (VII-34). Substituting the definition of K, which is $E(1 - \epsilon)A_f/V_f$, into the same equation, we obtain

$$\frac{\partial C}{\partial w'} = - \frac{A_f E C}{V_f \rho_f} \qquad \text{(VII-36)} .$$

Upon integration at constant time and collection efficiency, the result is

$$C = C_s \exp(- \frac{A_f E}{V_f \rho_f} w') \qquad \text{(VII-37)} .$$

Utilizing this result, Equation (VII-33) becomes

$$\frac{\partial C'}{\partial w'} = - \frac{A_f E \epsilon_s C_s}{V_f \rho_f (1 - \epsilon_s)} \exp(- \frac{A_f E}{V_f \rho_f} w') \qquad \text{(VII-38)} ,$$

so that upon integration again, we arrive at the solution:

$$C' = C'_s + \frac{\epsilon_s C_s}{1 - \epsilon_s} \left[1 - \exp\left(- \frac{A_f E}{V_f \rho_f} w'\right)\right] \qquad \text{(VII-39)} .$$

By converting the concentrations to mass ratios and $\underline{w}'$ to $\underline{w}$, the final solution becomes

$$\frac{m' - m'_s}{m_s} = 1 - \exp\left[- \frac{KW}{\rho_f (1 - \epsilon)} \left(1 - \frac{w}{W}\right)\right] \qquad \text{(VII-23)} ,$$

which turns out to be exactly the same as the incompressible case after all the involved mathematical manipulations. The reason for this result is implicit in the assumption of quasi equilibrium in slow filtration.

VIII. THEORETICAL TREATMENT OF FIBER RETENTION

The retention of fibers on a screen is treated statistically with the aid of the probability theory. This analysis was initiated by Estridge (III-11) and further developed by Nelson (II-1) and Abrams (VIII-1). At present only the idealized initial retention can be predicted. However, on the basis of the theory, the subsequent retention may be at least rationally described.

RETENTION PROBABILITY

Consider a suspension containing j types of fibers approaching a screen in the x-y plane. If the concentration of the ith-type fibers is C_i, expressed in the number of fiber centers per unit volume of the suspension, and the probability that this type of fibers will be retained is P_i, expressed as the number of fibers of the ith type retained to the total number of fibers originally in the suspension (provided that the total number is very large), then the number of the ith-type fibers dN_i removed from a volume dV_s, which reach the plane of the screen with a velocity $|u|$ in time dt is

$$\frac{dN_i}{dt} = \iint C_i P_i |u| dxdy \qquad \text{(VIII-1)} .$$

The total number of fibers retained is obtained by summing all types of fibers:

$$\frac{dN_t}{dt} = \Sigma \iint C_i P_i |u| dxdy \qquad \text{(VIII-2)} .$$

For convenience we define an average of $C_i P_i$ as

$$\overline{C_i P_i} = \frac{\iint C_i P_i u dxdy}{\iint u dxdy} \qquad \text{(VIII-3)} .$$

Since the denominator is simply the volumetric flow rate $d\underline{V}_s/d\underline{t}$, Equation (VIII-3) may be simply written as

$$\frac{dN_t}{dV_s} = \Sigma\overline{C_i P_i} \qquad \text{(VIII-4)} ,$$

provided $|\underline{u}|$ is independent of $\underline{x}$ and $\underline{y}$.

If $\underline{C}_i$ is not dependent on $\underline{x}$ and $\underline{y}$, the average of the product, $\overline{\underline{C}_i\underline{P}_i}$, will be the same as the product of $\overline{\underline{C}}_i$ and $\overline{\underline{P}}_i$. The subsequent development is then largely a matter of evaluating $\overline{\underline{P}}_i$.

INITIAL RETENTION

The initial retention of a fiber is dependent on (1) the position and orientation of the fiber at its close approach to the screen, (2) the dimensions, shape, rigidity, and surface characteristics of the fiber, (3) the geometry of the screen and the surface characteristics of the wires, (4) the hydrodynamic conditions near the screen, and (5) the interference and interaction of the neighboring fibers. It is not possible to account for all these factors in a quantitative manner; only the idealized case can be rigorously dealt with. In his pioneering work Estridge made the analysis of initial retention from a dilute uniform suspension of rigid cylindrical fibers flowing perpendicular to a screen constructed of very thin parallel and cross wires in a uniform arrangement.

Let the spacing between repeating parallel wires be $\underline{d}_o$ and that between cross wires be $\underline{d}_o'$, constituting a screen of rectangular meshes. The two extreme cases will be $\underline{d}_o'/\underline{d}_o = \infty$ for parallel wires and $\underline{d}_o'/\underline{d}_o = 1$ for square meshes. Now consider a suspension of fibers, differing only in their lengths, approaching a screen. For rectangular meshes the repeating geometric element is a right

triangle of two sides $d_o/2$ and $d_o'/2$. The average retention probability needs only to cover this elementary area:

$$\bar{P}_i = \frac{8}{d_o d_o'} \int_0^{d_o/2} \int_0^{d_o'/2} P_i dxdy \qquad \text{(VIII-5)} .$$

With all the preceding simplifications the probability function P_i is dependent only on the orientation of fibers, the length of fibers, the spacings of the wires, and the friction between the fibers and the wires.

When a fiber of length L_f approaches the screen at a certain orientation and strikes one wire, the fiber will be retained if it bridges across a second wire. By analyzing all the different combinations of the fiber-wire geometry, P_i may be evaluated as a function of the position x-y . The average probability $\bar{P}_i$ is then arrived at by evaluating the integrals of Equation (VIII-5). Upon repeating the analysis for various fiber lengths, $\bar{P}_i$ is derived as a function of L_f for a given screen. For different spacings the results may be related to d_o/L_f with the parameter d_o'/d_o . By this method of analysis Estridge derived the initial retention probabilities for the two extreme cases of parallel wires and square meshes.

Later, Nelson employed the Monte-Carlo method for evaluation of the initial retention probabilities on a digital computer. His method is based on the use of random numbers for the orientation of a fiber and the x and y co-ordinates of its center with respect to the wire spacings. By a large number of trials (10^4) moderate accuracy is easily achieved, but more precise results require a rapidly increasing volume of calculation. Nelson's results are shown in Fig. VIII-1, which are in agreement with Estridge's for the condition of little friction between fiber and wire.

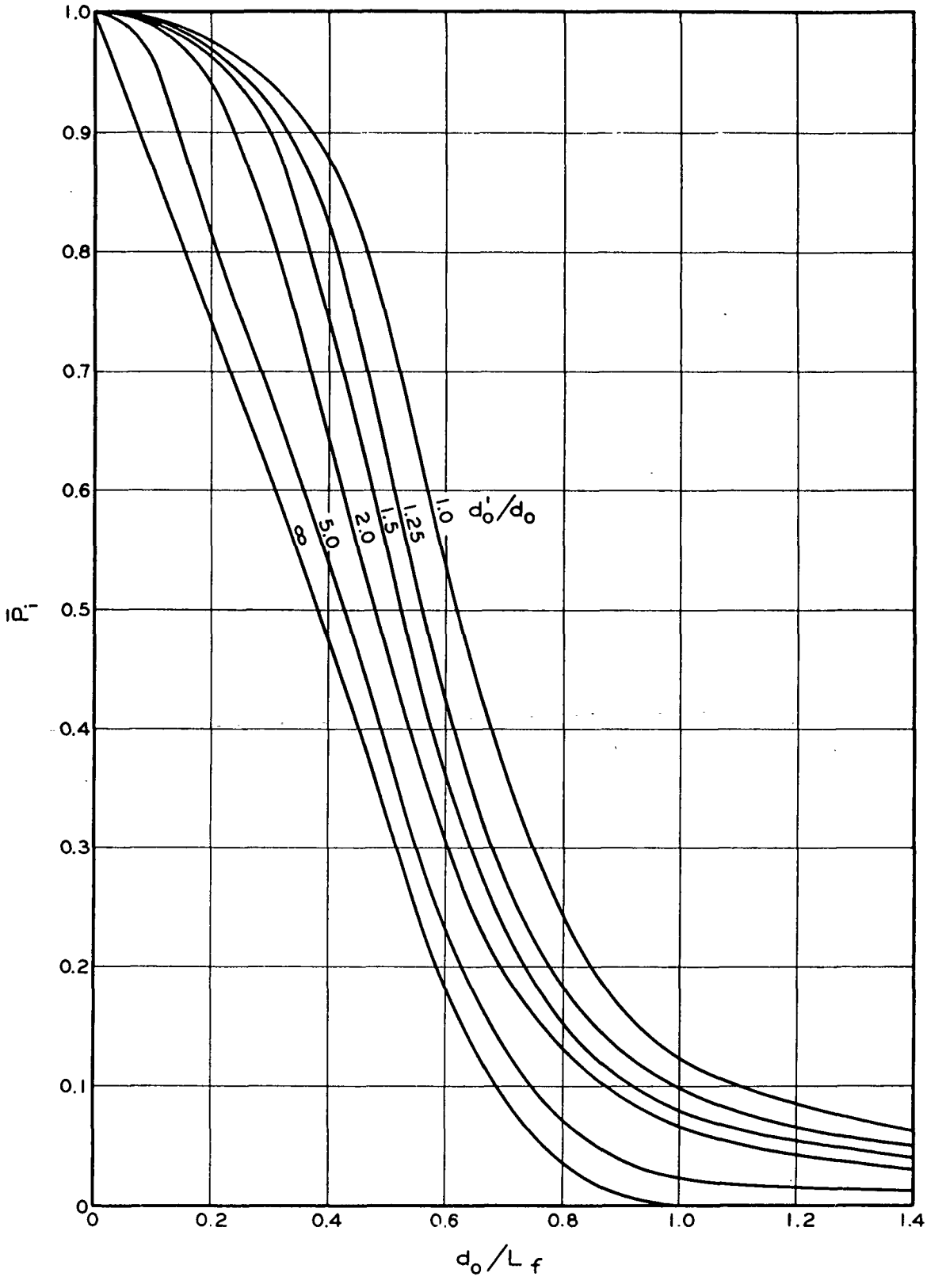

Figure VIII-1. Initial Fiber Retention Probabilities

Nelson and Abrams then developed the scanning line method predicated on the frequency function of the lengths of segments of scanning lines, falling within unobstructed areas in the plane of a screen. The results of initial retention calculated by this method again agree with those of the previous two methods.

SUBSEQUENT RETENTION

It is usually more convenient to deal with the mass rather than the number of fibers. The mass fraction of retention, which may be called retention efficiency, is related to the retention probability $\bar{P}_i$ by

$$\frac{dW}{dW_s} = \frac{1}{s} \Sigma s_i \bar{P}_i \qquad \text{(VIII-6)} ,$$

where s_i is the consistency of the ith-type fibers in the suspension.

A retention curve of W vs. W_s will have the slope at the origin, with a finite value of R_0 for initial retention, and end with a unity slope for complete retention. The intercept of the unity slope with the W_s axis at $W = 0$ gives the total loss of fibers through the screen.

The build-up of a fiber mat is much more difficult to treat theoretically. An analysis of subsequent retention would require a knowledge of how the geometry of the openings changes with the deposition of fibers and how this change affects the retention probability. At present the scanning line method offers some promise of dealing with this problem.

In the scanning line method the network dimensions may be specified by one angle and two distances (Fig. VIII-2), the angle being φ measured from the x axis, and the distance being L_1 and L_2 measured from the point x_c-y_c to

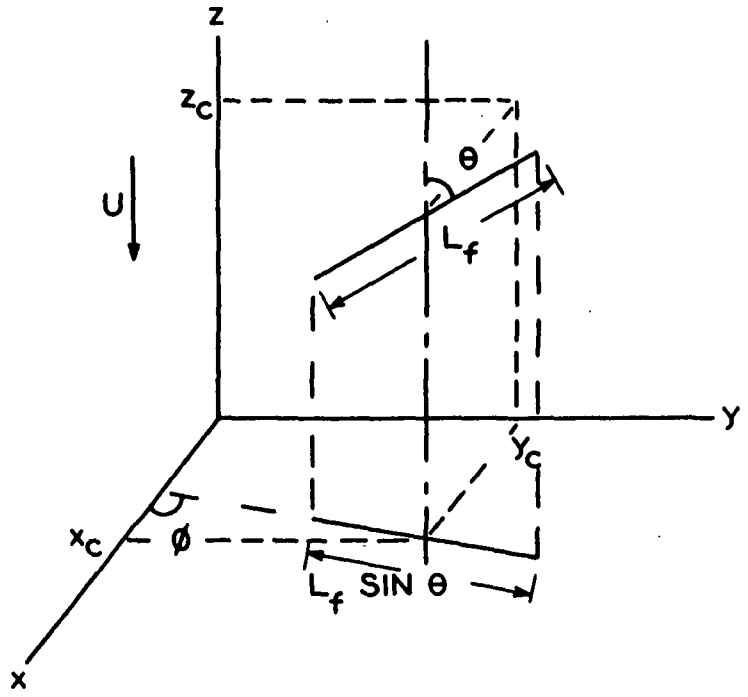

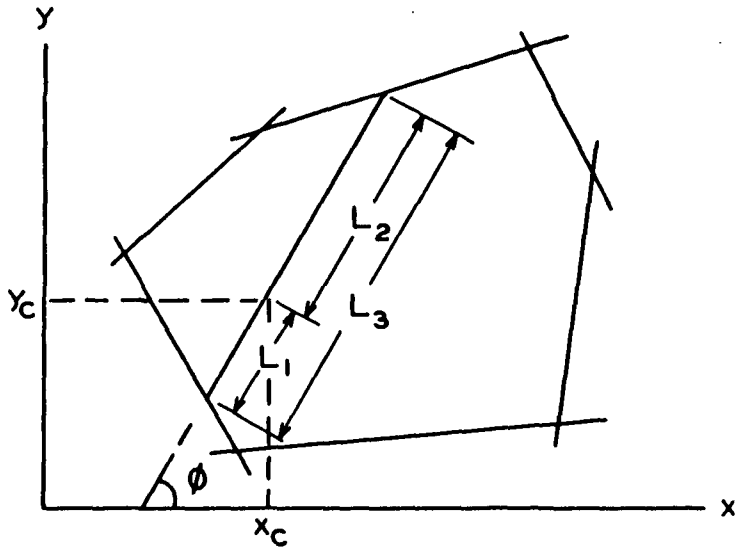

Figure VIII-2. Fiber Co-ordinates (top) and Network Dimensions (bottom)

the first crossing of a member of the network in the $\varphi + \pi$ and φ directions, respectively. The probability of retention can then be expressed as some complex relationship between the frequency distribution functions for $\underline{L}_3$ $(= \underline{L}_1 + \underline{L}_2)$, $\underline{L}_1$, and θ.

For negligible fiber-element friction the probability of retention for randomly oriented straight rigid fibers is given by

$$\bar{P}_i = \frac{1}{\bar{L}_3 L_f}\left\{\int_0^{L_f/2} f(L_3)\left[L_3\left(\frac{L_f^2}{4} - L_3^2\right)^{1/2} + \frac{L_f^2}{4}\arctan\frac{L_3}{(L_f^2/4 - L_3^2)^{1/2}}\right]dL_3\right.$$

$$\left. + \int_{L_f/2}^{L_f} f(L_3)\left[\frac{\pi L_f^2}{8} + \left(\frac{L_f}{2} - L_3\right)\left(L_3 L_f - L_3^2\right)^{1/2} + \frac{L_f^2}{4}\arctan\frac{L_f/2 - L_3}{(L_3 L_f - L_3^2)^{1/2}}\right]dL_3\right\}$$

(VIII-7).

The frequency function $f(\underline{L}_3)$ has been evaluated for networks composed of uniform rectangular openings:

for $0 \le L_3 \le d_o$, $\qquad f(L_3) = \frac{1}{d_o + d_o'}$ (VIII-8),

for $d_o \le L_3 \le d_o'$, $\qquad f(L_3) = \frac{d_o^2 d_o'}{(d_o + d_o')L_3^2(L_3^2 - d_o^2)^{1/2}}$ (VIII-9),

and for $d_o' \le L_3 \le (d_o^2 + d_o'^2)^{1/2}$,

$$f(L_3) = \frac{d_o^2 d_o'}{(d_o + d_o')L_3^2(L_3^2 - d_o^2)^{1/2}} + \frac{d_o d_o'^2}{(d_o + d_o')L_3^2(L_3^2 - d_o'^2)^{1/2}} - \frac{1}{d_o + d_o'}$$

(VIII-10).

Finally, for a network composed of randomly oriented fibers,

$$f(L_3) = (1/\bar{L}_3) \exp(-L_3/\bar{L}_3) \qquad \text{(VIII-11)} .$$

With these frequency functions Equation (VIII-7) may be integrated to yield the retention probabilities. The results of Abrams' calculations are shown in Fig. VIII-3..

RETENTION EXPRESSIONS

By the random network model the retention curve may be closely described by

$$\frac{dW}{dW_s} = 1 - (1 - R_0) \exp(-\alpha_0 L_f/\bar{L}_3) \qquad \text{(VIII-12)} ,$$

where α_0 has a theoretical value of 0.31, according to Abrams. From statistical considerations, the average network distance $\bar{L}_3$ is related to the mass of fibers retained by

$$\bar{L}_3 = \frac{\pi w_f}{2L_f W} \qquad \text{(VIII-13)} ,$$

where w_f is the mass per fiber. Integration of the combination of Equations (VIII-12) and (VIII-13) results in Estridge's expression:

$$W_s - W = \frac{1}{k_0} \ln \frac{1 - (1 - R_0) \exp(-k_0 W)}{R_0} \qquad \text{(III-13)} ,$$

with the additional implication:

$$k_0 = \alpha_0 \frac{2L_f^2}{\pi w_f} \qquad \text{(VIII-14)} .$$

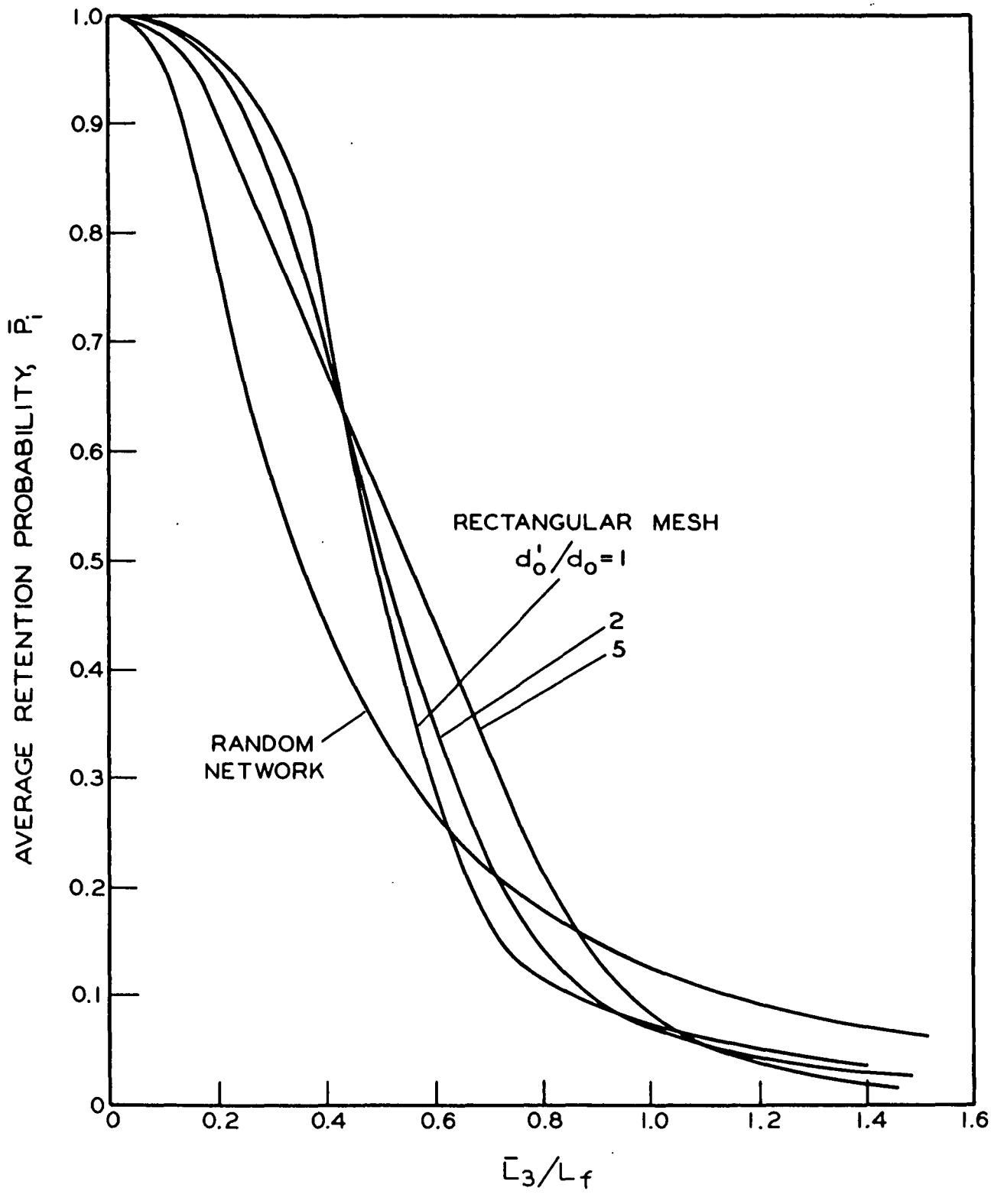

Figure VIII-4. Fiber Retention Probability for Random Network

By differentiating the fiber retention equation (III-13), we return to

$$\frac{dW}{dW_s} = 1 - (1 - R_o) \exp(-k_o W) \qquad \text{(VIII-15)} .$$

If the filtrate and suspension densities are nearly the same,

$$\frac{dW}{dW_s} = \frac{s - s_o}{s_o} \qquad \text{(VIII-16)} .$$

Combining with the previous equation, the result is Han's filtrate consistency expression:

$$s_o = s(1 - R_o) \exp(-k_o W) \qquad \text{(III-14)} .$$

IX. INTEGRATED SOLUTIONS FOR SIMPLE FILTRATIONS

In the elementary analysis of filtration, it is assumed that the presence of a screen would not affect the process in any way. The screen would offer no resistance to the flow of water and would retain the fibers completely. Furthermore, the fiber suspension is supposed to be well dispersed and the mat formed to be uniform in the x-y plane. The fibers are identical in their essential characteristics and constant in density.

If the suspension is dilute, the relative velocity is practically the same as the filtrate velocity. If the flow is slow, the fluid inertial effects may be ignored. The gravitational effect on the piezometric head is generally negligible. Under these simplifications the filtration process can be treated adequately by Darcy's law with the aid of the compressibility and porosity functions, as shown by Ingmanson (IX-1) and Whitney, Ingmanson, and Han (IX-2).

The somewhat more complicated cases of constant-pressure filtrations in rapid flow and with incomplete fiber retention have also been developed by Han and Ingmanson (IX-3).

FIBER BALANCE

The mass of fibers in the formed mat is directly proportional to the volume of the suspension. For unit area,

$$W = W_s = s\rho_s V_s \qquad \text{(IX-1)},$$

and the mass of the wet mat is the difference between the suspension and the filtrate,

$$\bar{m}W = \rho_s V_s - \rho V_0 \qquad \text{(IX-2)},$$

where $\underline{\bar{m}}$ is the average mat moisture expressed as the mass ratio of the wet to dry mat. Eliminating $\rho_{\underline{s}}\underline{V_s}$, we obtain, by virtue of a fiber balance,

$$W = \frac{s\rho V_0}{1 - s\bar{m}} \qquad \text{(IX-3)} .$$

SLOW DRAINAGE

When the flow is slow and practically constant through the mat, Darcy's law may be expressed in the form:

$$-U_0 = \frac{dV_0}{dt} = \frac{1}{a}\frac{dp}{dz} \qquad \text{(IX-4)} .$$

In early treatment of the subject, the specific filtration resistance $\underline{R}$ was introduced as

$$a = R\mu c \qquad \text{(IX-5)} ,$$

in order to put the resistance $\underline{R}$ on the basis of fiber mass. Its dimensions are length per unit mass.

Since by definition the local mat density is

$$c = \rho_f(1 - \varepsilon) = \frac{dw}{dz} \qquad \text{(IX-6)} ,$$

the Darcy equation is transformed, in terms of the readily measurable variables, to

$$\frac{dV_0}{dt} = \frac{1}{R\mu}\frac{dp}{dw} \qquad \text{(IX-7)} .$$

At any instant this simple filtration equation may be integrated at constant temperature to give

$$\int_{p_0}^{p_L} \frac{1}{R}\, dp = \frac{|\Delta p|}{\bar{R}} \qquad \text{(IX-8)},$$

where $\bar{R}$ is the average specific filtration resistance of the mat at $|\Delta p|$.

AVERAGE RESISTANCE

The integral in Equation (IX-8) may be evaluated with a compressibility function. Using the simple form (III-10) and the known viscous resistance from (V-13),

$$R = k_1 (S_v^2/\rho_f)(M p_f^N/\rho_f)^{1/2} [1 + k_2 (M p_f^N/\rho_f)^3] \qquad \text{(IX-9)}.$$

It will be shown later that for porosities larger than 0.9, the term containing k_2 is negligible compared with unity. Then, by the pressure relationship (II-11),

$$\int_{p_0}^{p_L} \frac{1}{R}\, dp = \frac{\rho_f^{3/2}}{k_1 S_v^2 M^{1/2}} \int_{p_{f,L}}^{p_{f,0}} p_f^{-N/2}\, dp_f \qquad \text{(IX-10)}.$$

The difference between Equations (II-12) and (II-13) yields

$$p_{f,L} - p_{f,0} = p_0 - p_L \qquad \text{(IX-11)}.$$

If we assume that at the mat-suspension boundary the mat density is practically zero, then the two limits are $p_{f,L} = 0$ and $p_{f,0} = p_L - p_0$. Hence the value of the integral is

$$\frac{\rho_f^{3/2} |\Delta p|^{1-N/2}}{k_1 S_v^2 M^{1/2} (1 - N/2)} .$$

From Equation (IX-8) we find

$$\bar{R} = k_1 (S_v^2/\rho_f^{3/2})(1 - N/2)(M|\Delta p|^N)^{1/2} \qquad \text{(IX-12)} .$$

For the sake of convenience, we define an average porosity $\bar{\epsilon}$ so that the average filtration resistance $\underline{\bar{R}}$ will yield the same flow as demanded by the integration of Equation (IX-7),

$$\bar{\epsilon} = 1 - (1 - N/2)^2 (M|\Delta p|^N/\rho_f) \qquad \text{(IX-13)} .$$

Hence,

$$\bar{R} = k_1 (S_v^2/\rho_f)(1 - \bar{\epsilon})^{1/2} \qquad \text{(IX-14)} .$$

For porosities less than 0.7, the Kozeny factor $\underline{k}$, or its equivalent α', in the viscous resistance $\underline{a}$ is nearly constant, so that

$$R = \frac{\alpha' S_v^2 (1 - \epsilon)^2}{\epsilon^3 M p_f^N} \qquad \text{(IX-15)} .$$

An average porosity may then be similarly derived to be

$$\bar{\epsilon} = 1 - (1 - N)(M|\Delta p|^N/\rho_f) \qquad \text{(IX-16)} .$$

The difference between the two average porosities is quite small because

$$(1 - N/2)^2 = 1 - N + N^2/4 \cong 1 - N \qquad \text{(IX-17)} ,$$

provided $\underline{N}$ is a small fraction. For example, when $\underline{N} = 0.3$, the discrepancy amounts to only 3%. If we choose the first definition, the average filtration resistance may be generalized to cover the range of porosities for which the Davis porosity function holds:

$$\bar{R} = k_1 (S_v^2/\rho_f)(1 - \bar{\epsilon})^{1/2}[1 + k_2(1 - \bar{\epsilon})^3] \qquad \text{(IX-18)} .$$

In constant-pressure filtrations the pressure drop across a mat is fixed, and consequently the flow decreases as the mat grows at constant moisture $\bar{m}$. Combining the fiber balance and the filtration equation, we have

$$V_0 dV_0 = \frac{(1 - s\bar{m})|\Delta p|}{s\rho\mu\bar{R}} dt \qquad \text{(IX-19)} .$$

Integrating at constant $\underline{s}$, the filtrate volume is

$$V_0 = \left[\frac{2(1 - s\bar{m})|\Delta p| t}{s\rho\mu\bar{R}}\right]^{1/2} \qquad \text{(IX-20)}$$

or

$$t = \frac{\mu\bar{R}(1 - s\bar{m})W^2}{2s\rho|\Delta p|} \qquad \text{(IX-21)} ,$$

which is the well-known parabolic law of constant-pressure filtration.

In constant-rate filtration the flow is fixed. Therefore, the pressure drop rises as the filtration proceeds. Since the basis weight is directly proportional to the filtration time, the resulting solution for constant-rate filtration is

$$t = \frac{(1 - s\bar{m})|\Delta p|}{s\rho\mu\bar{R}U_0^2} \qquad \text{(IX-22)} .$$

RAPID DRAINAGE

From the previous discussion of flow resistances, it is reasonable to expect that the permeation expression for transition flow will hold at any instant during simple filtrations:

$$\frac{|\Delta p|}{W} = \frac{\overline{\alpha'}(1 - \bar{\epsilon})(S_v^2 \mu/\rho_f)}{\bar{\epsilon}^3} |U_0| + \frac{b'\sqrt{\overline{\alpha'}}\,(S_v \rho/\rho_f)}{\bar{\epsilon}^3} U_0^2 \qquad \text{(IX-23)},$$

in which

$$\overline{\alpha'} = \bar{k} = k_1 \frac{\bar{\epsilon}^3}{(1 - \bar{\epsilon})^{1/2}} [1 + k_2 (1 - \bar{\epsilon})^3] \qquad \text{(IX-24)}.$$

The same expression may also be presented in the dimensionless form:

$$\overline{f'} = \frac{1}{\overline{Re'}} + b' \qquad \text{(IX-25)},$$

where

$$\overline{f'} = \frac{\bar{\epsilon}^3 |\Delta p| \rho_f}{\sqrt{\overline{\alpha'}}\, S_v \rho\, U_0^2\, W} \qquad \text{(IX-26)}$$

and

$$\overline{Re'} = \frac{\rho |U_0|}{\sqrt{\overline{\alpha'}}\,(1 - \bar{\epsilon}) S_v \mu} \qquad \text{(IX-27)}.$$

Because of the presence of the quadratic velocity term, the use of the average filtration resistance $\bar{R}$ becomes impractical, and instead, a filtration parameter will be introduced in the following treatment of simple filtration in transition flow.

Differentiating the fiber balance (IX-3) with respect to t, we obtain

$$|U_0| = \frac{dV_0}{dt} = \frac{1 - s\bar{m}}{s\rho} \frac{dW}{dt} \qquad \text{(IX-28)} .$$

Substituting this into Equation (IX-23), the result is

$$(\frac{dW^*}{dt})^2 + \frac{dW^*}{dt} - \frac{K^*}{W^*} = 0 \qquad \text{(IX-29)} ,$$

where

$$W^* = \frac{b'(1 - s\bar{m})W}{\sqrt{\overline{\alpha'}\,(1 - \bar{\epsilon})sS_v\mu}} \qquad \text{(IX-30)}$$

and

$$K^* = \frac{b'^2\bar{\epsilon}^3(1 - s\bar{m})\rho|\Delta p|}{\overline{\alpha'^2}(1 - \bar{\epsilon})^3 sS_v^4\mu^3/\rho_f} \qquad \text{(IX-31)} .$$

The solution at constant pressure with the new variable and parameter is

$$t = 2K^*\left[\frac{1}{\sqrt{1 + 4K^*/W^*} + 1} + \frac{1}{(\sqrt{1 + 4K^*/W^*} - 1)^2}\right.$$

$$\left. - \frac{1}{2} \ln \frac{\sqrt{1 + 4K^*/W^*} + 1}{\sqrt{1 + 4K^*/W^*} - 1}\right] \qquad \text{(IX-32)} .$$

For small values of K^* and large values of t the flow will be in Darcy's region, and the solution reduces to the parabolic law:

$$t = \frac{W^{*2}}{2K^*} \qquad \text{(IX-33)} .$$

In the other extreme for large values of K^* and small values of t, the viscous effect becomes negligible. The solution then assumes the form:

$$t = \frac{2}{3} \frac{W^{*3/2}}{K^{*1/2}} \qquad \text{(IX-34)} .$$

Figure IX-1 shows these relationships for $\underline{K}^* = 10^{-2}$ sec.

INCOMPLETE RETENTION

In the case of some fiber losses, the fiber balance calls for

$$W = s\rho_s V_s - \bar{s}_0 \rho V_0 \qquad \text{(IX-35)} .$$

Combining with Equation (IX-2), we obtain

$$W = \frac{(s - \bar{s}_0)\rho V_0}{1 - s\bar{m}} \qquad \text{(IX-36)} .$$

This equation may be differentiated at constant pressure to give

$$(1 - s\bar{m})dW = s\rho dV_0 - \rho d(\bar{s}_0 V_0) \qquad \text{(IX-37)} .$$

By definition,

$$\bar{s}_0 = \frac{1}{V_0} \int_0^{V_0} s_0 dV_0 \qquad \text{(IX-38)} ;$$

hence,

$$d(\bar{s}_0 V_0) = s_0 dV_0 \qquad \text{(IX-39)} .$$

The filtrate consistency expression has been introduced to be

$$s_0 = s(1 - R_0)e^{-k_0 W} = s'e^{-k_0 W} \qquad \text{(IX-40)} .$$

Combining Equations (IX-37), (IX-39), and (IX-40), we arrive at

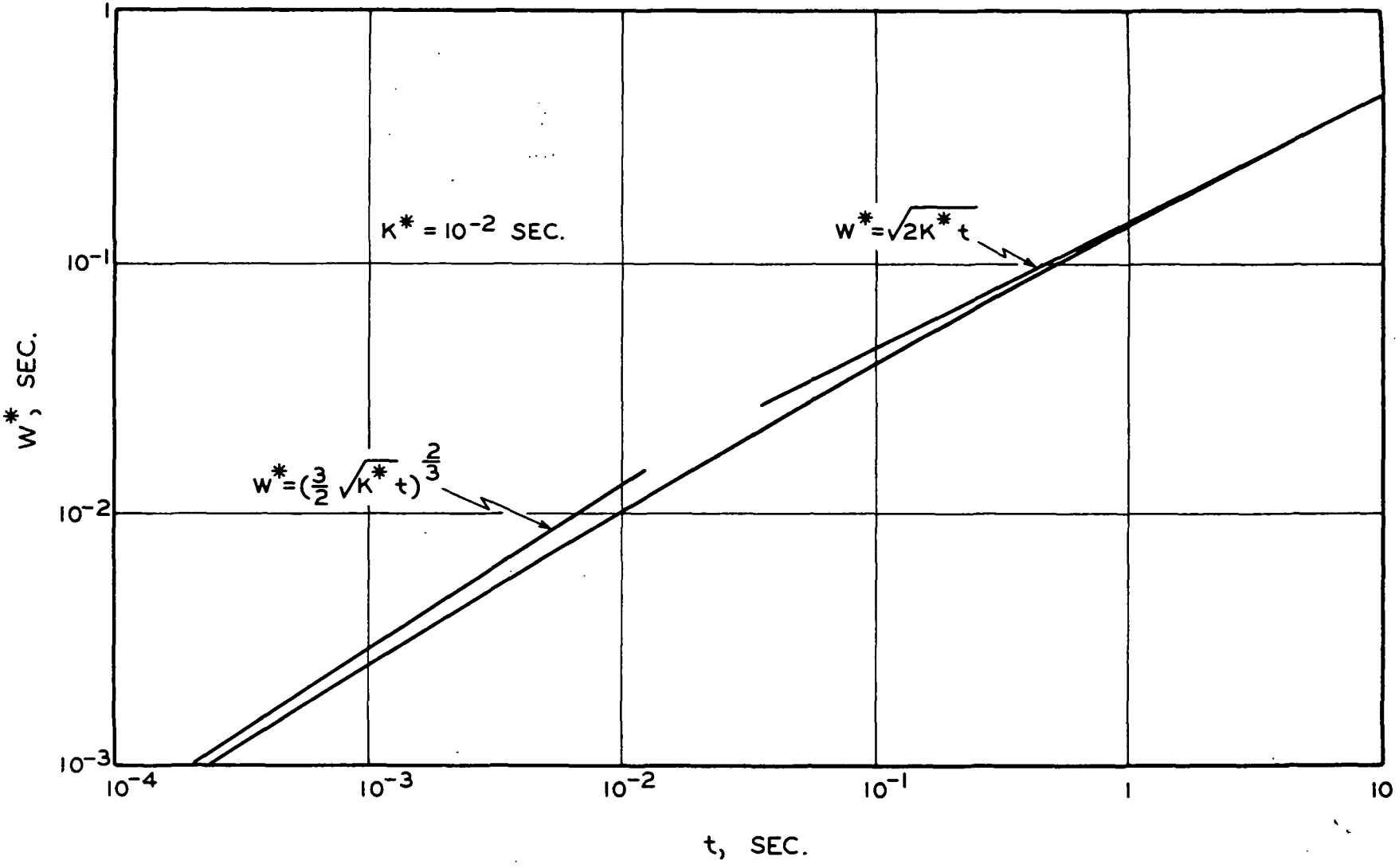

Figure IX-1. Constant-Pressure Filtration in Transition Flow

$$(1 - s\bar{m})dW = (s - s'e^{-k_o W})\rho dV_o \qquad \text{(IX-41)}\ .$$

Substituting this into Equation (IX-7) for slow filtration at constant pressure, utilizing Equation (IX-8), and arranging the result to a dimensionless form, we find

$$\frac{(k_o W)d(k_o W)}{1 - (s'/s)\exp(-k_o W)} = \frac{k_o^2 s\rho|\Delta p|dt}{\mu\bar{R}(1 - s\bar{m})} \qquad \text{(IX-42)}\ .$$

Let

$$W^o = k_o W \qquad \text{(IX-43)}$$

and

$$t^o = \frac{k_o^2 s\rho|\Delta p|t}{\mu\bar{R}(1 - s\bar{m})} \qquad \text{(IX-44)}\ ;$$

Equation (IX-42) is simplified to

$$\frac{W^o}{1 - (s'/s)\exp(-W^o)}\, dW^o = dt^o \qquad \text{(IX-45)}\ .$$

This equation has been solved numerically on a computer to yield $\underline{W^o}$ as functions of $\underline{t^o}$ with the parameter $\underline{s'/s}$. The results of evaluation are presented in Fig. IX-2.

At complete fiber retention the function reduces to the parabolic law:

$$t^o \approx \frac{1}{2}(W^o)^2 \qquad \text{(IX-46)}\ .$$

When there is some fiber loss, deviation from the parabolic law is significant only in early times of filtration, and diminishes rather rapidly, as filtration proceeds, by virtue of the exponential nature of the filtrate consistency

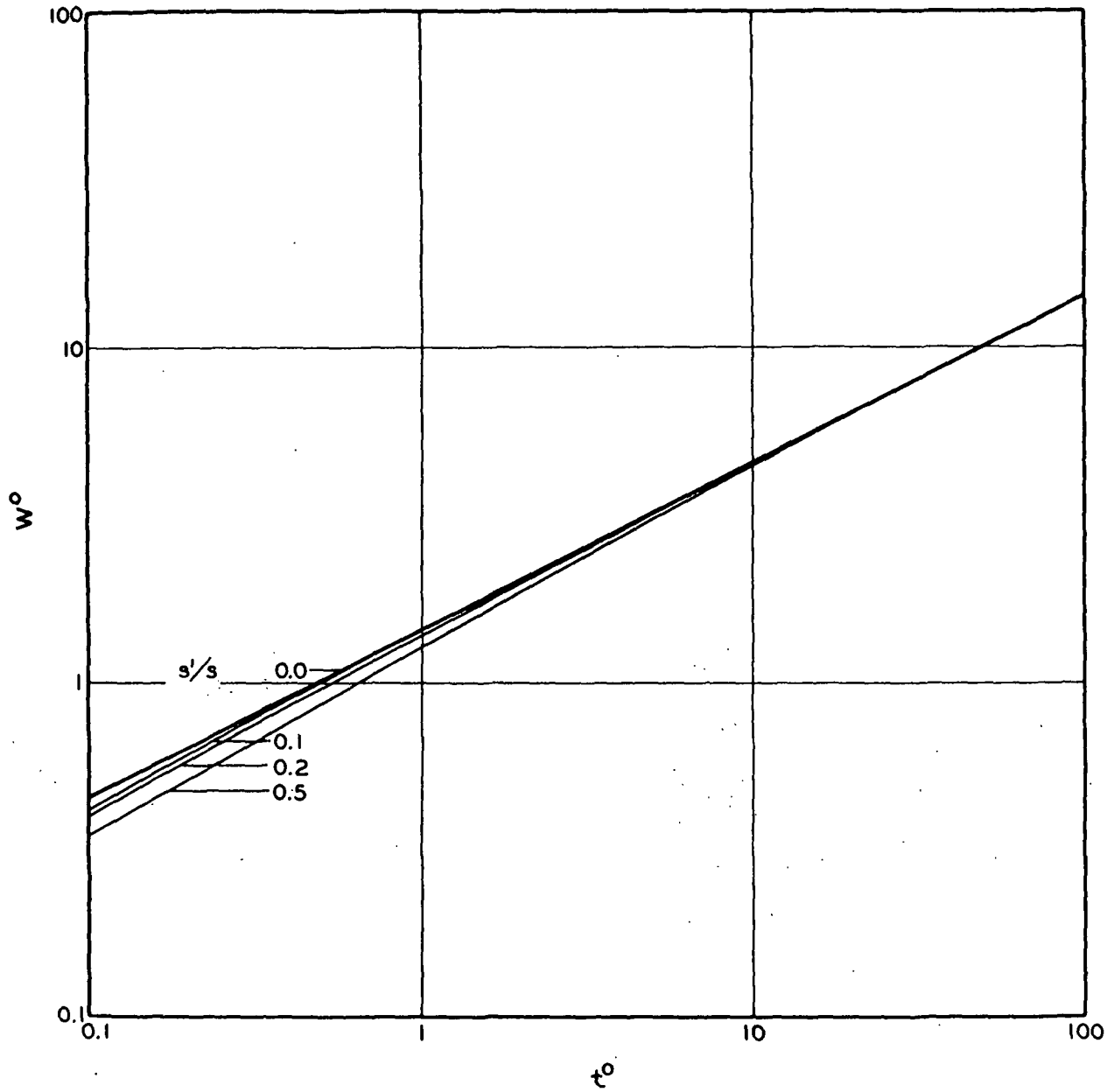

Figure IX-2. Effect of Fiber Loss on Constant-Pressure Filtration

$$\rho_f(1 - \epsilon) \frac{\partial p_f}{\partial z} = c \frac{\partial p_f}{\partial z} = \frac{\gamma}{M_o} c^\gamma \frac{\partial c}{\partial z} \qquad (X\text{-}4) .$$

Equation (X-3) is thereby transformed into

$$\frac{\partial c}{\partial t} + U_o \frac{\partial c}{\partial z} - \frac{\gamma}{M_o} \frac{\partial}{\partial z} \left(\frac{c^\gamma}{a} \frac{\partial c}{\partial z}\right) = 0 \qquad (X\text{-}5) ,$$

in which the constant ρ_f is cancelled out.

The mat-suspension boundary, $z = L(t)$, may be calculated by a fiber balance:

$$-s\rho_s U_s = -c_o U_o = \frac{d}{dt} \int_o^{L(t)} (c - c_o) dz \qquad (X\text{-}6) ,$$

where the mat density c_o at the boundary is assumed to be equal to the consistency of the suspension, which is taken to be constant. This condition is satisfied if the suspension or slurry is kept in a state of uniform dispersion. It is advantageous to treat the upper boundary as stationary by introducing a new independent variable $\eta = z/L$, so that

$$\frac{\partial}{\partial z} = \frac{1}{L} \frac{\partial}{\partial \eta} , \quad \frac{\partial}{\partial t} = \frac{\partial}{\partial t} - \frac{\eta}{L} \frac{dL}{dt} \frac{\partial}{\partial \eta} \qquad (X\text{-}7) .$$

The filtration equation (X-5) and the fiber balance (X-6) become, respectively, with the new variable

$$\frac{\partial c}{\partial t} + \frac{1}{L} \left(U_o - \frac{dL}{dt} \eta\right) \frac{\partial c}{\partial \eta} - \frac{\gamma}{M_o L^2} \frac{\partial}{\partial \eta} \left(\frac{c^\gamma}{a} \frac{\partial c}{\partial \eta}\right) = 0 \qquad (X\text{-}8)$$

and

$$-c_o U_o = \frac{d}{dt} \left[L \int_o^1 (c - c_o) d\eta\right] \qquad (X\text{-}9) ,$$

where the filtrate velocity is now expressed as

$$U_o = \frac{\gamma}{M_o L}\left(\frac{c^{\gamma-1}}{a}\frac{\partial c}{\partial \eta}\right)_{\eta=0} \qquad \text{(X-10)} .$$

CONSTANT PRESSURE

In the case of a constant-pressure filtration, we proceed to convert the partial differential equation (X-8) to an ordinary differential equation by introducing

$$c(\eta,t) = c^*(\eta^*) , \quad \eta^* = \eta_o^*\eta \qquad \text{(X-11)} ,$$

with η_o^* as a constant parameter. Noting that $\partial c/\partial t = 0$ in this case and letting

$$L = \eta_o^*\left(\frac{2\gamma t}{M_o}\right)^{1/2} \qquad \text{(X-12)} ,$$

Equation (X-8) now assumes the form:

$$\frac{d}{d\eta^*}\left(\frac{c^{*\gamma}}{a}\frac{dc^*}{d\eta^*}\right) + (\eta^* - I_o)\frac{dc^*}{d\eta^*} = 0 \qquad \text{(X-13)} .$$

Also, Equations (X-9) and (X-10) become, respectively,

$$-c_o^* I_o = \int_o^{\eta_o^*} (c^* - c_o^*)d\eta^* \qquad \text{(X-14)}$$

and

$$U_o = \left(\frac{\gamma}{2M_o t}\right)^{1/2} I_o \qquad \text{(X-15)} ,$$

with $$I_o = \left(\frac{c^{*(\gamma-1)}}{a}\frac{dc^*}{d\eta^*}\right)_{\eta^*=0} = \text{constant} \qquad (X\text{-}16)\ .$$

For a given constant pressure drop across the mat during filtration, the mat density at the screen is known from the compressibility function and the mat resistance by the viscous resistance formula. Therefore, Equation (X-13) may be solved numerically. However, if we make use of Emmons' (X-2) approximation:

$$a = a'c^{\gamma} = a'c^{*\gamma} \qquad (X\text{-}17)\ ,$$

where a' is a constant; putting

$$L = \eta_0^*\left(\frac{2\gamma t}{a'M_0}\right)^{1/2} \qquad (X\text{-}18)\ ,$$

Equation (X-13) is simplified to

$$\frac{d^2c^*}{d\eta^{*2}} + (\eta^* - I^*)\frac{dc^*}{d\eta^*} = 0 \qquad (X\text{-}19)\ ,$$

where $$I^* = \left(\frac{1}{c^*}\frac{dc^*}{d\eta^*}\right)_{\eta^*=0} \qquad (X\text{-}20)\ .$$

Equations (X-14) and (X-15) remain the same except that I_o is replaced by I^*. Equation (X-19) may be integrated to yield the mat density distribution:

$$c^*(\eta^*) = c^*_{\text{at } \eta^*=0}\left[1 + I^*\int_o^{\eta^*}\exp(I^*\eta^* - \eta^{*2}/2)d\eta^*\right] \qquad (X\text{-}21)\ .$$

Upon introducing the solution so obtained to (X-14) and (X-15), the resulting equations may be solved numerically for I^* and η_0^*.

CONSTANT RATE

A suitable transformation of the system of equations for constant-rate filtrations may be obtained by means of new variables:

$$c(\eta,t) = c_0 Y(\eta,t) ,$$

$$\tau = |U_0| t/L ,$$

and

$$L = \left(\frac{\gamma t}{a' M_0}\right)^{1/2} \qquad \text{(X-22)} .$$

The filtration equation and the fiber balance with the new variables are, respectively,

$$\frac{\partial^2 Y}{\partial \eta^2} + (\tau + \eta/2) \frac{\partial Y}{\partial \eta} - \frac{\tau}{2} \frac{\partial Y}{\partial \tau} = 0 \qquad \text{(X-23)}$$

and

$$-\left(\frac{\partial Y}{Y \partial \eta}\right)_{\eta=0} = \int_0^1 (Y - 1) d\eta \qquad \text{(X-24)} .$$

The initial and boundary conditions may be specified as

$$Y(\eta,0) = Y(1,\tau) = 1 \qquad \text{(X-25)} .$$

It can be shown that

$$Y(\eta,\tau) = 1 + \sum_{n=1}^{\infty} B_n(\eta) \tau^n \qquad \text{(X-26)} ,$$

where the coefficients B_n may be computed from

$$\frac{d^2 B_n}{d\eta^2} + \frac{\eta}{2}\frac{dB_n}{d\eta} - \frac{n}{2} B_n = -\frac{dB_{n-1}}{d\eta}, \quad n = 1,2,3,\ldots \qquad (X\text{-}27) .$$

The solutions must satisfy the condition

$$-\frac{dB_n}{d\eta} = B_n \int_0^1 B_n d\eta \quad \text{at} \quad \eta = 0 \qquad (X\text{-}28) ,$$

and so on until $\underline{B}_n(1) = 0$. For $\tau \ll 1$, the solution is

$$Y(\eta,\tau) \cong 1 + B_1(\eta)\tau ,$$

where $$B_1(\eta) = \{D_1[\exp(-\eta/2)^2 + (\sqrt{\pi}/2)\eta \overset{0}{\operatorname{erf}}(\eta/2)] - D_2^2\eta\}/(D_1 + D_2) ,$$

$$D_1 = \exp(-1/4) + (\sqrt{\pi}/2)\overset{0}{\operatorname{erf}}(1/2) ,$$

$$D_2 = \sqrt{\pi}\,[\overset{0}{\operatorname{erf}}(1/2) + \overset{1}{\operatorname{erf}}(1/2) - 2\overset{2}{\operatorname{erf}}(1/2)] ,$$

and $$\overset{n}{\operatorname{erf}}(x) = \int_0^x \overset{n-1}{\operatorname{erf}}(x)dx , \quad n = 1,2,3,\ldots, \quad \overset{0}{\operatorname{erf}}(x) = \operatorname{erf}(x) \qquad (X\text{-}29) .$$

Equation (X-23) is identical with Emmons' for the constant-rate case. His upper boundary, however, is placed at $\eta = \infty$ while we have $\eta = 1$. The solutions for mat density distribution are therefore different. The present solution indicates discontinuity at the mat-suspension boundary whereas Emmons describes an exponential decay-type layer.

MAT THICKENING

Filtration ends with the disappearance of a free slurry or suspension. Further removal of water from the formed mat is accomplished by compression. This process of thickening is considered complete when air begins to enter the

mat face. The analysis of mat thickening at constant rate was initiated by Hisey (II-4). We wish to make a new analysis in accordance with the present theory.

We assume that the mass of fibers remains constant during thickening. Thus,

$$L(t)\int_0^1 c\,d\eta = \text{constant} \qquad \text{(X-30)}.$$

At the upper mat face, $U_r = 0$. However, this layer moves with a superficial velocity

$$U_{f,L} = (1 - \epsilon_0)dL/dt \qquad \text{(X-31)}.$$

It follows that the filtrate velocity becomes simply

$$U_0 = dL/dt \qquad \text{(X-32)}.$$

We use Emmons' approximation (X-17) again and introduce the following nondimensional variables:

$$\lambda(\tau) = L/L_0 ,$$

$$\xi(\eta,\tau) = c/c_0^0 ,$$

and

$$\tau = \left(\frac{\gamma}{a' M_0 L_0^2}\right)t \qquad \text{(X-33)},$$

where L_0 is the mat thickness at $t = 0$ and c_0^0 a suitable reference mat density. The filtration equations are transformed into the thickening equations:

$$\frac{\partial^2 \xi}{\partial \eta^2} - \frac{1}{2} \frac{d\lambda^2}{dt} (1 - \eta) \frac{\partial \xi}{\partial \eta} - \lambda^2 \frac{\partial \xi}{\partial \tau} = 0 \qquad \text{(X-34)}$$

and

$$\left[\int_0^1 \xi d\eta\right]_{\tau=0} = \lambda \int_0^1 \xi d\eta = \text{constant} \qquad \text{(X-35)} .$$

The boundary conditions valid for $\tau > 0$ are

$$\left(\frac{\partial \xi}{\partial \eta}\right)_{\eta=0} = \frac{1}{2} \frac{d\lambda^2}{dt} \xi(0,\tau) ,$$

and

$$\left(\frac{\partial \xi}{\partial \eta}\right)_{\eta=1} = 0 \qquad \text{(X-36)} .$$

In constant-pressure thickening we assume a succession of dynamic equilibrium states so that

$$\lambda \int_0^1 \xi d\eta = \lambda_1 \xi_1 = 1 \qquad \text{(X-37)} .$$

The initial and boundary conditions now are

$$\xi(\eta,0) = 1 , \quad \lambda(0) = 1$$

$$\xi(\eta,\infty) = \xi_1 , \quad \lambda_1(\infty) = 1/\xi \qquad \text{(X-38)} .$$

However, for $0 < \tau < \infty$, the mat density distribution is continuously changing. Equation (X-34) may be solved numerically under these conditions.

The constant-rate thickening is characterized by

$$\frac{d\lambda^2}{dt} = \text{constant} = -2h \qquad \text{(X-39)} .$$

Introducing new variables:

$$\xi(\eta,\tau) = \xi^*(\eta,\tau^*) ,$$

$$\tau^* = -\frac{\gamma}{2a'M_b I_b} \ln\left(1 - \frac{2ha'M_b I_b}{\gamma}\tau\right)$$

and

$$\lambda^2 = 1 - \frac{2ha'M_b I_b}{\gamma}\tau \qquad \text{(X-40)} ,$$

the thickening equation becomes

$$\frac{1}{h}\frac{\partial^2 \xi^*}{\partial \eta^2} + (1 - \eta)\frac{\partial \xi^*}{\partial \eta} - \frac{\partial \xi^*}{\partial \tau^*} = 0 \qquad \text{(X-41)} ,$$

with Equation (X-35) unchanged, except the value of the constant being $\int_0^1 \xi(\eta,0)d\eta$, with $\xi(\eta,0)$ as a given initial mat density distribution. Equation (X-41) may be solved by separation of variables.

XI. GENERALIZED EQUATIONS FOR FILTRATION ANALYSIS

In the previous analysis of filtration it was assumed that the discrete fibers would be completely retained on a screen. To account for the effect of incomplete retention, the fibers are divided into two parts: retained and unretained. Furthermore, if there are several types of fibers in the suspension each type will have different retention probabilities at different locations. Thus, the mat will have an increasing number of retained fibers as the filtration proceeds until complete retention is reached.

The following treatment is due to Nelson (XI-1). Only the partial differential equations will be developed to describe the filtration process with incomplete fiber retention.

MODIFIED DEFINITIONS

For incomplete fiber retention the solid fraction is now defined by

$$1 - \epsilon = \Sigma(\omega_i + \omega_i^o) , \quad i = 1,2,3---j \qquad \text{(XI-1)} ,$$

where ω_i and ω_i^o are the volume fractions of the retained and unretained fiber of the ith type, respectively.

While the definition of the superficial fluid velocity remains the same as before,

$$U = \epsilon\bar{u} \qquad \text{(II-1)} ,$$

there are two superficial fiber velocities. For the unretained fibers of each type, the definition is

$$U_i^o = \omega_i^o \bar{u}_i^o \qquad \text{(XI-2)} ,$$

where the velocities $\bar{u}_i^o$ may, in general, differ from $\bar{u}$. For the retained fibers, however, there is a common velocity $\bar{u}_f$ so that

$$U_i = \omega_i \bar{u}_f \qquad \text{(XI-3)} .$$

On summing all types, we obtain

$$\bar{u}_f = \frac{\Sigma U_i}{\Sigma \omega_i} \qquad \text{(XI-4)} .$$

ADDITIONAL EQUATIONS

There is no change in the continuity condition for the incompressible fluid,

$$\frac{\partial \epsilon}{\partial t} = - \frac{\partial U}{\partial z} \qquad \text{(II-6)} .$$

If all types of fibers have the same density ρ_f, which remains constant, the equation of continuity for the ith-type fibers is

$$\frac{\partial}{\partial t} (\omega_i + \omega_i^o) = - \frac{\partial}{\partial z} (U_i + U_i^o) \qquad \text{(XI-5)} ,$$

and the summation of all types results in

$$\frac{\partial \epsilon}{\partial t} = \frac{\partial}{\partial z} \Sigma (U_i + U_i^o) \qquad \text{(XI-6)} .$$

In the case that the fibers are all of the same type and completely retained, the last equation reduces to the previous one (II-7).

The relative velocity is expressed the same as before,

$$U_r = U - \epsilon \bar{u}_f \qquad \text{(II-10)} ,$$

except that $\underline{\bar{u}}_f$ must satisfy Definition (XI-4). We now define a local retenti probability $\underline{P}_i^o$ for the ith-type fibers as the probability of capture in a thin layer of the mat, per unit thickness of the layer. The process of fiber retent in the undeformable case will then be described by

$$\frac{d\omega_i}{dt} = P_i^o |U_i^o| \qquad \text{(XI-7)} .$$

More generally, the derivative must be understood as a rate of change measured a a point fixed in the (retained) solid phase, and $\underline{U}_i^o$ must be replaced by $\underline{U}_{r,i}^o$ the relative superficial velocity of the unretained fibers of the given type. The latter is expressed as

$$\underline{U}_{r,i}^o = \underline{U}_i^o - \omega_i^o \underline{\bar{u}}_f \qquad \text{(XI-8)} .$$

In a stationary co-ordinate frame, the resulting equation of fiber retention becomes

$$\frac{\partial \omega_i}{\partial t} + \frac{\Sigma U_i}{\Sigma \omega_i} \frac{\partial \omega_i}{\partial z} = P_i^o |U_{r,i}^o| \qquad \text{(XI-9)} .$$

It should be noted that, in principle, there are differences between the local retention probability as defined here and the retention probability discussed previously. The incident fibers at a given level will no longer display the same kind of randomness in trajectory and orientation, and the presence of unretained fibers may modify the fluid flow. One possible consequence is that the local retention probability may depend, to some extent, on the relative superficial velocity.

PARTICLE RETENTION

To extend the previous discussion of fine particle retention, under the conditions of solid-phase heterogeneity and incomplete fiber retention, it becomes necessary to distinguish between several particle concentrations and fluxes. In principle, a fine particle concentration and its flux must be associated with the fluid, for each type of unretained fibers, and for each type of retained fibers. In addition, it will be necessary to consider separately the attachment of free particles to unretained and to retained fibers of each type.

The definitions of the particle fluxes are $\underline{UC}$ for free particles, $\underline{U}_i^o \underline{C}_i^o$ for bound particles attached to the unretained fibers of the $\underline{i}$th type, and $\underline{U}_i \underline{C}_i'$ for bound particles attached to the retained $\underline{i}$th-type fibers. The conservation of small particles requires that

$$\frac{\partial}{\partial t}\left[\epsilon C + \Sigma(\omega_i C_i' + \omega_i^o C_i^o)\right] = -\frac{\partial}{\partial z}\left[UC + \Sigma(U_i C_i' + U_i^o C_i^o)\right] \qquad \text{(XI-10)} .$$

In any case where the definitions of particle fluxes are satisfactory, and the fluid is incompressible, Equation (XI-10) may be simplified somewhat by application of the equation of continuity for the fluid (II-6). The new particle continuity equation reduces to the old one (II-5) under the previously prescribed conditions.

We now have to describe the processes by which fibers are retained, and by which free particles become attached to them. For the first of these, we have

$$\frac{d\omega_i}{dt} = P_i^o \left| U_{r,i}^o \right| \qquad \text{(XI-11)} .$$

There will also be a relation

$$\frac{dC_i^o}{dt} = \zeta \qquad \text{(XI-12)},$$

which will be discussed further below, and

$$\omega_i \frac{dC_i'}{dt} = K_i |U_r| C + P_i^o |U_{r,i}^o| C_i^o \qquad \text{(XI-13)}.$$

In the last equation, the first term on the right side represents the acquisitior of free small particles from the fluid, where the attenuation coefficient is related to the collection efficiency by

$$K_i = E_i \frac{A_{f,i}}{V_{f,i}} \omega_i \qquad \text{(XI-14)}.$$

The second term represents the effect of the addition of fibers of the given type as these are retained at the locality in question.

Concerning the unspecified function ζ, information will be required from other sources. The attachment of free particles to unretained fibers may depend on relative motion with respect to the fluid, on diffusion, on saturation, and possibly on other effects in addition to the probable dependence on free particle concentration. A circumstance which might be realized under suitable conditions is that each C_i^o may be a constant, determined by the manner of preparation of the suspension.

The generalization outlined above serves as a basis for future development.

XII. STATISTICAL DESCRIPTIONS OF POROUS STRUCTURES

The objective of the sheet-forming process is to form a fiber mat of a desirable structure. Because of its complexity the porous structure has so far defied a complete description. Certain efforts have lately been made in the various fields dealing with porous media to initiate some more rigorous analysis of the problem than previously. All work is based on the statistical treatment. We attempt here to present a brief survey of such work.

PORE GEOMETRY

Chalkeley, Cornfield, and Park (XII-1) studied pore geometry by the statistical method. Debye, Anderson, and Brumberger (XII-2) used the same principle to determine the specific surface of porous catalysts. Their work is summarized in the following, based primarily on a recent paper by Prager (XII-3).

A function $f(\vec{r})$ of a position vector $\vec{r}$ within the porous medium is introduced such that the function has the value of unity if $\vec{r}$ is in the void region and zero if $\vec{r}$ is in the solid region. A complete knowledge of $f(\vec{r})$ would amount to a detailed specification of the pore geometry. In its nature, $f(\vec{r})$ is a stochastic function.

The volume average of the function itself is the porosity or void fraction:

$$\epsilon = \langle f(\vec{r}) \rangle = \frac{1}{V} \int_V f(\vec{r}) d\vec{r} \qquad \text{(XII-1)} ,$$

where $\langle f(\vec{r})\rangle$ is called the one-point average. It represents the probability that if a pin is thrown at random on a much enlarged cross section of an isotropic porous medium, the pin head will land in the void region. Thus,

$$\epsilon = \lim_{N_t \to \infty} \frac{N_0}{N_t} \qquad \text{(XII-2)} ,$$

where N_0 denotes the number of times when the pin head is in the void region and N_t the total number of throws. The porosity so determined is the total porosity including sealed pores, such as isolated bubbles or fiber lumina.

The surface of the void region may be ascertained by adding a length vector $\vec{\delta}$ to the position vector $\vec{r}$ and carrying out the averaging process over all possible orientations of $\vec{r}$. The resulting two-point average,

$$S(\vec{\delta}) = \langle f(\vec{r}) f(\vec{r} + \delta)\rangle \qquad \text{(XII-3)} ,$$

indicates the probability that a pin having the length and direction of the vector $\vec{\delta}$ will land with both its ends in voids. Again, for an isotropic medium, $S(\vec{\delta})$ will depend on the magnitude of $\vec{\delta}$ only. At $\delta = 0$, the product of $f(\vec{r})$ by itself is obviously unity and its volume average is simply ϵ. At $\delta = \infty$, the probabilities of two events in two voids wide apart are independent of each other; the volume average of each being ϵ, the product is therefore ϵ^2. Thus, the correlation function $S(\delta)$ decays continuously from ϵ to ϵ^2 as δ varies from 0 to ∞.

If one end of a pin length δ is fixed in a void, the probability that the other free end will also be in void is

$$P_{11} = S(\delta)/\epsilon \qquad \text{(XII-4)} ,$$

and the probability that the free end will be in solid is obviously

$$P_{10} = 1 - P_{11} = 1 - S(\delta)/\epsilon \qquad \text{(XII-5)} .$$

If the pin is thrown randomly, it is equally probable that the ends will be in different environments,

$$P_{01} = \frac{\epsilon}{1 - \epsilon} P_{10} = \frac{\epsilon - S(\delta)}{1 - \epsilon} \qquad \text{(XII-6)} ;$$

thus the probability of "dissimilar ends" can be written as

$$P_d = \epsilon P_{10} + (1 - \epsilon)P_{01} = 2[\epsilon - S(\delta)] \qquad \text{(XII-7)} .$$

If we allow δ to become very small and to take on all possible spatial orientations, while restricting its two ends to remain always in different environments, the pin must cut and follow the surface between solid and void. From geometric considerations the probability of dissimilar ends may be derived.

The end of the pin situated at an origin in solid must be within some distance $\underline{h} < \delta$ from the surface. For a range of values of this distance between $\underline{h}$ and $\underline{h} + d\underline{h}$, the volume which can be covered by the pin per unit volume of the porous medium is $S_0 d\underline{h}$. Furthermore, only certain orientations of the pin, so fixed at one end, will allow the free end to penetrate the surface. The probability of penetration is

$$P_h = \frac{2\pi\delta(\delta - h)}{4\pi\delta^2} S_0 dh \qquad \text{(XII-8)} ,$$

and the probability of dissimilar ends is twice the integrated value of penetration:

$$P_d = 2S_o\int_o^\delta \frac{\delta - h}{2\delta}\, dh = \frac{S_o\delta}{2} \qquad \text{(XII-9)}$$

By comparing this result with Equation (XII-7) it is seen that the specific su is

$$S_o = -4\left[\frac{S(\delta) - \epsilon}{\delta}\right] \qquad \text{(XII-10)}$$

When δ becomes small as previously stated, $\underline{S}(\delta)$ approaches ϵ, and the value in the bracket approaches that of the derivative of $\underline{S}(\delta)$ with respect t δ at $\delta = 0$, and

$$S_o = -4\left(\frac{dS}{d\delta}\right)_{\delta=0} \qquad \text{(XII-11}$$

where the derivative is always negative.

Debye, et al. proceeded to establish the form of the correlation function $\underline{S}(\delta)$ for a completely random and isotropic porous medium. If the of length δ has one end fixed in void, $\underline{P}_{11}$ will change only if the additio of $\Delta\delta$ will allow the pin to cross the surface of void into solid or vice ver

The free end of the pin must lie within a sheet of thickness $\Delta\delta\cos$ to allow $\delta + \Delta\delta$ to cross into solid, φ being the angle which the pin makes with the normal to the surface. The average value of this thickness is given by the integral over all possible orientations of δ :

$$\frac{\Delta\delta}{2}\int_o^{\pi/2} \sin\varphi\cos\varphi\, d\varphi = \frac{\Delta\delta}{4} \qquad \text{(XII-12}$$

The change in $\underline{P}_{11}$, when δ is changed by $\Delta\delta$ is

$$\Delta P_{11} = -\left(\frac{S_o}{\epsilon}\right)\left(\frac{\Delta\delta}{4}\right) P_{11} \qquad \text{(XII-13)} .$$

Since it is possible for the free end of the pin to be already in solid, an additional term is introduced to account for the positive contribution to $\underline{P}_{11}$ by the growth of δ into another void region. Thus,

$$\Delta P_{11} = -\left(\frac{S_o}{\epsilon}\right)\left(\frac{\Delta\delta}{4}\right) P_{11} + \left(\frac{S_o}{1-\epsilon}\right)\left(\frac{\Delta\delta}{4}\right) P_{10} \qquad \text{(XII-14)} ,$$

which in the limit becomes

$$\frac{dP_{11}}{d\delta} = -\frac{S_o}{4}\left[\frac{P_{11}}{\epsilon} - \frac{P_{10}}{1-\epsilon}\right] \qquad \text{(XII-15)} .$$

Substituting Equations (XII-4) and (XII-5) for $\underline{P}_{11}$ and $\underline{P}_{10}$, respectively, we obtain

$$\frac{dS(\delta)}{d\delta} = -\frac{S_o}{4}\left[\frac{S(\delta) - \epsilon^2}{\epsilon(1-\epsilon)}\right] \qquad \text{(XII-16)} ,$$

the solution for which is

$$\frac{S(\delta) - \epsilon^2}{\epsilon(1-\epsilon)} = \exp\left[-\frac{S_o \delta}{4\epsilon(1-\epsilon)}\right] \qquad \text{(XII-17)} .$$

Thus, for an isotropic medium with a random distribution of voids and solid elements, the correlation function is exponential. In order to define the shapes of the pore region, at least a three-point average is necessary. Such a treatment becomes very involved mathematically. Furthermore, the extension of the theory to anisotropic porous media such as fiber mats perhaps needs substantial modifications.

Prager proceeded to outline a general method of predicting the permeability of an isotropic medium by the principle of the least energy dissipation. Using the three-point average, Weissberg and Prager (XII-4) calculated the viscous resistance of a bed of widely dispersed spheres to be 25% below the true value.

PORE INTERCONNECTIONS

The often-used term "pore size" is not well defined. A common way of characterizing the pore-size distribution is made in terms of capillary pressure in a partially saturated medium, such as Parker's work (XII-5) on fiber mats. Across a curved interface between two fluid phases occupying a capillary, a pressure difference exists, arising from the surface tension of the liquid. The pressure on the concave side of a liquid meniscus is always greater than that on the convex side.

In a system of capillaries, a quantity of liquid will distribute itself in the small pores until a state of equilibrium is reached, at which all of the liquid-gas interfaces will have the same curvature. Conversely, if a pressure difference is imposed on the system of capillaries completely filled with liquid, the liquid will be displaced from the system by a gas until the remaining liquid is just sufficient to occupy the small pores in accordance with the capillary law The volume of liquid retained per unit volume of the void space is called saturation. By measuring the capillary pressures at various degrees of saturation, th equivalent radii or pore sizes may be calculated on the construction of a capilla model.

To describe the pore geometry adequately, not only the pore-size distribution, but also the interconnection of the pore spaces must be considered. Fatt (XII-6) proposed a network model in two dimensions, in which cylindrical

tubes of a certain radius distribution are interconnected in a definite manner. The choice of size distribution and network form were left open to provide flexibility in model construction. The number of cross connections per tube is called the β_o factor, a number depending on the network form. Two models of Fatt, a square and a triple hexagonal network, have β_o factors of 6 and 10, respectively.

By taking a certain pore-size distribution and network form, the capillary pressure-desaturation or pore-size distribution curve may be constructed with the aid of a random number table and with the assumption that the length of a segment of a tube between two cross connections varies with its radius in a definite manner such as

$$L_s = \beta_o r_o^{\gamma_o} \qquad \text{(XII-18)} ,$$

β_o and γ_o are dependent on the network form and porosity.

The network model is reduced to a bundle of tubes if $\gamma_o = 0$ and $\beta_o = \infty$. By analysis of these networks Fatt arrived at the following conclusions: (1) The form of the capillary pressure curve obtained on a porous medium is determined almost entirely by the pore-size distribution while the network structure has little or no effect. (2) The observed dynamic properties of porous media, such as permeability, are determined entirely by network structure while pore-size distribution has little or no effect.

Rose (XII-7) further expanded the square network to three dimensions and called it a tetrahedron 3-D network. The β_o factor for tetrahedron is 22. By choosing a certain pore-size distribution and a certain tube segment length-radius function, the model may be constructed by programming on a computer.

It is then possible to predict permeability of this model. However, such predictions have not yet been made because of considerable calculations involved.

From the above brief review of the recent advance in model simulation of porous media, it appears that a major defect is in the omission of pore shape. In spite of all the elaborate construction of pore-size distribution and cross connections, some empirical factor may still have to be introduced to bring the models into agreement with the experimental data.

FIBER INTERSECTIONS

Some workers such as Kallmes and Corte (XII-8) have approached the problem of fiber structure by dealing with the solid elements, rather than the pores. From such a standpoint, the treatment must begin with an account of fiber intersections in the structure. The following analysis is due to Nelson (XII-9).

Let us consider straight fibers of a single length L_f and of negligible transverse dimensions. The fibers are to be arranged in space in such a way that the centers of their projections on the x-y plane occur randomly and uniformly in some region, the number of centers per unit area being N_f. The orientation of each fiber will be specified by a polar angle θ measured from the positive z axis, and an azimuth φ which is the angle between the positive x axis and the projection of the fiber, as shown in Fig. VIII-2. For convenience, a preferred direction along each fiber (and its projection) will be chosen, such that $0 \leq \theta \leq \pi/2$. We must now determine, or assume, a frequency function $g(\theta)$, for the angle θ, and it will be supposed that this has been normalized so that

$$\int_0^{\pi/2} g(\theta)d\theta = 1 \qquad \text{(XII-19)}.$$

To complete the specification, the values of the azimuth φ are to be random and uniform on the interval $0 \leq \varphi \leq 2\pi$, and it is assumed that θ, φ, and the fiber center location in the $\underline{x}$-$\underline{y}$ plane are uncorrelated. We wish to calculate the frequency of intersections in the $\underline{x}$-$\underline{y}$ plane.

The frequency function $f(\underline{R}_f)$ for the projection $\underline{R}_f$ of half the fiber length will be required in the sequel, and from the relation $\underline{R}_f = (\underline{L}_f/2)\sin\theta$ we conclude that

$$f(R_f) = \frac{2}{L_f}\frac{g(\theta)}{\cos\theta} = \frac{2}{L_f}\frac{g(\arcsin[2R_f/L_f])}{\sqrt{1 - [2R_f/L_f]^2}} \qquad \text{(XII-20)} .$$

Let the center of the projection of one fiber fall at point $\underline{H}$ in the $\underline{x}$-$\underline{y}$ plane (Fig. XII-1) and let the value of $\underline{R}_f$ for this fiber be $\underline{R}'_f$. All other fiber projections are to be considered in classes, within each of which the azimuth φ' has nearly the same value. The number of fiber projections, per unit area, having values of φ' within a small interval $\Delta\varphi'$, is $\underline{N}_1\Delta\varphi'$, where $\underline{N}_1 = \underline{N}_f/(2\pi)$. For one such class of fiber projections, we select those cases for which the center lies in a narrow strip (having the azimuth φ') of width $\Delta\underline{h}$, at a distance $\underline{h}$ from $\underline{H}$. We consider first the intersections which may result when the azimuth of the fiber projection with center at $\underline{H}$ has a given value, φ.

The probable number of centers of fiber projections, of the class considered, falling within a rectangle of area $\Delta\underline{h}\Delta\underline{R}_f$, at a distance $\underline{R}_f$ from point $\underline{J}$, is $\underline{N}_1\Delta\varphi'\Delta\underline{h}\Delta\underline{R}_f$. Of these, a fraction will have polar angles θ such that actual intersections will result. Allowing for this, the count is

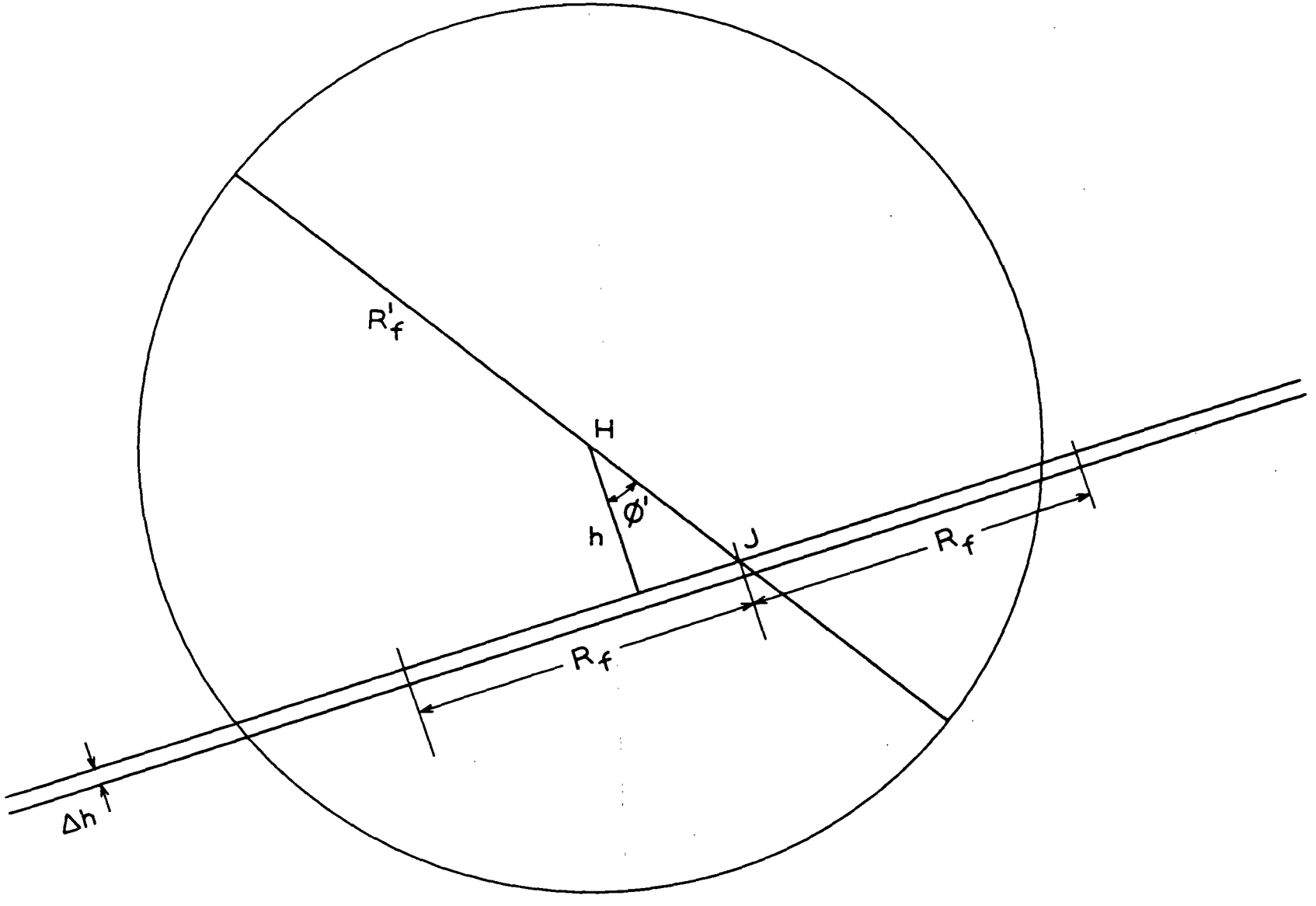

Figure XII-1. Evaluation of Fiber Intersections

$$N_{c,1} = N_1 \Delta\varphi' \Delta h \Delta R_f \int_{R_f}^{L_f/2} f(R_f'')dR_f'' \qquad \text{(XII-21)} .$$

Integration with respect to $\underline{R_f}$ yields

$$N_{c,2} = N_1 \Delta\varphi' \Delta h \times 2 \int_0^{L_f/2} \int_{R_f}^{L_f/2} f(R_f'')dR_f''dR_f \qquad \text{(XII-22)}$$

or

$$N_{c,2} = 2N_1 \Delta\varphi' \Delta h \int_0^{L_f/2} R_f'' f(R_f'')dR_f'' \qquad \text{(XII-23)} .$$

The probability that φ will fall in a given small interval $\Delta\varphi$ is $\Delta\varphi/(2\pi)$. We now multiply by this probability and integrate over the allowable range, inserting first a factor of 2 to account for equivalent orientations of the projection which has its center at $\underline{H}$. The result is

$$N_{c,3} = 2N_{c,2} \frac{2}{2\pi} \arccos \frac{h}{R_f'} \qquad \text{(XII-24)} .$$

We may now integrate with respect to $\underline{h}$, obtaining

$$N_{c,4} = \frac{4}{\pi} N_1 \Delta\varphi' \int_0^{L_f/2} R_f'' f(R_f'')dR_f'' \times 2R_f' \qquad \text{(XII-25)} .$$

The variable $\underline{R_f'}$ has the frequency function $f(\underline{R_f'})$; multiplying by this, and integrating with respect to $\underline{R_f'}$, we find

$$N_{c,5} = \frac{4}{\pi} N_1 \Delta\varphi' \int_0^{L_f/2} R_f'' f(R_f'')dR_f'' \times 2 \int_0^{L_f/2} R_f' f(R_f')dR_f' \qquad \text{(XII-26)}$$

or

$$N_{c,5} = \frac{8}{\pi} N_1 \Delta\varphi' \left[\int_0^{L_f/2} R_f f(R_f) dR_f\right]^2 \qquad \text{(XII-27)} .$$

Integration over the various strip orientations φ' now gives

$$N_{c,6} = \frac{8}{\pi} N_f \left[\int_0^{L_f/2} R_f f(R_f) dR_f\right]^2 \qquad \text{(XII-28)} .$$

Fiber projections, such as the one having its center at $\underline{H}$, occur so as to provide, on an average, $\underline{N_f}$ centers per unit area. We therefore multiply the last result by $\underline{N_f}$, but we must also divide by 2, inasmuch as we will have counted every fiber intersection twice. The expectation value of the number of intersections per unit area is thus

$$N_{c,7} = \frac{4}{\pi} N_f^2 \left[\int_0^{L_f/2} R_f f(R_f) dR_f\right]^2 \qquad \text{(XII-29)} .$$

If all the fibers lie in the $\underline{x}$-$\underline{y}$ plane, or are parallel to it, we have $g(\theta) = 0$ when $0 \leq \theta \leq \pi/2$, and thus $g(\theta)$ is singular in the manner of a delta function at $\pi/2$. The quantity in the square bracket in Equation (XII-29) becomes $\underline{L_f}/2$, and we find

$$N_{c,7} = (1/\pi) N_f^2 L_f^2 \qquad \text{(XII-30)} ,$$

which is Equation (VI-1).

If the fiber orientation is isotropic, we have $g(\theta) = \sin\theta$. The quantity in the square bracket in Equation (XII-29) is found to be $(\pi/8)\underline{L_f}$, which gives

$$N_{c,7} = (\pi/16)N_f^2 L_f^2 \qquad \text{(XII-31)} .$$

As might be expected, this quantity is smaller than that computed from (XII-30), given the same $\underline{N}_{\underline{f}}\underline{L}_{\underline{f}}$ product; the ratio is approximately 1.621:1.

XIII. INITIAL EXPLORATION OF FIBER-WIRE INTERACTION

Aside from its effect on fiber retention, a wire screen also contributes resistance to flow. In the later period of a prolonged filtration the wire resistance can be safely neglected, compared with that of a thick mat. During the intermediate times the assumption that the pressure drops across the mat and the wire are additive is reasonable. However, in the beginning of filtration such an assumption may lead to serious errors in predicting drainage because of hydrodynamic interactions between a thin mat and its supporting structure. The following analysis is an initial attempt by Meyer (XIII-1) to resolve this problem.

IRROTATIONAL FLOW

The hydrodynamic potential theory dealing with irrotational flow of an ideal fluid (constant ρ and zero μ) is a mathematical abstraction of a real system in which vorticity generated in the boundary zone does not appreciably disturb the main flow (IV-2). Such flow follows the Laplace equation:

$$\nabla^2 \varphi = 0 \qquad \text{(XIII-1)},$$

where the potential φ is a scalar function applicable to fields such as electrical, magnetic, gravitational, temperature, and pressure. A vector called its gradient can be derived from a potential by partial differentiation. For irrotational flow, φ is the velocity potential ($u_x = \partial\varphi/\partial x$, $u_y = \partial\varphi/\partial y$, $u_z = \partial\varphi/\partial z$

Meyer considered steady two-dimensional irrotational flow through an array of parallel cylinders (Fig. XIII-1) as a simplified simulation of a wire screen. Introducing the stream function ψ , such that

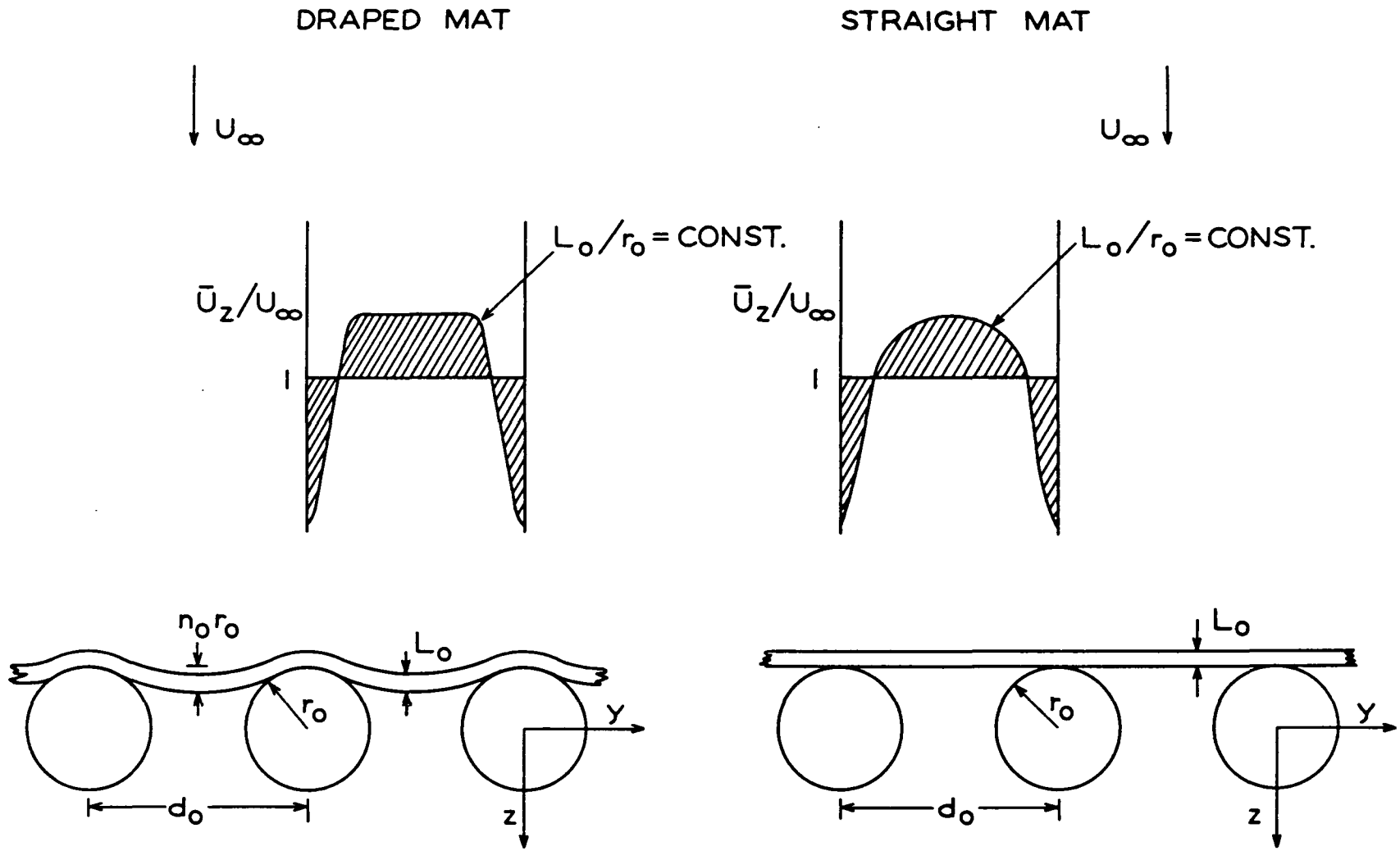

Figure XIII-1. A Simplified Diagram of Fiber-Wire Interaction

$$u_x = 0 , \quad u_y = - \frac{\partial \psi}{\partial z} , \quad u_z = \frac{\partial \psi}{\partial y} \qquad \text{(XIII-2)} ,$$

the equation of continuity (IV-5) calls for

$$\nabla^2 \psi = 0 \qquad \text{(XIII-3)} .$$

Furthermore, the velocity at the surface can only be tangential, that is,

$$\frac{d\psi}{dS} = 0 \qquad \text{(XIII-4)} ,$$

where $\underline{S}$ represents the surface element; thus, at the surface,

$$dS^2 = dy^2 + dz^2 \qquad \text{(XIII-5)} .$$

Let $\underline{r_o}$ be the radius of the cylinders and $\underline{d_o}$ the center-to-center distance between the cylinders. For potential flow around a single cylinder with the approach velocity $\underline{U_\infty}$, the well-known solution of Equations (XIII-1), (XIII-3), and (XIII-4) is expressed in terms of the complex potential:

$$\varphi + i\psi = U_\infty (Z + \frac{r_o^2}{Z}) \qquad \text{(XIII-6)} ,$$

where $\underline{Z}$ is the complex variable, $\underline{z} + \underline{iy}$. Now for flow through an infinite array of cylinders with spacing $\underline{d_o}$, it can be shown that the solution is

$$\varphi + i\psi = U_\infty [Z + \frac{d_o}{\pi} \sinh^2 (\frac{\pi r_o}{d_o}) \coth (\frac{\pi Z}{d_o})] \qquad \text{(XIII-7)} .$$

Upon taking the imaginary part of the solution we have

$$\psi = U_\infty \left[y - \frac{d_o}{\pi} \sinh^2 \frac{\pi r_o}{d_o} \frac{\sin(2\pi y/d_o)}{\cosh(2\pi z/d_o) - \cos(2\pi y/d_o)} \right] \qquad \text{(XIII-8)} .$$

Because of the symmetry of the array it is sufficient to evaluate ψ in the range of $0 \leq \underline{y} \leq (\underline{d}_D/2)$ and $-\infty \leq \underline{z} \leq +\infty$.

For a real fluid there will be an irreversible loss of pressure as a result of the flow. We assume that the velocity distribution remains the same from $\underline{z} = -\infty$ to $\underline{z} = 0$, and all energy dissipation occurs in the downstream because of flow separation.

FLOW CONVERGENCE

The macroscopic viscous flow through a homogeneous fiber mat follows the Laplace equation:

$$\nabla^2 p = 0 \qquad \text{(XIII-9)} ,$$

in which the gravitational effect is neglected, and $\underline{p}$ may be treated as the potential φ . For two-dimensional flow, the superficial velocity components may be expressed in terms of the stream function ψ :

$$U_x = 0 , \quad U_y = -\frac{\partial \psi}{\partial z} , \quad U_z = \frac{\partial \psi}{\partial y} \qquad \text{(XIII-10)} ;$$

then according to Darcy's law and continuity condition, we arrived at the same equation as (XIII-3). In view of the similarity between the viscous flow through the mat and the potential flow through the simplified screen, we consider that the previous solution (XIII-8) would also be applicable to the mat-wire combination if we interpret the approach velocity to be $\underline{U}_\infty$. For an isotropic mat with constant resistance, we modify the Darcy law for two-dimensional flow as

$$-\frac{1}{a}\frac{\partial p}{\partial z} = \frac{\partial \psi}{\partial y} = U_\infty \kappa(y,z) \qquad \text{(XIII-11)} ,$$

where

$$\kappa(y,z) = 1 - 2\sinh^2\left(\frac{\pi r_o}{d_o}\right) \frac{\cosh(2\pi z/d_o)\cos(2\pi y/d_o) - 1}{[\cosh(2\pi z/d_o) - \cos(2\pi y/d_o)]^2} \quad \text{(XIII-12)} .$$

This is equivalent to saying that the streamlines of superficial flow through a thin mat, originally straight in the flow direction, become curved, owing to the obstruction of the cylinders, the dimension of which is very large compared with that of fibers. Via such an abstraction we proceed to integrate Equation (XIII-12). The integration is performed first in the z direction over the mat thickness and then in the y direction to obtain an average $\bar{\kappa}$ for the flow.

The mat with thickness L_b may lie flat on or drape slightly over the cylinders, as shown in Fig. XIII-1. For the sake of simplicity, its deflection contour is described by

$$\delta_o = n_o r_o \sin^2(\pi y/d_o) \quad \text{(XIII-13)}$$

with the maximum deflection $n_b r_o$ located at the midpoint between the cylinders. The deflection parameter n_b may vary from zero for a flat mat to $(1/2)(\pi r_o/d_o)$ for the draped mat. The integration limits may be specified as

$$z_1 = -r_o[1 + L_b/r_o - n_o \sin^2(\pi y/d_o)] \leq z \leq z_1 + L_b$$

and

$$0 \leq y \leq d_o/2 .$$

The result is expressed as

$$\frac{1}{a}\frac{|\Delta p|}{L_b} = U_\infty \bar{\kappa} \quad \text{(XIII-14)}$$

where

$$\bar{\kappa} = \frac{2}{L_b d_o} \int_0^{d_o/2} \int_{z_1}^{z_1+L_b} \kappa(y,z)\,dz\,dy \qquad \text{(XIII-15)} .$$

In this way $\bar{\kappa}$ is obtained as a function of the deflection parameter n_b, the relative mat thickness parameter $L_b r_o$, and the cylinder spacing parameter r_o/d_o. The double integral has been evaluated numerically, and the results are shown in Fig. XIII-2 in terms of these parameters at $r_o/d_o = 0.227$, equivalent to a screen porosity 0.65. It is seen that $\bar{\kappa}$ is either equal to or larger than unity. At a finite n_b, its value increases rapidly with decreasing L_b/r_o for thin mats. Conversely, it approaches unity as the mat becomes relatively thick. The pressure drop calculated from Equation (XIII-14) includes the additional energy loss in the mat due to curved flow in the presence of downstream cylinders. For a flat mat, $n_b = 0$, and $\bar{\kappa} = 1$, indicating no effect of flow convergence by this analysis.

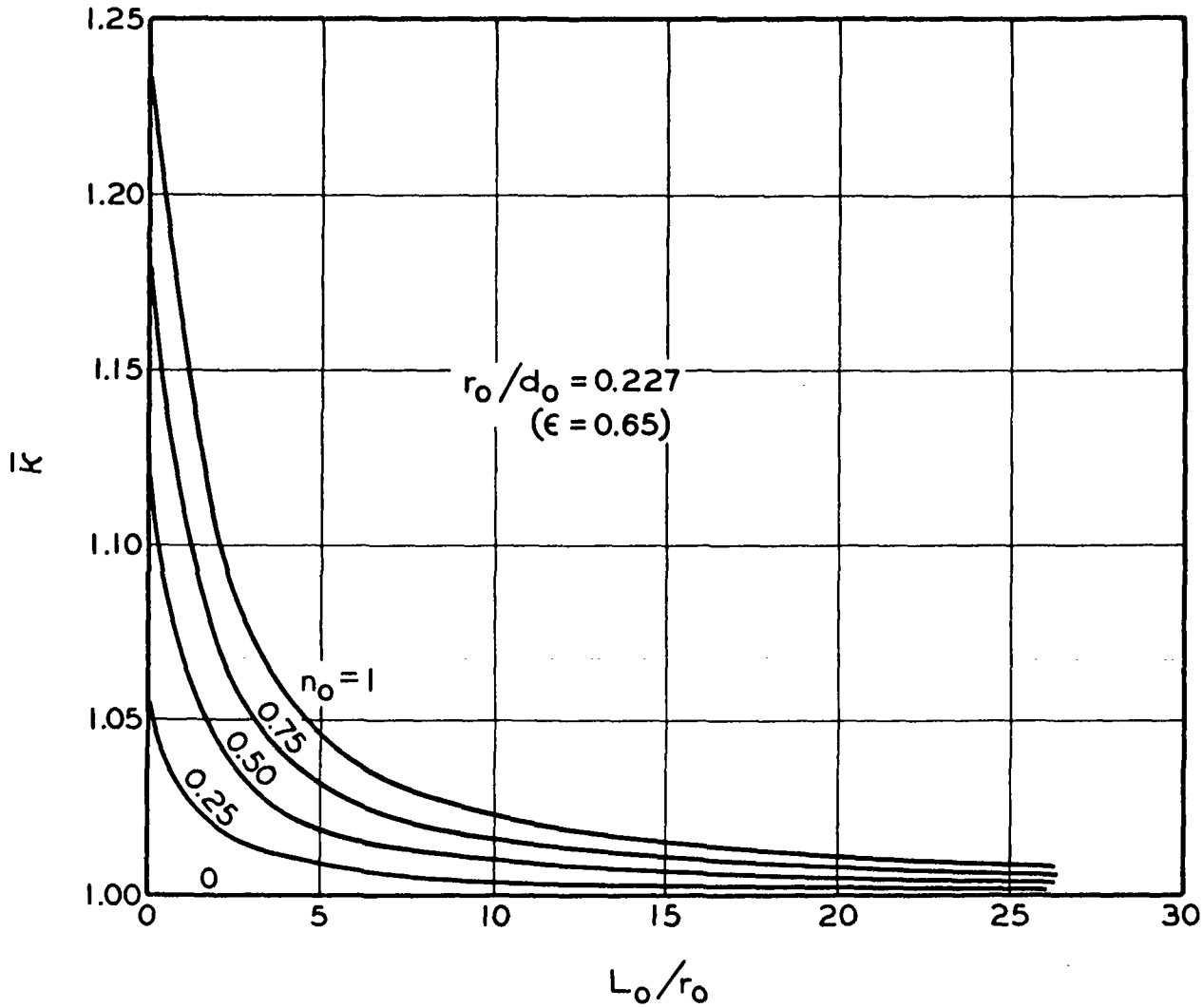

Figure XIII-2. Correction Factor for Fiber-Wire Interaction

XIV. HYDRODYNAMIC APPROACHES TO FIBER FLOCCULATION

The problem of fiber flocculation is of such a complex nature that it has so far defied a precise definition. Broadly speaking, the flocculation of fibers in a fluid consists of fiber motion, collision, and interaction in a field of forces. The forces involved arise from mechanical, electrostatic, and molecular origins. For the sake of clarity and at the risk of oversimplification, we shall restrict our discussion largely to an aqueous suspension of cylindrical fibers.

FIBER MOTION

In order for the collision of fibers to take place, they must approach one another by virtue of their motion. The motion of fibers is governed by hydrodynamic forces. The simplest case is slow translation in a viscous fluid. The steady linear motion of an infinitely long cylinder in a direction perpendicular to its axis in an infinite expanse of a Newtonian fluid (its stress being directly proportional to the rate of strain) follows Lamb's solution (XIV-1):

$$F_\infty = \frac{4\pi\mu U L_f}{2.002 - \ln Re_f} \qquad \text{(XIV-1)} ,$$

where F_∞ is the force required to maintain a linear velocity U. The Reynolds number, Re_f, is defined as $\rho d_f U/\mu$, which is restricted to much less than unity.

It is obvious that Lamb's solution is the limiting case of a finite cylinder. Burgers (XIV-2) developed an expression for slow translation of a finite cylinder with a large axis ratio as

$$F_\infty = \frac{4\pi\mu U L_f}{\ln (2L_f/d_f - 1/2)} \qquad \text{(XIV-2)} .$$

This is closely related to Oberbeck's solutions for ellipsoids (XIV-3). Solutions for curved cylinders have been developed by Tchen (XIV-4). For a cylinder with a uniform radius of curvature r and an angle ψ between r at one end and the bisector, Tchen's general result is

$$F_\infty = 2\pi\mu U r \psi f_\infty \qquad \text{(XIV-3)} ,$$

where the friction coefficient, $\pi\mu f_\infty$, is a known function of ψ and L_f/d_f, depending on the direction of motion. Tchen's solution reduces to Burgers' for straight cylinders.

The wall effect on the motion of a particle was recently generalized by Brenner (XIV-5) to be

$$\frac{F}{F_\infty} = \frac{1}{1 - k_w[F_\infty/(3\pi\mu U d_w)]} \qquad \text{(XIV-4)} ,$$

in which d_w is the diameter of a circular wall or the distance between two flat walls. The constant k_w is supposed to be dependent only on the shape of the boundary. The two particular values of k_w are 2.104 for a circular wall and 1.004 for two parallel infinite flat walls. In both cases the particle must move parallel to and symmetrical with the walls.

For somewhat higher Reynolds numbers ($Re_f \cong 1$) the inertial effect must be taken into account. Brenner suggested the generalized correction:

$$\frac{F}{F_\infty} = 1 + \frac{F_\infty}{16\pi\mu U d_f} Re_f \qquad \text{(XIV-5)} .$$

Above the unity Reynolds number flow separation begins to occur and a wake of eddies is developed behind the moving particle. The drag coefficient, defined similarly as the friction factor, becomes a complex function of the Reynolds number.

When a number of particles are present in a confined space, their motion is influenced by one another as well as by the boundaries. Even the simplest case of gravitational settling of spheres in a very dilute suspension requires involved mathematical solutions of the hydrodynamic equations. Happel (XIV-6) has attained partial success in this analysis, but encountered difficulties in dealing with agglomeration of particles, which is of chief interest in the phenomenon of flocculation.

When a fiber is present in a shear field, its center will follow the motion of the fluid, provided its inertia is negligible. In addition, it will execute rotation under the influence of a torque arising from the velocity gradient. As a consequence of rotation, it develops a force which imparts perturbations to the shear field, as manifested by an apparent increase of the fluid viscosity. In the simplest case of fibers suspended in a Newtonian fluid undergoing viscous flow with a linear shear field, the ends of a fiber will rotate in a spherical elliptical orbit, describing a surface roughly corresponding to a double cone, with the period of rotation directly proportional to the axis ratio and inversely proportional to the velocity gradient in accordance with Jeffrey's analysis (XIV-7) of ellipsoids. Burgers analyzed the effect of rotation on the shear field for a very dilute suspension and concluded that the apparent viscosity of the suspension would increase by the following amount:

$$\frac{\mu_s}{\mu} = 1 + \alpha^{\rho} C \qquad \text{(XIV-6)},$$

where

$$\alpha^{o} = \frac{(L_f/d_f)^2}{6[\ln(2L_f/d_f) - 1.80]} \overline{\sin^4\theta \sin^2 2\varphi} \qquad \text{(XIV-7)} .$$

$\underline{C}$ is the volume concentration (volume of fibers per unit volume of suspension), and α^{o} a coefficient to account for the effects of axis ratio and average rotating orbit. The spherical co-ordinates θ and φ, describing the orientation of a single fiber, are defined in Fig. XIV-1.

For higher concentrations, Blakeney (XIV-8) introduced a correction term to Burgers' expression as follows:

$$\frac{\mu_s}{\mu} = 1 + \alpha^{o} C + \beta^{o} (\alpha^{o} C)^2 \qquad \text{(XIV-8)} ,$$

where β^{o} is an empirical factor.

FLOC FORMATION

When two fibers approach each other and result in a collision, a disturbance in the motion of either fiber must occur. For neutral fibers a doublet is formed, which is a temporary association of the two fibers in a common motion at the instant of collision. The doublet has a finite life, at the end of which the two fibers separate from each other. The collision involves an interpenetration of the rotating orbits and the separation results in different orbits from the original ones. By analogy with the earlier analysi of spheres, Mason (XIV-9) asserted that the collision frequency of rigid fibers in a dilute suspension is proportional to the product of concentration and velocity gradient. He further suggested that above a certain concentration such interaction becomes almost continuous. The concentration at which free rotatior

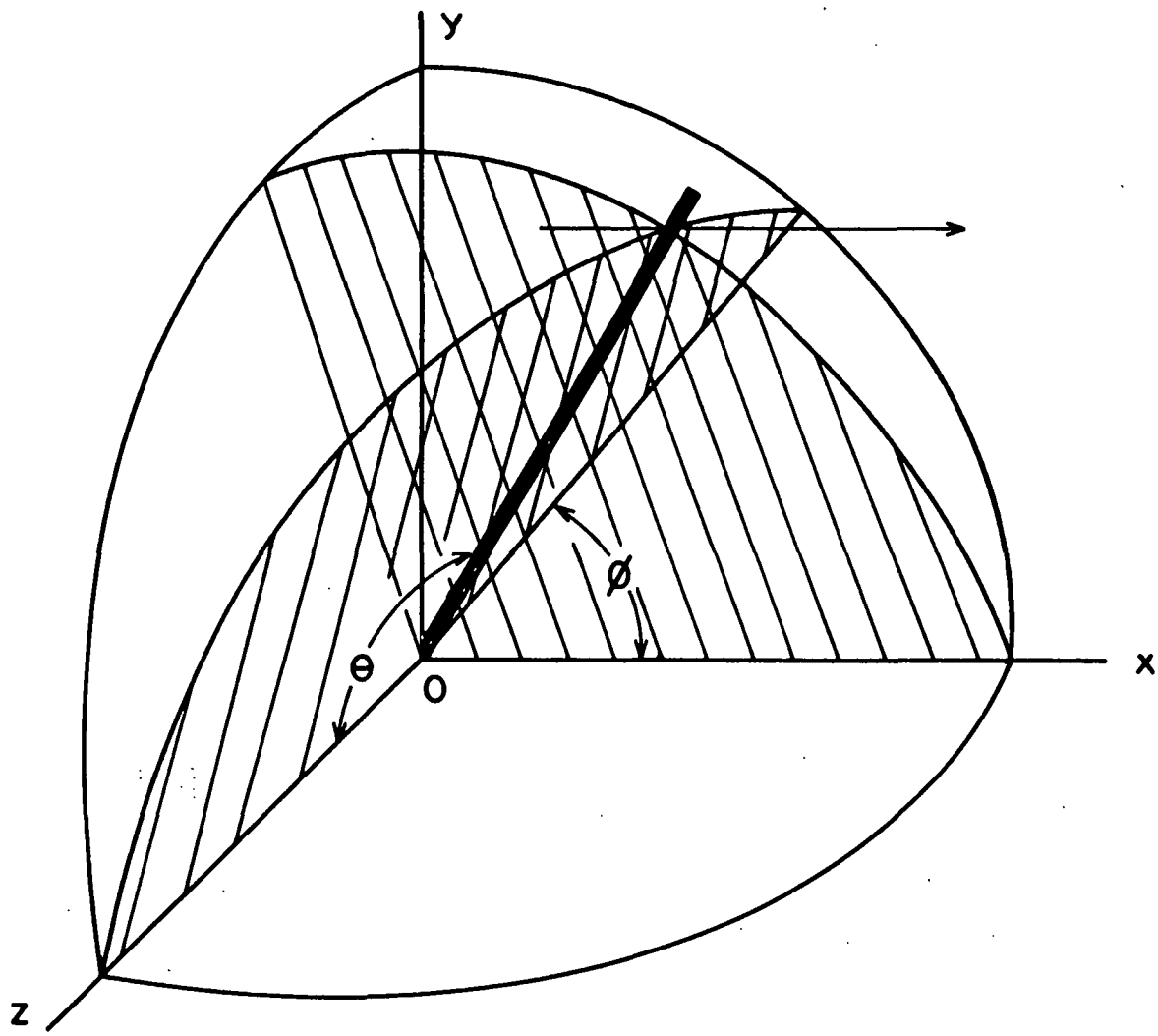

Figure XIV-1. Co-ordinates of a Rotating Fiber

are inhibited was shown to be inversely proportional to the square of the axis ratio. At higher concentrations the formation of multiplets becomes highly probable.

The motion, collision, and interaction of fibers in a shear field were viewed by Mason as the hydrodynamic process of floc formation. In this way a floc can grow in size upon acquiring more fibers. Meanwhile the flocs are progressively broken down under the fluid shearing action. A dynamic equilibrium is established between the growth and breakdown of the flocs. The state of dynamic equilibrium shifts to the direction of higher dispersion with increasing dilution and shear.

The interaction of neutral fibers in a floc is dependent on their distance of separation. In investigations of water-solid interfaces, some workers, especially Derjaguin (XIV-10), hypothesized the existence of a rigid water layer with a shear modulus from 10^{-6} to 10^{-4} dynes/cm.^{2} at a thickness of the order of 10^{-5} cm. The rigidity was attributed to the orientation of polar molecules on the solid surfaces. It was also possible to conceive an "immobile" water layer associated with microscopic roughness of an apparently smooth surface (XIV-11). With such a concept the average distance of separation could be from 10^{-4} to 10^{-6} cm., depending on the surface roughness. In any case a very thin layer of water must adhere to the surface. If the layer consists of only two to three molecules, its thickness would be of the order of 10^{-7} cm.

Once the fibers come into close proximity, further reduction in the distance of separation would necessitate viscous flow of the water in the mobile layer. This is a time-dependent process, the frictional force being inversely proportional to the time of interaction. In view of the possible existence of

a rigid or immobile layer, the magnitude of such forces could be large at short times, or the final distance of separation could be appreciable at a high velocity of approach. From the foregoing discussion of the hydrodynamic factors involved in a floc, it appears that the possible range of separation is somewhere between 10^{-4} and 10^{-7} cm., and the probable average value is of the order of 10^{-5} to 10^{-6} cm.

The attractive forces which tend to hold fibers together are always present. For neutral molecules the Van der Waals-London potential energy of attraction due to the dispersion effect is very nearly proportional to the distance of separation raised to the negative 6th power. The attraction potential between two macroscopic bodies appears to be inversely proportional to the 2nd or 3rd power of separation (XIV-12). Accordingly, the attractive force decreases with the separation to the power -3 or -4. Roughly speaking then, if the distance of separation is 10^{-5} cm., the potential energy of attraction is negligible while at 10^{-6} the attractive forces become appreciable. In light of the previous account for the distance of separation, the attraction between fibers would be, in general, rather small, but could be very large at some points of virtual contact.

Most practical fibers are not neutral. Cellulosic fibers carry weak negative charges in distilled water. The existence of zeta potential and the possibility of increased thickness of the immobile water layer have also been demonstrated (XIV-13). In the presence of ionic compounds certain ions tend to adsorb preferentially onto the fiber surfaces, then a diffuse layer of the opposite ions will be surrounding the fibers. As a result of the ionic interaction, the fibers become strongly repulsive to one another. The electrostatic repulsion is of the exponential nature beginning at a separation of about 10^{-4} cm.

Cellulose fibers possess hydroxyl groups which are polarizable. Consequently, attraction potential due to orientation and induction effects should also be taken into consideration. On the other hand, they are also composed of glucose polymers, the ends of which are soluble in water. If these dissolved ends constituting a part of the fiber surface tend to orient with one another in an orderly manner between approaching fibers, it would mean a decrease in entropy, and therefore would prevent themselves from doing so. This phenomenon may be called the entropic barrier. The entropic repulsion is also of the exponential nature beginning at a separation of about 10^{-5} cm. (XIV-14). Thus, either attraction or repulsion may be reinforced by introducing a suitable polymer which would adsorb on the fiber surfaces, the result depending on the nature of the polymer.

From the above review of the possible mechanisms of floc formation, perhaps only one point has emerged clearly: Fiber flocculation is an extremely complex phenomenon.

FLOC DISPERSION

Aside from the chemical means of preventing fibers from flocculation, the state of dispersion is maintained by shear stress. An initial attempt to describe flocculation would be to establish the size of a floc subject to its stresses. Meyer's approach (XIV-15) to this problem is interesting; a brief account of his analysis follows.

Consider an isolated floc as a porous sphere of fibers suspended in a simple shear field, such as shown in Fig. XIV-1. A rigid sphere will execute a uniform spin about the z axis with the angular velocity ω, which has been shown to be directly proportional to the velocity gradient G in the x-y plane.

If we now boldly assume that flow takes place through a porous floc without causing significant perturbations in the external flow field, the floc, subject to tension and compression, would tend to deform into a prolate ellipsoid. The maximum tensile stress sustained by a floc of radius r_o is estimated to be

$$\sigma_{max} \cong \frac{aG}{4} r_o^2 \qquad \text{(XIV-9)} ,$$

where a is the viscous flow resistance of the floc. Conversely, if we know the tensile strength of a floc, the maximum floc size would be determinable from the velocity gradient and viscous resistance. This approach might lead to an approximate description of the state of flocculation in a turbulent shear field provided the interactions of flocs among themselves and with the flow field would not render the analysis untenable.

XV. RATIONAL ANALYSIS OF TABLE-ROLL SUCTION

The analysis of table-roll suction was initiated by Wrist (XV-1), independently formulated by Taylor (XV-2), and recently extended by Meyer (XV-3) This development, concurrent with the work on filtration by Ingmanson, Han, and Nelson, signaled a new approach to the modern art of sheet forming. It is worthy of a critical review for the simple reason that an appropriate union of t two interdependent factors, suction force and flow resistance, will greatly clarify drainage on the fourdrinier machine.

ORIGINAL CONCEPTION

Wrist's conception of table-roll suction involved only simple physical reasoning. He first assumed that as the wire moves away from the contact with the roll, the two adjacent points remain almost in a vertical line and separate with the velocity xU_w/r_o (Fig. XV-1). If the drainage velocity U_0 is equal to this value, the suction can be calculated as that which would be produced in a cylinder with a porous top by the downward motion of a piston. Assuming that the flow is viscous through the porous medium at constant resistance a_o, the suction would be $a_o U_w x/r_o$.

Wrist's contention would then lead to the prediction that the suction in the table-roll nip should increase indefinitely with x. To explain why th suction stops increasing, he proceeded to make a second assumption that it ceas to increase at the point at which the inertia of a stream moving at U_w reache atmospheric pressure against an adverse pressure gradient. This assumption would predict the existence of a maximum suction equal to $\rho U_w^2/2$, which would occur at $x = (1/2) r_o \rho U_w/a_o$.

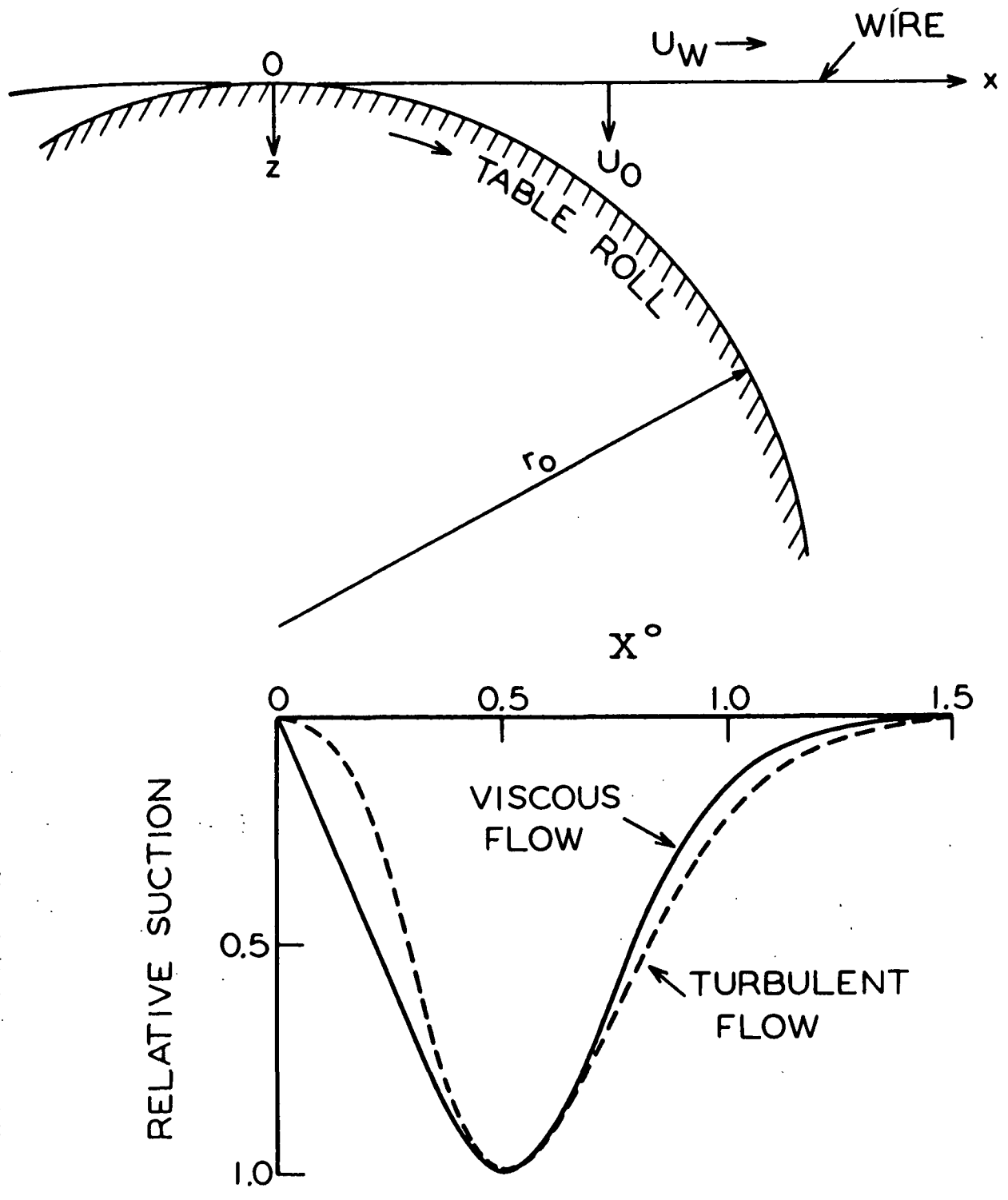

Figure XV-1. A Diagram of Table-Roll Suction

The two assumptions are incompatible with each other, as pointed out Taylor. The first implies no lateral pressure gradient in the nip while the second affirms the existence of such a gradient except at the point of the maxi suction. In spite of this inconsistency, Wrist's work has cleared away the previous misconceptions and led to a rational analysis of the table-roll action.

According to Wrist's simple theory, the drainage (volumetric flow rate per unit width is equal to $(1/8)\underline{r_o^2}\rho^2\underline{U_w^3}/\underline{a_o^2}$ from zero to maximum suction.

HYDRODYNAMIC ANALYSIS

Referring to Fig. XV-1, Taylor began his analysis with the contention that the pressure at any point in the nip varies with $\underline{x}$ only, the small variation with respect to $\underline{z}$ being ignored. In general, the drainage velocity is a function of the suction:

$$U_o = f(p_o) , \quad p_o = p_a - p \qquad (XV-1) ,$$

where $\underline{p_o}$ is the suction which is the difference between the atmospheric pressu $\underline{p_a}$ and the hydrostatic pressure $\underline{p}$.

If there is no mixing of the water in the nip, the variation of the velocity and pressure along a streamline such as $\underline{x} - \underline{x^o}$ follows the Bernoulli law:

$$p_o^o - p_o = \tfrac{1}{2}\rho[(u_x^o)^2 - U_w^2] \qquad (XV-2) .$$

For a stream with unit width and depth $\underline{dz}$, the condition of continuity require

$$U_o dx = u_x^o dz \qquad (XV-3) .$$

The combination of the last two equations results in

$$U_0 dx = [U_w^2 + \frac{2}{\rho}(p_0^0 - p_0)]^{1/2} dz \qquad \text{(XV-4)} .$$

A further condition which must be satisfied is that the nip is completely filled with water. Since the nip is narrow, its depth may be taken as

$$z^0 \cong \frac{(x^0)^2}{2r_0} = \int_0^{z^0} dz \qquad \text{(XV-5)} ,$$

and the condition of complete filling may be expressed as

$$\frac{(x^0)^2}{2r_0} = \int_0^{x^0} \frac{U_0 dx}{[U_w^2 + \frac{2}{\rho}(p_0^0 - p_0)]^{1/2}} \qquad \text{(XV-6)} .$$

In the case of viscous flow through the mat and the wire, the drainage is assumed to be proportional to the suction:

$$p_0 = a_0 U_0 \qquad \text{(XV-7)} .$$

Then Equation (XV-6) at constant a_0 becomes

$$\left[\frac{a_0 x^0}{r_0 \rho U_w}\right]^2 = \int_0^{x^0} \frac{[p_0/(\frac{1}{2}\rho U_w^2)][a_0/(r_0 \rho U_w)dx]}{[U_w^2 + \frac{2}{\rho} p_0^0 - \frac{2}{\rho} p_0]^{1/2}/U_w} \qquad \text{(XV-8)} ,$$

which has been rendered to the dimensionless form:

$$(X^0)^2 = \int_0^{X^0} \frac{P_0}{[1 + P_0^0 - P_0]^{1/2}} dX \qquad \text{(XV-9)} .$$

In the other extreme of turbulent flow through the mat-wire system, the drainage is assumed to be proportional to the square root of the suction:

$$p_o = b_o U_o^2 \qquad \text{(XV-10)} .$$

If b_o remains constant, Equation (XV-6) may be similarly expressed in the dimensionless form:

$$(X^o)^2 = \int_o^{X^o} \left[\frac{P_o}{1 + P_o^o - P_o} \right]^{1/2} dX \qquad \text{(XV-11)} ,$$

in which P_o and P_o^o remain as before, and

$$X^o = \frac{x^o}{r_o} \sqrt{\frac{b_o}{2\rho}} , \qquad X = \frac{x}{r_o} \sqrt{\frac{b_o}{2\rho}} \qquad \text{(XV-12)} .$$

The solutions of Equations (XV-9) and (XV-11) under the boundary conditions: $p_o^o = 0$, at $x^o = 0$ and $p_o^o = 0$, as $x^o \to \infty$, were given by Miller (XV-4). The general shape of the suction distribution curves are similar for both cases, as sketched in Fig. XV-1. They reach the maximum value $\rho U_w^2/2$ at $X^o = 1/2$ a fall to practically zero at $X^o = 1.5$. The suction is always higher for viscous drainage than that for turbulent drainage prior to the maximum. The reverse is true after the maximum.

The drainage per unit width for the viscous case is

$$q_o = \int_o^\infty U_o dx = \frac{1}{a_o} \left(\frac{1}{2} \rho U_w^2\right) \left(\frac{r_o \rho U_w^2}{a_o}\right) \int_o^\infty X^o dX^o \qquad \text{(XV-13)} .$$

Integrating numerically with Miller's values, the result was found to be $0.295 r_o \rho^2 U_w^3 / a_o^2$.

Taylor also analyzed the case of complete mixing by turbulence in the nip without surface friction. For viscous drainage he concluded that the maximum suction will increase by a factor of 1.4 over the nonmixing case.

Bergström (XV-5) dealt with wire wrapping around the roll. He concluded, on the basis of Taylor's theory, that the suction profile would have the same general bell shape with the identical maximum suction but a narrower spread, as a result of the change in the nip geometry. He further demonstrated that increasing drainage resistance along the nip would still produce similar suction profiles, again with a narrowing spread compared with that for constant resistance.

POSSIBLE EXTENSION

Meyer extended Taylor's analysis to include both viscous and inertial effects in the nip. He treated the flow as two-dimensional ($\underline{x}$,$\underline{z}$) and showed that the boundary-layer equations apply. For viscous flow through the mat and wire, he arrived at the drainage equation

$$q_o = (r_o \rho^2 U_w^3 / a_o^2) f\left[\frac{U_w - U_R}{U_w}, \left(\frac{\rho U_w}{a_o}\right)^3 \left(\frac{2 r_o \rho U_w}{\mu}\right)\right] . \qquad \text{(XV-14)} .$$

The first parameter in the function represents the effect of the differential wire-roll speed. For a foil, $\underline{U}_R = 0$. For a table roll without slipping, $\underline{U}_R = \underline{U}_w$. In both cases this parameter becomes inconsequential. The second parameter accounts for the combined effects of the mat resistance and the flow pattern in the nip. Meyer's contention is that the second parameter will account for a maximum suction different from Taylor's constant value ($\rho \underline{U}_w / 2$) due to the additional energy loss in the nip.

XVI. EXPLORATORY DISCUSSION OF TWO-WIRE FORMING

High-consistency and symmetrical drainage are desirable features of two-wire forming for high-speed machines. In view of its future importance, we have made a preliminary analysis of two-wire formers, based on the filtration theory. The following is a brief summary of Meyer's recent work (XVI-1), which is subject to experimental verification and further modification. A schematic diagram of two possible wire arrangements is shown in Fig. XVI-1.

CONSTANT PRESSURE

The top sketch in Fig. XVI-1 shows a hypothetical forming zone between two stationary symmetrical straight wires converging at small angles θ. For viscous flow of a pure fluid at constant resistance a_o maintained at a constant external pressure p_o, the internal pressure p_i and the drainage velocity U_O would remain constant along the forming zone:

$$U_O = U_o \sin\theta = \frac{p_i - p_o}{a_o} \qquad \text{(XVI-1)}$$

and

$$p_i + \frac{1}{2}\rho U_o^2 \cong \text{constant} \qquad \text{(XVI-2)},$$

where U_o is jet velocity.

Accordingly, as shown in the bottom sketch, for wires moving at the horizontal velocity U_w equal to U_o the angle θ must decrease in order to accommodate increasing web thickness at constant pressure for an incompressible material:

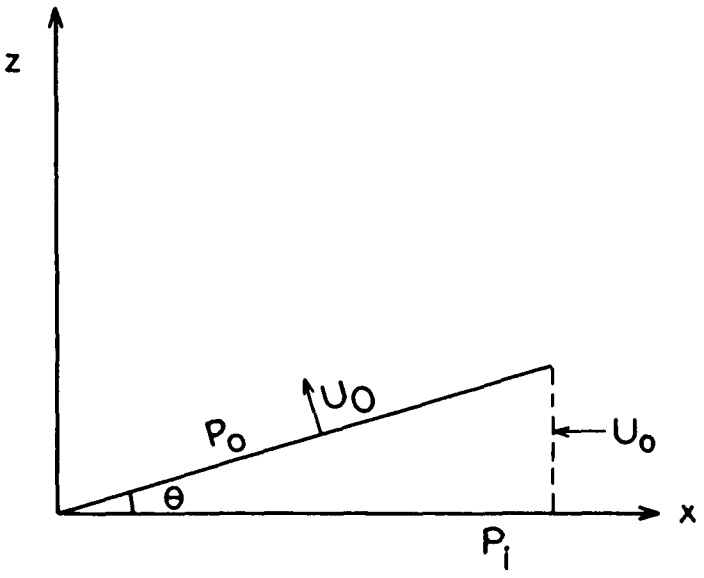

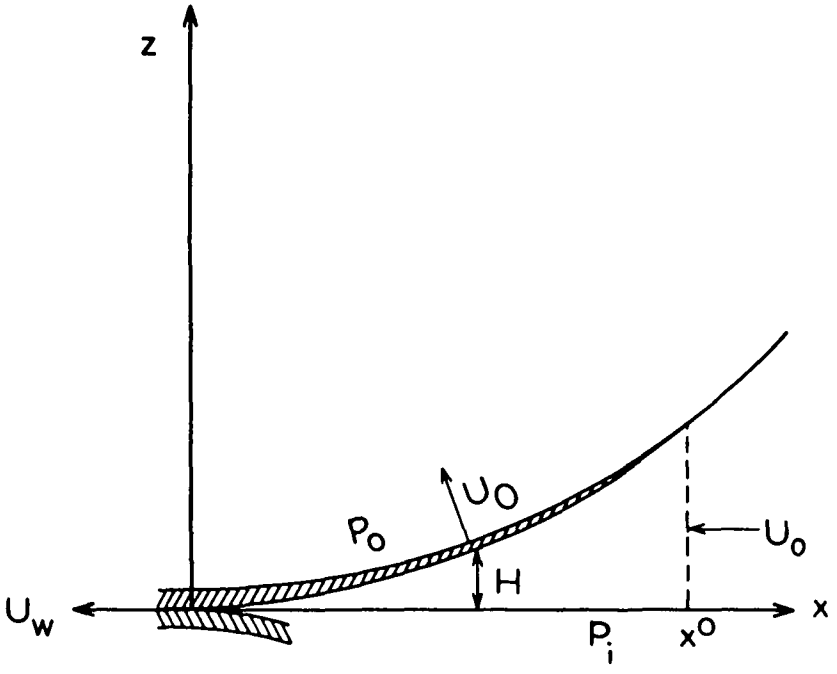

Figure XVI-1. Diagrams of Symmetrical Two-Wire Forming Zone

$$p_i - p_o = aLU_w \sin\theta = \mu R_t U_o \qquad \text{(XVI-3)} .$$

By a simple fiber balance the basis weight may be calculated from

$$W = \rho s \int_o^t U_o dt = \frac{c_o}{U_w} \int_x^{x^o} U_o dx \qquad \text{(XVI-4)} .$$

Assuming no fiber-wire interaction and a constant wire resistance R_w, we have

$$\Delta p = \mu(R_w + RW)U_o = \mu\left(R_w U_o + \frac{c_o R U_o}{U_w} \int_x^{x^o} U_o dx\right) \qquad \text{(XVI-5)} ,$$

which may be solved to yield the drainage velocity:

$$U_o = \frac{\Delta p}{\mu R_w}\left[1 + \frac{2c_o R \Delta p}{\mu R_w^2 U_w}(x^o - x)\right]^{-1/2} \qquad \text{(XVI-6)} ,$$

where x^o is the forming length for the desired final basis weight W_f as

$$x^o = [(1 + RW_f/R_w)^2 - 1]/[2c_o R\Delta p/(\mu R_w^2 U_w)] \qquad \text{(XVI-7)} .$$

The contour of the wires follows the equation:

$$H = \frac{U_w}{\mu R c_o}\left\{\left[1 + \frac{2c_o R \Delta p x^o}{\mu R_w^2 U_w}\right]^{1/2} - \left[1 + \frac{2c_o R \Delta p}{\mu R_w^2 U_w}(x^o - x)\right]^{1/2}\right\} \qquad \text{(XVI-8)} .$$

From this analysis the major conclusion is that the approach flow will remain uniform at constant pressure provided the wires are symmetrically convex shaped. However, the wire contour will have to change with operating conditions in order to insure satisfactory formation.

VARYING PRESSURE

If straight symmetrical, rigidly supported wires are used, the internal pressure will change at constant external pressure. Assuming again viscous flow at constant wire and specific resistance, the filtration equations may be solved for θ and $\underline{x}^{o}$. In this case, adjustment of these two geometric factors of the forming zone together with applied suction would accommodate a range of operating conditions provided the internal pressure rise would not cause serious difficulties in mechanical operation and sheet formation. Furthermore, this concept is also applicable to compressible mats. It can be shown that the internal pressure would rise to a maximum and then fall to the initial value. The drainage would be less than the constant-pressure case at the same maximum pressure for the same forming length.

"How sound a theory actually is can be shown by experience alone. To b subject to mathematical analysis, practically any problem in fluid motion must be idealized to some extent, but it is experience which limits the assumptions of the theorist to those which are physically reasonable rather than merely mathematicall convenient. In problems not too far afield from others already solved, prior experience is often sufficient. Wholly new problems, on the other hand, may well require new experience, else unguided simplifications will very likely lead to physically impossible conclusions. Mathematical analyses, in other words, must not only be limited to realistic hypotheses but must ultimately be subjected to experimental verification."

(Rouse, Hunter, Ed., Advanced mechanics of fluids.
Chap. I. p. 3. New York, John Wiley & Sons, 1959

PART TWO

EXPERIMENTS AND RESULTS

XVII. MAT COMPRESSIBILITY BY STATIC COMPRESSION

The behavior of a fiber mat in response to compressive stresses is far from being a simple phenomenon because of the complex structure of the mat and the viscoelastic nature of most fibers. The experimental studies of Ingmanson (III-9), Wilder (III-10), Jones (XVII-1), and Elias (XVII-2) have clarified a number of important points, but many questions remain to be answered.

In review of the static compressibility experiments we restrict the systems to the unbonded wet state under a uniformly applied load. Our primary purpose is to establish the compressibility functions introduced in Part One. We also attempt to explain some of the underlying factors so far as our present understanding permits.

COMPRESSIBILITY TESTS

A rather elaborate device was used by Wilder and Jones in their experiments, as shown in Fig. XVII-1. The major features of the apparatus are (1) forming a uniform mat, (2) minimizing the edge effects, (3) applying a steady load, and (4) providing a swift and precise measurement of the mat thickness.

A uniform mat is formed on a septum from a very dilute and well-dispersed fiber suspension at a slow constant rate. The forming method will be described in detail in a subsequent chapter. To minimize edge effects the mat is made relatively large (3 to 5 in. diameter) and kept unconfined by removing the forming tube and trimming the mat circumference if necessary. The steady application of a load is achieved by means of a movable piston guided in its downward travel and counterbalanced by a weight; additional weights are then gently placed on the piston. The initial mat thickness is measured with a

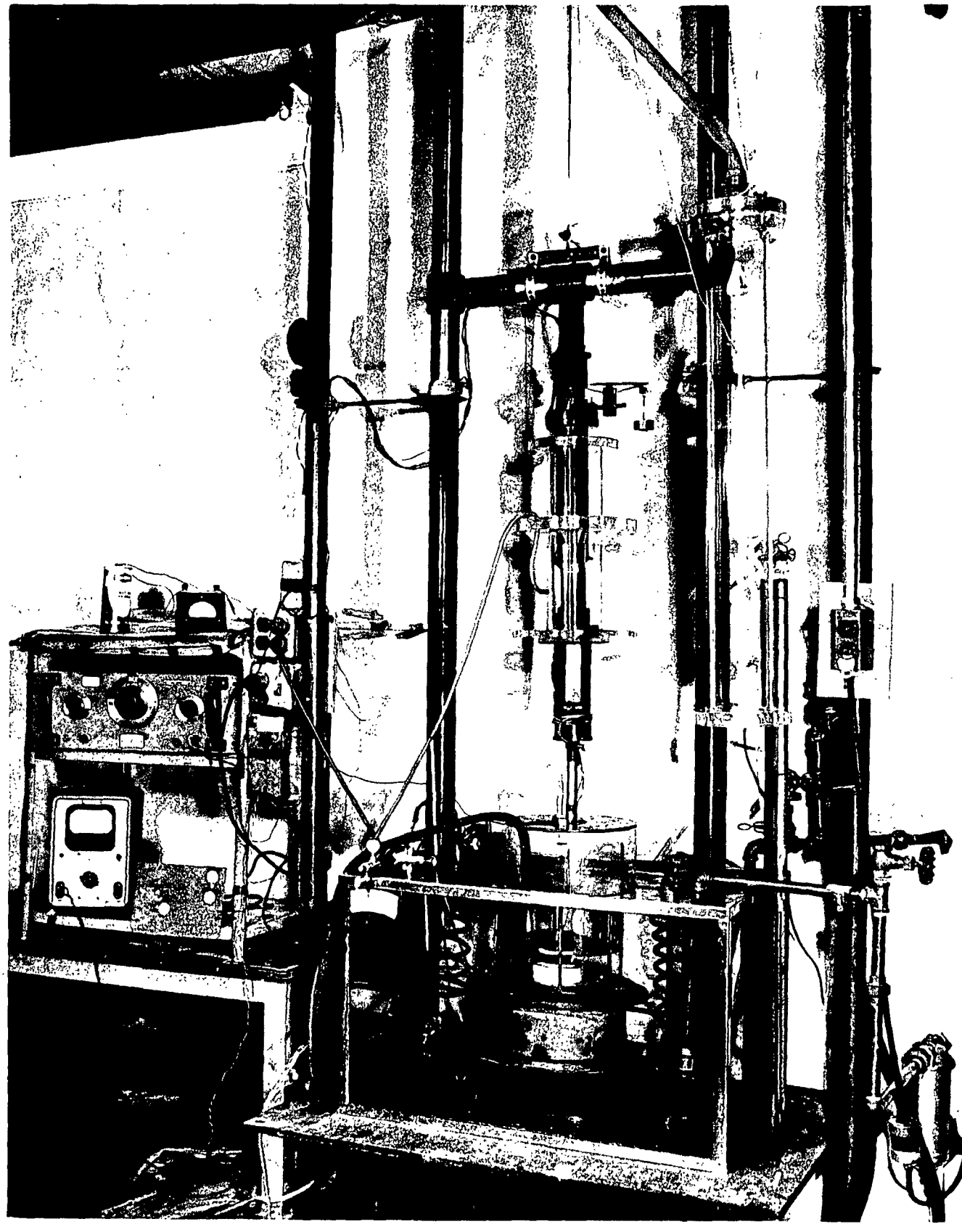

Figure XVII-1. Compressibility Apparatus

cathetometer or a dial micrometer and the change of thickness with a linear variable differential transformer in conjunction with an audio oscillator and a vacuum tube voltmeter. With such apparatus data may be obtained for compression and recovery, as well as creep and recovery.

GENERAL BEHAVIOR

The complex response of a fiber mat to compression and recovery is illustrated in Fig. XVII-2, taken from Jones' study. These data are for loblolly pine summerwood pulp, prepared by the kraft process, bleached to 0.3% residual lignin, and classified for the removal of fines. In the log-log plot the first-compression data of mat density vs. applied pressure for a freshly formed mat under successively increasing loads may be divided into linear and curved regions. The linear region extends upward from approximately 10 g./sq. cm. in applied pressure. Toward lower pressures the data tend to curve with diminishing slopes. It is also to be noted that two sets of the first-compression data taken at two different time intervals (5 and 15 min.) under identical loads have closely the same slopes, but slightly different positions, in the entire experimental range. The gradual change of deformation in response to compression with respect to time at constant load is called "creep."

At any time during the first compression, if the load is decreased, the mat loosens, but never recovers to the full extent corresponding to the original lower compression. The recovery, which is also time dependent, proceeds with further decrease of load. At a certain point of recovery, if the mat is subjected to compression again, the deformation in the second compression will be less than that of the first. Thus, the compression-recovery cycles exhibit hysteresis. The portion of data indicated in the figure represents the sixth cycle.

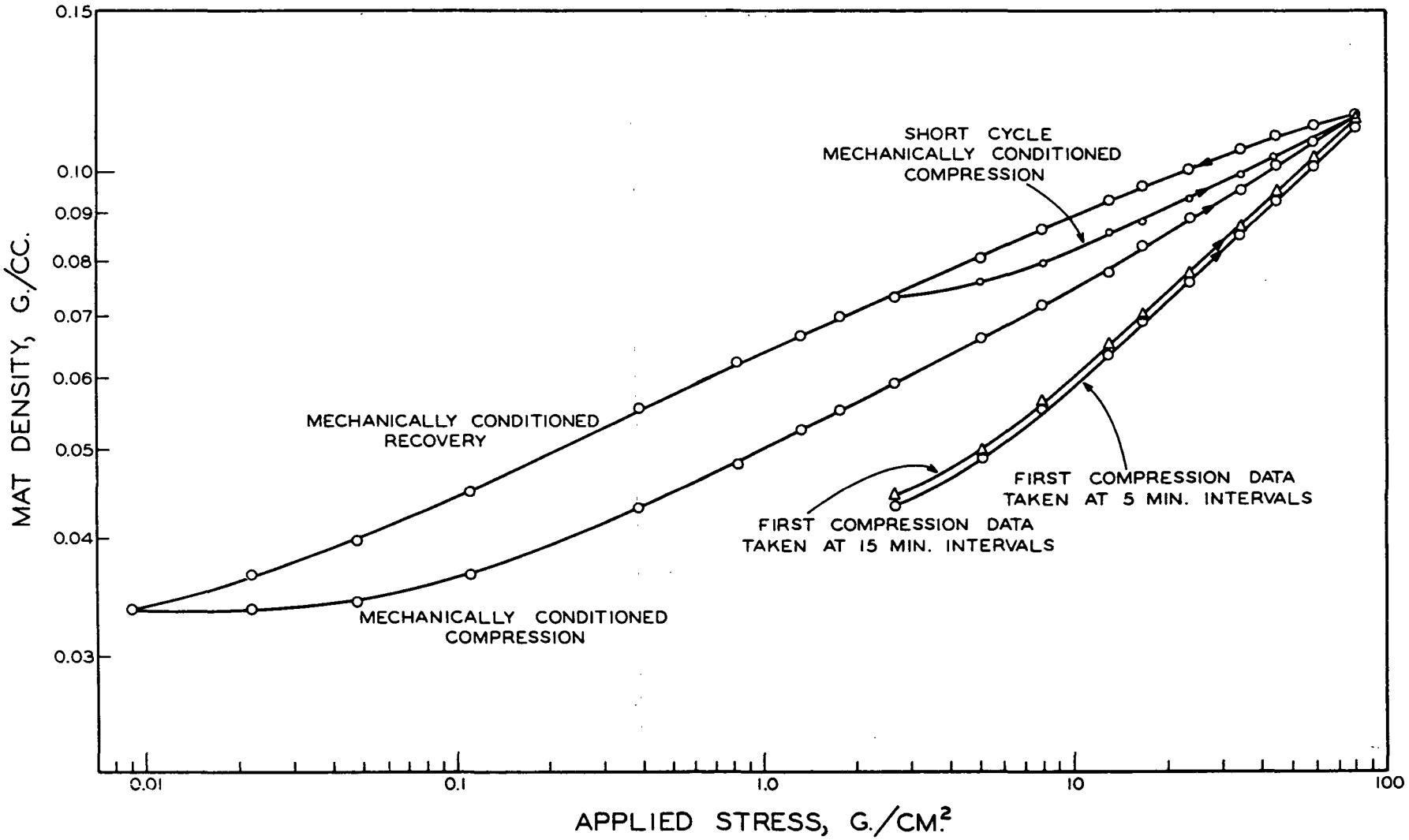
0.15
0.10
0.09
0.08
0.07
0.06
0.05
0.04
0.03
MAT DENSITY, G./CC.
SHORT CYCLE
MECHANICALLY CONDITIONED
COMPRESSION
MECHANICALLY CONDITIONED
RECOVERY
FIRST COMPRESSION DATA
TAKEN AT 5 MIN. INTERVALS
FIRST COMPRESSION DATA
TAKEN AT 15 MIN. INTERVALS
MECHANICALLY CONDITIONED
COMPRESSION
0.01
0.1
1.0
10
100
APPLIED STRESS, G./CM.²

To clarify some of these and other complications, supporting experimental evidence will be cited.

POWER FUNCTION

The linear region of first-compression data may be represented by a power function:

$$c = (1 - \epsilon)/v = Mp_f^N \qquad \text{(XVII-1)},$$

where p_f is understood to be the applied pressure. The swollen specific volume is defined as

$$v = \frac{V_f + V}{V_f \rho_f} \qquad \text{(XVII-2)},$$

V_f and V being the volumes of dry fiber and fluid, respectively. For solid fibers v is simply the reciprocal of the pycnometric density, ρ_f.

The lower limit of p_f in such experiments is related to the maximum fluid drag forces, Δp, attained in forming the mat. The larger the final fluid stresses, the higher will be the lower limit of the power function. On the other hand, the upper limit appears to be indefinite; its value is as high as the applied pressures of the known experiments have reached.

Jones' data for cylindrical fibers (nylon, dacron, and glass) indicated clearly that both M and N increase with the axis (length-diameter) ratio until a "critical" value is reached, beyond which they remain practically constant. The critical value for nylon is about 100 and for glass about 500. The difference between the two fibers appears to be attributable, at least, to the modulus of elasticity and interfiber friction. The first factor has to do with reversible

and the second with irreversible effects on compressibility. For the time bei we shall confine our attention to the systems above their critical axis ratios further clarification of the compressibility constants.

The dependence of compressibility on modulus of elasticity is demonstrated in Wilder's equation (VI-14), which may be grossly simplified to

$$c \propto \left[\frac{\rho_f^5}{E} p_f\right]^{1/(4\gamma_0 - 1)} \qquad \text{(XVII-3)}$$

If γ_0 is 3/2, $\underline{N}$ will be 1/5, and $\underline{M}$ will be directly proportional to ρ_f and inversely proportional to $\underline{E}^{1/5}$. Jones' data are summarized in Table XVII-1.

TABLE XVII-1

DATA FOR CYLINDRICAL FIBERS

Fiber	ρ_f, g./cc.	d_f, microns	E, g./sq. cm. x 10^{-7}	N
Nylon	1.14	16.8-46.2	0.31-1.33	0.20
Dacron	1.39	22.7	14.7	0.25
Glass	2.56	5.1-12.9	74.4-103	0.26

When the experimental values of $\underline{M}$ for all these fibers are adjuste to the nylon density by direct proportionality, they correlate with the moduli of elasticity as

$$M \propto \left(\frac{1}{E}\right)^{0.24} \qquad \text{(XVII-4)}$$

It is to be noted that both theoretically and experimentally, fiber diameter does not appear to be explicitly involved in compressibility. In Wilder's development the diameter comes into play in both contact points and moment of inertia in the opposite way, and its effects are cancelled out. Jones' results seem to support this implication. The value of $\underline{N}$ being less than 1/3 or γ_o being greater than unity is somewhat puzzling from the viewpoint of the current theory (Chapter VI).

The power function may also be developed in other manners. By dimensional analysis one may arrive at

$$\frac{c}{\rho_f} \propto \left(\frac{L_f}{d_f}\right)^{N_b}\left(\frac{p_f}{E}\right)^{N} \qquad \text{(XVII-5)} .$$

Above the critical axis ratio, $N_b = 0$, and $\underline{M} \propto \rho_f/\underline{E}^{N}$, as assumed before. From bulk modulus considerations Wrist (XVII-3) proposed the following expression:

$$\frac{c}{c_o} = \left(\frac{p_f}{p_{f,o}}\right)^{N} \qquad \text{(XVII-6)} ,$$

where c_o is the mat density at the reference pressure $p_{f,o}$. By his contention, the modulus of elasticity, but not the density, is implicated in $\underline{M}$.

Mechanical conditioning involving compression-recovery cycles removes a part of the irreversible effects in mat response to further compression. According to Jones, the nonrecoverable deformation (hysteresis) arises primarily from repositioning of the fibers due to slippage. The hysteresis loop becomes narrower and narrower for each subsequent cycle. After a number of cycles, the mat is said to be mechanically conditioned. When this state is reached, the response to further compression becomes stabilized although there remains

partial recovery or minor hysteresis. Disregarding the more complicated proble of recovery, the high-pressure region for mechanically conditioned compression may still be represented by the simple power function. Its slope is smaller, while its position is higher, than in the corresponding case of the first compression. From Jones' data for the same fibers:

$$M \propto \left(\frac{1}{E}\right)^{0.21} \qquad \text{(XVII-7)} .$$

THREE-PARAMETER MODELS

To extend the correlation to the curved region, it is necessary to incorporate a third parameter in the compressibility function. A logical choic is to introduce the quantity c_o . In both Ingmanson's form,

$$c - c_o = Mp_f^N \qquad \text{(III-8)} ,$$

and Wilder's form,

$$c^\gamma - c_o^\gamma = M_o p_f \qquad \text{(III-9)} ,$$

c_o is meant to be the mat density at zero applied load. The value of c_o , however, has not yet been precisely determined. Since mat density involves fiber density or specific volume, a more appropriate quantity to use for the purpose of comparison is solid fraction $(1 - \epsilon)$. Ingmanson estimated a value of solid fraction to be about 0.02 for an expanded wood fiber mat formed at a lo pressure drop of the order of one cm. of water. The value from Elias' work on glass fiber mats was also about 0.02. Wilder obtained a value of 0.04 from his creep data for wood fiber mats. Using the fiber sedimentation technique, Jones arrived at the value 0.04 for glass fiber mats, corrected for the compressive

stress due to the weight of the fibers themselves. This value is also in rough agreement with that extrapolated approximately from his first-compression data.

In view of the apparent uncertainty, we merely consider c_o as an adjustable parameter and proceed to compare the above two forms of compressibility functions by statistical correlation of some selected data of Jones. The data quoted in Table XVII-2 are for mechanically conditioned mats of glass fibers and kraft pulp. By using a linear least-squares-regression technique the appropriate values of the slope and intercept of the lines plotted from the data may be determined by assigning a series of values for the exponents N and γ. If the lowest point is excluded in each case, the correlation is excellent for either compressibility function. However, deviations in the low range are also apparent, as shown in Fig. XVII-3 and XVII-4. It appears that Wilder's form is slightly superior to Ingmanson's at very low loads. There is no significance in the extrapolated values of c_o in these correlations.

COMPLICATING EFFECTS

Most fibers are viscoelastic in nature. Their response to stress is time dependent. The creep of wood fiber mats in compression was first reported in (III-9). These data indicated a linear relationship between mat density and logarithm of time over a range of 20 sec. to 25 min. Wilder established that for both first compression and mechanically conditioned compression, as well as recovery from compression, his data may be correlated by incorporating the time effect as follows:

$$c - c_o = (M_1 + M_2 \log t)p_f^N \qquad \text{(XVII-8)}.$$

This represents a four-parameter model applicable to times as short as 10^{-1} sec.

TABLE XVII-2

MECHANICALLY CONDITIONED COMPRESSIBILITY DATA

Glass fibers: d_f = 12.9 microns; L_f = 6.3 mm.;
ρ_f = 2.37 g./cc.; E = 74.4 x 10^9 g./sq. cm.

Kraft pulp: d_f = 43.6 microns; L_f = 2.8 mm.;
v = 3.5 cc./g.

Glass Fiber Mat		Kraft Pulp Mat	
p_f, g./sq. cm.	c, g./cc.	p_f, g./sq. cm.	c, g./cc.
0.385	0.0439	0.043	0.0341
0.824	0.0497	0.106	0.0364
1.32	0.0542	0.385	0.0432
1.77	0.0575	0.824	0.0486
2.69	0.0627	1.32	0.0526
5.04	0.0725	1.77	0.0554
7.94	0.0805	2.69	0.0594
13.0	0.0890	5.04	0.0662
16.8	0.0947	7.94	0.0721
23.5	0.1014	13.0	0.0793
34.3	0.1095	16.8	0.0833
45.4	0.1156	23.5	0.0894
59.5	0.1219	34.3	0.0966
80.2	0.1293	45.4	0.1024
		59.5	0.1086
		80.2	0.1162

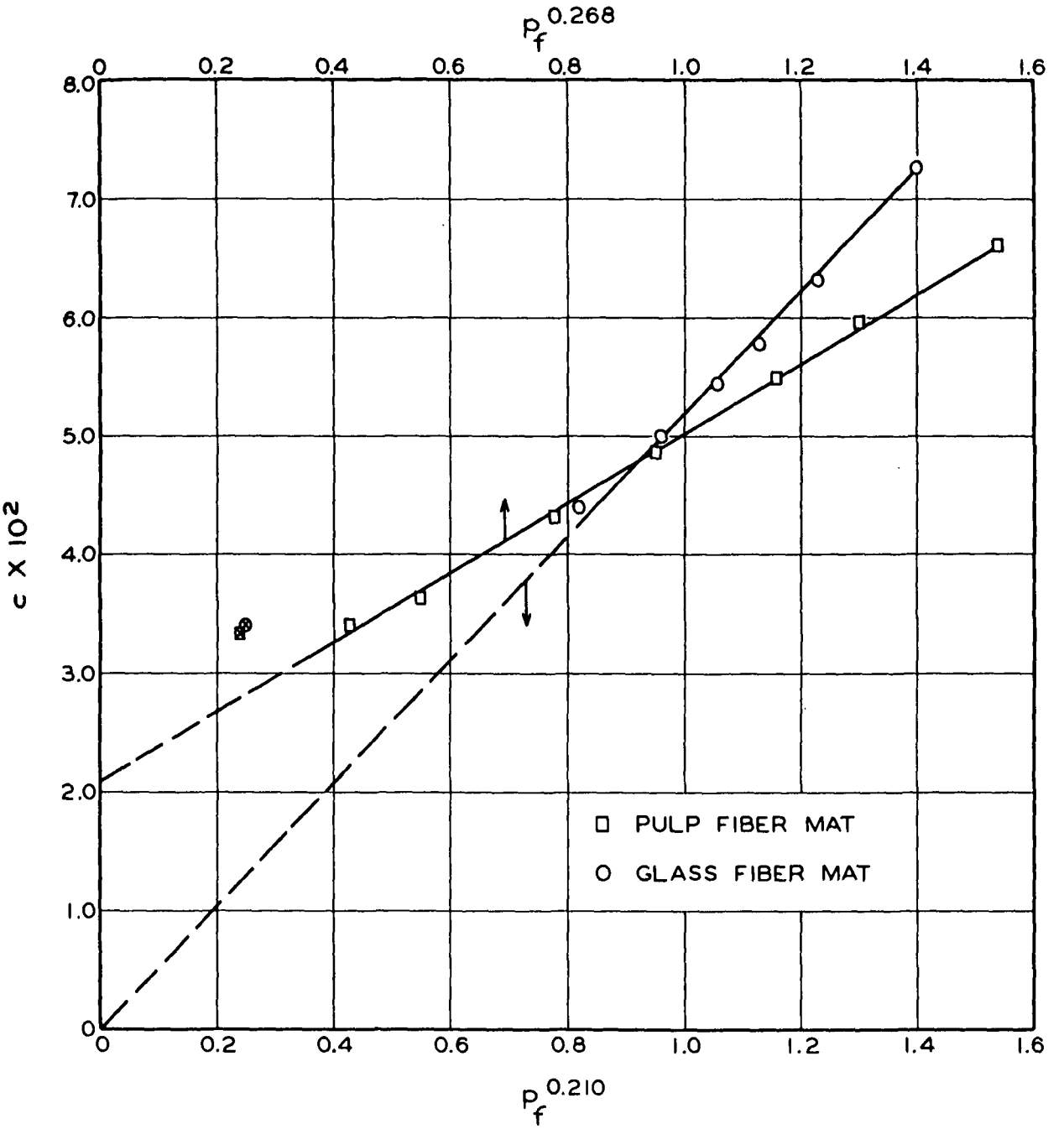

Figure XVII-3. Test of Ingmanson's Compressibility Function

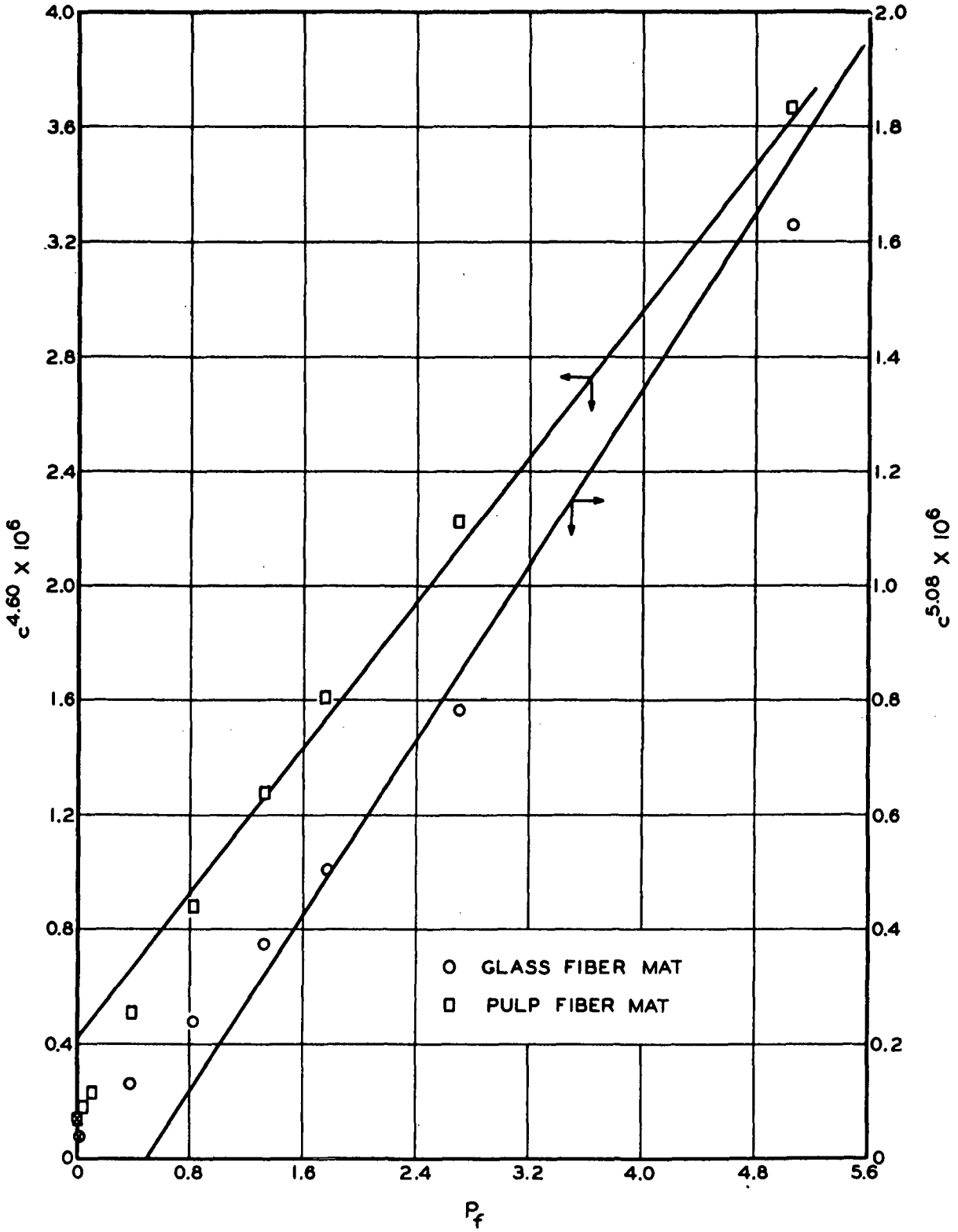

Figure XVII-4. Test of Wilder's Compressibility Function

Rapid cycles of pressures, such as vibrations, produce a more compressed mat. This effect has been observed in static compressibility tests, the vibrations arising from a pump used in forming the mat. Figure XVII-5 reveals the marked difference in the first-compression response of kraft pulp mats under normal conditions and under vibrations.

When a mat is formed in a filtration tube, the fibers close to the wall tend to drag themselves along the wall in their downward flow, resulting in some orientations with the z direction around the circumference of the formed mat. The more rigid and the higher surface friction of the fibers such as glass fibers, the more pronounced is this edge effect. With more flexible fibers such as nylon and cellulosic fibers, the edge effect is not critical provided the mat is sufficiently large and thick. For most compressibility tests a well-formed mat 3 in. in diameter and 1/4 in. thick is adequate.

Since friction is involved in the edge effect during compression, the surface of the confining tube in a compressibility tester may also influence the test results. With certain pulps such discrepancies between Lucite and brass have been detected. Aside from its surface characteristics, Lucite or Plexiglas being transparent, is preferred to brass as a material for the confining tube. The clearance between the tube and the piston should be about 0.0025 to 0.005 in. Too little or too much clearance may incur difficulties in piston operation or cause edge effects.

We have formed mats from relatively high-consistency suspensions (up to 0.5%) in the compression tube by simply stirring the suspension until it is well dispersed and letting the fibers settle under gravity. A permeable piston is then lowered smoothly and slowly in the tube till the settled fibers are compressed into

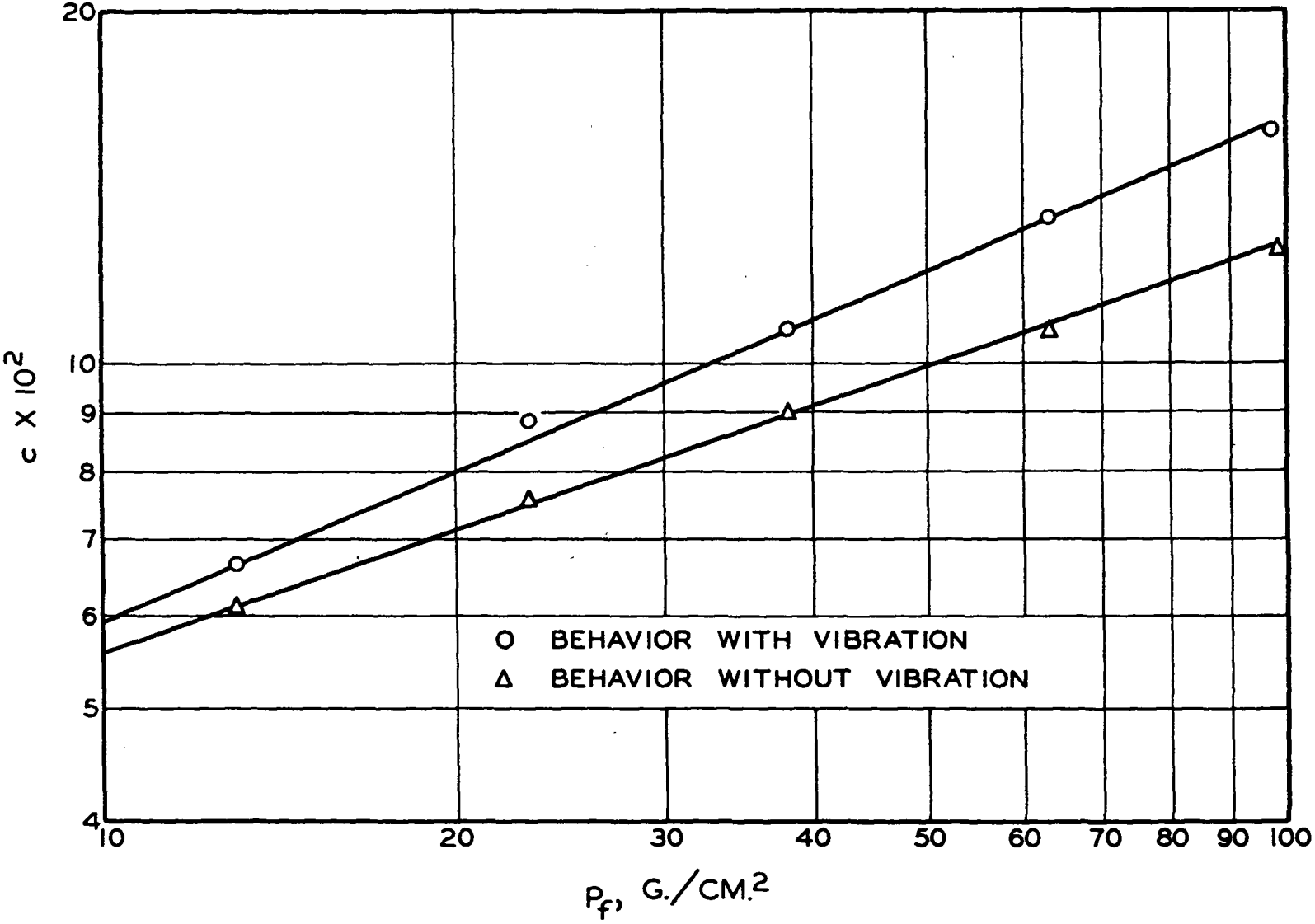
20
10
9
8
7
6
5
4
c X 10²
10
20
30
40
50
60
70
80
90
100
P_f, G./CM.²
O BEHAVIOR WITH VIBRATION
Δ BEHAVIOR WITHOUT VIBRATION

a high-porosity mat. In this way we avoid the possible hysteresis involved in the time-consuming method of mat forming by slow filtration of a dilute suspension. For all practical purposes the compressibility results by the settling method are the same as by the filtration method.

As mentioned before, Jones found the change of compression response below the critical fiber axis ratio. In general, the lower the modulus of elasticity, the lower is the critical ratio. However, this ratio is also dependent on fiber repositioning. By means of his ingenious apparatus (Fig. XVII-6), Elias observed the existence of z orientations of glass fibers in a newly formed mat and the effect of such orientations on the mat compression behavior. As the axis ratio decreased, the average z orientation increased. This effect became very pronounced below the axis ratio 250 and was appreciable even at 500. Compaction of the mat reduced the z orientation of the fibers. He concluded that the segment length at a given solid fraction increased as the mean z orientation of the fibers decreased, in agreement with the Onogi-Sasaguri theory. Elias also found that the interfiber friction had an appreciable effect on the compression response, in accord with Jones' findings. Low friction increased compressibility.

Wood pulps generally exhibit slopes or N values higher than 1/3. It has been suggested that this fact may be partially due to fiber curl. Such a view seems to be supported by Jones' results of a compressibility test on curled nylon fibers. As shown in Fig. XVII-7, they have larger slopes than straight nylon fibers. The higher values of N may be a consequence of z orientations.

THIN MATS

The compressibility measurements for thin mats involved considerably more difficulties than for thick ones. Most of these experimental problems were solved

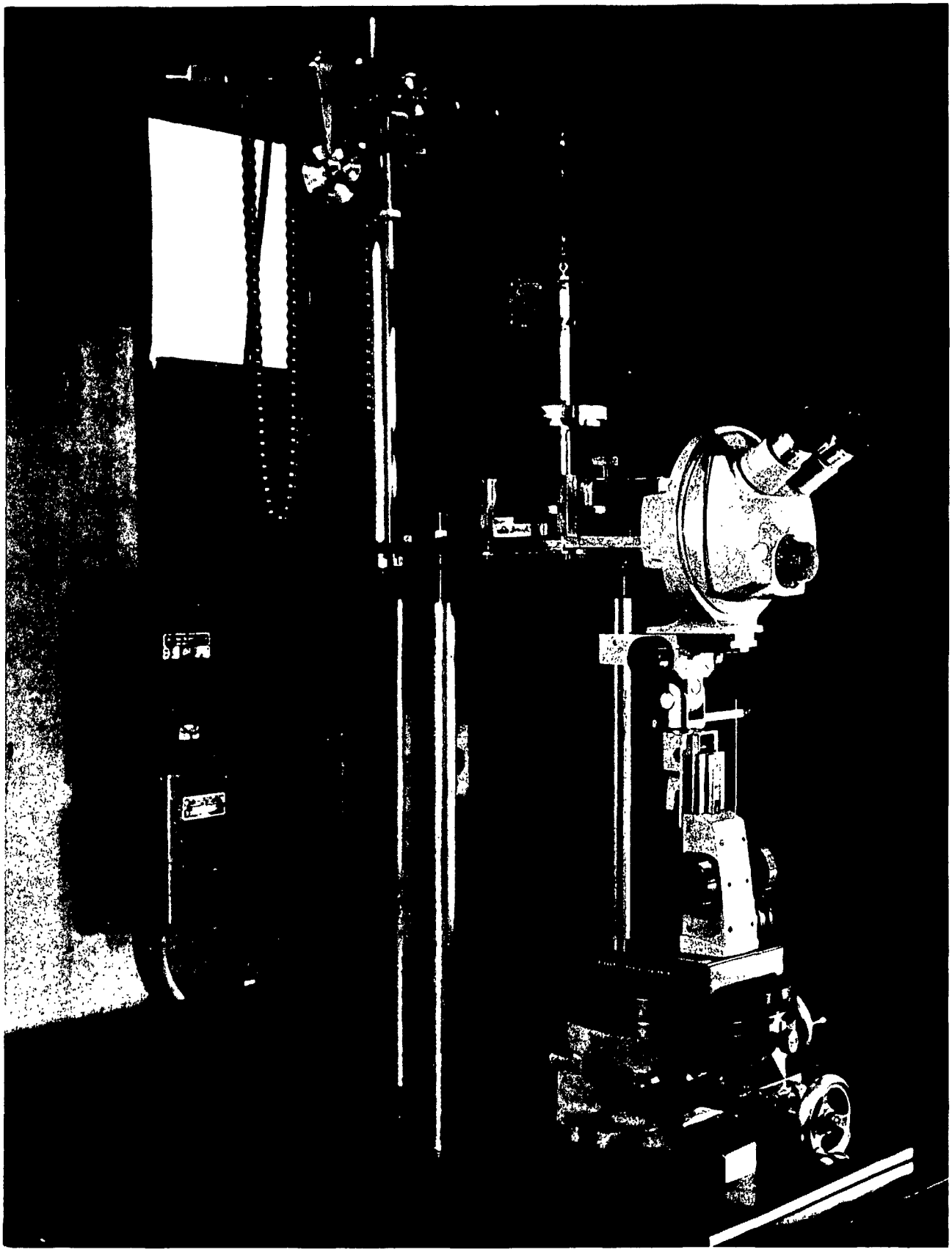

Figure XVII-6. Apparatus for Observation of Fiber Orientations Under Compression

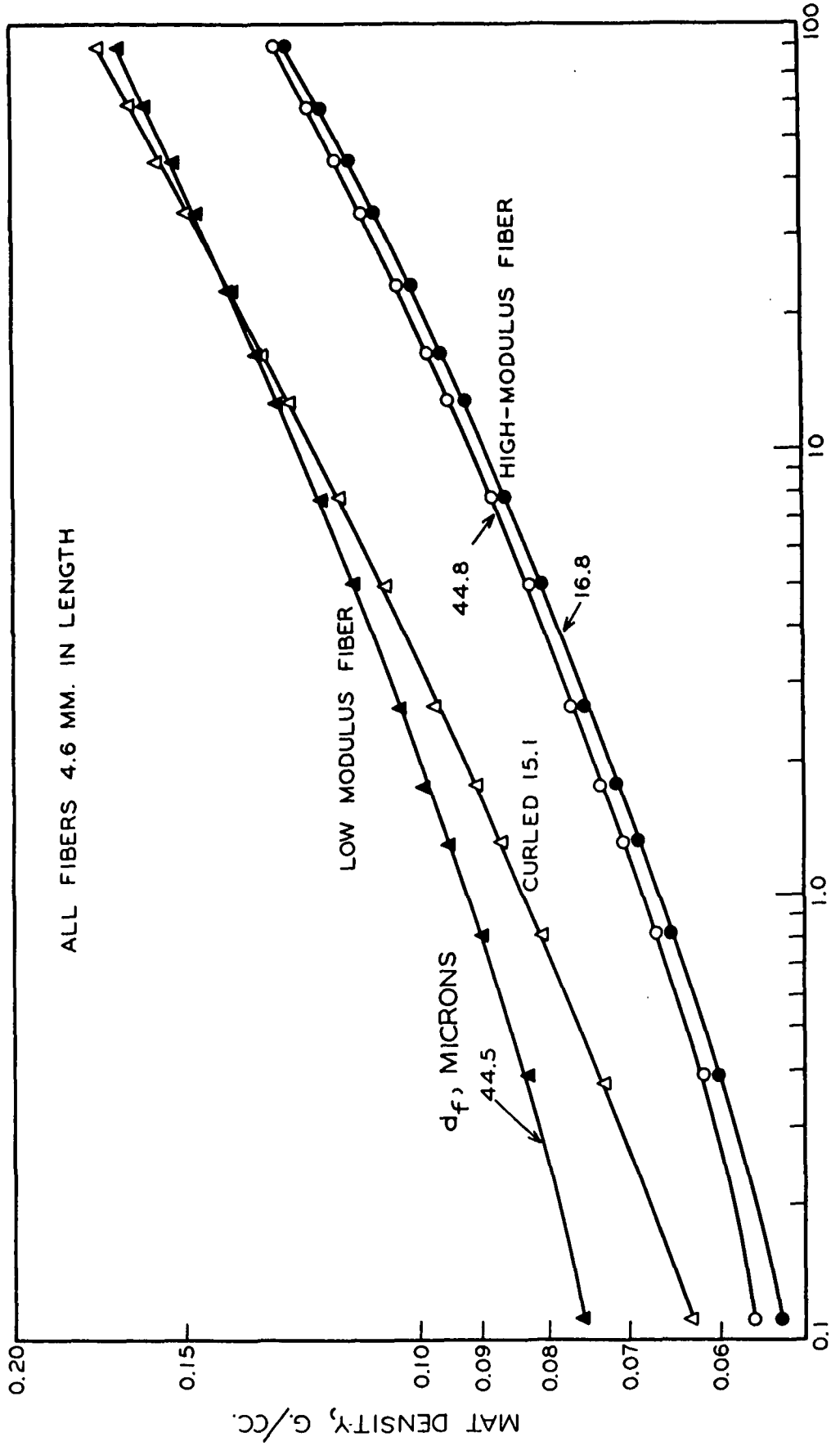

Figure XVII-7. Effect of Fiber Curl on Compressibility

by Chang (XVII-4). The mats were formed by the filtration method without using a pump to avoid vibrations. To facilitate transfer of the mats to the compressi bility apparatus, the septum of the filtration tube was covered by a piece of tea-bag tissue. The mat, together with the tissue, was placed face down on a solid brass plate to maintain a flat mat surface, and the tissue was then peeled off. The plate was inserted in the Jones apparatus and rigidly supported by a stainless steel plate. The solid piston was lowered with the guidance of a Jacobs chuck for precise alignment and fixed positioning during the addition of weights (Fig. XVII-8). Dacron and classified sulfite fibers were used in these experiments.

As the wet mat was compressed between two solid parallel plates with ar unconfined circumference, it began to bulge laterally when a load was applied. Under such a condition the internal stress and density distributions could not be uniform in the radial direction. The bulging part of the mat was trimmed for separate weight determination. It was found that for both dacron and sulfite fibers the bulging fraction tended to decrease with increasing load; this tendenc was more pronounced with more compressible sulfite mats. The average percentage of bulge by weight were 8.2 and 7.1 for dacron and sulfite, respectively.

By an approximate analysis it may be shown that the average mat density at a given load should be based on the plate area and corrected for the bulge as

$$\bar{c} \cong \frac{W(1 - B_b/3)}{L} \qquad \text{(XVII-9)}$$

where B_b is the weight fraction of bulge based on W. Since the values of B were less than 10^{-1}, the correction was applied to the compressibility constant using the average values of B_b instead of each data point.

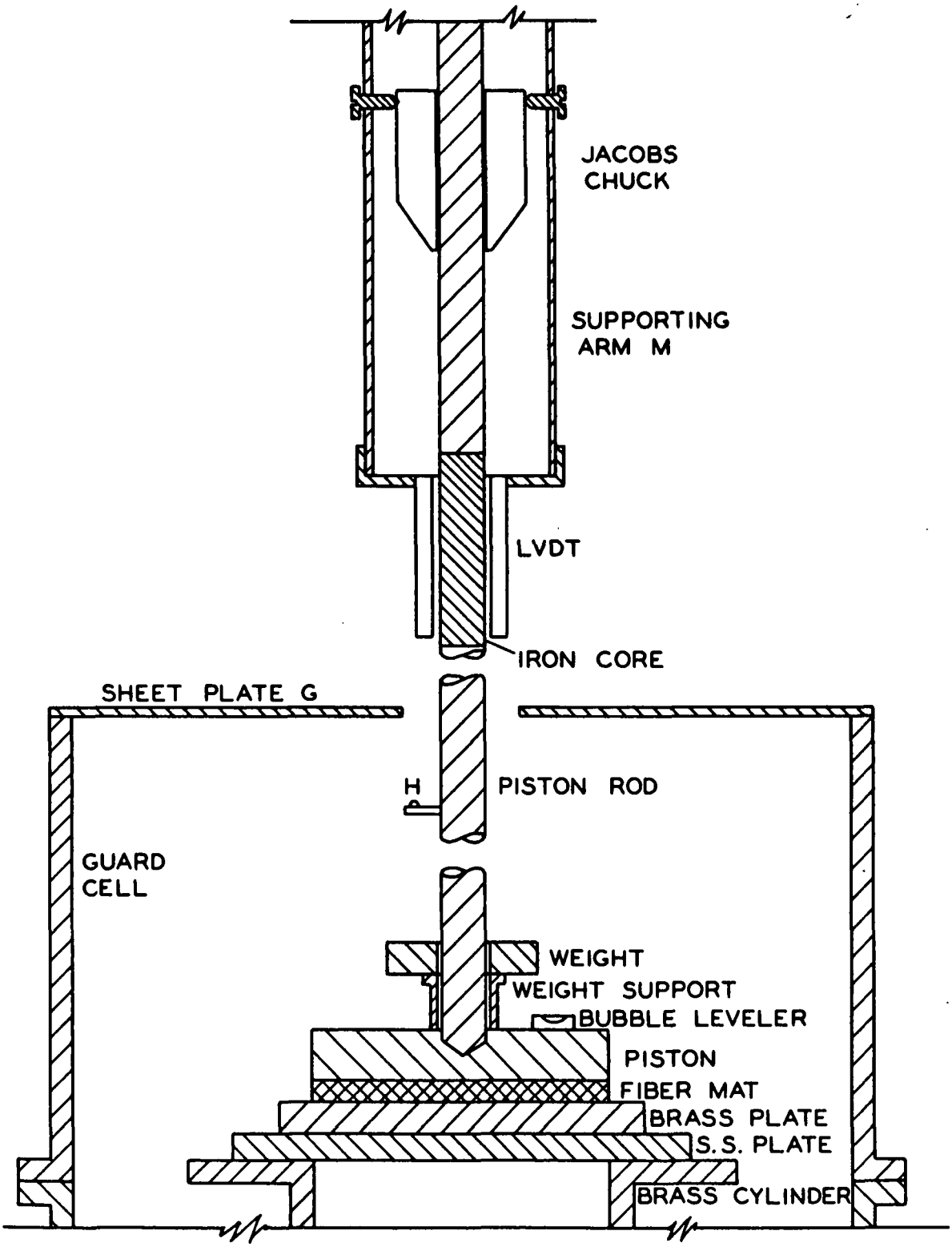

Figure XVII-8. Thin Mat Compressibility Apparatus

Chang's results are presented in Fig. XVII-9 and XVII-10, in which the solid line represents arbitrarily a basis weight of 100 g./sq. m. The dotted curve above the solid line is for thicker mats and that below for thinner mats. These curves are the limits of the range investigated, roughly from 14 to 570 g. per sq. m. It should be mentioned that variations of $\underline{N}$ with basis weight were quite small, less than ±5%, but deviations in $\underline{M}$ spread from -9 to +22%. However, the deviations were random in both cases.

Data were also obtained for the same fibers with the edges confined. The average values of the compressibility constants for both unconfined and confined conditions are reported below:

	Unconfined		Confined	
	$\underline{M}$	$\underline{N}$	$\underline{M}$	$\underline{N}$
Dacron	0.0091	0.29	0.0066	0.25
Sulfite	0.0025	0.38	0.0022	0.38

$\underline{M}$ in (g./cc.)/(dynes/sq. cm.)$^{\underline{N}}$.

From these data it appears that thin mats behave very similar to thick mats in first compression, which is a rather surprising finding. In fact, experimental conditions generally account for more discrepancies in compressibility tests than basis weight, whatever its actual minor influences may be.

DATA CORRELATION

To conclude this chapter on static compressibility we present a comprehensive set of first-compression data in Table XVII-3, which have been accumulated in the past years since Ingmanson's work. Both synthetic and

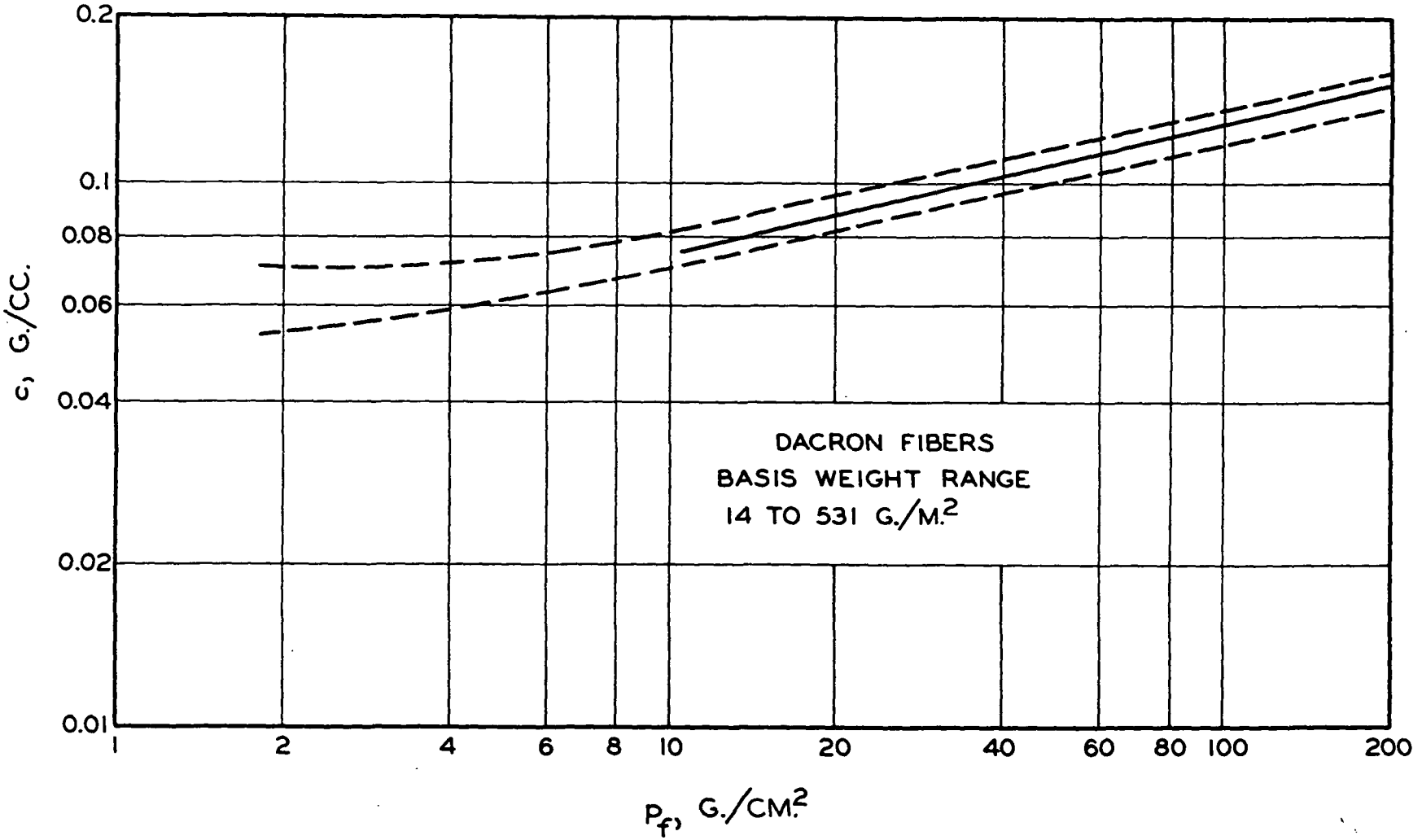

Figure XVII-9. Thin Mat Compressibility

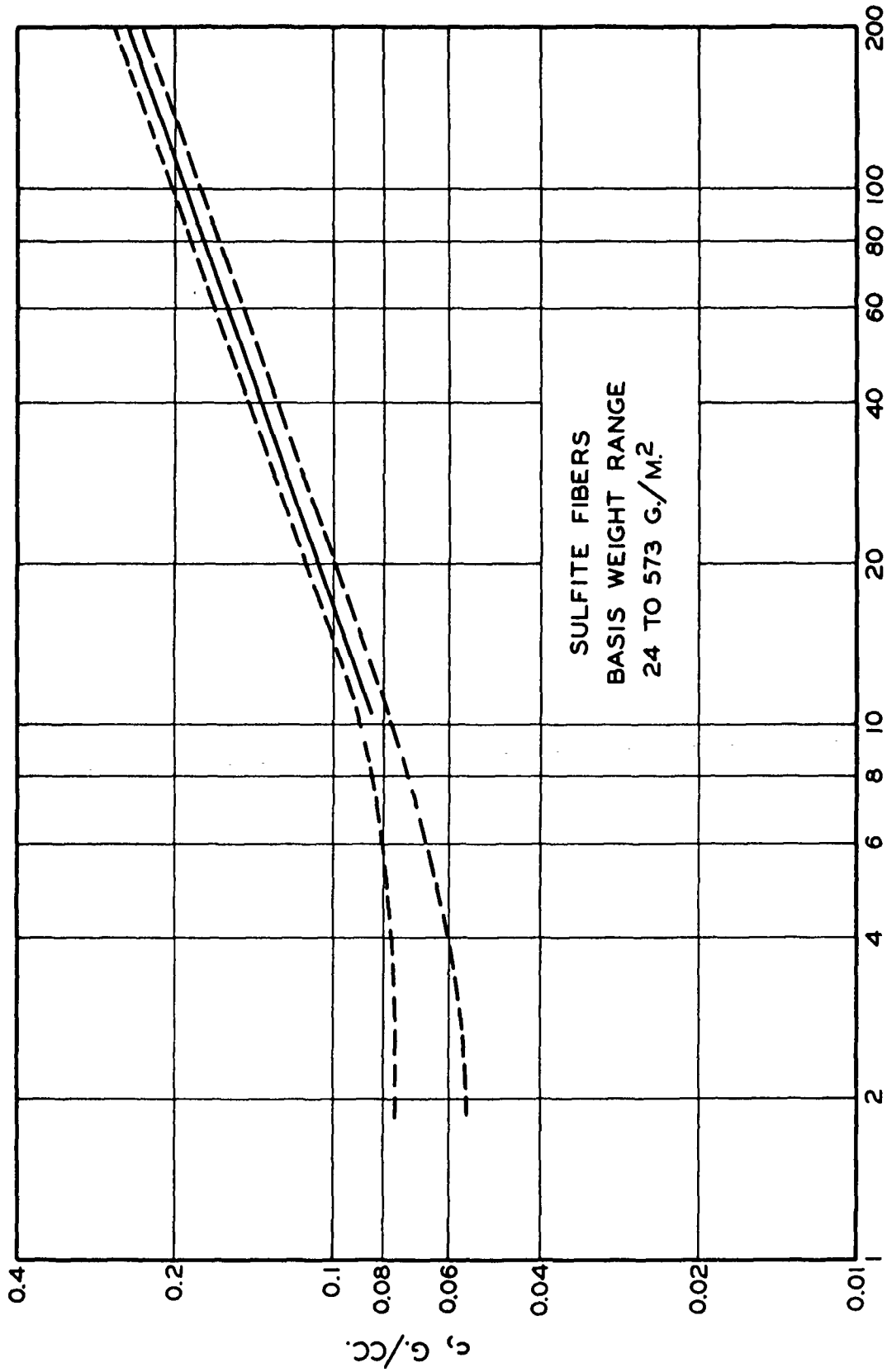
SULFITE FIBERS
BASIS WEIGHT RANGE
24 TO 573 G./M.2
ρ, G./CC.
0.4
0.2
0.1
0.08
0.06
0.04
0.02
0.01
1
2
4
6
8
10
20
40
60
80
100
200
Pf, G./CM.2

TABLE XVII-3

COMPRESSIBILITY CONSTANTS

First compression: $\underline{N}$, dimensionless

$\underline{M}$, (g./cc.)/(dynes/sq. cm.)$^{\underline{N}}$

Hydrodynamic properties: $\underline{v}$, cc./g.

$\underline{S}_w$, sq. cm./g.

Pressure range: 10^4 - 10^5 dynes/sq. cm.

Fibers	$\underline{N}$	$\underline{M} \times 10^3$	$\underline{v}$	$\underline{S}_w \times 10^{-3}$
Nylon	0.225	10.4	0.904	1.82
Dacron	0.254	6.6	0.725	1.70
Glass	0.271	6.32	0.391	6.15
Orlon	0.286	4.55	0.826	2.19
Pulps				
Bagasse	0.230	8.68	3.38	8.3
Cotton linters (1)	0.276	6.65	1.57	12.3
White oak	0.300	5.32	2.76	14.5
Groundwood	0.326	3.95	2.85	53.9
Cotton linters (2)	0.332	3.12	1.43	7.9
Douglas-fir summerwood (1)	0.362	1.93	2.54	5.7
Western hemlock (1)	0.370	2.27	1.95	10.6
Aspen (1)	0.373	2.07	2.51	11.1
Western hemlock (2)	0.375	2.15	2.35	5.4
Douglas-fir summerwood (2)	0.383	1.50	2.35	4.9
Spruce (1)	0.387	1.81	2.55	10.0
Jack pine	0.391	1.33	3.42	13.3
Douglas-fir springwood (1)	0.396	1.27	3.75	16.8
Jack pine (1)	0.395	1.62	2.52	9.7
Aspen (2)	0.400	1.52	2.96	14.8
Spruce (2)	0.406	1.57	2.55	11.7
Jack pine (2)	0.415	1.20	3.48	21.1
Douglas-fir springwood (2)	0.437	0.78	4.12	15.6
Southern pine	0.451	0.71	2.54	5.3

cellulosic fibers are included. Among the latter the majority is wood while range extends from bagasse to cotton. The processes involved in the preparat of these fibers were extremely diverse, covering the conventional commercial pu as well as some laboratory specialties. While the data are generally for the unrefined state, refining does not affect the compressibility constants to a significant extent for most pulps.

It is interesting to add Han's (XVII-5) analysis of these data in lig of Wilder's compressibility function:

$$c^{4\gamma_o - 1} - c_o^{4\gamma_o - 1} = \frac{M'(4\gamma_o - 1)\rho_f^5}{E c_o^{6-4\gamma_o}} p_f \qquad \text{(VI-14)},$$

where M' is $\pi^8/(16^3 N')$. In the pressure range of the data, the second ter may be neglected. The equation reduces to

$$c = \left[\frac{M'(4\gamma_o - 1)\rho_f^5}{E c_o^{6-4\gamma_o}} p_f\right]^{1/(4\gamma_o - 1)}$$

or

$$c = \left[\left(\frac{M'}{E}\right)^N \frac{\rho_f^{5N}}{N^N c_o^{5N-1}}\right] p_f^N \qquad \text{(XVII-10)}.$$

Thus,

$$\log\left[\frac{M N^N c_o^{5N-1}}{\rho_f^{5N}}\right] = N \log\left[\frac{M'}{E}\right] \qquad \text{(XVII-11)}.$$

A plot of the first logarithmic term against N would be linear provided M'/E were constant. Such a plot is shown in Fig. XVII-11. The value of c_o was chosen to be 10^{-2} g./cc. and the values of ρ_f are indicate in the plot. From the slope of this plot the value of M'/E is evaluated to

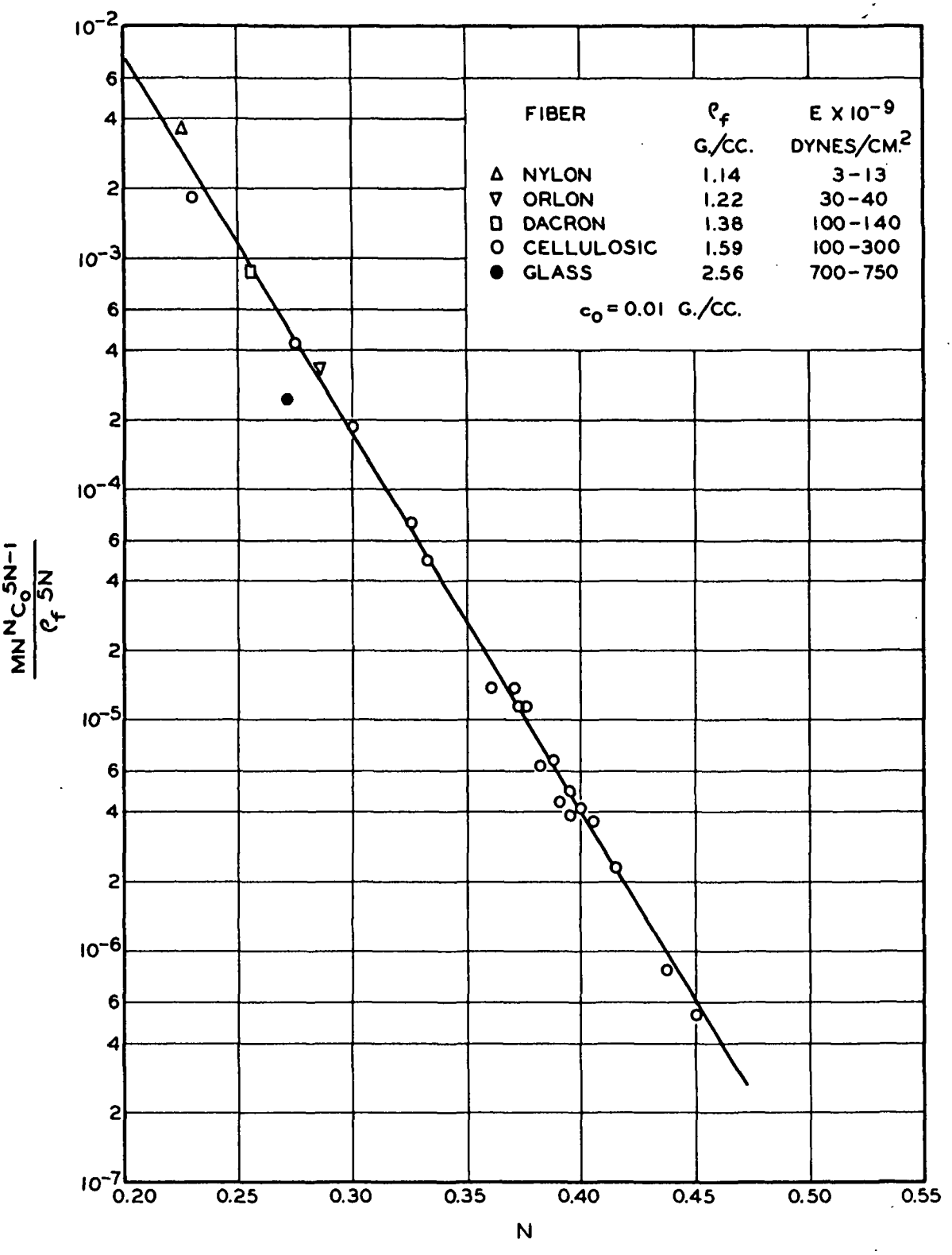

Figure XVII-11. Correlation of Compressibility Constants

10^{-16}. When $\underline{E}$ is 10^{11} dynes/sq. cm., $\underline{M}'$ is of the order of 10^{-5}, and $\underline{N}'$ of the order of 10^{6}. The intercept of the line is about 10, i.e., as $\underline{N}$ approaches zero, the first term approaches unity.

In Wilder's development the number $\underline{N}'$ has to do with the mode of fiber bending or deflection, which is dependent on the distributions of load and support Then the empirical evidence of $\underline{M}'$ being linear with $\underline{E}$ indicates that the compression behavior responds, directly and indirectly, to the modulus of elasticity alone. Since the fibers included here are viscoelastic in nature, the indication of such an oversimplified picture is rather surprising. Nevertheless, this finding is an interesting one which may lead to new thinking about mat compressibility.

On reflection, the present evidence would also cast some doubt about the legitimacy of Jones' correlation (XVII-4) that $\underline{M}$ is inversely proportional to $(\rho_{\underline{f}}^{5}/\underline{E})^{\underline{N}}$ without taking into account the possible effects of other factors such as $\underline{c}_{o}$, $\underline{M}'$, and $\underline{N}$ itself. All these results serve to show the importance of interaction in dealing with fibrous materials, especially those of cellulosic origin.

XVIII. STEADY PERMEATION OF CYLINDRICAL-FIBER MATS

In Part One the concept of resistance to flow through fiber mats was developed in a partially analytical manner. We now proceed to demonstrate its validity, as well as its limitations, by the results of carefully controlled experiments. In these experiments flow through relatively thick mats formed from very dilute suspensions of selected types of fibers was systematically investigated in order to determine those known factors governing permeation. The suspension must be sifficiently dilute to achieve uniform dispersion and the mat sufficiently thick to minimize the effects of the supporting septum. The results of such experiments reported by Ingmanson, Andrews, and Johnson (XVIII-1) and by Ingmanson and Andrews (XVIII-2) are summarized here.

EXPERIMENTAL SYSTEMS

The experimental setup is shown in Fig. XVIII-1, which is self-explanatory. The details of the permeation tube assembly are illustrated in Fig. XVIII-2. These diagrams represent the actual apparatus then in use after considerable modifications of the initial version.

A general procedure for permeation experiments is outlined as follows: Dry and clean fibers are introduced into hot water in a suction flask which is then gradually evacuated to a gently boiling condition for the purpose of deaeration. The deaerated fiber slurry is siphoned over into the dilution water in a feed tank, care being taken to prevent the free surface from disturbances which might cause the entrainment of air bubbles on the fiber surfaces. The dilute fiber suspension in the tank is mildly agitated to break up any fiber bundles and to maintain a state of uniform dispersion, the consistency of the suspension being about 0.01%.

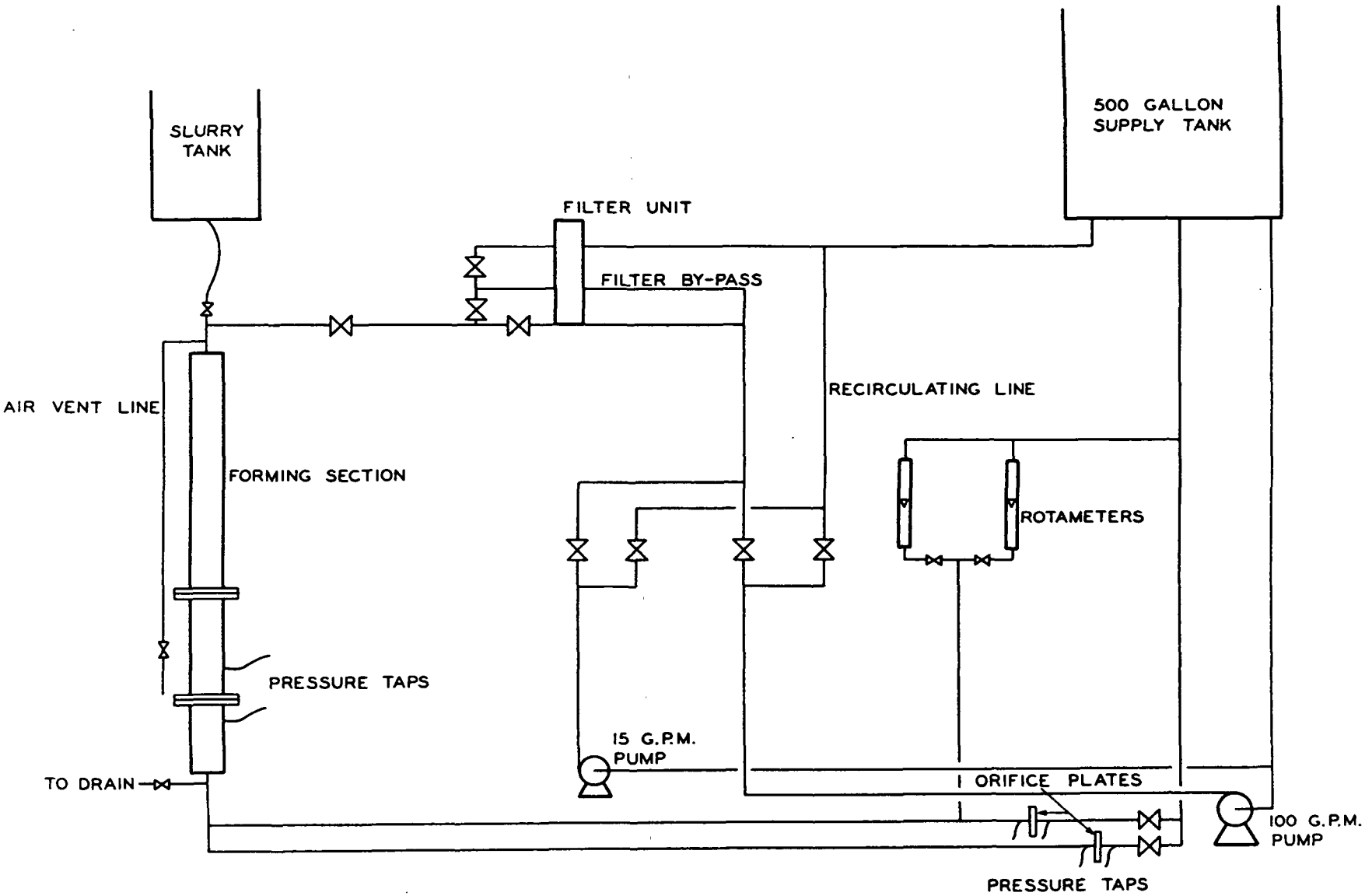
SLURRY TANK
500 GALLON SUPPLY TANK
FILTER UNIT
FILTER BY-PASS
AIR VENT LINE
FORMING SECTION
RECIRCULATING LINE
ROTAMETERS
PRESSURE TAPS
15 G.P.M. PUMP
TO DRAIN
ORIFICE PLATES
100 G.P.M. PUMP
PRESSURE TAPS

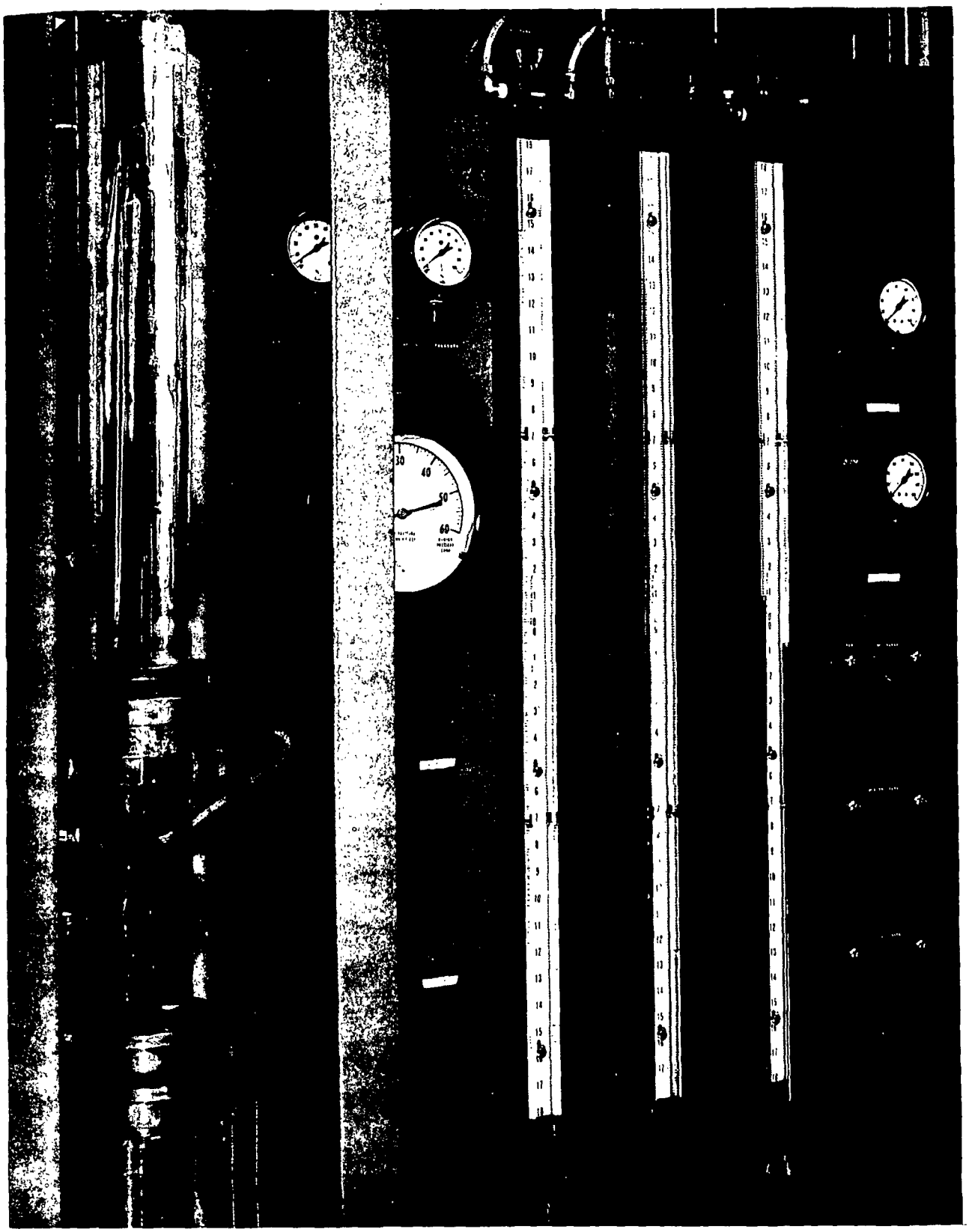

Figure XVIII-2. Permeation Tube Assembly

The septum which is a perforated plate covered with a coarse backing w (35 mesh) and a fine face wire (100 mesh) is thoroughly cleaned and dried. Aft it is assembled with the permeation tube, flushing water flows upward through th tube to wet the septum and to remove air bubbles. The tube is then completely filled with water, and the fiber suspension is admitted to the tube beneath the surface. A mat is formed at a constant flow rate, sufficiently high to maintai mild turbulence in the tube but low enough to avoid large-scale eddies.

A permeable piston is lowered and compresses the mat to the desired po ity by weights as in the compressibility test. The water-recirculating line is connected to the tube, and any air entrapped in the system is removed by bleedin through a suitable vent. Flow through the mat is then initiated and slowly increased to the desired rate. At a steady state the corresponding pressure dr is noted and corrected for that of the septum. A series of successive points a increasing flow rates is obtained in a single permeation run. The last datum p is limited to a pressure drop not exceeding 1% of the load in order to maintain uniform porosity. The mat thickness may be measured with a cathetometer or dia micrometer, and the basis weight determined by drying and weighing the fibers. The water used in permeation is deionized and distilled. The recirculating wat is thoroughly filtered in each cycle, or some decay of permeability will occur because of contaminations.

Glass, dacron, and nylon fibers were used in these experiments. Thei dimensions can be precisely determined microscopically and their densities pycnc metrically. In the case of nylon fiber which is known to be slightly swollen i water, its pycnometric specific volume may be corrected for swelling (about 3%) from microscopic measurements of the fiber cross sections in a wet state. The compressibility constants of the simple power function may be established from

first-compression tests in the range of pressure drops to be used in the permeation runs. The characterization of these fibers is summarized in Table XVIII-1.

TABLE XVIII-1

CHARACTERIZATION OF CYLINDRICAL FIBERS

Fiber	$\bar{L}_f$, [a] mm.	$\bar{d}_f$, [b] mm.	S_v, [c] sq. cm./cc.	v, [d] cc./g.	M, [e] c.g.s. units	N [f]
Glass	0.94	16.5	2420	0.384	-	-
Dacron	5.30	17.1	2340	0.709	0.0066	0.254
Nylon	6.47	19.5	2050	0.904	0.0104	0.225

[a] $\bar{L}_f = \Sigma N_i L_f^2 / \Sigma N_i L_f$.

[b] $\bar{d}_f = \Sigma N_i d_f^2 / \Sigma N_i d_f$.

[c] $S_v = 4/\bar{d}_f$.

[d] For nonswelling fibers, $v = 1/\rho_f$.

[e] $(g./cc.)/(dynes/sq.\ cm.)^N$.

[f] Dimensionless.

UNIFORM MATS

Glass fibers, being relatively rigid, can be formed into mats of very high porosities, but they are not satisfactory for lower porosities (<0.8) because of their fragile nature. Nylon fibers are suitable for the intermediate porosity range by virtue of their low modulus of elasticity, but not feasible for porosities larger than 0.9 because extremely low pressure drops are required to form such high-porosity mats. Dacron fibers occupy an intermediate position.

An example of permeation data for glass fibers is given in Fig. XVIII-3, in which the flow rate is plotted vs. the pressure drop across the mat with porosity as the parameter. Within the experimental range the data indicate direct proportionality, in agreement with Darcy's law. From the slopes of these lines the permeability coefficients (μK_D) may be calculated with the known values of th mat thickness and the water viscosity.

Proceeding with the evaluation of the Kozeny factor in accordance with the Kozeny-Carman equation, it becomes apparent at once that k is far from being a constant for these high-porosity mats. In fact, its value increases rapidly with increasing porosity, as shown in Table XVIII-2.

TABLE XVIII-2

VARIATION OF KOZENY FACTOR

μK_D, sq. cm. x 10^6	ε, cc./cc.	k	
		Experimental	Happel's Prediction
1.69	0.911	9.57	11.5
1.31	0.900	8.75	10.7
1.00	0.879	7.84	9.4
0.67	0.852	7.23	8.8
0.36	0.805	6.51	7.4

As discussed in Chapter V, variation of the Kozeny factor with porosity is to be expected. Upon checking the experimental value of k with Happel's prediction by his free-surface model, the general trend appears to be correct, but the discrepancy is quite large. For this reason the Davis form with two adjustable parameters seems to be more suitable for correlation. Considerably more data have been collected with nylon fibers to extend the range of interest.

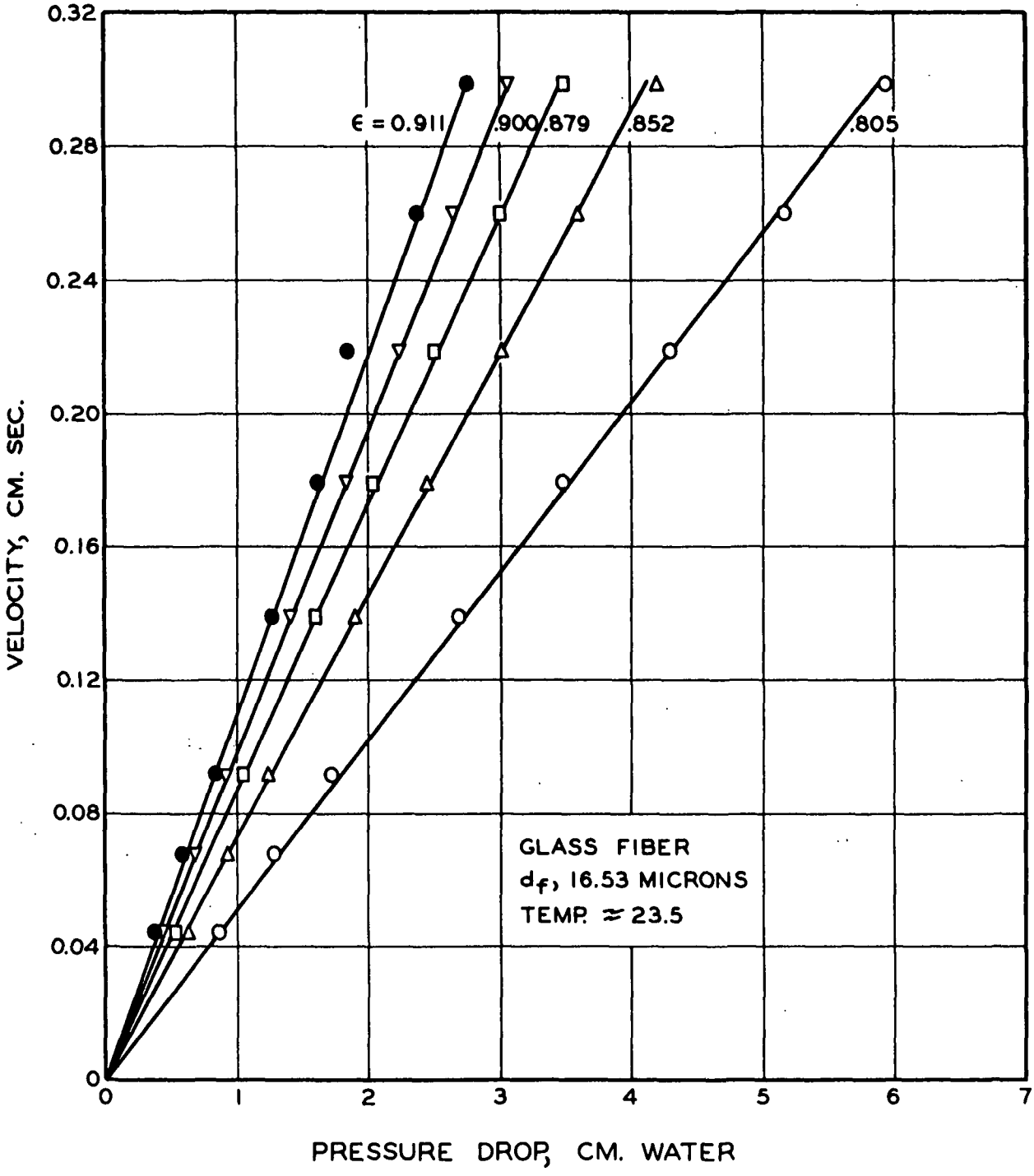

Figure XVIII-3. Permeation Data of Uniform Fiber Mats

The final correlation is shown in Fig. XVIII-4. From these data the Davis correlation was established as

$$k = 3.5 \frac{\epsilon^3}{(1-\epsilon)^{1/2}} [1 + 57(1-\epsilon)^3] \qquad \text{(XVIII-1)} .$$

The original Davis values for k_1 and k_2 were 4.0 and 56, respectively based on air permeability data for fiber filters. It is to be mentioned that the Davis equation should not be used for low porosities as it will yield rapidly decreasing values of k while it has been amply demonstrated that the Kozeny factor remains nearly constant at relatively low porosities. Figure XVIII-4 indicates the average value of k for fiber mats to be 5.5, which has been commonl accepted for porosities less than 0.75. Happel's equation predicts 5.6 for porosity 0.60. For many types of porous media with porosities between 0.3 and 0.7 the Kozeny factor lies between 4 and 6, according to Carman (XVIII-3).

Carroll's (III-4) three-parameter correlation overcomes the shortcoming of Davis' correlation at low porosities. They are compared in the same figure. It is seen that Carroll's curve fits the whole experimental range better than does Davis'. The Carroll correlation is

$$k = 5.0 + \exp[14(\epsilon - 0.80)] \qquad \text{(XVIII-2)} .$$

PRESSURE DISTRIBUTION

A special tube with multiple pressure taps was used to measure the internal fluid pressures in thick mats under fluid stresses during permeation. Data were taken with increasing flow rates to avoid hysteresis effects. The pressure distribution data for dacron and nylon fibers are shown in Fig. XVIII-5.

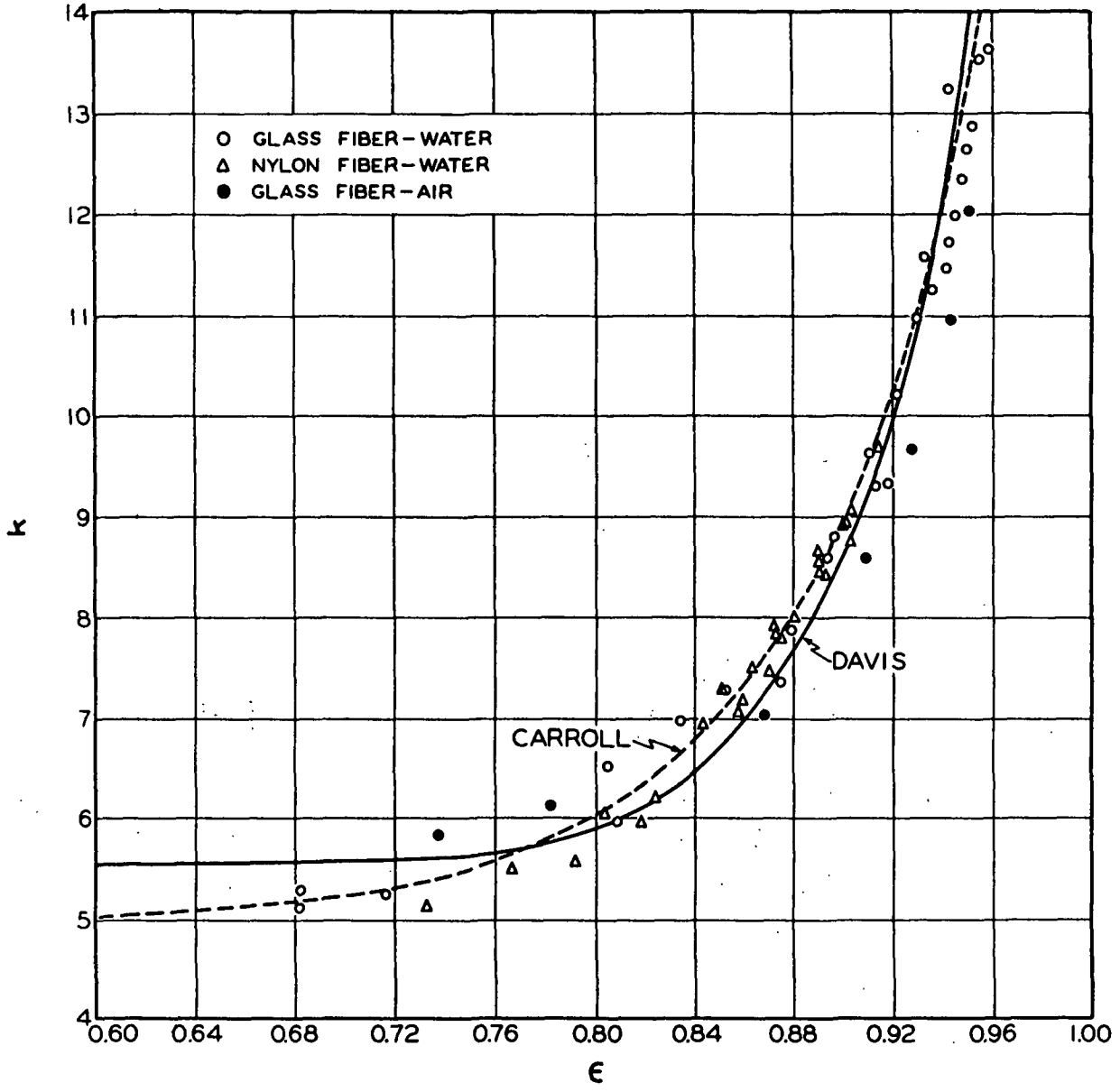

Figure XVIII-4. Correlation of Kozeny Factor with Porosity

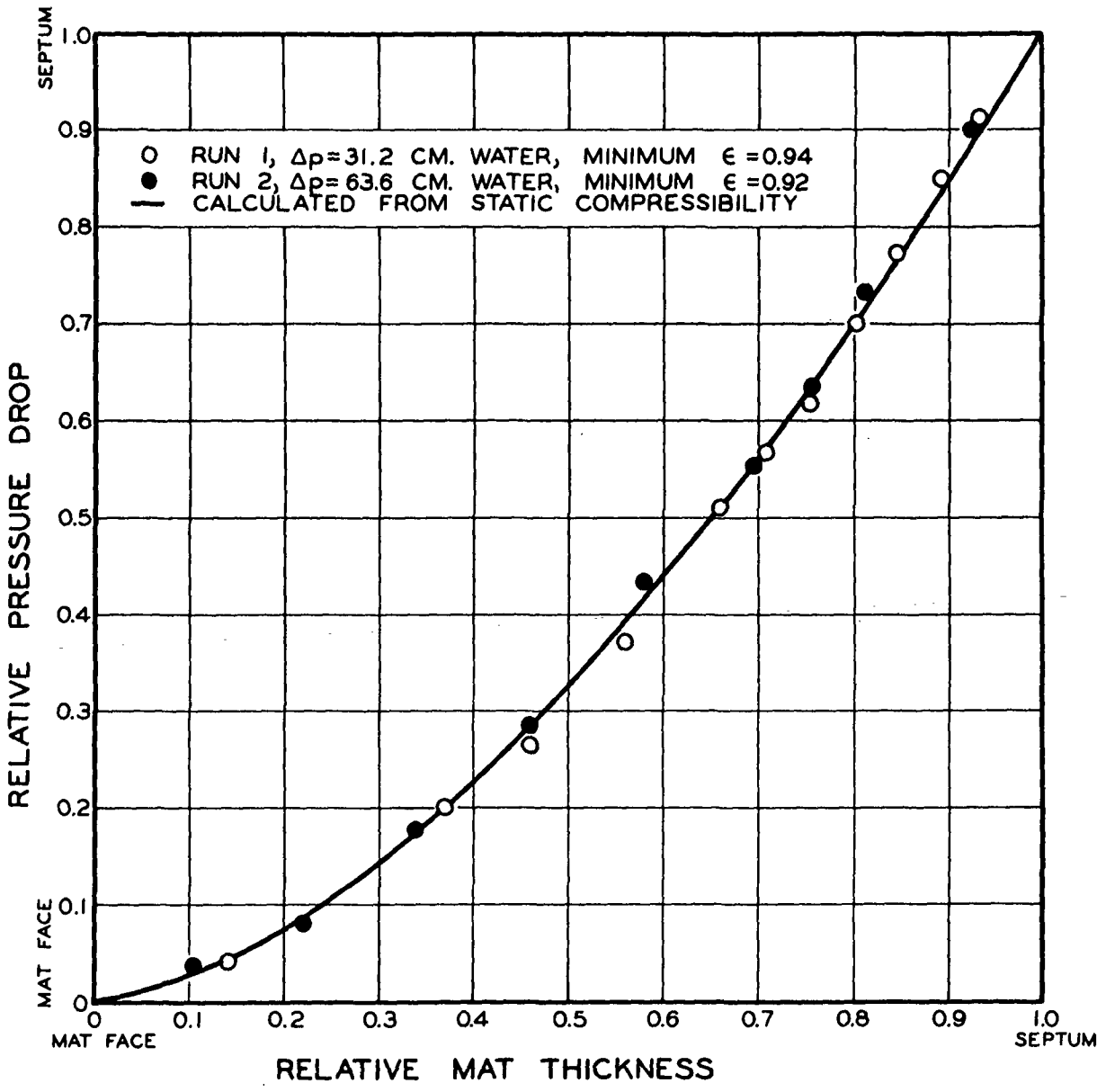

Figure XVIII-5. Pressure Distribution in a Nonuniform Mat

The permeation expression for slow flow through uniform fiber mats of high porosities, using Davis' porosity function is

$$\frac{|\Delta p|}{L} = k_1 (1 - \epsilon)^{3/2} [1 + k_2 (1 - \epsilon)^3] S_v^2 \mu |U| \qquad \text{(XVIII-3)} .$$

The pressure gradient is, therefore, constant.

When a mat is subjected to fluid stresses, an internal pressure distribution will develop. By an analysis similar to that for the average filtration resistance in Chapter IX, we may arrive at a pressure distribution with respect to $\underline{z}$. Substituting the simple compressibility function for the solid fraction, omitting the factor in the brackets for porosities larger than 0.9, which is justified by Equation (XVIII-1), and differentiating the resulting expression, we obtain

$$- \frac{dp}{dz} = \frac{dp_f}{dz} = k_1 \mu S_v^2 U [v M p_f^N]^{3/2} \qquad \text{(XVIII-4)} .$$

Upon integration over the mat thickness from 0 to $\underline{L}$ and the corresponding pressure drop from $-\Delta \underline{p}$ to 0, the result is

$$\frac{p_L - p_0}{L} = k_1 \mu S_v^2 |U| (1 - 3N/2) [v M (p_L - p_0)^N]^{3/2} \qquad \text{(XVIII-5)} .$$

The integration may also be performed from 0 to $\underline{z}$, yielding the same expression applicable to any position $\underline{z}$. Dividing one by another, the pressure distribution is expressed by

$$\frac{p - p_0}{p_L - p_0} = \left[\frac{z}{L}\right]^{1/(1-3N/2)} \qquad \text{(XVIII-6)} .$$

This power function is represented by the solid curve in Fig. XVIII-5. Its agreement with the experimental data for high-porosity mats is excellent in both cases. For an incompressible mat, $\underline{N}$ is equal to zero, and the pressure distribution becomes linear as previously stated.

In a similar manner the high-porosity viscous flow expression may be derived on the fiber mass basis:

$$\frac{p_L - p_0}{W} = k_1 \mu S_v^2 |U| (1 - N/2) v^{3/2} [M(p_L - p_0)^N]^{1/2} \qquad \text{(XVIII-7)} .$$

Thus, from Equations (XVIII-5) and (XVIII-7) the over-all mat density $\underline{c^o}$ is related to the over-all pressure drop by a modified compressibility function:

$$c^o = \frac{W}{L} = \left(\frac{2 - 3N}{2 - N}\right) M(p_L - p_0)^N \qquad \text{(XVIII-8)} .$$

The validity of this relation is demonstrated in Fig. XVIII-6, in which the data points are compared with the solid line representing the equation for nylon fiber mats under fluid stresses.

For intermediate porosities the quantity in the brackets of Equation (XVIII-3) should be taken into account. The resulting differential expression may be integrated graphically with the aid of the static compressibility data to arrive at a pressure distribution. Since porosity distribution cannot be readily measured, it may be calculated from the pressure distribution. The results of such calculations for dacron and nylon fibers are shown in Fig. XVIII-7, in which a wood pulp mat is included. The dashed part of each curve implies uncertainty because it is based on extrapolation of the compressibility data.

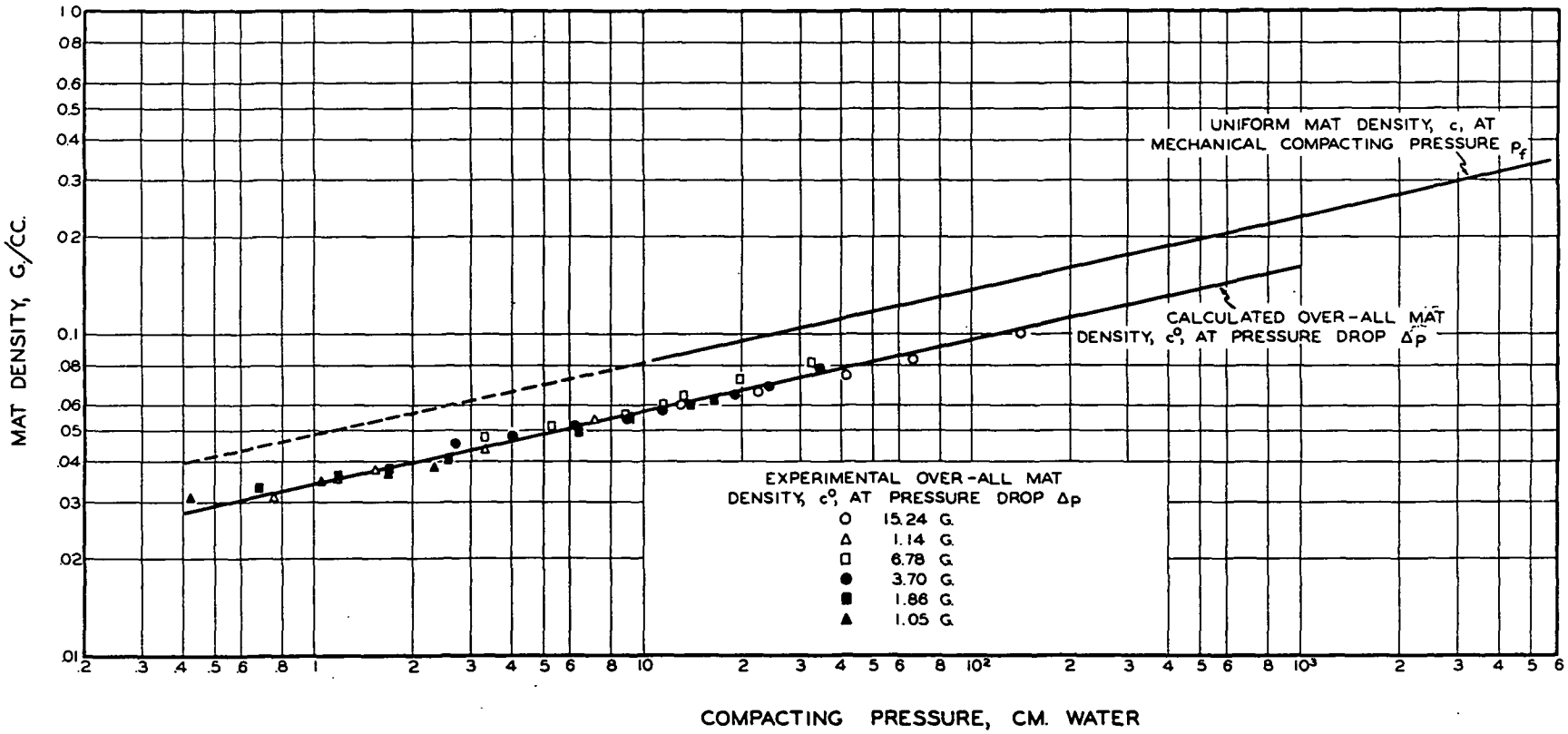

Figure XVIII-6. Comparison of Uniform and Over-all Mat Densities

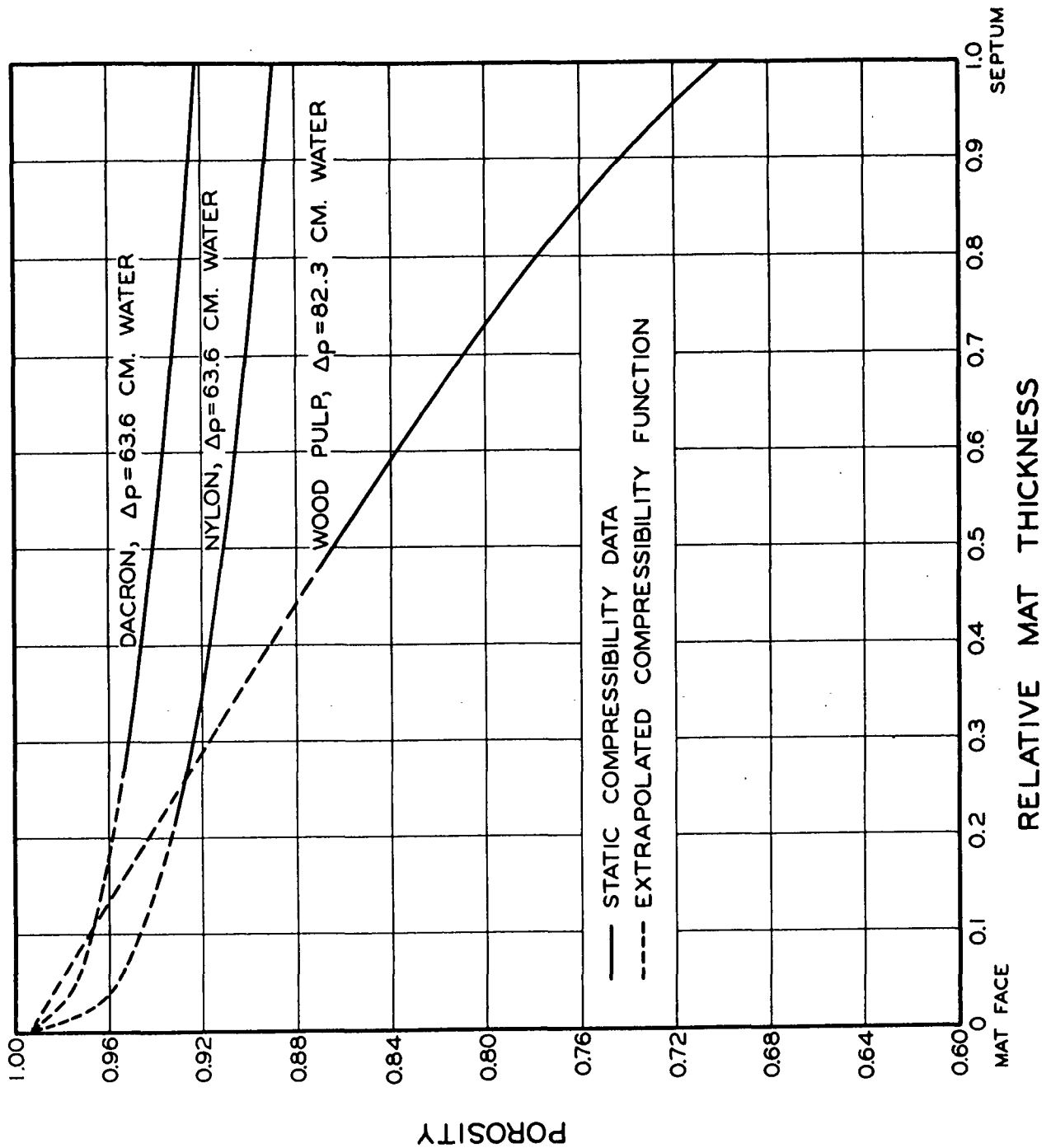
DACRON, Δp=63.6 CM. WATER
NYLON, Δp=63.6 CM. WATER
WOOD PULP, Δp=82.3 CM. WATER
STATIC COMPRESSIBILITY DATA
EXTRAPOLATED COMPRESSIBILITY FUNCTION
POROSITY
1.00
0.96
0.92
0.88
0.84
0.80
0.76
0.72
0.68
0.64
0.60
MAT FACE
0
0.1
0.2
0.3
0.4
0.5
0.6
0.7
0.8
0.9
1.0
SEPTUM
RELATIVE MAT THICKNESS

TRANSITION FLOW

It has been shown in Part One that a more general flow expression for uniform mats including both viscous and inertial effects is

$$\frac{\epsilon^3 |\Delta p|}{\sqrt{\alpha'}(1 - \epsilon) S_v \rho U^2 L} = \frac{\sqrt{\alpha'}(1 - \epsilon) S_v \mu}{\rho |U|} + b' \qquad \text{(XVIII-9)} .$$

For compressible mats this expression may be used with the following average quantities:

$$\alpha'_{av} = k_{av} = 3.5 \frac{\epsilon_{av}^3}{(1 - \epsilon_{av})^{1/2}} [1 + 57(1 - \epsilon_{av})^3] \qquad \text{(XVIII-10)} ,$$

and

$$\epsilon_{av} = 1 - (1 - 3N/2)^{2/3} v M |\Delta p|^N \qquad \text{(XVIII-11)} .$$

Similarly, the flow expression may also be written on the mass basis:

$$\frac{\bar{\epsilon}^3 |\Delta p|}{\sqrt{\bar{\alpha'}}\, v S_v \rho U^2 W} = \frac{\sqrt{\bar{\alpha'}}(1 - \bar{\epsilon}) S_v \mu}{\rho |U|} + b' \qquad \text{(XVIII-12)} ,$$

in which the average quantities have been defined by Equations (IX-24) and (IX-13) as

$$\bar{\alpha'} = \bar{k} = 3.5 \frac{\bar{\epsilon}^3}{(1 - \bar{\epsilon})^{1/2}} [1 + 57(1 - \bar{\epsilon})^3] \qquad \text{(XVIII-13)}$$

and

$$\bar{\epsilon} = 1 - (1 - N/2)^2 v M |\Delta p|^N \qquad \text{(XVIII-14)} .$$

The two mean expressions of Equation (XVIII-9) are equivalent to each other thr the relationship (XVIII-8). For filtration purposes, however, the latter base fiber mass is more convenient to use, and consequently has been presented in th simple form:

$$\overline{f'} = \frac{1}{\overline{Re'}} + b' \qquad \text{(IX-25)}$$

A large amount of experimental data has been collected with cylindric fibers. All data are plotted as $\overline{f'}$ vs. $\overline{Re'}$ in Fig. XVIII-8. The value of was determined to be 0.1. It is interesting to note that in terms of pressure drop, the inertial resistance is 9% of the total at unity $\overline{Re'}$ and 91% at 100. Flow below unity $\overline{Re'}$ may be considered to be in Darcy's region.

SCREEN RESISTANCE

The resistance of grids, screens, and fabrics to fluid flow has been extensively investigated. Previous attempts at correlations were based on simplified models of flow through orifices and around cylinders. In his study air flow through open-weave fabrics, Robertson (XVIII-4) adopted the orifice mod and accordingly correlated the discharge coefficient with the Reynolds number. He found that at high flow rates the discharge coefficient was larger than unity in contrast to the case of a single orifice. Wieghardt (XVIII-5) and Cornell (XVIII-6) considered flow around cylinders and used the drag coefficients for th purpose of correlation. Grootenhuis (XVIII-7) succeeded in correlating air flo through screens of square meshes in terms of the friction factor and the Reynold number. In all these correlations the major parameter was the fractional open area.

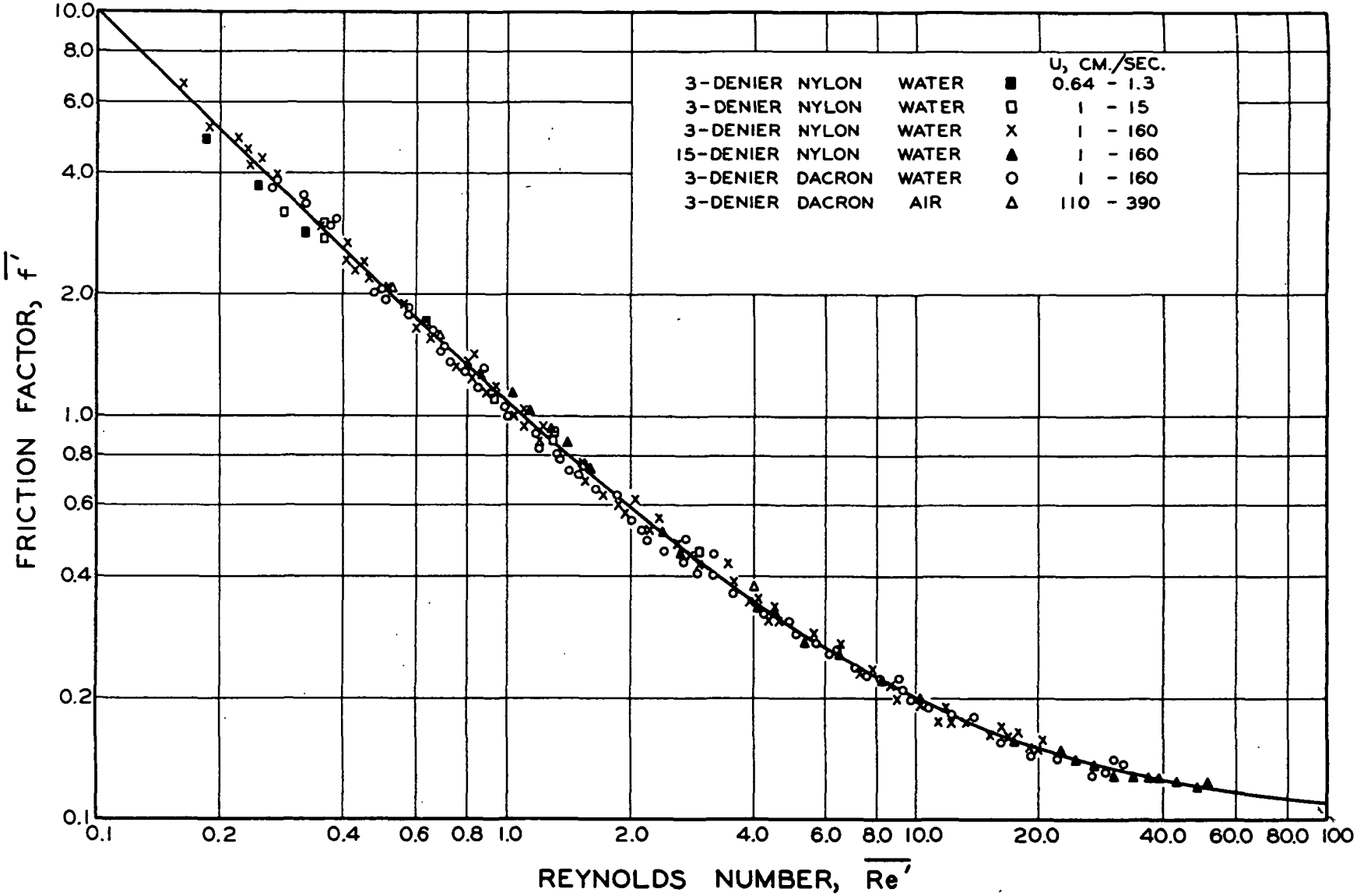

Figure XVIII-8. Correlation of Flow Data for Cylindrical-Fiber Mats

We have treated the papermaking wire screens as a porous structure (XVIII-8), and assumed that the flow resistances follow Forchheimer's law (III-5). By this concept the correlation (XVIII-9) would be applicable also to wire screen.

Furthermore, for turbulent flow the inertial resistance coefficient b' becomes a mild function of the Reynolds number, as was demonstrated by Ergun (III-6) with flow through packed beds:

$$b' = \frac{b^o}{(Re')^n} \qquad \text{(XVIII-15)} .$$

The value of n is about 0.1 based on data compiled by Carman (XVIII-3). With this knowledge we modified our correlation to

$$f' = \frac{1}{Re'} + \frac{b^o}{(Re')^n} \qquad \text{(XVIII-16)} .$$

For a given screen and fluid this equation reduces to

$$\frac{\Delta p}{U} = a_o + b_o |U|^{1-n} \qquad \text{(XVIII-17)} .$$

Upon differentiation we obtain

$$\frac{d(\Delta p/U)}{d|U|} = b_o (1 - n)|U|^{-n} \qquad \text{(XVIII-18)} .$$

Thus, a logarithmic plot of the derivative vs. U would result in a straight line. This method was used to correlate the water flow data for conventional twill-weave 54 to 100-mesh screens and yielded the average value 0.11 for n. The second plot of $f'(Re')$ vs. $(Re')^{1-n}$ would give the slope b^o. The value so obtained was 0.2. This correlation is shown in Fig. XVIII-9. In the same figure the correlation for fiber mats is indicated by the dashed curve. It

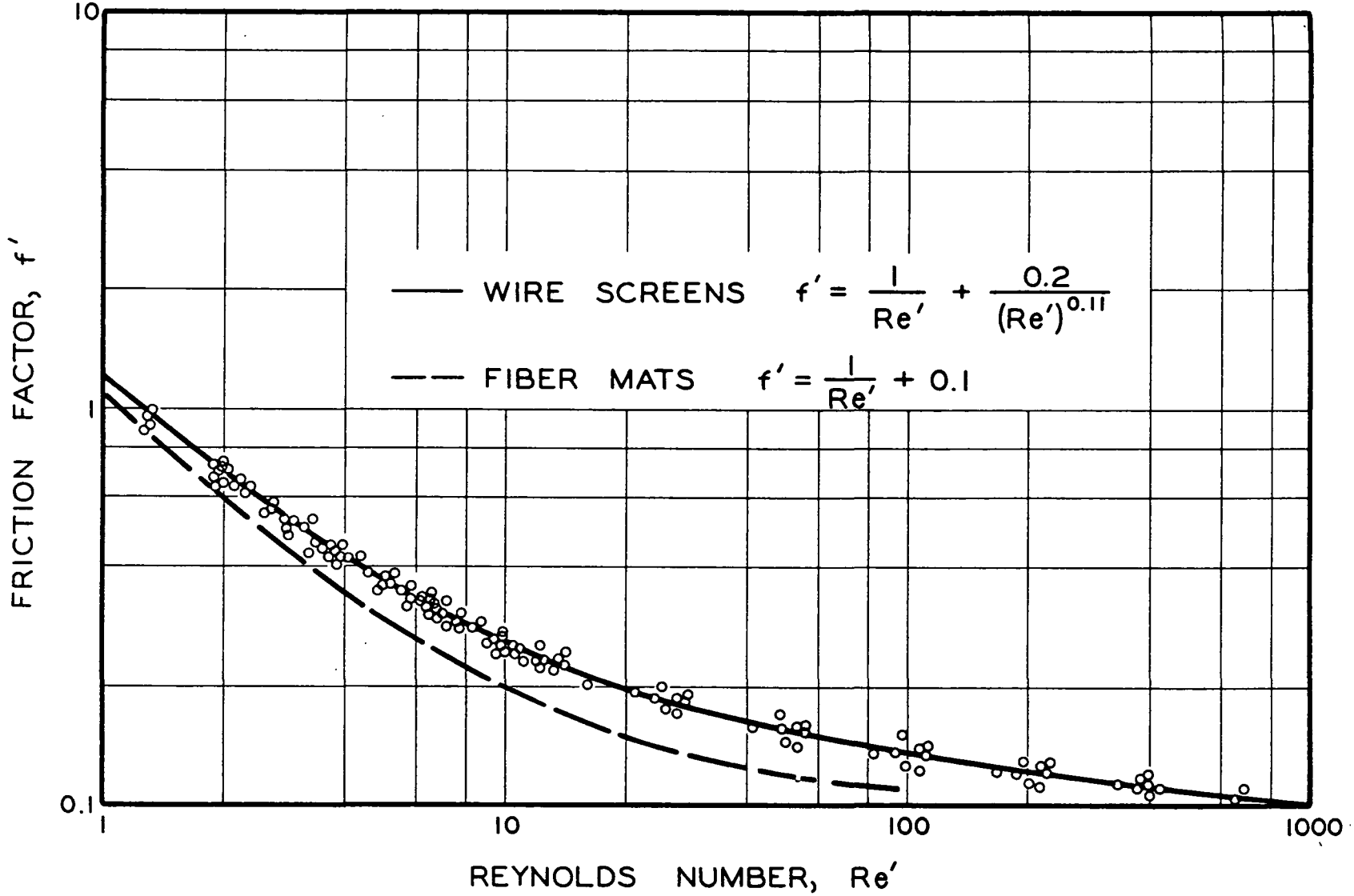

Figure XVIII-9. Correlation of Flow Through Screens

appears that the inertial effects in the transition flow ($1 < \underline{Re}' < 100$) for wire screens are somewhat larger than for fiber mats. This is probably due t eddies formed behind the screen as a result of flow separation from the indivi wires. At either lower or higher Reynolds numbers the two curves are expecte to approach each other.

In the correlation the measured average porosity and thickness of th screens were used. The surface area was calculated from the diameters of the strands. The average value of the Kozeny factor evaluated from the low flow c is 5.1 in the porosity range 0.6-0.7. This value is in the range of the previ cited values for porous media. The maximum deviation of the data from the cu is ±10%. By introducing an additional parameter, the pitch-diameter ratio, t correlation was improved to about ±6%. There was some evidence that very coa screens and some fabric wires do not follow this particular correlation. Sinc the resistance of a screen can be so easily measured, it is questionable if fu refinement of the correlation is worthwhile.

XIX. HYDRODYNAMIC PROPERTIES OF CELLULOSIC FIBERS

Cellulosic fibers have wide distributions of dimensions. Their cross sections are more nearly elliptical than cylindrical. They are not only flexible in bending, but also conformable on contact. They have a high capacity for swelling and a tendency to deswell at increasing pressure and temperature. Their geometric properties are neither uniform nor continuous along their length. The ease with which they become fibrillated complicates their surfaces, which are not precisely definable even on a macroscopic scale.

These complications have necessitated the use of gross properties which are only approximately interpretable in terms of the behavior observed experimentally. Nevertheless, the hydrodynamic method of evaluation has been found useful for the reason that several important steps in the processing of pulps are essentially hydrodynamic in nature. Two commonly accepted properties are specific surface and volume. Experimental values for the same fibers used in compressibility tests have been included in Table XVII-3.

TESTING METHODS

The determination of these two properties was initiated by Robertson and Mason (XIX-1), using the permeation method. They encountered two major experimental difficulties: permeability decay and nonuniform porosity. The problem of decay, as manifested by creeping increase of pressure drop or decrease of flow rate, will be discussed later. The necessity of maintaining a uniform mat (because the porosity function had not then been established) by compressing it with a substantial load and using low pressure drops limited the useful range of data and rendered subsequent evaluation less reliable.

Ingmanson (IX-1) used constant-pressure filtration for the same purpose. In this method, while a mat is formed at a constant head, the filtrate volume is measured in consecutive time intervals. As an experimental technique it also involves certain inherent problems. The initial portion of data must be discarde on account of the septum effects. Several runs must be made in order to cover a sufficient range of pressure drops for the subsequent analysis. The mat is also subject to creep during the run.

Ingmanson (III-9) then adopted the constant-rate filtration method. Hi latest version of the apparatus is shown in Fig. XIX-1. Its essential feature is to record the pressure rise as a mat is formed at a known flow rate. For the purpose of pulp evaluation the following experimental conditions should be satisfied:

1. A dilute suspension of soaked, deaerated, and classified fibers kept in mild agitation and constant temperature flows smoothly into a filtration tube filled with water.

2. The flow is turbulent in the tube but viscous through a sufficiently thick mat.

3. Vibrations from pump and other sources are to be avoided.

The constant-rate method has largely overcome the two last-mentioned difficulties with the constant-pressure method.

DATA ANALYSIS

From the known suspension consistency and flow rate, the basis weight of the mat at any time (discarding the initial period) is calculated from the fiber

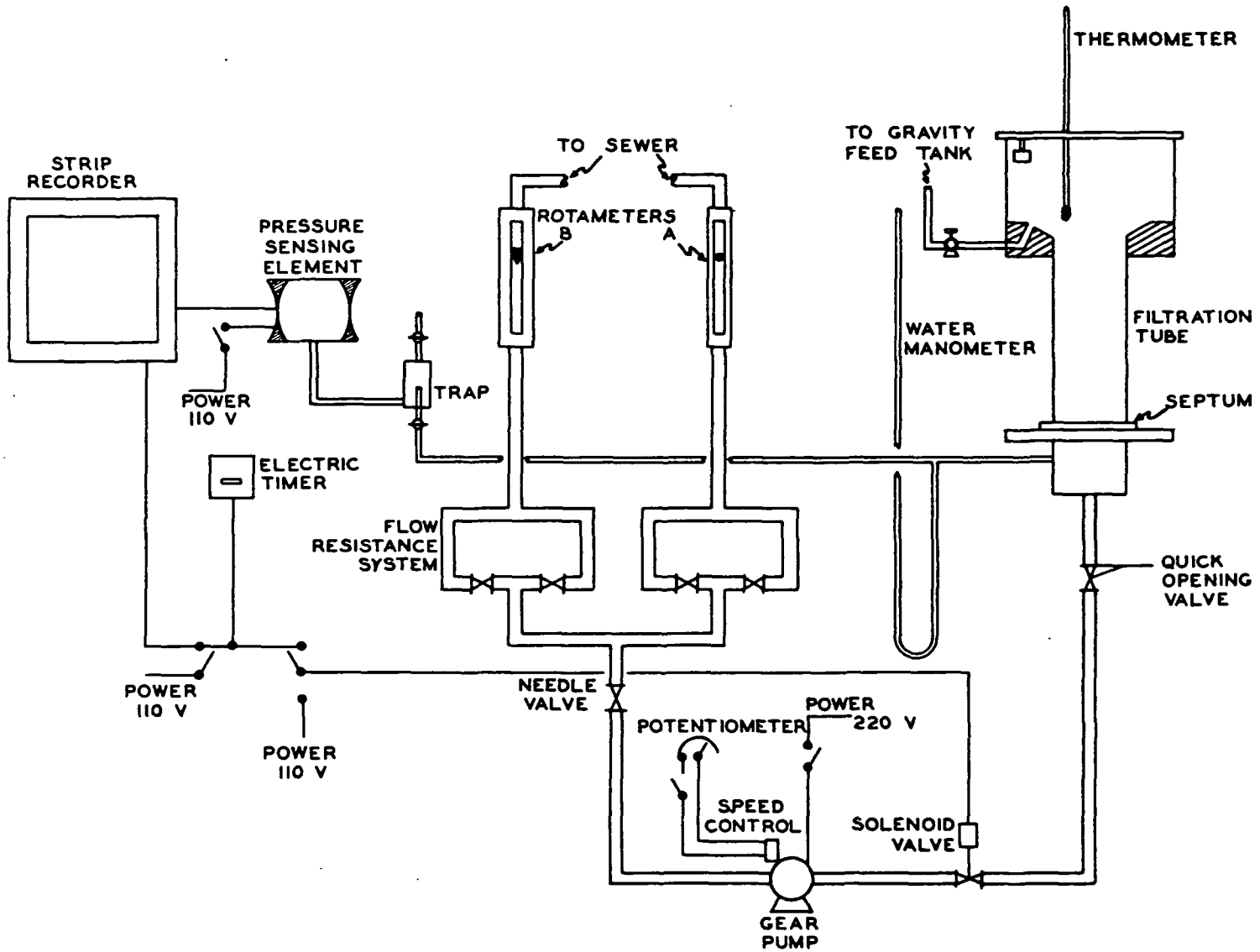

Figure XIX-1. A Constant-Rate Filtration System

balance (IX-3). The corresponding pressure drop across the mat is read from t recorded pressure-time curve, and corrected for the septum resistance. The average specific filtration resistance is then calculated from the constant-rat filtration equation:

$$\bar{R} = \left(\frac{1 - s\bar{m}}{s\rho_s \mu U_0^2}\right) \frac{|\Delta p|}{t} \qquad \text{(IX-22}$$

$\bar{R}$ may then be plotted or tabulated as a function of Δp, usually in the rang 10-100 cm. of water. A comprehensive set of filtration resistance data for wo pulps is shown in Fig. XIX-2 and XIX-3. The correlation of $\bar{R}$ with "freeness' illustrated in Fig. XIX-4. It is obvious that freeness is insensitive in both high and low regions.

The differential constant-rate filtration equation may be rearranged i the so-called rectified form:

$$\frac{d|\Delta p|}{\sqrt{c}\, dt} = \frac{k_1 S_w^2}{B^0 \sqrt{v}} (1 + k_2 v^3 c^3) \qquad \text{(XIX-1)}$$

where S_w is the specific surface based on the fiber mass, and is equal to vS B^0 is called the filtration constant and represents the quantity $(1 - s\bar{m})/(s\rho_s$ in Equation (IX-22). If the suspension consistency is much less than 0.1%, B^0 reduces to $1/(s\rho\mu U_0^2)$. The mat density c at the septum is calculated from th simple compressibility function. By taking the slopes from the corrected press time chart at various pressure drops, Equation (XIX-1) may be plotted as slope/ vs. c^3. If the resulting plot is a straight line, then S_w and v can be evaluated from its slope and intercept. This procedure involves a loss of experimental precision. Instead of taking derivatives, the pressure drops may

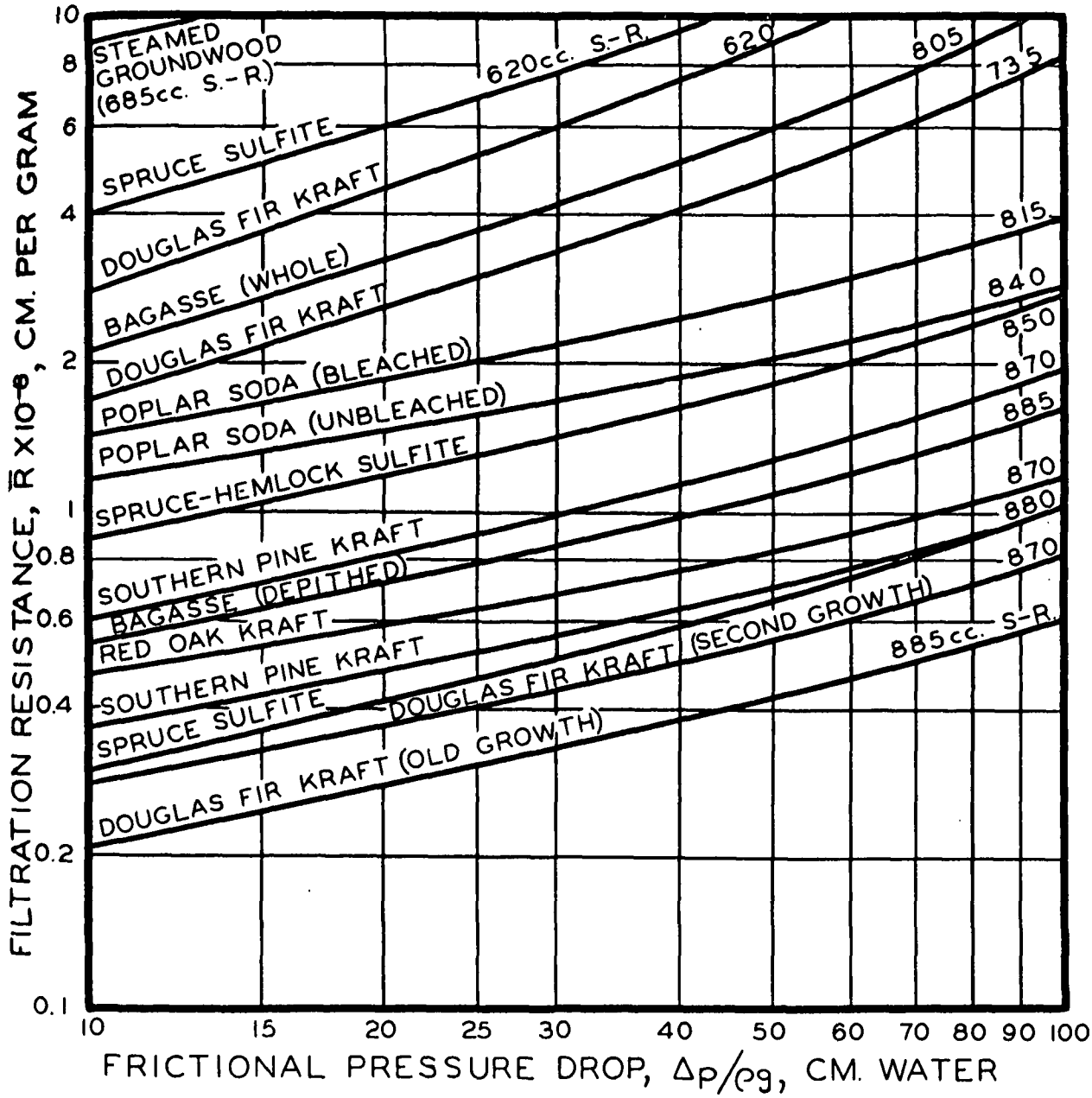

Figure XIX-2. Filtration Resistances of Cellulosic Fibers (Low Range)

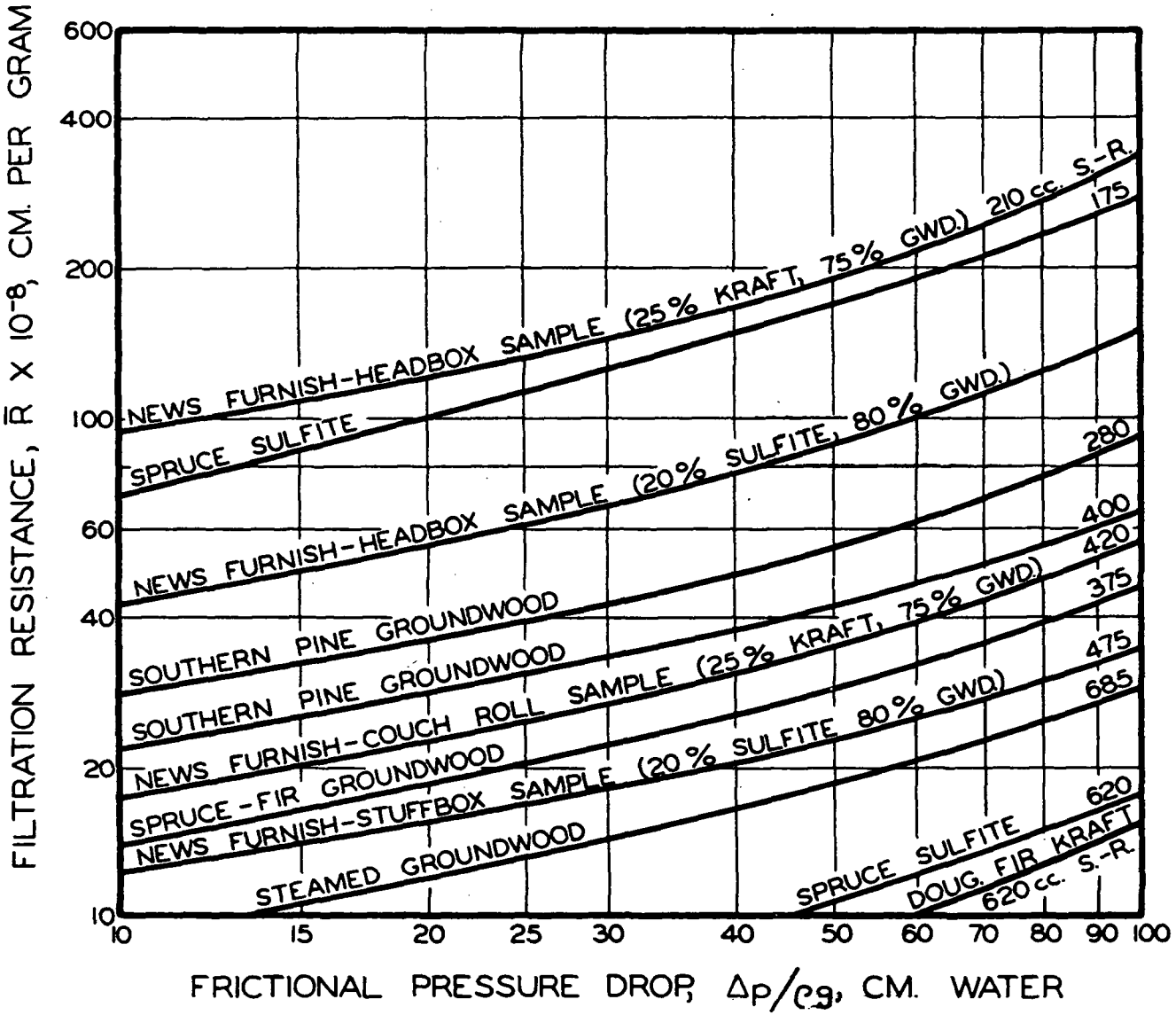

Figure XIX-3 Filtration Resistance of Groundwood

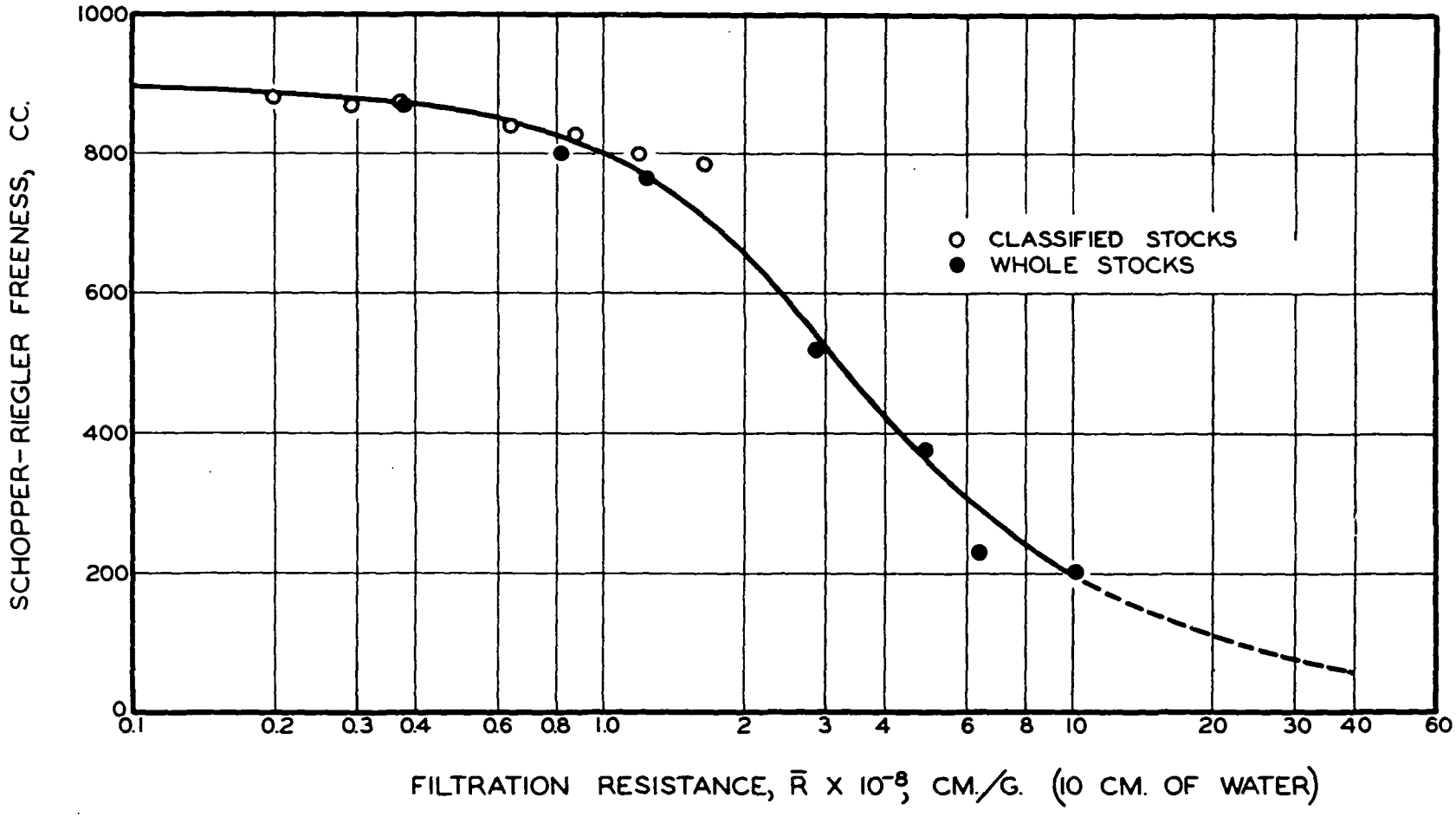

Figure XIX-4. Correlation of Filtration Resistance with "Freeness"

read and corrected from the chart at various times, as in the calculation of the average filtration resistance. The rectified equation now assumes the integrate form:

$$\frac{|\Delta p|}{\sqrt{c}\, t} = \frac{k_1 (1 - N/2) S_w^2}{B^o \sqrt{v}} [1 + k_2 v^3 (1 - N/2)^6 c^3] \qquad \text{(XIX-2)} .$$

By introducing the average mat density in accordance with its definition (IX-13):

$$\bar{c} = (1 - \bar{\epsilon})/v = (1 - N/2)^2 M |\Delta p|^N = (1 - N/2)^2 c \qquad \text{(XIX-3)} ,$$

the alternate form of Equation (XIX-2) becomes

$$\frac{|\Delta p|}{\sqrt{\bar{c}}\, t} = \frac{k_1 S_w^2}{B^o \sqrt{v}} [1 + k_2 v^3 \bar{c}^3] \qquad \text{(XIX-4)} .$$

The following example from Ingmanson and Andrews (XIX-2) may be given as an illustration of the constant-rate method:

Pulp	classified bleached sulfite
U_o	1.80 cm./sec.
μ	0.827×10^{-2} g./(cm.)(sec.)
s	0.0196×10^{-2} g./g.
B^o	1.90×10^3 (sq. cm.)(sec.^{3})/g.^{2}

The filtration and compressibility data are shown in Fig. XIX-5. The data are then plotted in Fig. XIX-6 in the rectified form (XIX-4). The result is nonlinea curving concave-downward. If linearity is forced to fit most of the data and extrapolated to zero mat density, such as shown by the dashed line, the resulting values for specific surface and volume are 5030 sq. cm./g. and 2.16 cc./g., respectively, using 3.5 for k_1 and 57 for k_2 . These are obviously sort of

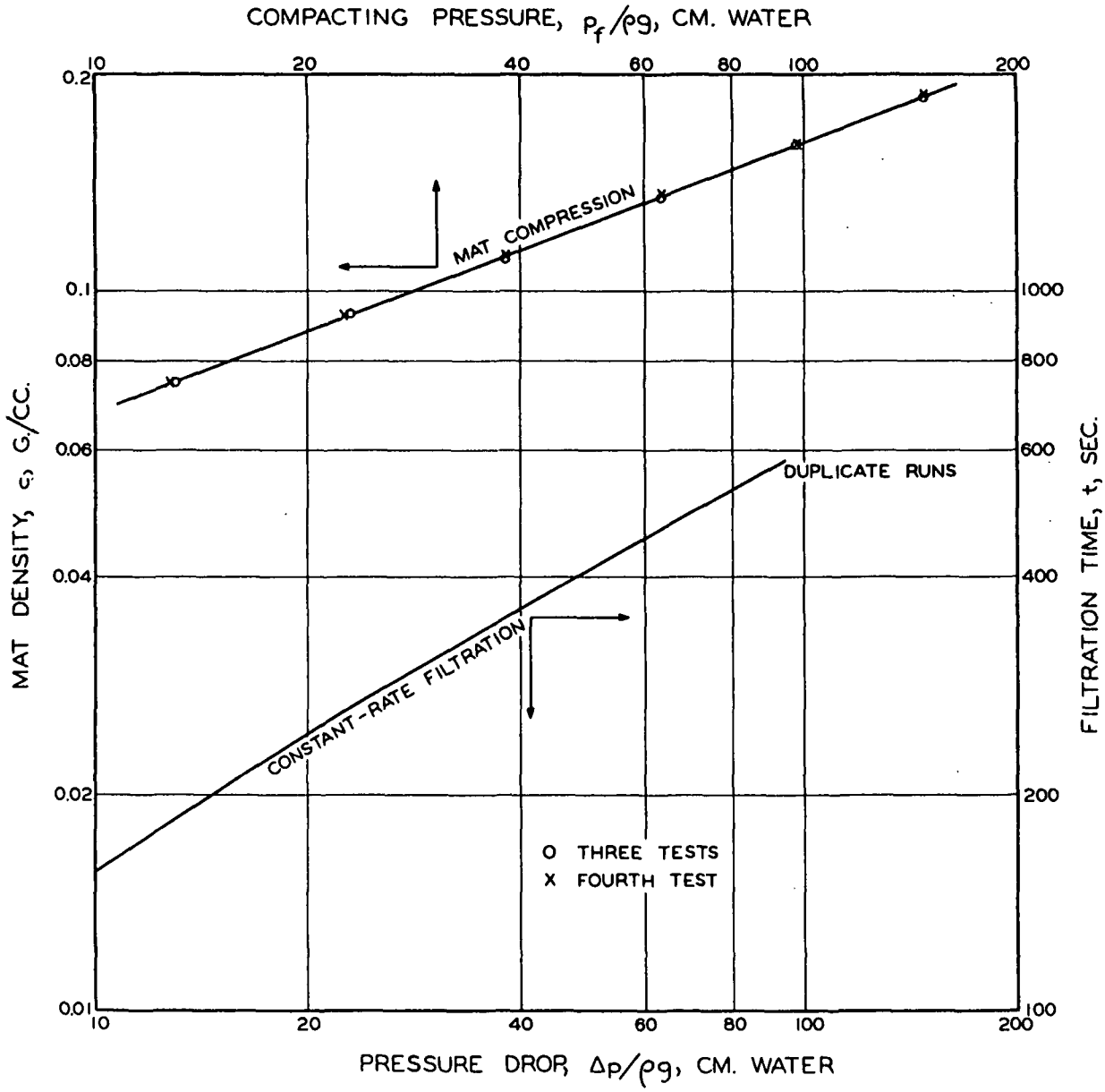

Figure XIX-5. Filtration and Compressibility Data

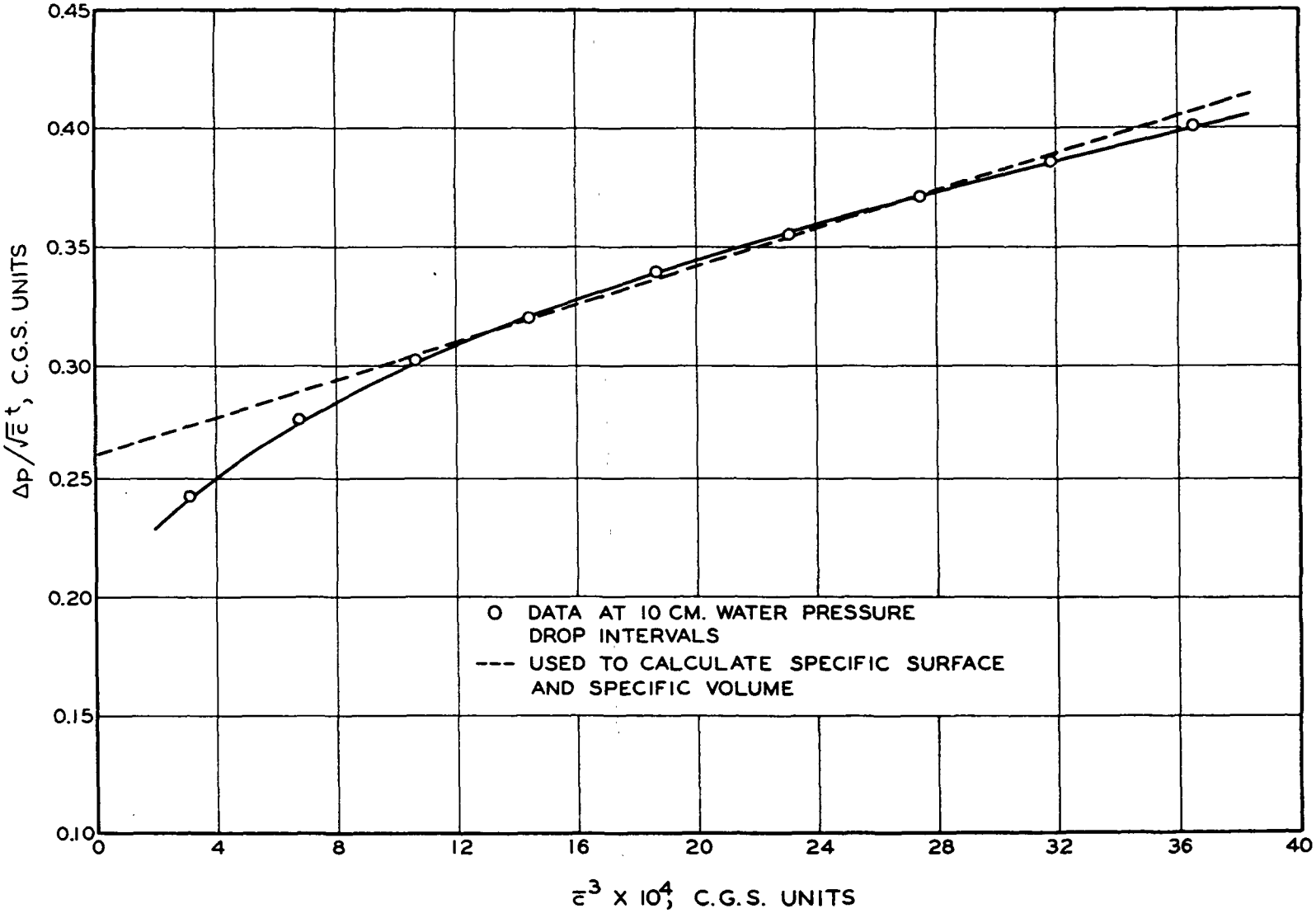

Figure XIX-6. Rectified Plot of Filtration Data

average values. They may be compared with the average values determined microscopically, which are 5,370 and 1.64, respectively. It should be mentioned that the microscopic method always yields a lower specific volume because of the difficulty in preparing fiber cross sections in a fully swollen state.

COMPENSATING FACTORS

The deviation from linearity should be examined in some detail. At the outset one may question the legitimacy of the integration process from which the definition of the average mat density or porosity has been derived, i.e., the evaluation of the integral (IX-10):

$$\int f(1 - \epsilon)dp_f \ .$$

In connection with this question there are two points to be clarified. One is the doubtful assumption of unity porosity or zero mat density at the mat-suspension boundary. However, whatever reasonable value is chosen for the solid fraction at the mat face, it will not affect the integration result to a significant extent as the flow resistance is determined predominantly by the rest of the mat at substantially lower porosities. The other point has to do with the use of the abbreviated Davis porosity function, which is only valid for porosities greater than 0.9, in order to perform the integration analytically. If the integration is carried out numerically for lower porosities, using the Davis function in its complete form, the results are not more than 7% lower than those based on the average porosity definition (XIX-3). Furthermore, the small discrepancies are nearly the same for a large number of different pulps throughout the porosity range concerned. We therefore conclude that the use of average porosity is justifiable and the cause of deviation from linearity lies somewhere else.

It is entirely possible that the porosity function based on cylindrica fibers may vary with fiber shape and contact area, thus rendering its use for cellulosic fibers questionable. Bliesner (XIX-3) prepared flattened synthetic fibers of approximately elliptical cross section and with an average aspect (wid to thickness) ratio 3-4. Using the theory of Onogi and Sasaguri (VI-1) for contact points and the equation of Van den Akker (XIX-4) for projected contact area, he demonstrated considerable departure of the porosity function for flatte fibers from cylindrical ones, based on his air permeability data with the assump of the maximum possible projected area. Labrecque (XIX-5) proceeded to recalcu Bliesner's data to account for incomplete contact, as estimated from Bliesner's photomicrographs of fiber arrays, and arrived at porosity functions as shown in Fig. XIX-7. For both nylon and orlon fibers the Kozeny factor increases with increasing aspect ratio at the same porosity while the general trend of the functions remains the same and tends to converge at high porosities. In the dynamic sense, resistance increases with fiber flattening (a larger pore shape factor than unity for cylindrical fibers) and decreases with contact area (a smaller surface area available to flow), the former being a stronger influence i the practical porosity range.

The data for wood pulp (Fig. XIX-3), however, indicate that for the intermediate porosity range the deviation from linearity is the least. This may indicate a fortuitous compensation by a third factor which is thought to be the deswelling of cellulosic fibers under pressure. Deswelling will cause a higher porosity or lower resistance at the same mat density. The inclusion of the deswelling factor would also account for the larger deviation of both higher and lower porosities. As the pressure drop increases, deswelling increases the actual porosity while the Kozeny factor remains relatively constant at a value

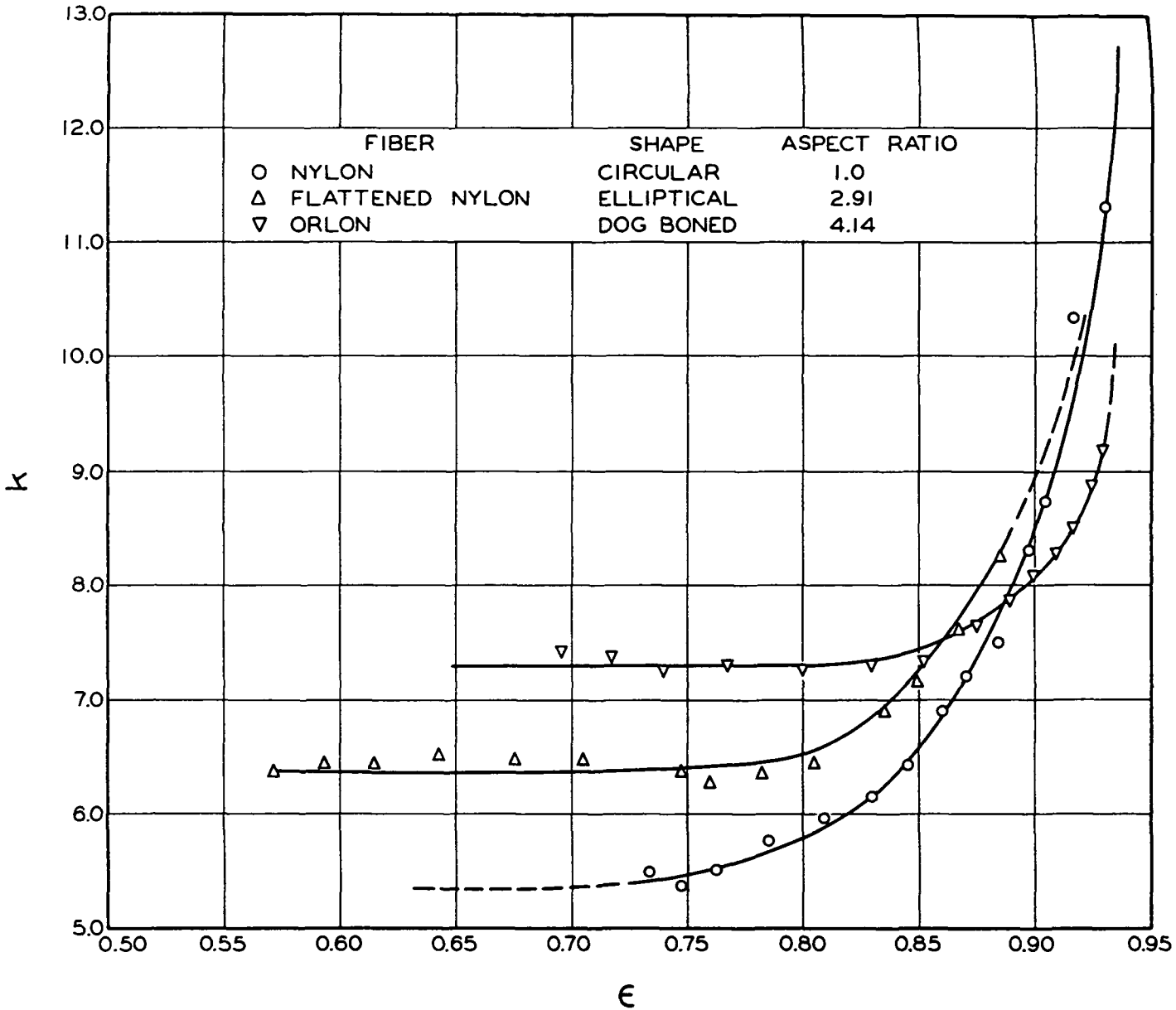

Figure XIX-7. Effect of Fiber Shape on Kozeny Factor

higher than previously assumed. Thus, the discrepancy would become larger with the increasing mat density. In the other direction, as the pressure drop decrea the Kozeny factor tends to the assumed function whereas deswelling continues to increase the actual porosity, resulting in a lower resistance than expected.

DESWELLING ESTIMATE

In light of the experimental evidence and its interpretation, Meyer (XIX-6) suggested an approximate method of finding the dependence of specific volume and surface on compacting pressure. He put Equation (XIX-4) in a modified form:

$$p^* = k_1^* \frac{S_w^2}{\sqrt{v}} [1 + k_2^* v^3 c^3] \qquad \text{(XIX-5)} .$$

Assuming v and S_w to have some representative mean values for any two points 1 and 2 along a short segment of the curve (Fig. XIX-6) and using Lagrange's interpolation formula, he estimated their dependence on pressure from the following equations:

$$v = \left[\frac{p_1^* - p_2^*}{k_1^* (c_1^3 p_2^* - c_2^3 p_1^*)} \right]^{1/3} \qquad \text{(XIX-6)}$$

and

$$S_w = \left[\frac{c_1^3 p_2^* - c_2^3 p_1^*}{k_1^* (c_1^3 - c_2^3)} \right]^{1/2} v^{1/4} \qquad \text{(XIX-7)} .$$

The results of calculation for the sulfite pulp are shown in Fig. XIX-8. It is seen that the specific surface on the mass basis increases only mildly while the specific volume decreases pronouncedly with increasing pressure drops.

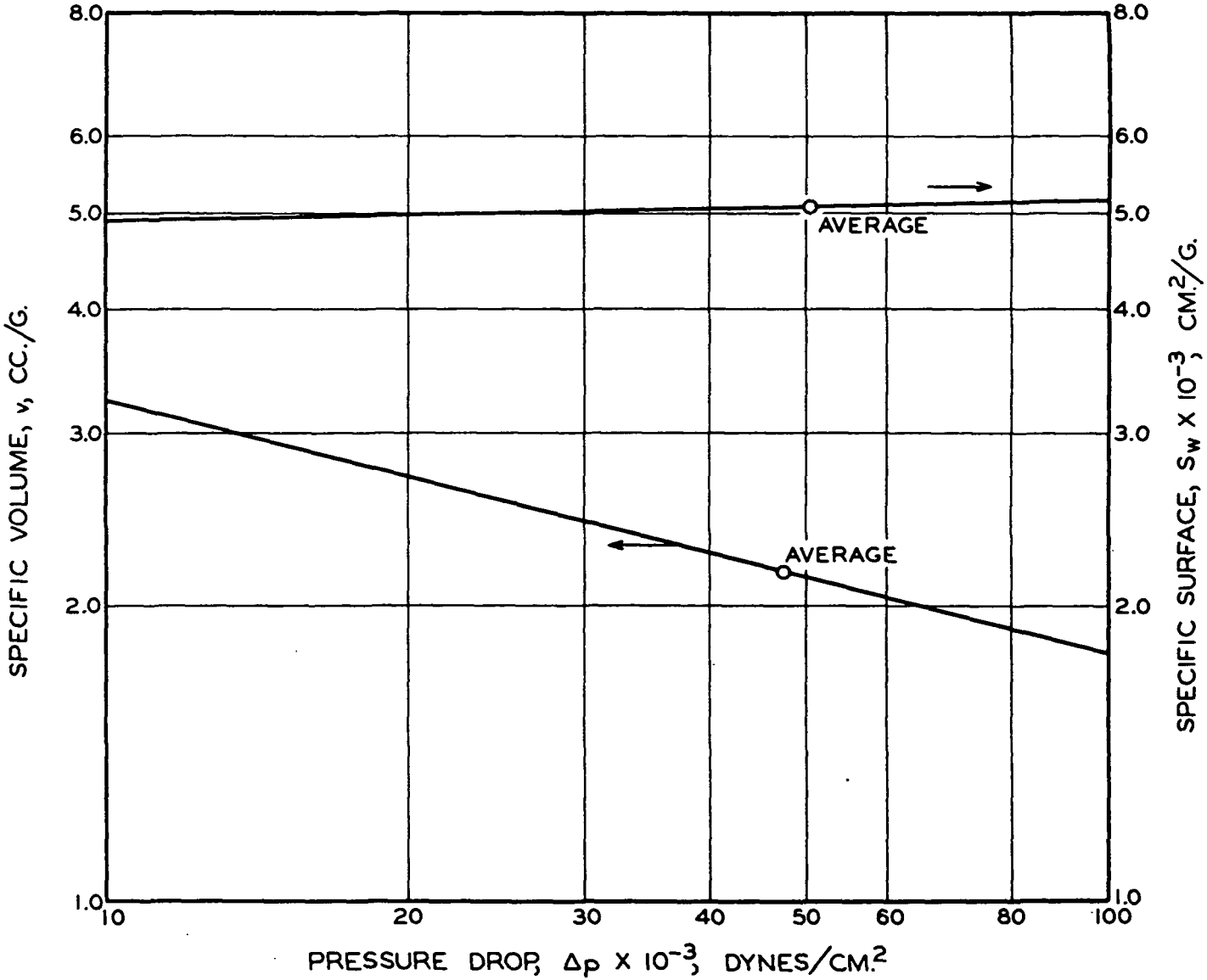

Figure XIX-8. Variation of Specific Volume and Surface

PERMEABILITY DECAY

The decay of permeability of wood pulp mats is a familiar phenomenon An example is illustrated in Fig. XIX-9. The first experimental factor causi decay is the gradual retention of foreign particles in a mat from a large volu of water flowing through the mat. By thoroughly cleaning the entire system ar using distilled and filtered water, this source of trouble may be eliminated, b only with extreme care. A second factor is the fines in wood pulp, which may partially overcome by extra classification.

With these precautions a permeation experiment was carried out by Andrews (XIX-7). A mat of 105 g./sq. m. was formed, and the pressure drop readings were taken quickly over a flow range of 10-160 cm./sec. When the highest flow was reached, the velocity was successively decreased, allowing the mat to expand slowly until the lowest point was reached again. After repeatin the procedure for six cycles, it was found that the same pressure drop-velocity curve could be attained. The whole conditioning process took eight hours, aft which permeation was maintained at the highest flow for one hour. During this hour no decay was observed.

The results of this experiment agree with the known effect of mechani conditioning on compressibility behavior (Chapter XVII). The power of the com pressibility function reduces from that for the first compression to about less than half the original value in the case of a conditioned mat. This serves to explain the decay of a freshly formed mat in the previous permeation experiment

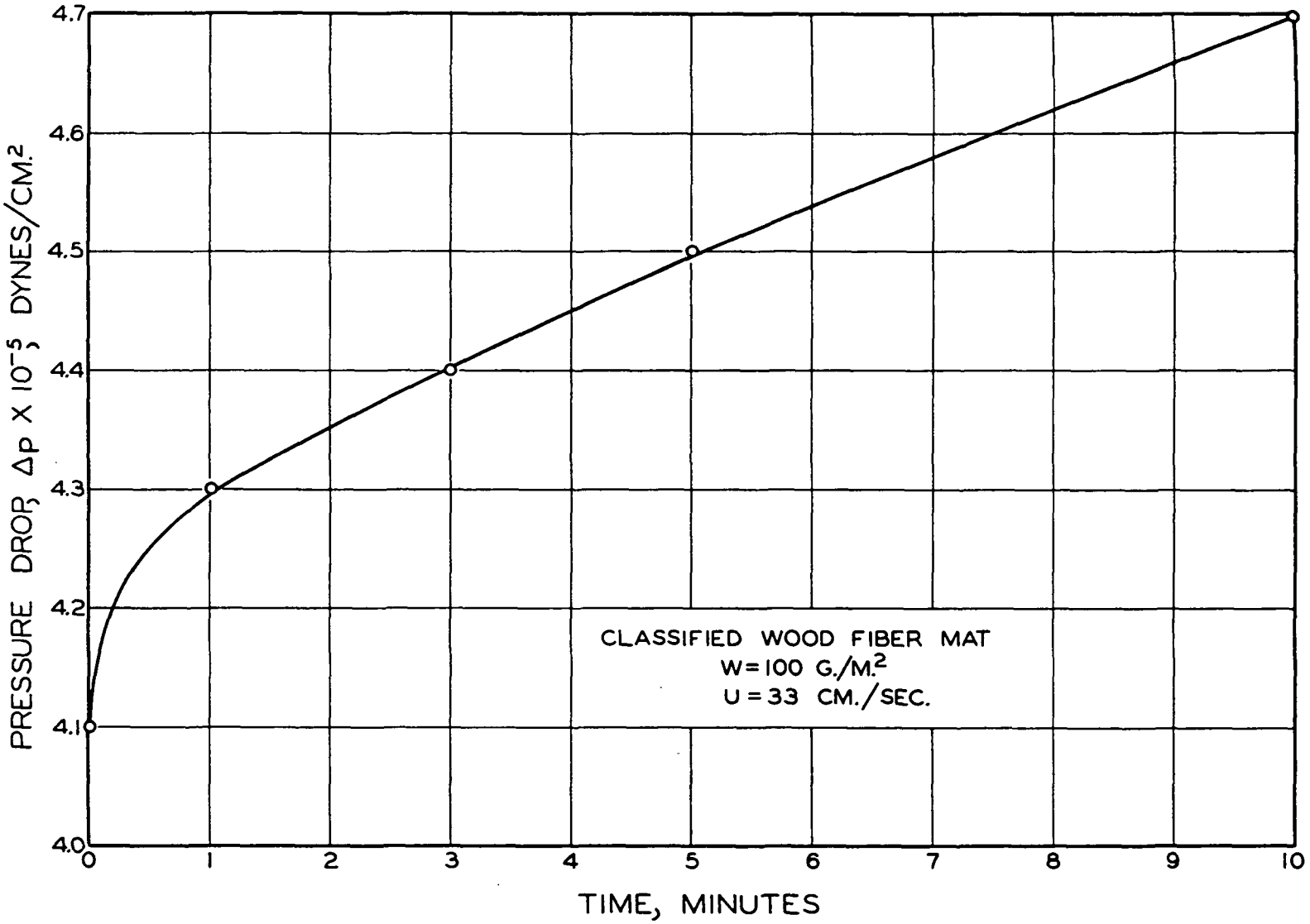

Figure XIX-9. Permeability Decay

XX. DYNAMIC EFFECTS IN CONSTANT-RATE FILTRATION

In simple filtrations so far described, possible dynamic effects have b
either avoided or discounted. When drainage of a fiber suspension is suddenly initiated by an external force, the fluid must undergo acceleration because of th unbalanced forces acting on the system. With viscoelastic fibers the response o the mat to the compacting force is time dependent. This is another factor to be taken into consideration in "dynamic" drainage. Finally, if the system is subje to disturbances, instability may set in, depending on the nature and magnitude of the disturbances as well as the ability of the system in damping them.

To clarify some of these factors, we have used a dynamic drainage teste which is capable of performing a complete filtration test in a relatively short time. The experiments were performed by White (XX-1) and Andrews (XX-2).

DRAINAGE TESTER

The tester consists of a tube and piston with a driving mechanism. Th Lucite tube is 7.6 cm. in diameter and 100 cm. tall. The top of the tube is fit with two flanges between which a wire screen is clamped. The open end is enclos in a box for the flow to return through a pipe by gravity into a receiver. The steel piston has a Teflon sleeve in contact with the tube wall to improve lubrica tion and sealing. The piston is rigidly connected with a driving member. The original driving mechanism was a rack and pinion system connected to a variable speed reducer and engaged by a hand-operated clutch. It was later changed to a hydraulic system with actuating and control valves. The former system is shown in Fig. XX-1. Both systems operate in the speed range of 1-100 cm./sec.

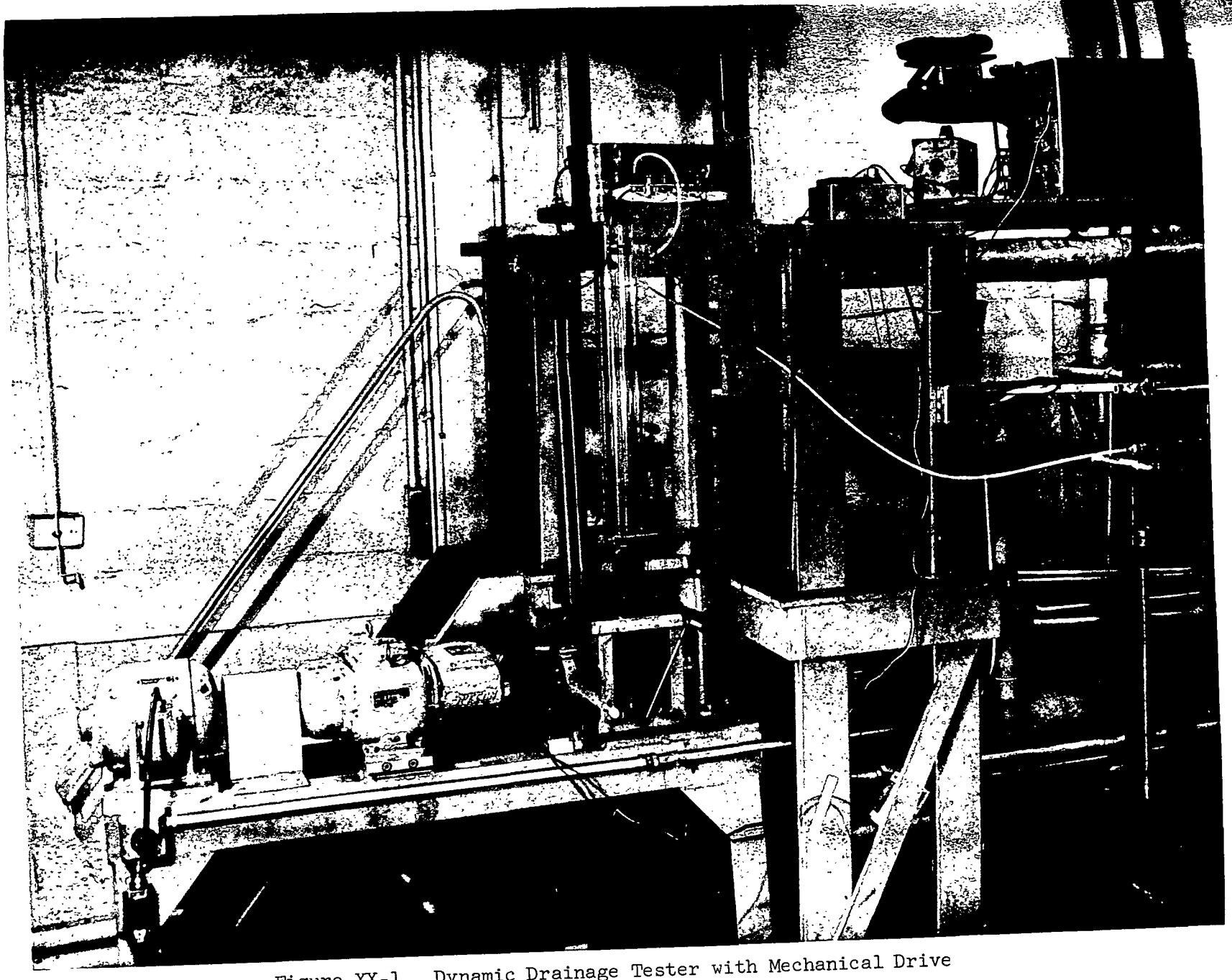

Figure XX-1. Dynamic Drainage Tester with Mechanical Drive

Near the lower flange on the tube wall is located a pressure tap which is connected by a plastic tubing to one of two transducers covering a pressure range up to 700 cm. of water and calibrated with a manometer. The output of either transducer is received by an oscilloscope. The pressure trace on the oscilloscope is recorded by a Polaroid camera.

With the rack and pinion mechanism, when the clutch is engaged, the inertial system consisting of the piston, rack, pinion, and the driven member of the clutch undergoes rapid acceleration to reach the driving speed. This initial acceleration as measured by means of an accelerometer is shown in Fig. XX-2. The acceleration rises to a maximum, then falls to a minimum, and finally oscillates about the zero value. This period lasts within 0.05 sec. Thus, the piston accelerates from zero to a mean velocity in this short period of time and then continues to oscillate about the mean velocity with a major frequency of the gear teeth number per stroke time and an amplitude less than one cm./sec. The pressur of the water in the tube also oscillates about a mean value with the same major frequency and an amplified amplitude due to external disturbances. The temporal mean values of velocity and pressure, however, are reliable.

TEST RESULTS

Preliminary sheet-forming tests were made with 3-denier dacron fibers and 52-mesh screen. The tube was rapidly filled with a dilute suspension in upward flow. As soon as the suspension reached the screen, the clutch was engaged and at the same instant an electric timer and the pressure-recording instrument were activated through microswitches. The piston motion was arrested by a mechanical clutch release when the piston reached the screen. The stroke ti was of the order of one second. After the run the fibers on the screen were collected, dried, and weighed.

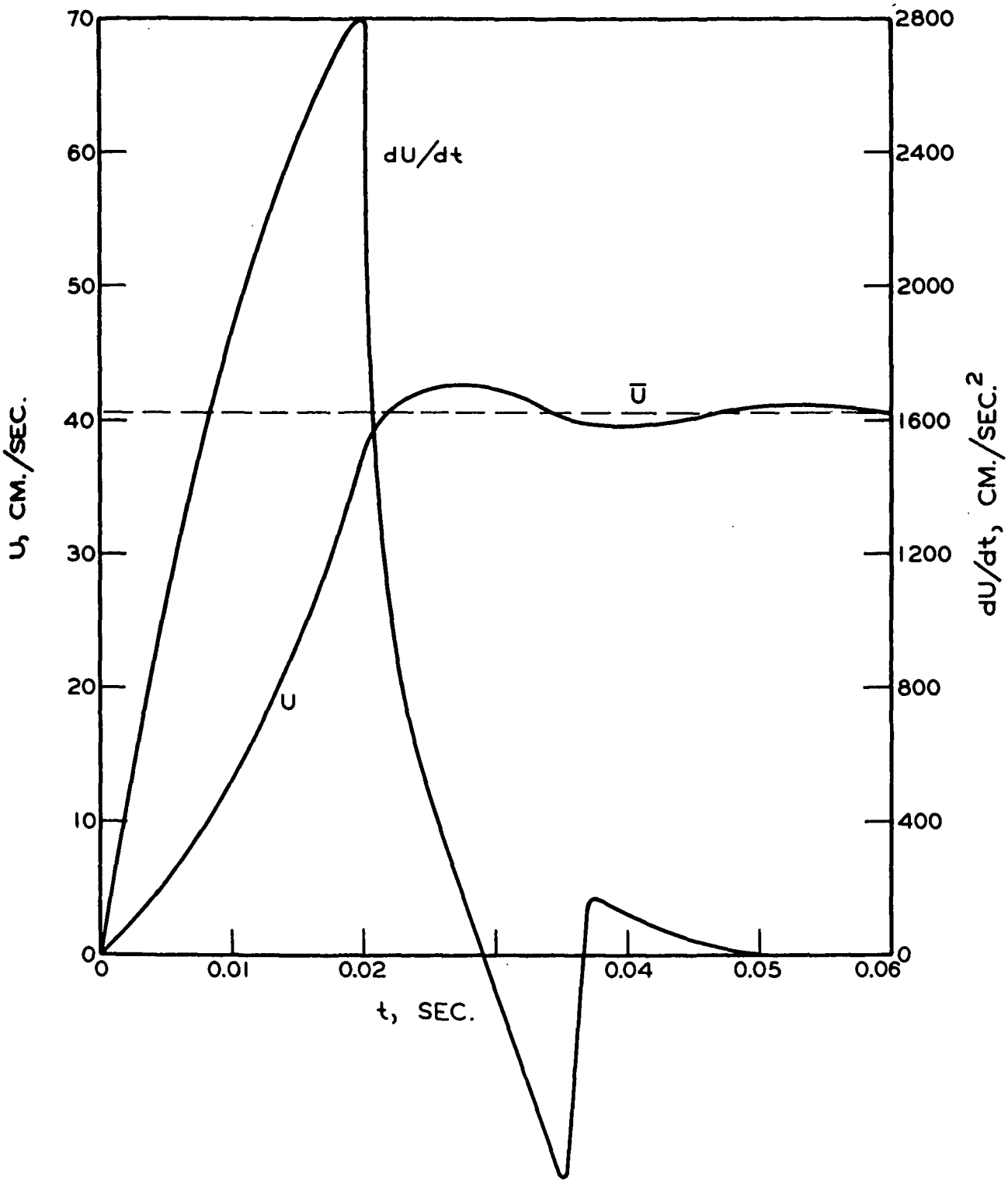

Figure XX-2. Piston Velocity and Acceleration

For each run the pressure drops $\overline{\Delta p}$ were translated from the pressur trace and corrected for the screen resistance at arbitrary intervals. The corresponding basis weights were determined by

$$W = \rho s \bar{U}(t - t_o) \qquad \text{(XX-1)}$$

where t_o is the time lag in synchronizing the initiation of drainage and pres trace by extrapolating the latter to zero pressure.

In a series of duplicate runs it was found that their discrepancies we as large as 50% at early times and became as close as 6% toward the end. The early large discrepancies were attributable to various sources of random errors experimental measurements and translations. The average data of several duplic runs were reliable. These results are shown in Fig. XX-3 and compared with the previously established correlation (XVIII-12). The maximum deviation is 10%.

The apparent absence of nonequilibrium effects in the average results these experiments may be attributed to three factors: (1) low compressibility c dacron fiber mats, (2) dilute suspensions, and (3) insufficiently short forming times. The low compressibility is reflected by the nearly linear relationship between the pressure drop and the basis weight. Flow pulsations and pressure fluctuations in the tester were probably not of sufficient magnitudes to affect the compressibility. As the mats were formed from a dilute suspension, the mot of fibers, once deposited, was negligible. The mats were in a state of quasi-equilibrium just as in slow filtrations. The time scale from slow filtration i the regular apparatus to rapid drainage in the dynamic tester was two decades. This reduction might not be enough to show the time-dependent effects. Further more, while the compressibility behavior is dependent on the rate of pressure

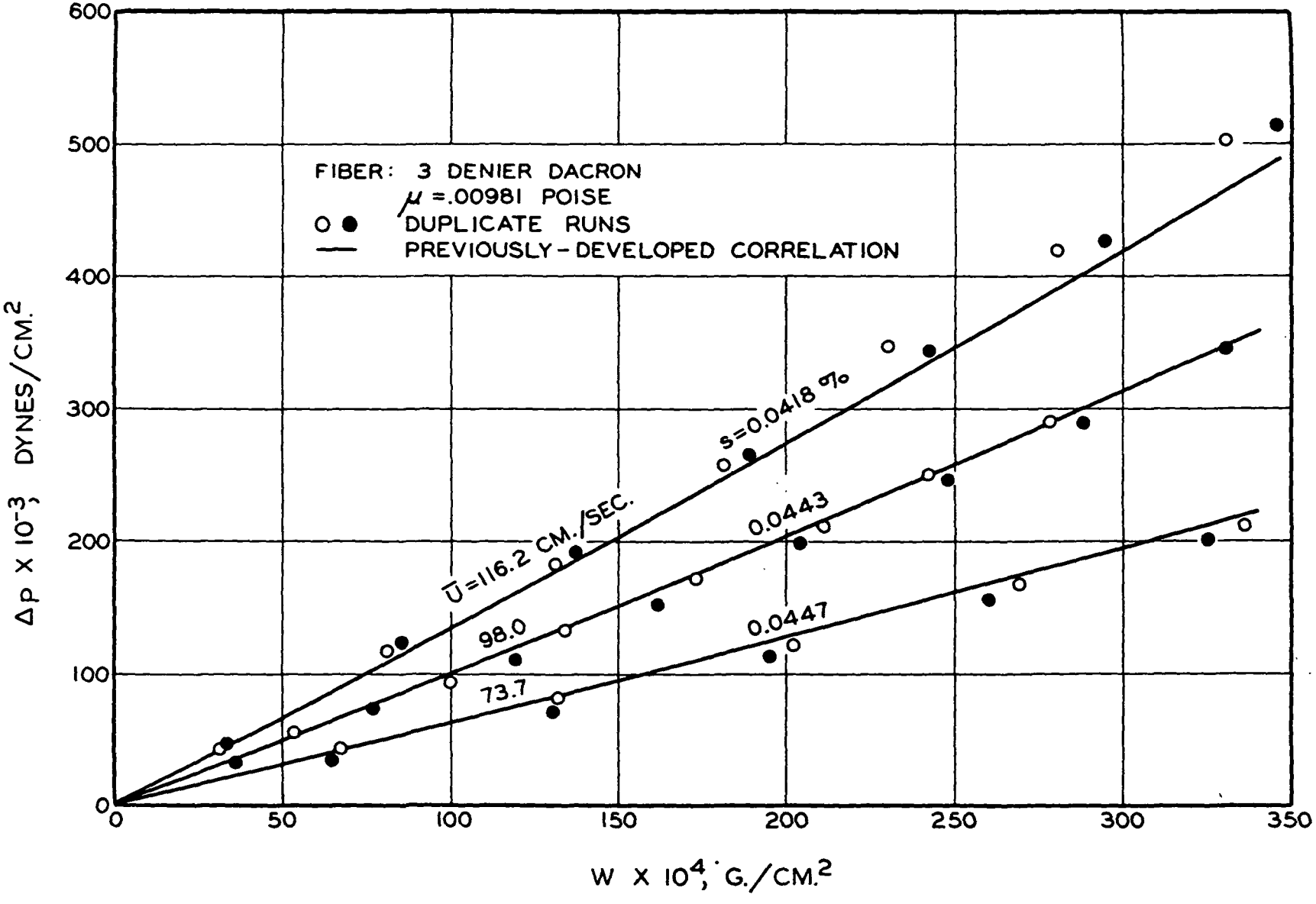

Figure XX-3. Dynamic Drainage Test Data

rise, the considerable increase in the tester, as shown below, might still be insufficient for dacron mats.

	Slow Filtration	Rapid Drainage
Forming time, sec.	10	10^{-1}
Pressure rise, dynes/(sq. cm.)(sec.)	10^{3}	10^{6}

A classified bleached sulfite pulp was then used in the dynamic drainage tester with a 100-mesh screen in a speed range from 20 to 100 cm./sec The reproducibility was again satisfactory, about 3-8%. However, upon compar with the known correlation, the pressure drop from the test results was always higher than the calculated value for the same filtration time, the discrepancy increasing with increasing velocities. Such a comparison is shown in Fig. XX for the high-velocity range. Because of the low consistency (about 0.004%) tl high-velocity runs covered basis weights up to about 30 g./sq. m.; even the lo velocity data with a 0.01% consistency extended the basis weights to only 70 g. per sq. m. For further analysis the complete set of data were smoothed and transformed into pressure drop-basis weight curves which are shown in Fig. XX-5

In view of the large discrepancies, the initial step of analysis was check the data for linearity by the differential form of the Forchheimer law:

$$\frac{1}{\bar{U}} \frac{d|\overline{\Delta p}|}{dW} = R\mu + R'\rho\bar{U} \qquad \text{(XX-1)}$$

where the resistances $\underline{R}$ and $\underline{R}'$ are understood to be functions of the pressu drop. Therefore, at a given pressure drop, the data should show a straight li with slope $\underline{R}'\rho$ and intercept $\underline{R}\mu$. The results of this analysis at several chosen pressure drops indicated definite concave-upward curvatures in the whole

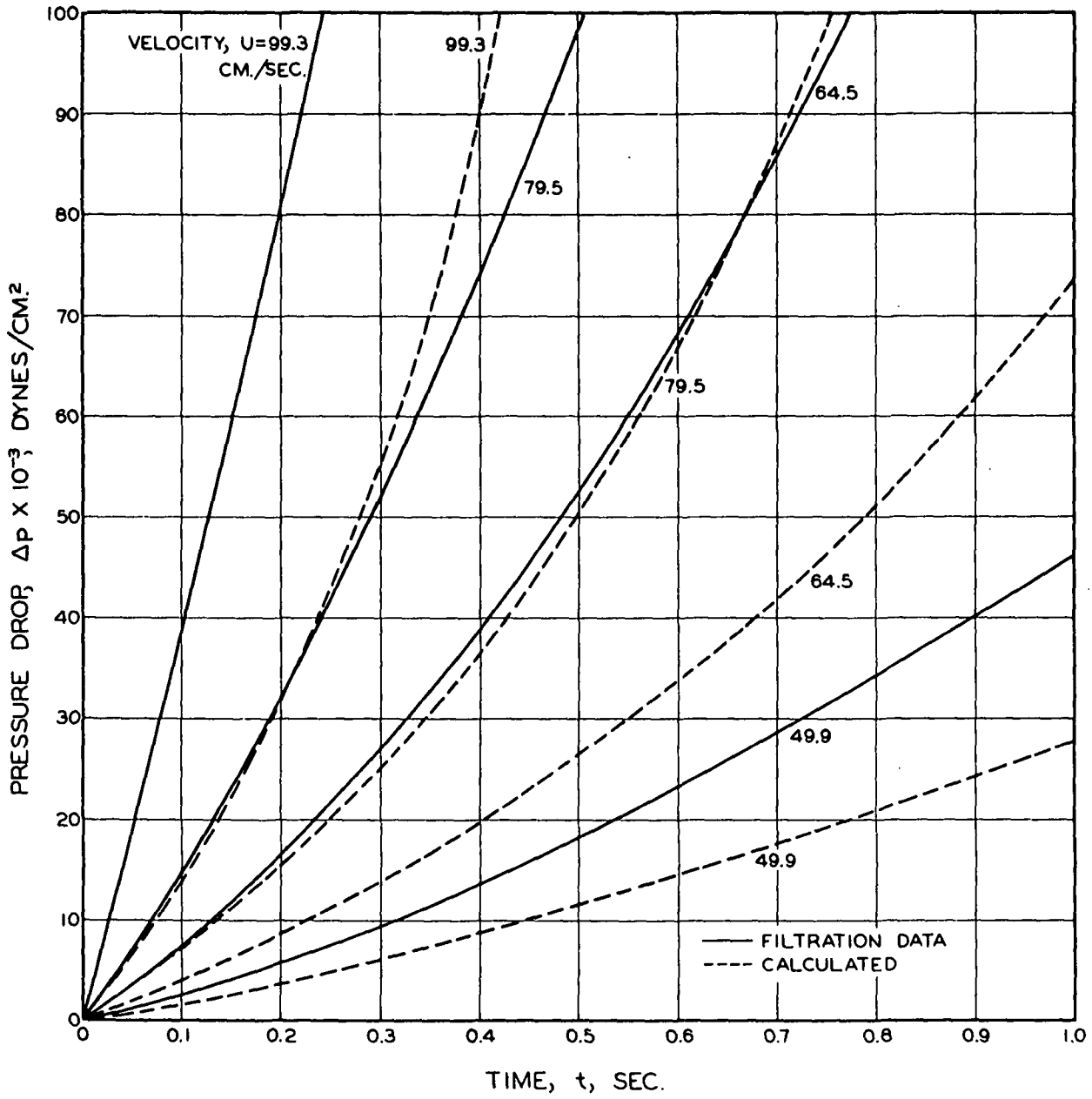

Figure XX-4. Drainage Data for Thin Sulfite Mats

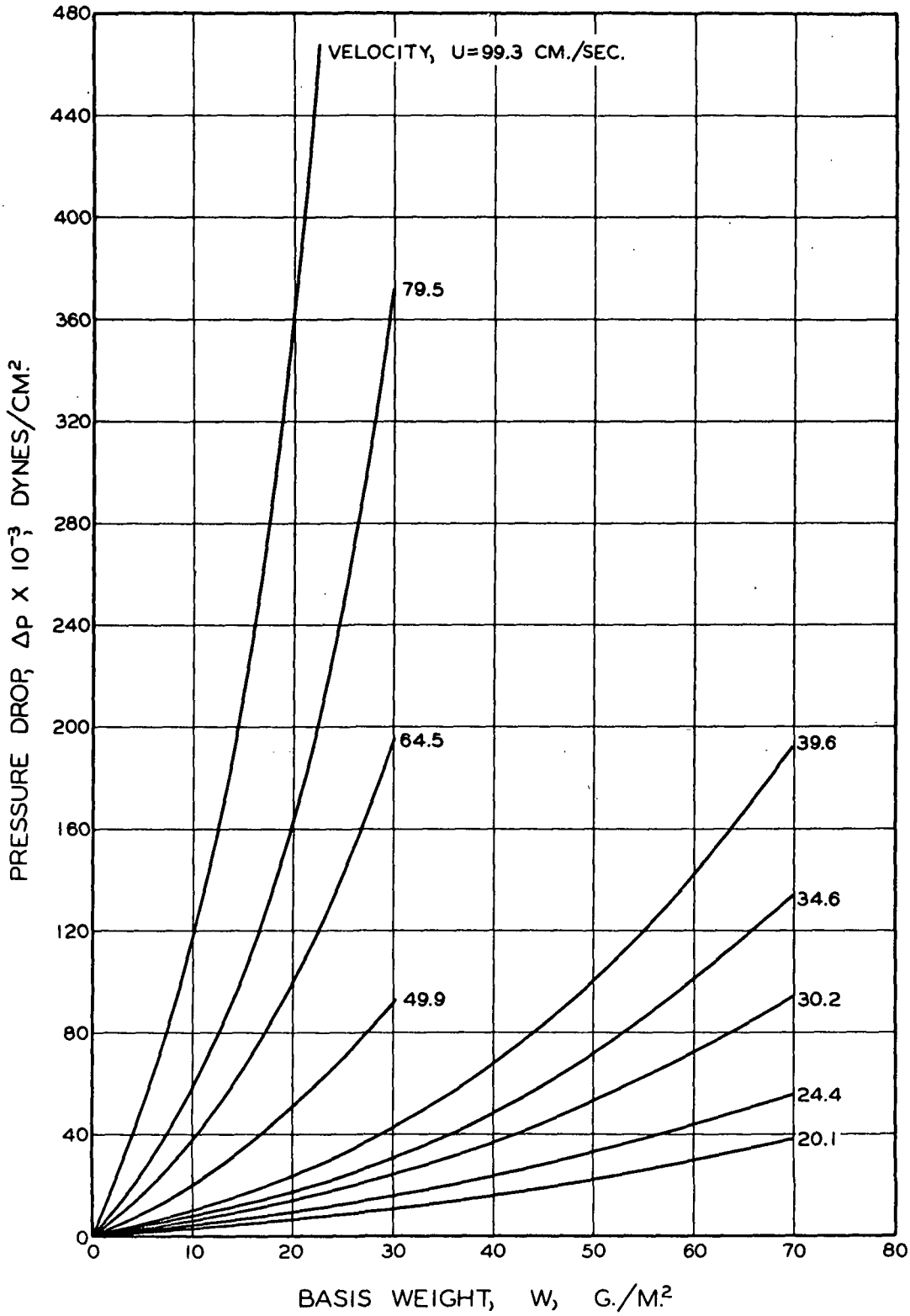

Fig. XX-5. Drainage Data for Sulfite Mats

range of velocities. By further analysis it was revealed that the discrepancy became smaller and smaller as the basis weight approached 50 g./sq. m.

The possible causes of such discrepancies were thought to be the change of compressibility behavior and the fiber-wire interaction. The change of compressibility behavior could be due to pressure pulsations or inherent in thin mats. The first factor could not be very large in view of the previous agreement secured in the same tester in the case of dacron fibers. The second factor, which was originally thought to be important, turned out to be also minor when the experimental evidence for the compressibility of thin mats showed nearly the same behavior as thick ones, as presented in Chapter XVII. A tentative conclusion was that the additional flow resistance was probably caused by the fiber-wire interaction. Figure XX-6 shows photomicrographs of a thin mat and a relatively thick mat of the sulfite fibers used. For the former the mat may be only 2 to 3 fibers thick, while the latter amounts to about a dozen fiber diameters. What is called the fiber-wire interaction was viewed by Ingmanson (XX-3) primarily as the bending of the flow lines around the individual wires of the screen, as discussed in Chapter XIII. The convergence of flow through the screen openings was thought to incur additional energy losses.

Before proceeding to explore the problem of fiber-wire interaction, we conclude this chapter by stating again that the time-dependent dynamic effects which we were seeking have failed to reveal any particular significance in these rapid drainage results.

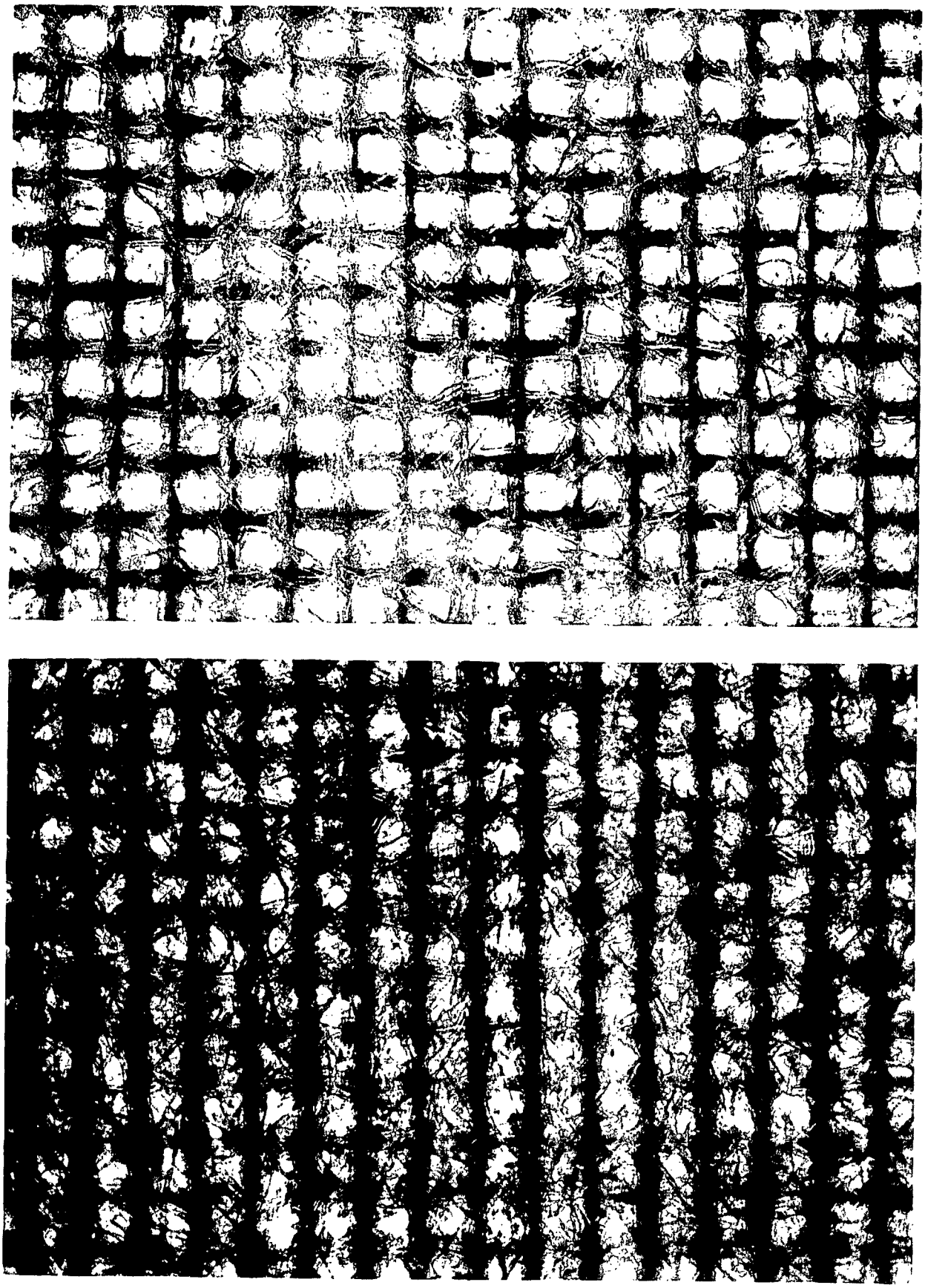

Figure XX-6. Photomicrographs of Sulfite Mats
(Top: 12.1 g./sq. m. and bottom: 37.7 g./sq. m., both 40X)

XXI. FIBER-WIRE INTERACTION IN SHEET FORMING

The resistance of a wire screen supporting a thick mat can be justifiably neglected. As the basis weight is reduced to less than 300 g./sq. m., the wire resistance becomes proportionately important, the pressure drops across the mat and the wire being additive. For cylindrical fibers this rule applies to basis weight as low as 50 g./sq. m. However, for thin sheets of cellulosic fibers there are complications involved other than fiber-wire interaction. Our attempt to clarify the different effects is necessarily of an exploratory nature. The experimental work was performed by Andrews (XXI-1) and the data analysis by Meyer (XXI-2).

EXPERIMENTAL RESULTS

The dynamic drainage tester described in the last chapter exhibited pressure pulsations caused by mechanical vibrations. To reduce their possible influences on the test results, a hydraulic drive was substituted for the rack-and-pinion mechanism. The modified apparatus is shown in Fig. XXI-1. The hydraulic drive consisted of a pump, an actuating valve, a control valve, and a cylinder. The cylinder, with a 36-in. stroke and cushioned on the rod end, was rigidly mounted to maintain alignment with the flow tube.

With the aid of an accelerometer the initial accelerating period of the piston was found to be reduced to a maximum of 0.01 sec. The piston velocity was established by motion pictures aiming at a 10-cm. span and cross checked by the pressure trace. The results agreed with each other. Vibrations were still noticeable in the pressure trace, but they were much less severe than before.

The screens used were 100-mesh plain weave, 48-mesh plain weave, and 74 x 58 semitwill weave. They were calibrated both in the permeability apparatus

Figure XXI-1. Dynamic Drainage Tester with Hydraulic Drive

and the drainage tester over a velocity range of 1-100 cm./sec. The results are shown in Fig. XXI-2.

A dilute suspension of classified bleached sulfite fibers was used in this work. The average fiber length determined microscopically was 2.05 mm. In one experiment the fiber length was cut to 1.25 mm. without altering the cross sections significantly.

Since the screens were unsupported by a backing plate, they were subjected to deformation. To minimize the screen deformation, the highest basis weight was limited to 100 g./sq. m. at a velocity of 20 cm./sec. With the improved sensitivity of a second pressure transducer it was possible to reduce the basis weight to as low as 4 g./sq. m. The set of low basis weight data is shown in Fig. XXI-3, in which the pressure drop has been corrected for the screen resistance by subtracting the calibrated value for the screen (Fig. XXI-2) from the measured value for the mat-screen combination.

DATA REDUCTION

The raw data were replotted in the form of pressure drop vs. flow velocity with basis weight as the parameter in selected increments from 10 to 100 g./sq. m. Two sets of data are shown in Fig. XXI-4 and XXI-5. The former corresponds to Fig. XXI-3 and the latter differs only in fiber length.

On inspection the data showed certain definite trends. (1) With the same screen the shorter fibers cause higher pressure drops. (2) For both fiber lengths there is little difference between the semitwill- and plain-weave data. (3) The 100-mesh screen shows lower pressure drops at lower basis weights. The differences due to screens tend to vanish with increasing basis weights, as expected.

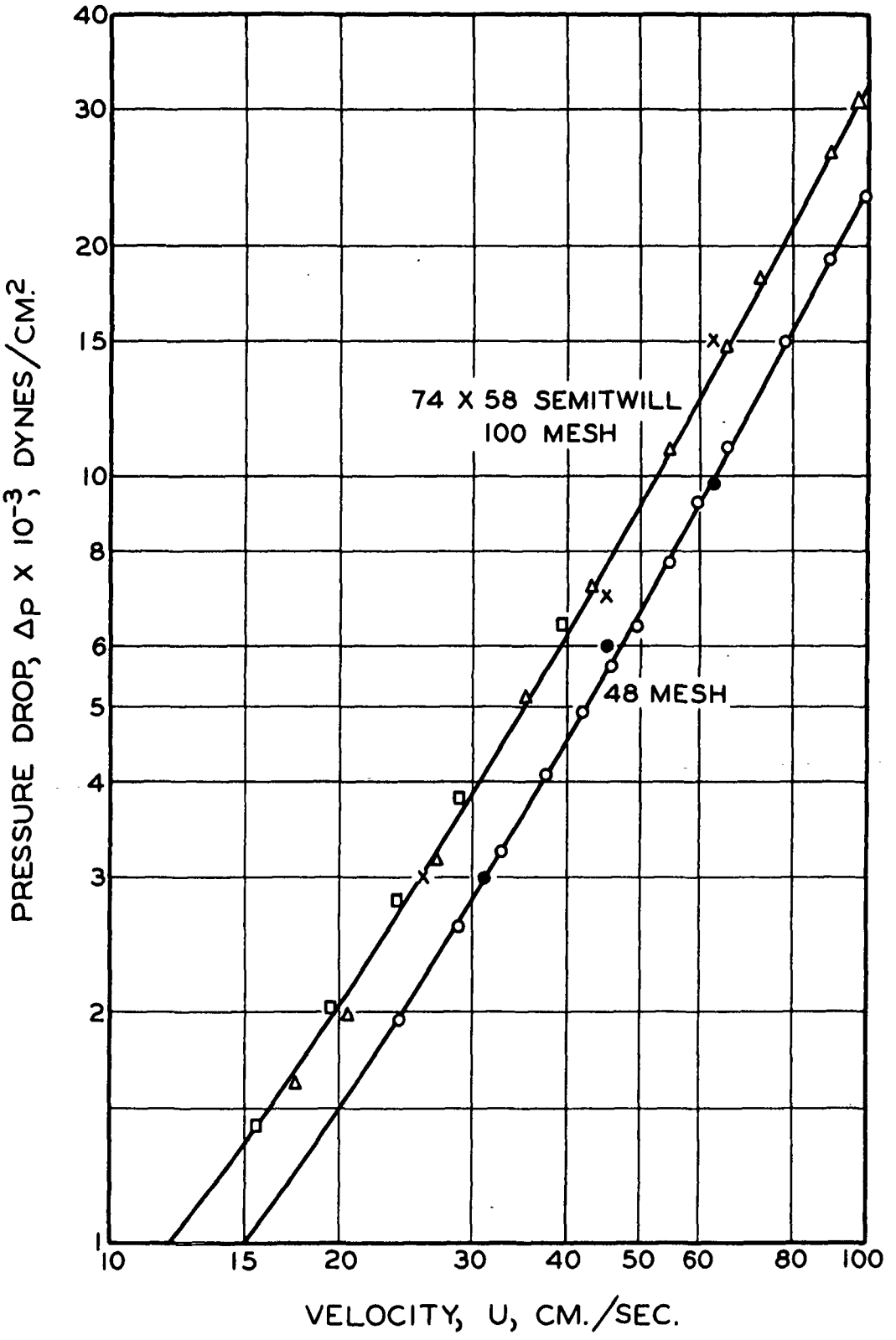

Figure XXI-2. Screen Resistances

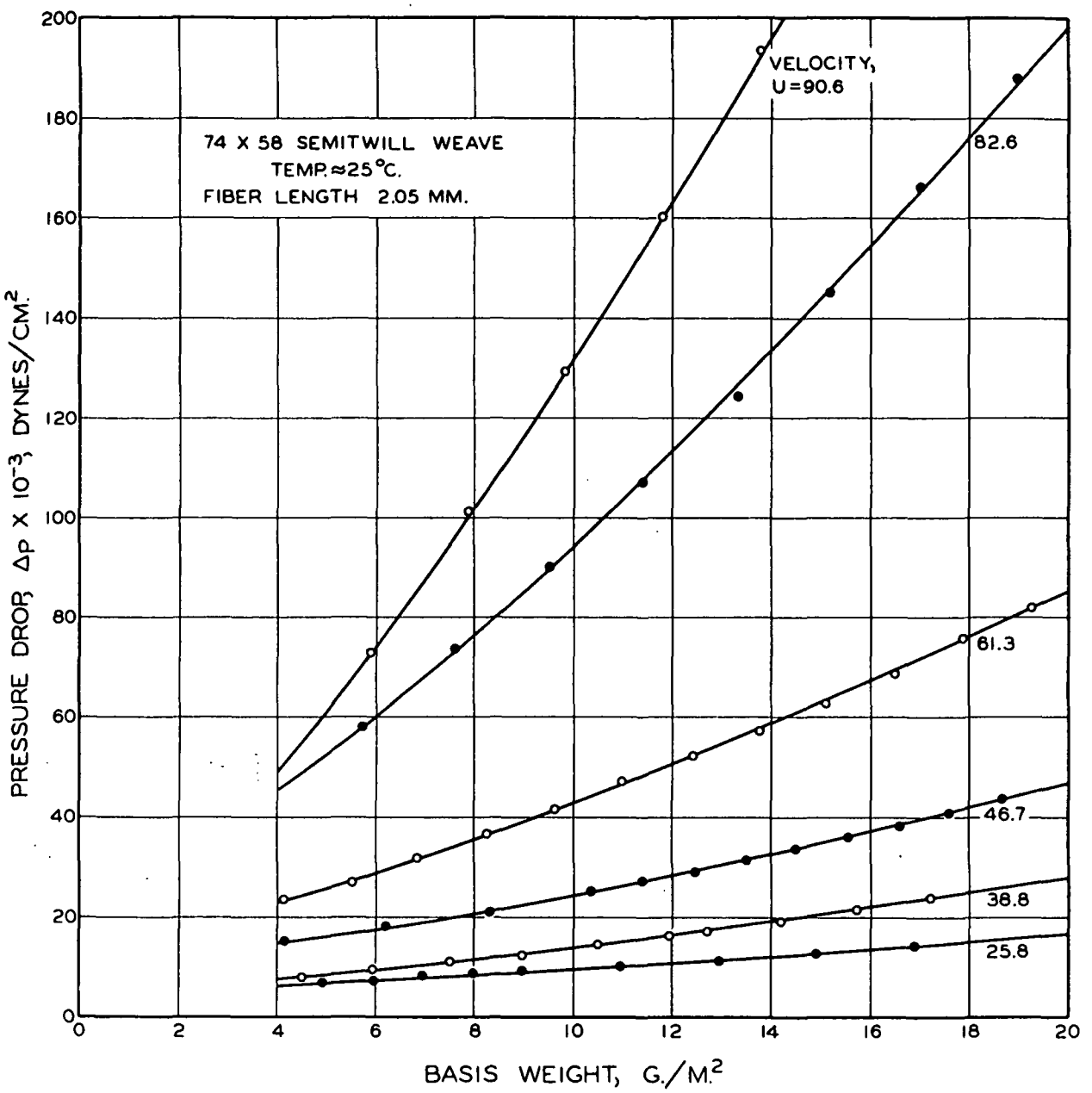

Figure XXI-3. Drainage Data for Low Basis Weights

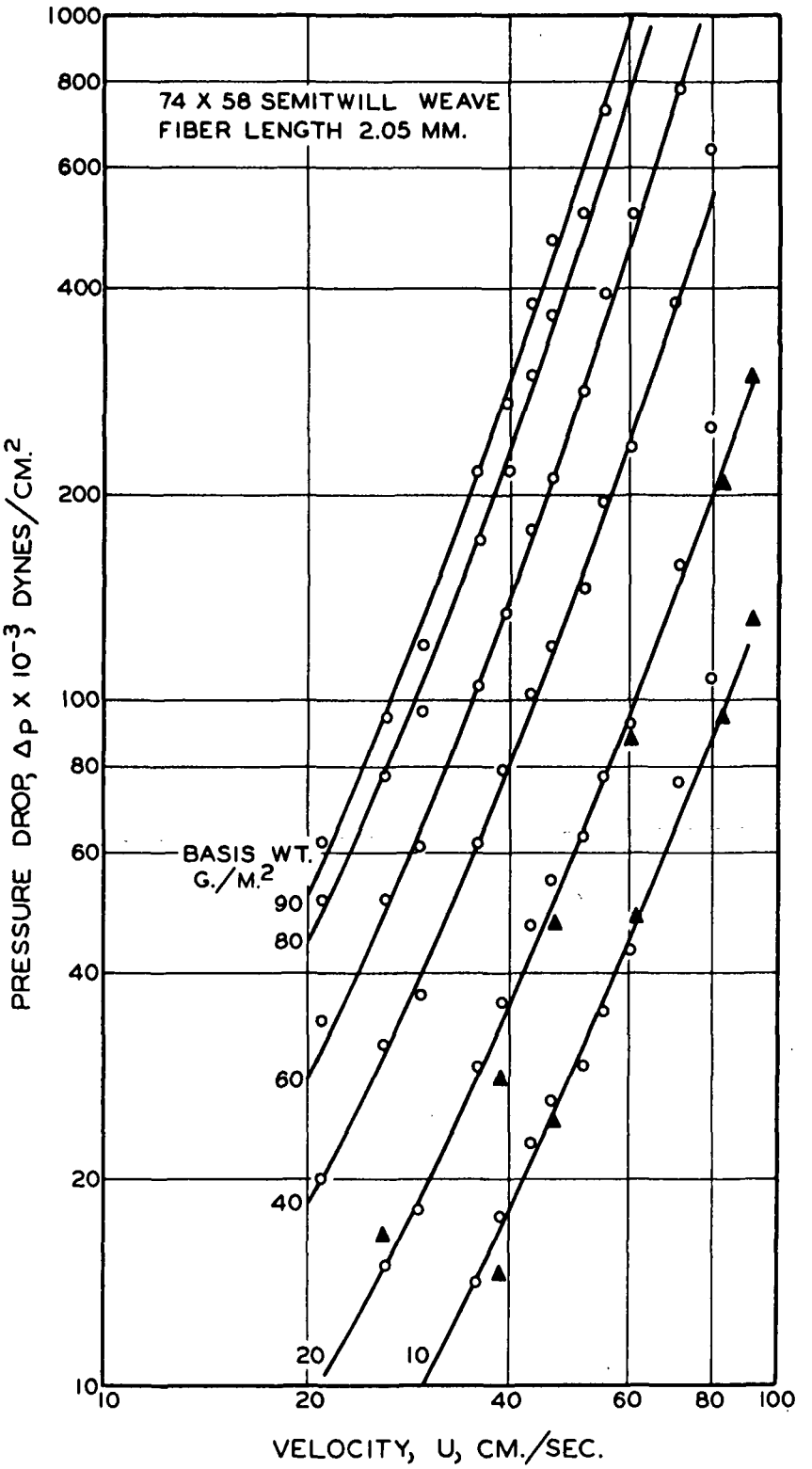

Figure XXI-4. Drainage Data for Original Fibers

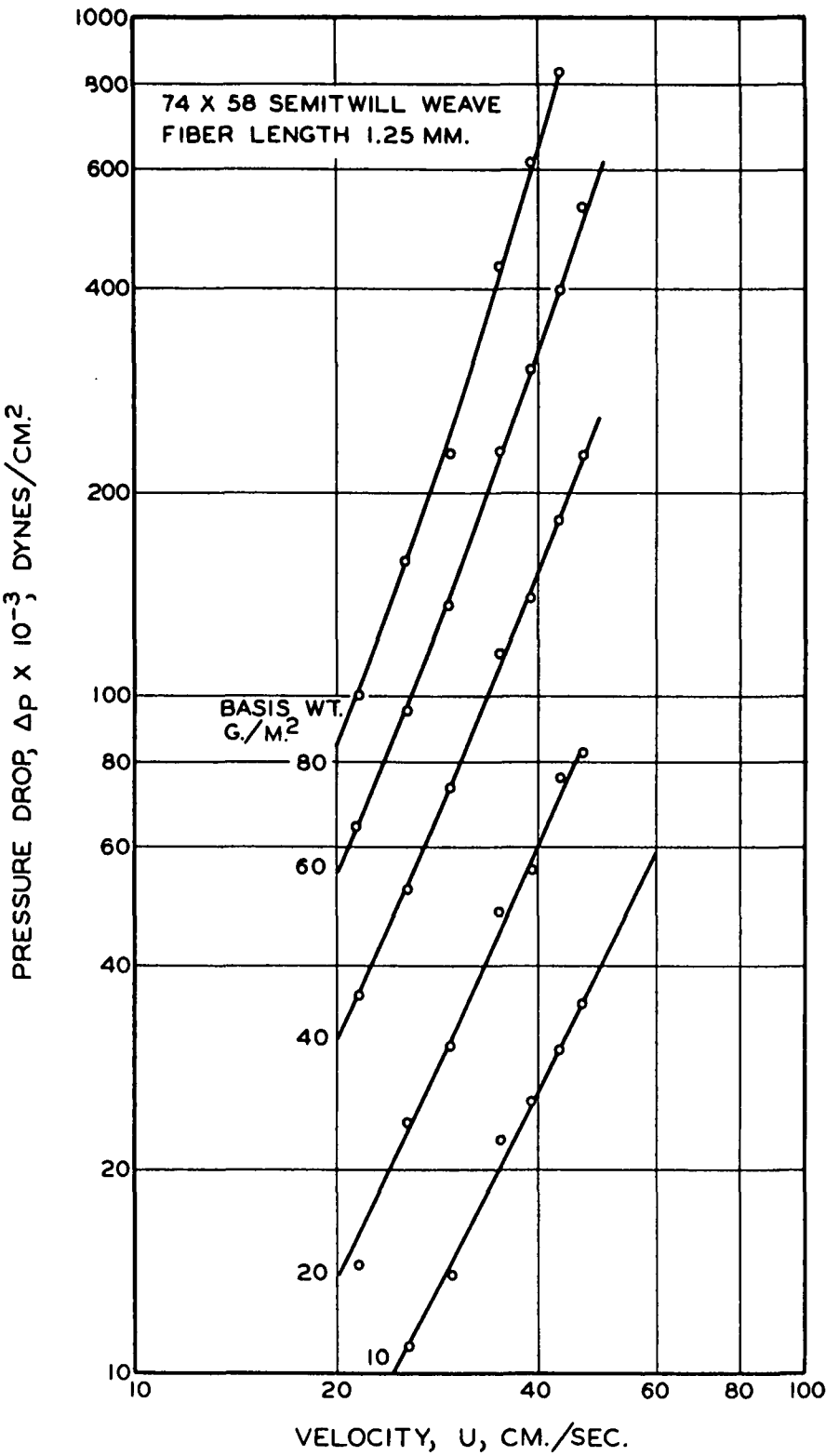

Figure XXI-5. Drainage Data for Cut Fibers

Using the analysis presented in Chapter XIII, the Forchheimer formula may be rewritten as

$$\frac{|\Delta p|}{W} = (\bar{R}\mu + \bar{R'}\rho\bar{\kappa}U)\bar{\kappa}U \qquad \text{(XXI-1)}$$

where Δp is the pressure drop corrected for flow through the screen alone, U the approach or piston velocity (equivalent to the previous U_∞) and $\bar{\kappa}$ is the interaction factor due to flow convergence. It is assumed without justification that the analysis based on viscous flow could be extended to transition flow provided the inertial term is not dominant.

The compressibility of thin mats for these fibers was presented in Chapter XVII. Under the confined condition the compressibility function was

$$c = \frac{1 - \epsilon}{v} = 0.0022|\Delta p|^{0.38} \qquad \text{(XXI-2)}$$

By the analysis in Chapter XIX for the dependence of the hydrodynamic properties c cellulosic fibers, the specific surface and volume of these fibers were found to b correlated by

$$S_w = 425|\Delta p|^{0.022} \qquad \text{(XXI-3)}$$

and

$$v = 12.6|\Delta p|^{-0.15} \qquad \text{(XXI-4)}$$

The values of $\bar{R}$ and $\bar{R'}$ may now be evaluated from (XVIII-12):

$$\bar{R} = \bar{k}\frac{(1 - \bar{\epsilon})}{\bar{\epsilon}^3}\frac{S_w^2}{v} \qquad \text{(XXI-5)},$$

$$\overline{R'} = 0.1 \frac{\sqrt{\overline{k}}}{\overline{\epsilon}^3} S_w \qquad \text{(XXI-6)},$$

$$\overline{\epsilon} = 1 - (1 - N/2)^2 \nu M |\Delta p|^N \qquad \text{(XXI-7)},$$

$$\overline{k} = 3.5 \frac{\overline{\epsilon}^3}{(1 - \overline{\epsilon})^{1/2}} [1 + 57(1 - \overline{\epsilon})^3] \quad \text{for} \quad \epsilon > 0.76 \qquad \text{(XXI-8)},$$

and

$$\overline{k} = 5.5 \quad \text{for} \quad \epsilon < 0.76 \qquad \text{(XXI-9)}.$$

From these relationships the value of $\overline{\kappa}$ was determined from Equation XXI-1, using the experimental data of $\Delta \underline{p}$, $\underline{W}$, and $\underline{U}$.

Because of the assumptions involved in both the previous analysis (Chapter XIII) and the present data reduction, a direct comparison of theory and experiment is not yet feasible. However, the general characteristics of the analytical curves in Fig. XIII-2 may be approximated by

$$\overline{\kappa} \cong 1 + \exp[n_b' - (L_b/r_o)'] \qquad \text{(XXI-10)},$$

where $\underline{n_b'}$ is proportional to the mat deflection factor $\underline{n_b}$, and $(\underline{L_b}/\underline{r_o})'$ to the relative mat thickness parameter, $\underline{L_b}/\underline{r_o}$. By use of the following relationships:

$$\epsilon_o = 1 - \frac{\pi}{2} \frac{r_o}{d_o} \qquad \text{(XXI-11)}$$

and

$$c = \frac{W}{L_b} \qquad \text{(XXI-12)},$$

we find that

$$\frac{L_0}{r_0} = \frac{\pi}{2} \frac{W}{d_0 (1 - \epsilon_0) M (1 - N/2)^2 |\Delta p|^N} \qquad \text{(XXI-13)},$$

where d_0 is the center-to-center spacing of the wires or approximately the dimension of the screen openings, and ϵ_0 the screen porosity. Equation (XXI-10) may now be transformed to

$$\ln (\bar{\kappa} - 1) = K_1 n_0 - K_2 \left[\frac{W}{d_0 (1 - \epsilon_0) M (1 - N/2)^2 |\Delta p|^N} \right] \qquad \text{(XXI-14)},$$

where K_1 and K_2 are two constants for a given fiber-wire combination.

The results so plotted are shown in Fig. XXI-6 for the semitwill screen. It is seen that the logarithm of $(\bar{\kappa} - 1)$ is linear with the basis weight up to about 40 g./sq. m. at constant pressure drop, and $(\bar{\kappa} - 1)$ decreases with increasi pressure drop at constant basis weight. This qualitative agreement merely serves to indicate a reasonable method of accounting for the fiber-wire interaction.

In fact, Ingmanson (XX-3) has previously considered thin mats as having a uniform porosity and suggested using the same flow correlation (XVIII-12) by introducing a correction factor I for the average porosity:

$$\bar{\epsilon} = 1 - Ivc \qquad \text{(XXI-15)}$$

and

$$I = (1 - N/2)^2 + (N - N^2/4)\exp(-K_3 W) \qquad \text{(XXI-16)},$$

where K_3 is to be experimentally determined. Thus, as the basis weight decreases I increases and $\bar{\epsilon}$ decreases, resulting in a higher velocity at a pressure drop defined by (XXI-1) or conversely a higher pressure drop across the mat than that

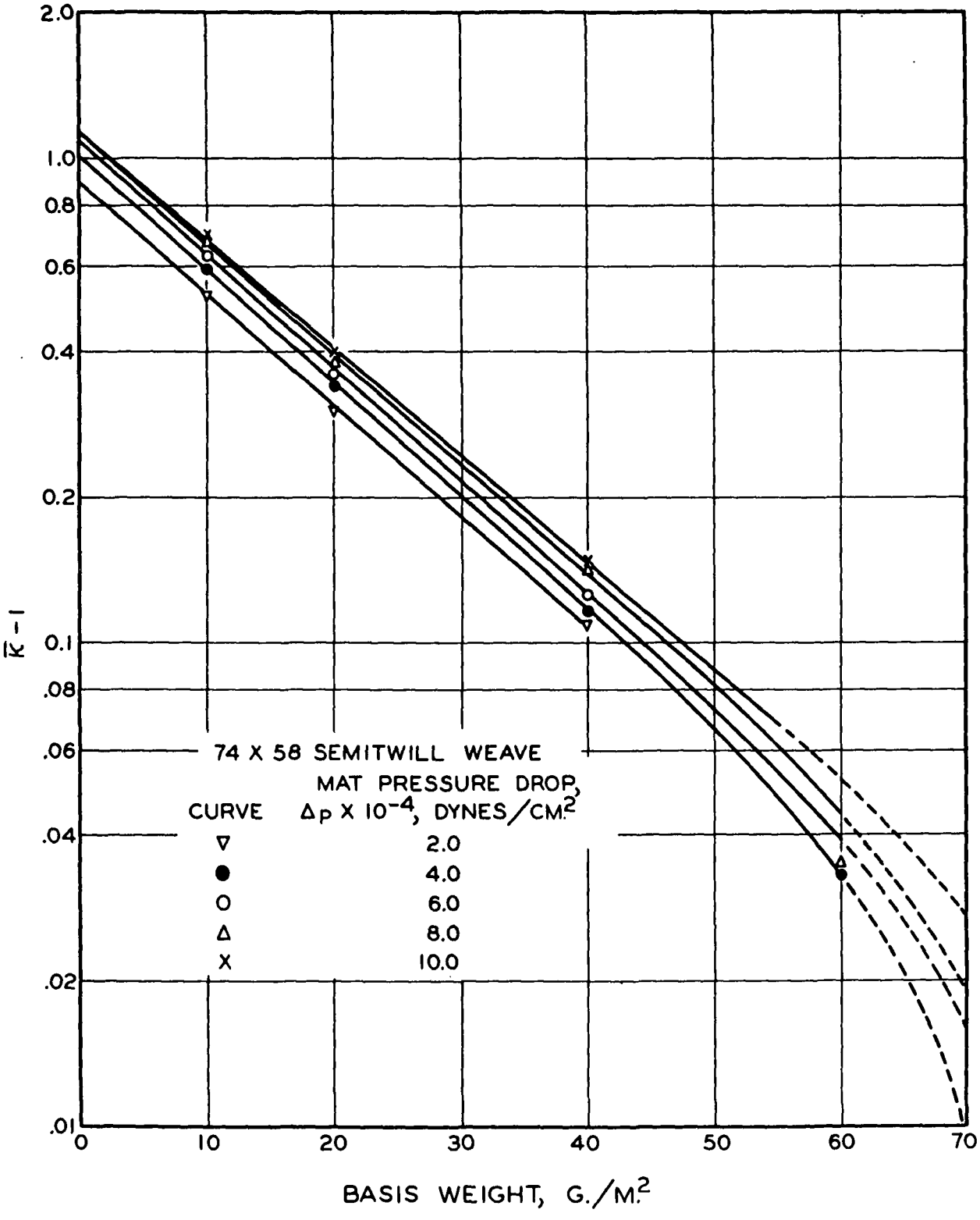

Figure XXI-6. Fiber-Wire Interaction Factor

without a supporting screen at the actual approach velocity. In the other direc-
tion as the basis weight increases, $\underline{I}$ decreases exponentially and approaches th
value of $(1 - \underline{N}/2)^2$, which satisfies the original definition of average porosi-
(XXI-7).

XXII. GRAPHICAL RESULTS OF HIGH-CONSISTENCY FILTRATION

In filtration of high-consistency suspensions the relative superficial velocity must be taken into account. An analytical procedure has been presented in Chapter X. However, the final solutions remain to be computed. Previously, Ingmanson (II-2) employed a graphical method for the same analysis. His results are outlined below.

LOW VELOCITY

The macroscopic continuity equation may be written on the fiber mass basis as

$$\frac{v}{c}\frac{\partial c}{\partial t} = \frac{\partial U}{\partial w} = -\frac{\partial U_f}{\partial w} \qquad \text{(XXII-1)} .$$

For slow flow with complete fiber retention and negligible fiber-wire interaction, the macroscopic equation of motion reduces, with Darcy's law, to

$$U_r = -\frac{1}{R\mu}\frac{\partial p}{\partial w} \qquad \text{(XXII-2)} ,$$

which may be converted at constant t to the integral form:

$$\int_w^W U_r dw = -\int_p^{p_L} \frac{1}{R\mu}\, dp \qquad \text{(XXII-3)} .$$

In terms of the Davis porosity function,

$$R = k_1 S_v^2 v^{3/2} c^{1/2} [1 + k_2 (vc)^3] \qquad \text{(XXII-4)} ,$$

and using the Ingmanson compressibility function:

$$c = c_o + M|p - p_L|^N \qquad \text{(XXII-5)}$$

the right side of Equation (XXII-3) is integrable at constant μ, $\underline{S_v}$, and $\underline{c_o}$. For the left side the relative superficial velocity may be expressed by its definition as

$$U_r = U - \frac{1 - vc}{vc} U_f = \frac{U - (1 - vc)U_o}{vc} \qquad \text{(XXII-6)}$$

Since the continuity condition (XXII-1) relates the temporal rate of change of the local mat density to the velocity gradient on the mass basis, it is possible to evaluate the left integral by a trial-and-error graphical technique for specific conditions. An example is given as follows:

Pulp	Classified, bleached sulfite fibers
$\underline{S_v}$	3800 sq. cm./cc.
$\underline{v}$	2.35 cc./g.
$\underline{c_o}$	0.01 g./cc.
$\underline{\rho_f}$	1.6 g./cc.
$\underline{N}$	0.411
$\underline{M}$	0.00132 (g./cc.)/(dynes/sq. cm.)$^{\underline{N}}$
$\underline{s} \times 10^2$	0.01, 0.1, 0.5, 0.8, 1.0 g./g.
$\underline{U_o}$	1.29 cm./sec.
μ	0.00934 g./(cm.)(sec.)
ρ	1.0 g./cc.

The constant-rate filtrations specified above will show the largest effect of high consistency on mat density.

In the beginning of the analysis, the assumption of constant U being equal to U_0 is made. Then Equation (XXII-3) results in

$$U_0(W - w) = f(\Delta p) \qquad \text{(XXII-7)},$$

where $f(\Delta p)$ is graphically evaluated from the right-side integral with the given conditions. Since the local mat density is related to the pressure drop by the compressibility function, we may express c as a function of w, corresponding to Δp for a given basis weight W or time t. In the process we need to know the average mat moisture $\bar{m}$ from the following relations:

$$W = \frac{s\rho}{1 - s\bar{m}} |U_0| t \qquad \text{(XXII-8)}$$

and

$$\bar{m} = 0.38 + \frac{1}{W} \int_0^W \frac{1}{c} \, dw \qquad \text{(XXII-9)},$$

the constant 0.38 being derived from the known values of ρ_f and ρ. The evaluation of $\bar{m}$ is carried out graphically. The results are a family of c vs. w curves with t as the parameter. Under the assumption $U = U_0$, these mat density distribution curves are alike, only being displaced outward from the origin as the filtration proceeds. Each curve terminates at c_0 at the mat face W.

By cross plotting, the distribution curves are converted to c vs. t curves at constant W. Slopes are then taken from these curves, and the product $(v/c)(\partial c/\partial t)$ so obtained is numerically the same as $\partial U/\partial w$ according to the continuity condition. Thus, a plot of velocity "gradient" vs. w will yield a

family of curves at various times. By graphical integration of these curves, the velocity change from the origin to any position is obtained:

$$U - U_0 = -U_f = f(w) \quad \text{at} \quad t \qquad \text{(XXII-10)},$$

from which the values of $\underline{U}$, which has been assumed to be the same as $\underline{U_0}$, may now be evaluated, as a first approximation, by the difference of $\underline{U_0} - \underline{U_f}$. Finally, $\underline{U_r}$ is obtained from its definition (XXII-6) and plotted against $\underline{w}$ at time $\underline{t}$. By integrating graphically these relative velocity distribution curves, a new set of mat density distribution functions is evaluated with the aid of Equation (XXII-3). This completes the first trial. The procedure is repeated until a new set of mat density curves agrees closely with the previous one. The final results are for a given suspension consistency, and the entire process must be repeated for other consistencies.

The results of two trials for 0.5% consistency are shown in Fig. XXII-1. The effect of consistency on porosity distribution is shown in Fig. XXII-2.

HIGH VELOCITY

Ingmanson (XXII-1) proceeded to analyze the case of transition flow in high-consistency filtration. The filtrate velocity was taken to be 65 cm./sec., and the other conditions remained the same as before. The flow equation is now written as

$$-\frac{\partial p}{\partial w} = R\mu U_r + R'\rho U_r^2 \operatorname{sgn}(U_r) \qquad \text{(XXII-11)},$$

where

$$R' = b' k_1^{1/2} S_v v^{3/4} c^{-1/4} (1 - vc)^{-3/2} [1 + k_2 (vc)^3]^{1/2} \qquad \text{(XXII-12)}.$$

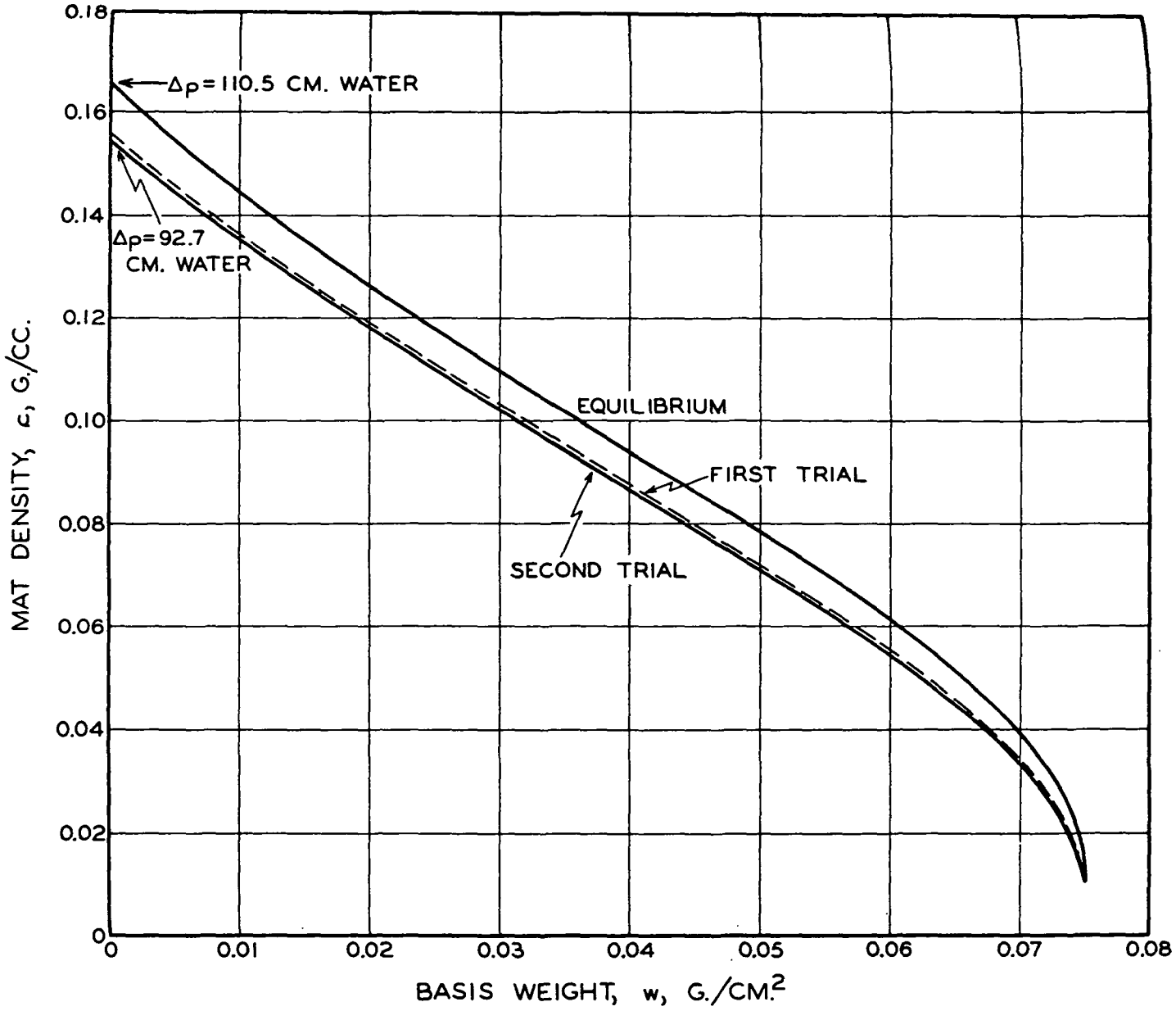

Figure XXII-1. Mat Density Distributions for 0.5% Consistency

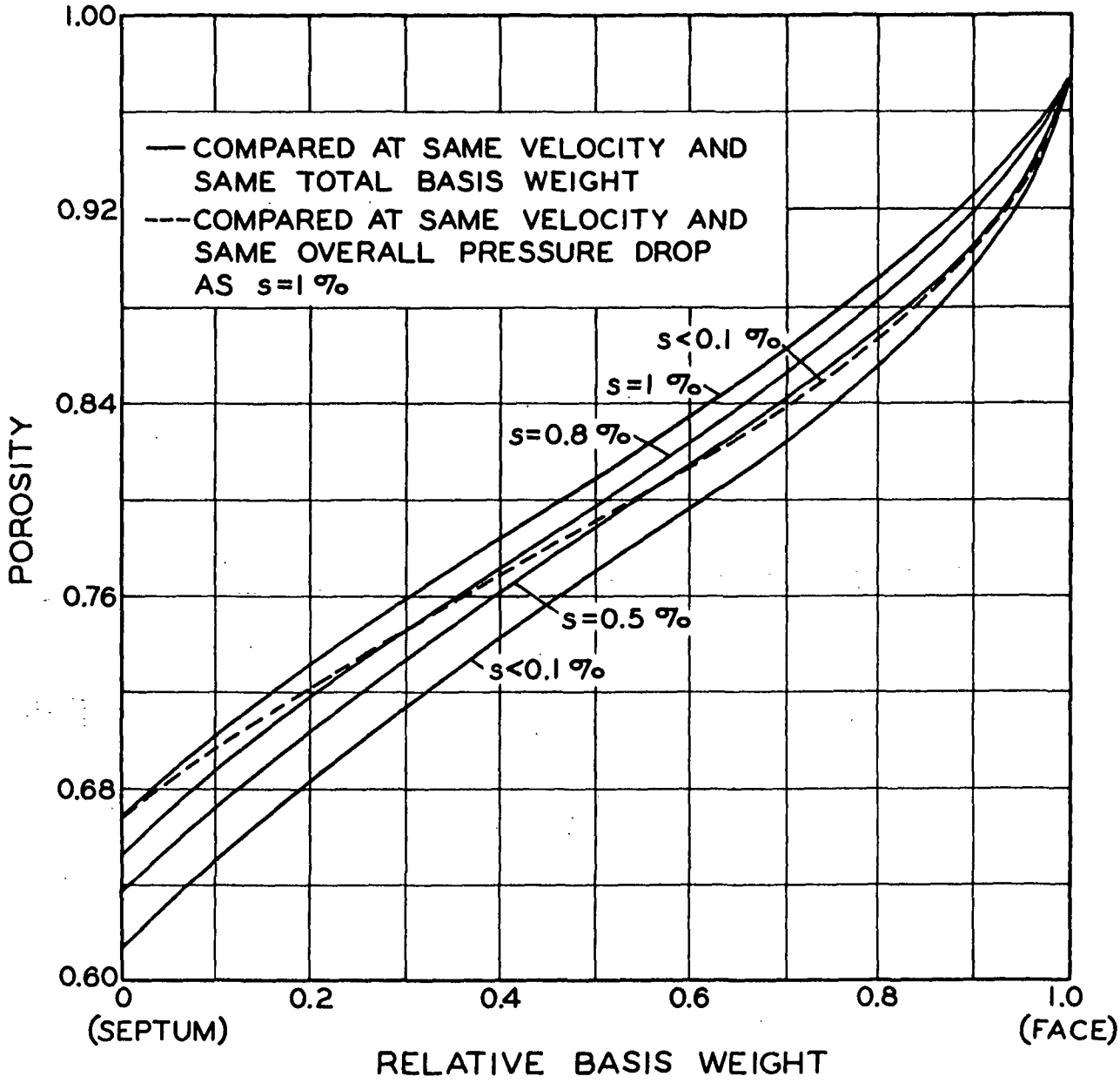

Figure XXII-2. Effect of Consistency on Porosity Distribution

The integral form of Equation (XXII-11) used for analysis becomes

$$\int_0^W dw = -\int_{p_0}^{p_L} \frac{1}{R\mu|U_r| + R'\rho U_r^2} dp \qquad \text{(XXII-13)} .$$

In the initial step, $\underline{U}_r$ was again assumed to be $\underline{U}_0$, and a master curve of $\underline{c}$ vs. $\underline{W}$ at $\underline{t}$ was constructed. The remaining procedure was carried out as before; only it became more complicated because of the presence of the quadratic velocity term. The results of the analysis were very similar to the previous case of viscous flow. At the given velocity the inertial resistance amounted to about 20% of the total resistance in terms of pressure drops.

MAJOR INDICATIONS

The main effect of high-consistency forming is a more diffuse structure with a higher moisture content than the mat formed from a dilute suspension when the comparison is made at the same pressure drop and flow rate. Such a comparison is shown in Fig. XXII-3. In essence, a significant part of water is merely squeezed out of the mat formed from high consistency. Thus, less pressure drop is required to reach the same basis weight than in the case of low-consistency forming at the same rate.

Since high-consistency filtrations involve flocculation to a pronounced extent, Ingmanson used the permeation experiments to demonstrate the effect of high consistency on mat structure. An entire suspension of the specified fibers at a known consistency was introduced into the filtration tube and thoroughly agitated to result in an apparently uniform fiber network. Water was then admitted to the tube and allowed to permeate the network at a very low rate. The flow was slowly increased until the pressure drop reached the desired range of

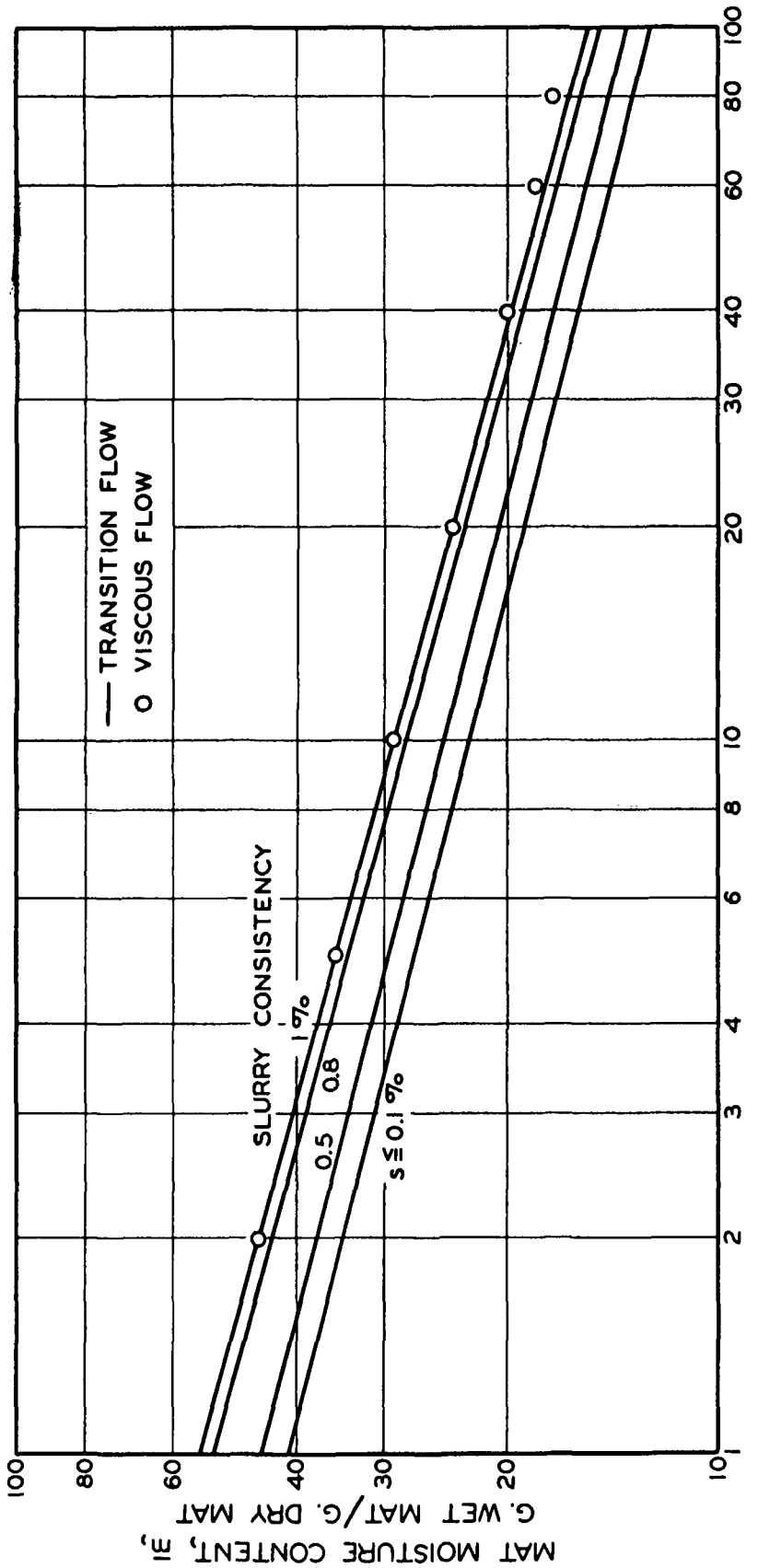
MAT MOISTURE CONTENT, $\overline{w}$,
G. WET MAT/G. DRY MAT
100
80
60
40
30
20
10
PRESSURE DROP, $\Delta p/\rho g$, CM. WATER
1
2
3
4
6
8
10
20
30
40
60
80
100
— TRANSITION FLOW
O VISCOUS FLOW
SLURRY CONSISTENCY
1%
0.8
0.5
s ≦ 0.1 %

10-90 cm. of water. These experiments were satisfactory for 1% consistency at which the initial structure was strong enough to minimize fiber settling and network disintegration into flocs.

The permeation data for one basis weight from 1% consistency are shown in Fig. XXII-4. They are compared with the filtration results for 0.01% consistency at which both flocculation and relative velocity effects are negligible. The agreement between the two sets of results indicates that the mat formed from a three-dimensional fiber network has the same specific resistance and therefore the same two-dimensional structure as one formed from the free deposition of individual fibers. This evidence should remove some of the persistent doubt about the usefulness of the laboratory filtration results under idealized conditions to the practical sheet-forming process. However, the effect of flocculation, in the sense of floc formation, on drainage and sheet structure remains to be clarified. Generally speaking, flocculation resulting in a large-scale nonuniform sheet will increase drainage, but this effect should be distinguished from that of relative flow of water and fiber through a structure macroscopically homogeneous in the $\underline{x}$-$\underline{y}$ plane. Flocculation tends to decrease the specific filtration resistance while relative velocity merely reduces the driving force or pressure drop.

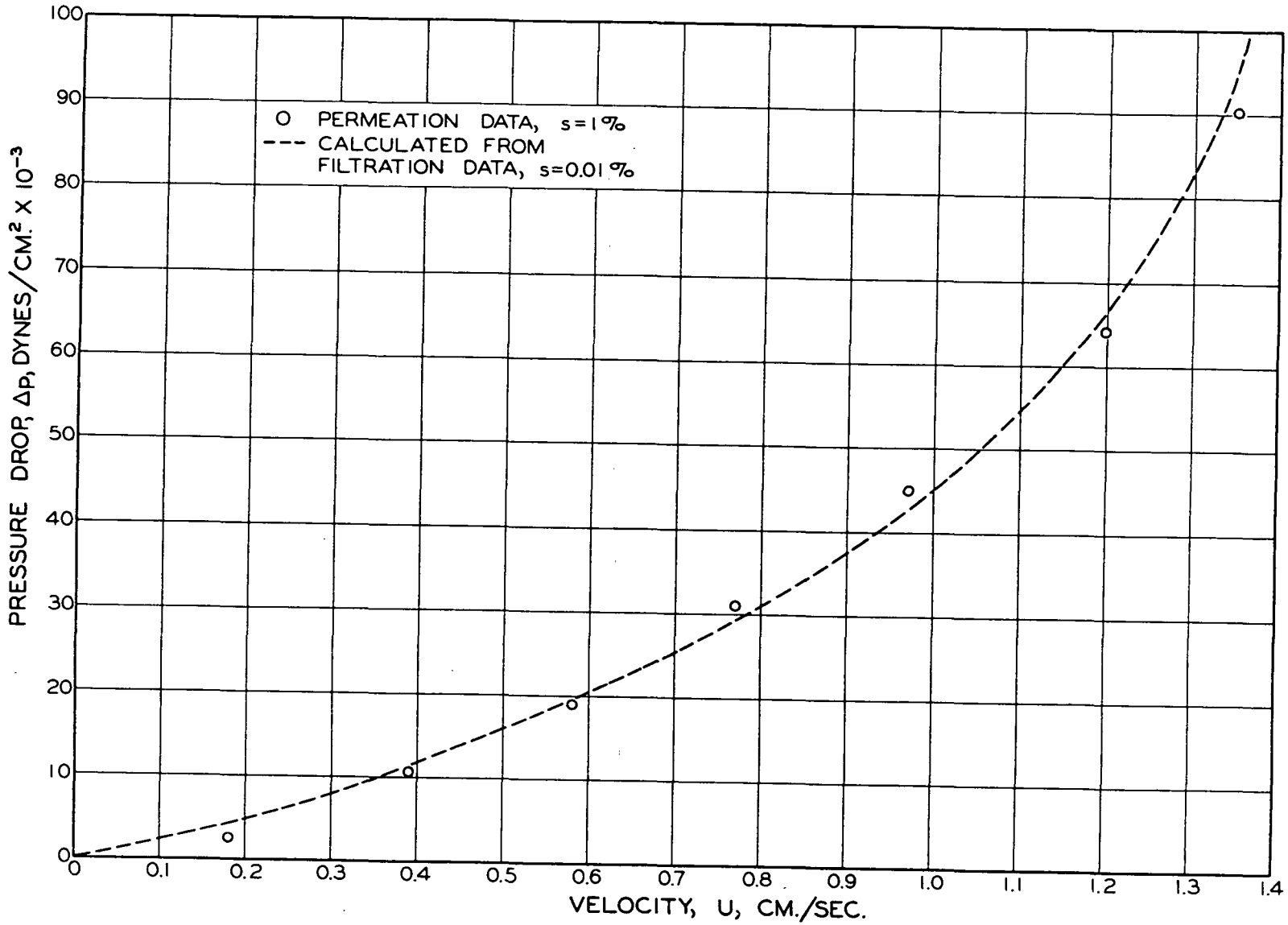

Figure XXII-4. Comparison of Mat Structure by Permeation and Filtration

XXIII. EXPERIMENTAL VERIFICATION OF PARTICLE-FILTRATION THEORY

The theory of fine-particle filtration has been presented in Chapter VII. The experimental verification of the analytical results for both incompressible (II-3) and compressible cases by Han and Chang (XXIII-1) will be presented here. A brief study of particle removal by permeation will also be reported.

INCOMPRESSIBLE MATS

Dacron fibers of high modulus of elasticity were used in forming incompressible mats. Titanium dioxide particles which had been treated on their surfaces with sodium hexametaphosphate as a dispersing agent were chosen for the initial experiments. The particles were made into a slurry of 73% solids, stirred in a Waring Blendor until a minimum viscosity was reached (in about 20 min.), and kept, after dilution, in a slowly rotating jar to prevent the particles from settling.

In order that the particles could be retained to a measurable extent, the dispersing action of the phosphate ions was partially counteracted by introducing to a dilute suspension certain ionic compounds which would not adsorb on the particles. Calcium, sodium, and hydrogen chlorides were found to be effective for this purpose. The suspensions of particles and fibers, both adjusted to the desired ionic condition, were mixed in an agitated tank.

Filtration was performed with the mixed suspension in the usual manner until a very thick mat was formed at constant rate. At the end of the filtration, the water in the tube was drained slowly through the mat until it reached the mat face, and the water below the septum was emptied by bleeding air through a tap

located just under the septum. After its removal from the tube, the mat was sectioned by hand into several layers which were dried and weighed. The dried layers were ashed, and the ash was converted to the sulfate form. Hydrogen peroxide was used to form a stable color in the solution, which was measured with a spectrophotometer. By comparing light transmission of the peroxide sample with the original sample without peroxide at the same temperature, the result in percentage transmission was converted to the titanium dioxide concentration by the use of a calibration curve.

The cumulative masses of particles and fibers in successive layers were plotted against each other, and the slopes were determined on the smooth curve. These were experimental values of $\underline{m}'$ in Equation (VII-23) simplified to

$$-\ln\left(1 - \frac{m' - m'_s}{m_s}\right) = K'\left(1 - \frac{w}{W}\right) \qquad \text{(XXIII-1)},$$

where

$$K' = \frac{KW}{\rho_f(1 - \epsilon)} = \frac{4EW}{\pi d_f \rho_f} \qquad \text{(XXIII-2)}.$$

The value of $\underline{m}'_s$ was also determined, with some uncertainty, from the last data point of the curve, corresponding to the mat face. That of $\underline{m}_s$ was calculated from the difference between the known value of the total mass of free and bound particles per unit mass of fibers in the suspension and the value of $\underline{m}'_s$. The data were plotted in accordance with Equation (XXIII-1), and a linear relationship resulted, as shown in Fig. XXIII-1. From the slope of the line the value of collection efficiency $\underline{E}$ was determined from Equation (XXIII-2).

Permeation experiments were carried out under the same ionic conditions for the purpose of determining the collection efficiency of a preformed mat according to Equation (III-11):

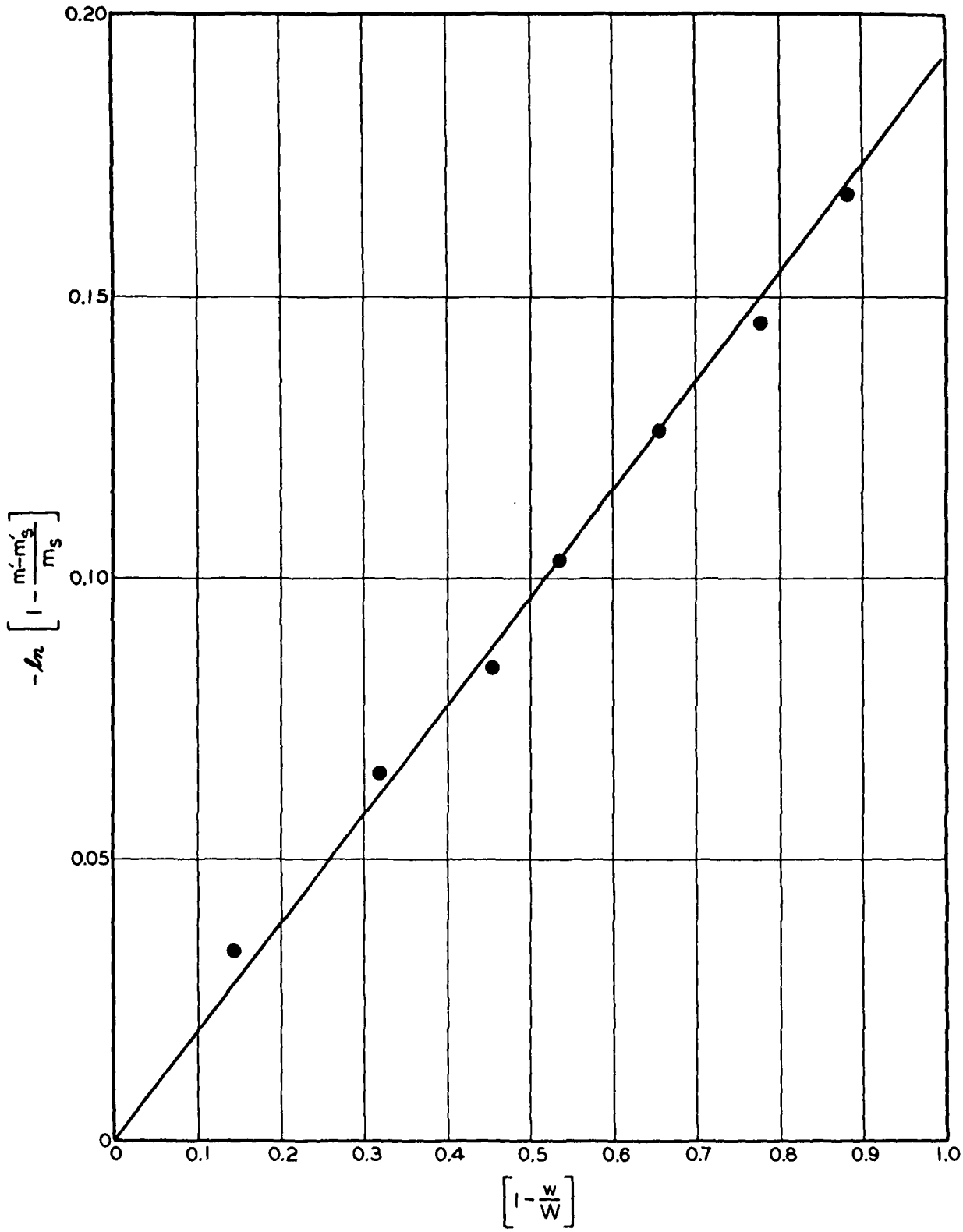

Figure XXIII-1. Particle Distribution in an Incompressible Mat

$$E = \frac{\pi d_f}{4(1 - \epsilon)L} \ln \frac{C_L}{C_0} \qquad \text{(XXIII-3)} .$$

The value so determined served as a check against that from filtration.

The results of these experiments are summarized in Table XXIII-1. The discrepancy between the filtration and permeation values of collection efficiency was about 13%. This rather large discrepancy was attributable to the experimental errors. The major part probably occurred in the particle measurement. In the case of permeation, a single determination of the retained particles was sufficient for the evaluation of $\underline{E}$. For filtration, however, the involved colorimetric analysis of titanium dioxide was performed on each layer of the mat. In any single analysis the sample had to be ashed, chemically treated, and transferred. All these manipulations entailed some losses of the particles. The total loss could conceivably account for the smaller value of $\underline{E}$ from filtration.

COMPRESSIBLE MATS

In the subsequent experiments a classified sulfite pulp was used in forming compressible mats. The average fiber length $\underline{L_f}$ was 2.11 mm. and the average width $\underline{D_f}$ was 0.039 mm. The specific volume $\underline{v}$ was 2.26 cc./g., and the number of fibers per gram $\underline{n_f}$ was 2.78×10^6. The projected area per unit volume of the fibers was calculated to be 10^3 sq. cm./cc. from

$$\frac{A_f}{V_f} = \frac{n_f L_f D_f}{v} \qquad \text{(XXIII-4)} .$$

The particles were fines from the same sulfite pulp. They were obtained by dry and wet grinding of the fibers to the size range of 0.5-2 microns in the first batch and 0.05-0.5 micron in the second batch. An electron

TABLE XXIII-1

VERIFICATION OF PARTICLE RETENTION

Particle	TiO_2
$\underline{d}_p$	0.15 micron
ρ_p	3.9 g./cc.
Fiber	dacron
$\underline{d}_f$	0.0169 mm.
ρ_f	1.41 g./cc.
Suspension	
TiO_2 concn.	2.31×10^{-6} g./cc.
Fiber concn.	6.84×10^{-5} g./cc.
$CaCl_2$ concn.	1.9×10^{-5} g.-moles/cc.
pH	3.6
$\underline{T}$	23°C.
$\underline{U}$	1.0 cm./sec.
$\Delta\underline{p}$ (final)	1.9 cm. H_2O
Mat	
$\underline{L}$	4.0 cm.
ϵ	0.98
$\underline{E}$ (from filtration)	3.5×10^{-3}
$\underline{E}$ (from permeation)	4.0×10^{-3}

micrograph of the second batch of fines is shown in Fig. XXIII-2. The fines wer tagged with radioactive silver-110. The radioactivity was measured with a Geiger-Müller counter in counts per minute (c.p.m.), corrected for background radioactivity, under a fixed geometry over the sulfated ash of the fines in a planchet. The counting results were significant only on a relative basis.

When a suspension of the fines and fibers was prepared by dilution, it was found that the retention of fines in the mat was insufficient (almost none) for a precise measurement of their radioactivity. By providing similar ionic conditions as in the hydrophobic system of titanium dioxide particles and dacron fibers, retention was considerably improved. However, at low pH values there occurred serious leaching of radioactivity to the solution. A leaching test the showed that at pH 6.5 only 5% of the radioactivity was lost. The final procedure was to add only calcium chloride dihydrate or sodium chloride to the suspension without the use of hydrochloric acid to lower the pH.

It is interesting to mention that in the other extreme a uniform particle distribution in a mat could also be achieved by imposing highly favorabl colloidal and hydrodynamic conditions to the particle-fiber suspension. When a relatively concentrated suspension of the sulfite fines and fibers was stirred intermittently for 25 hr. at pH 6.4 with a sufficient concentration of calcium chloride and then diluted to make a filtration run, the resulting mat exhibited an almost uniform fines distribution, as shown in Fig. XXIII-3. In this case nearly all fines were bound to the fibers prior to the filtration or the fibers became so saturated with fines that further collection was negligible during the filtration.

Under a majority of experimental conditions the sulfite system behaved in a manner somewhere between the two extremes of little retention and pseudo

Figure XXIII-2. Electron Micrograph of Sulfite Fines

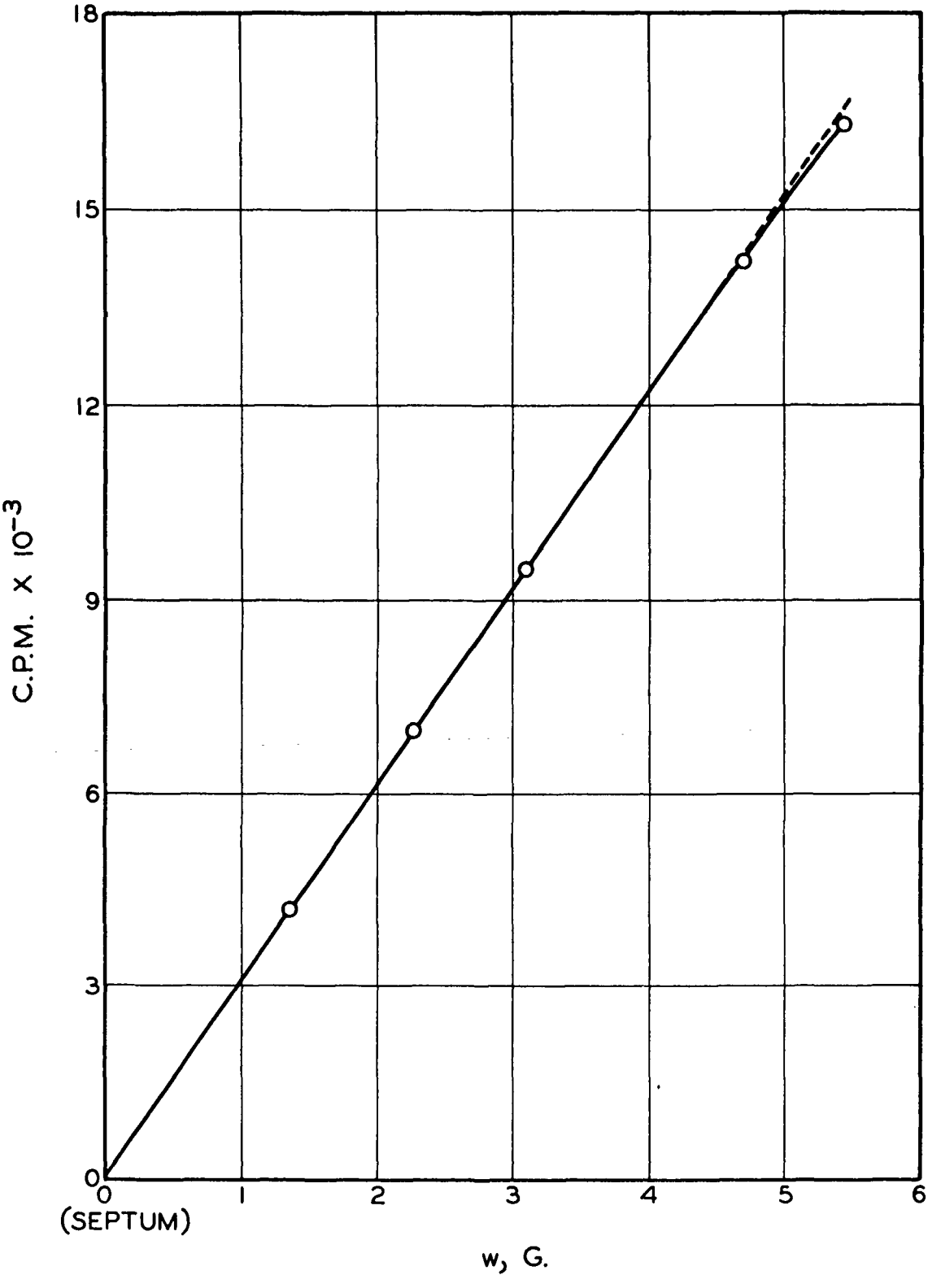

Figure XXIII-3. Uniform Particle Distribution

saturation. Such data are shown in Fig. XXIII-4. It is seen that the top part of a mat from its face downward is a sloping line in agreement with the theory while the bottom part near the septum, being a horizontal line, indicates a condition of saturation. The unsaturated and saturated regions are joined by a curve of an uncertain transition region. The lower the collection efficiency and basis weight, the shorter is the saturation region. We wish to emphasize that the so-called saturation is probably a pseudo stable state which may be easily altered by small disturbances.

From the discussion in Chapter XIV on flocculation, we may conceive that the hydrodynamic, electrostatic (colloidal), and molecular forces are operative between fines and fibers and among themselves. To carry the analogy farther, we may imagine that the energy of interaction would vary along the surfaces. In a given force field, the rates of attachment and detachment might become temporarily equalized so that a precarious dynamic equilibrium could be so maintained.

Further experiments were conducted to show possible particle distribution in thin mats. These mats were divided into layers with a Beloit sheet splitter. The results for thin mats as shown in Fig. XXIII-5 are in excellent agreement with the theory. This is perhaps another demonstration of the usefulness of a mathematical model and controlled experiments in the research of a complex subject. Table XXIII-2 summarizes the results of the sulfite system. The agreement in collection efficiency between the filtration and permeation experiments is much better than in the titanium dioxide-dacron system because of the sensitive measurement of radioactivity.

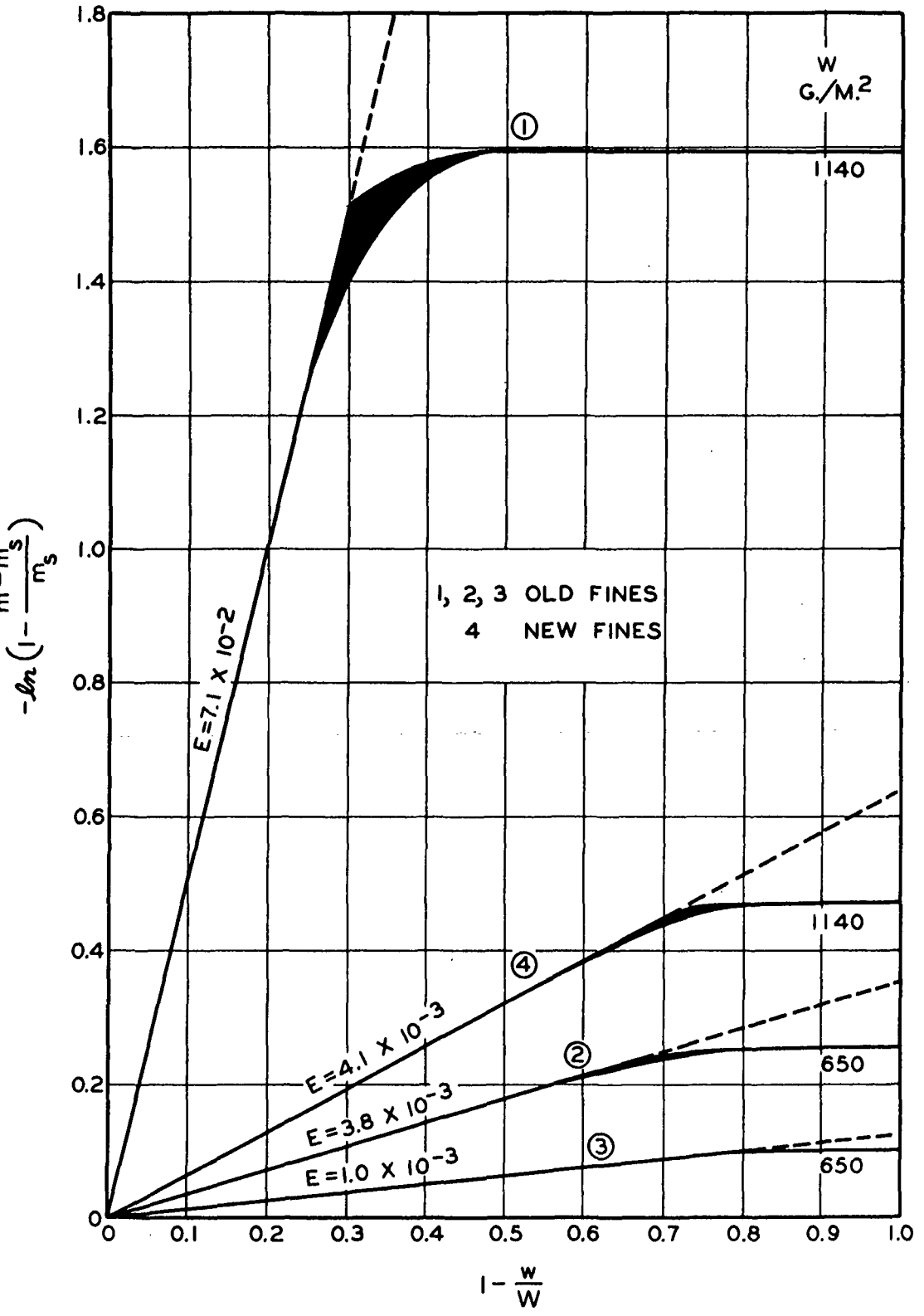

Figure XXIII-4. Particle Distributions in Thick Mats

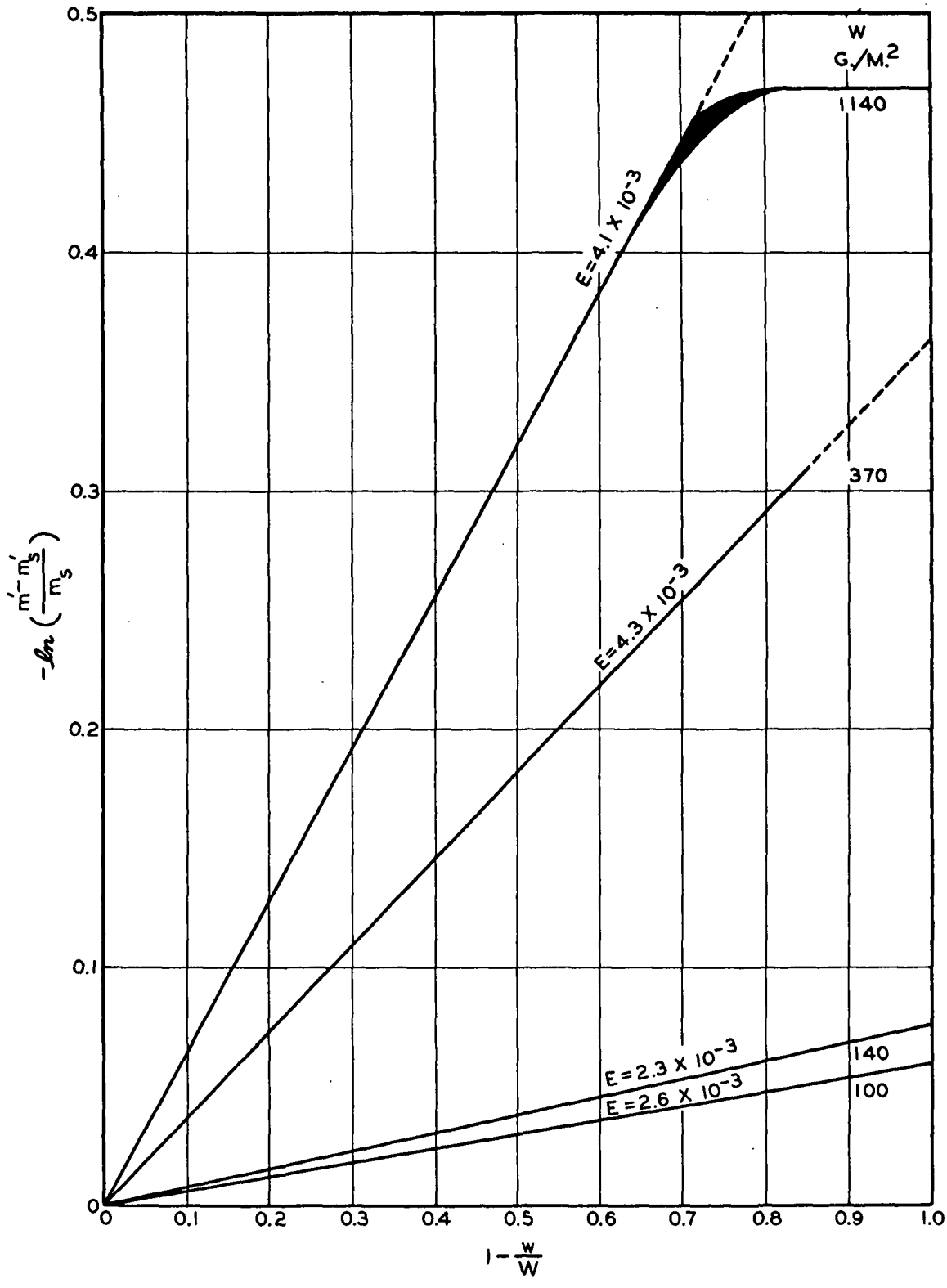

Figure XXIII-5. Particle Distributions in Thin Mats

TABLE XXIII-2

RETENTION OF FINES IN COMPRESSIBLE MATS

Fines, micron	0.5-2			0.05-0.5			
$CaCl_2$ concn. x 10^5, g.-moles/cc.	1.9			1.9	1.9		
NaCl concn. x 10^5, g.-moles/cc.		1.0	1.1			1.0	1.0
pH	6.4	5.8	5.1	6.3	6.0	6.2	6.3
$\underline{T}$, °C.	23	21	21	26	21	26	26
$\underline{W}$, g./sq. m.	1140	650	650	1140	370	140	110
$\underline{E}$ x 10^3							
Filtration	71	3.8	1.0	4.1	4.3	2.3	2.6
Permeation	70				4.5	2.5	2.7

FINES REMOVAL

A thick mat was formed from the sulfite suspension under the conditions of nearly complete attachment of the fines to the fibers prior to the filtration. A solution of the same ionic concentrations as those in the suspension was permeated through the mat at a fixed velocity. During permeation, the radioactivity of the mat was monitored as illustrated in Fig. XXIII-6. The results are shown in Fig. XXIII-7. As suggested by Nelson (XXIII-2), these curves may be represented by the function:

$$m' - m_0' = A_0 \exp(-t/t_0) \qquad \text{(XXIII-5)},$$

where the total number of bound particles $\underline{m}'$ is proportional to the measured radioactivity. The values of $\underline{A_0}$, $\underline{m_0'}$, and $\underline{t_0}$ were thus evaluated from the data.

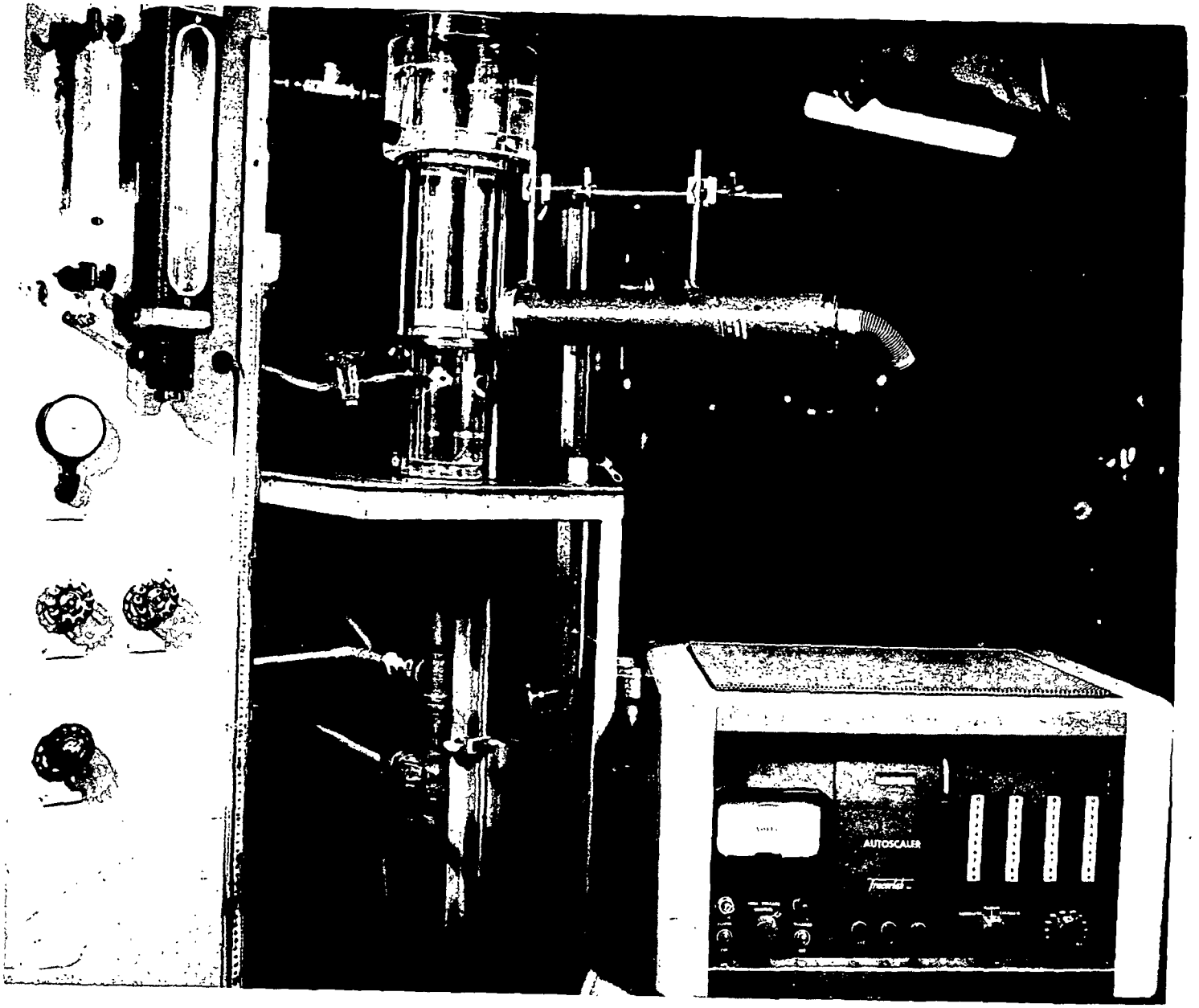

Figure XXIII-6. Fines Removal Experiment

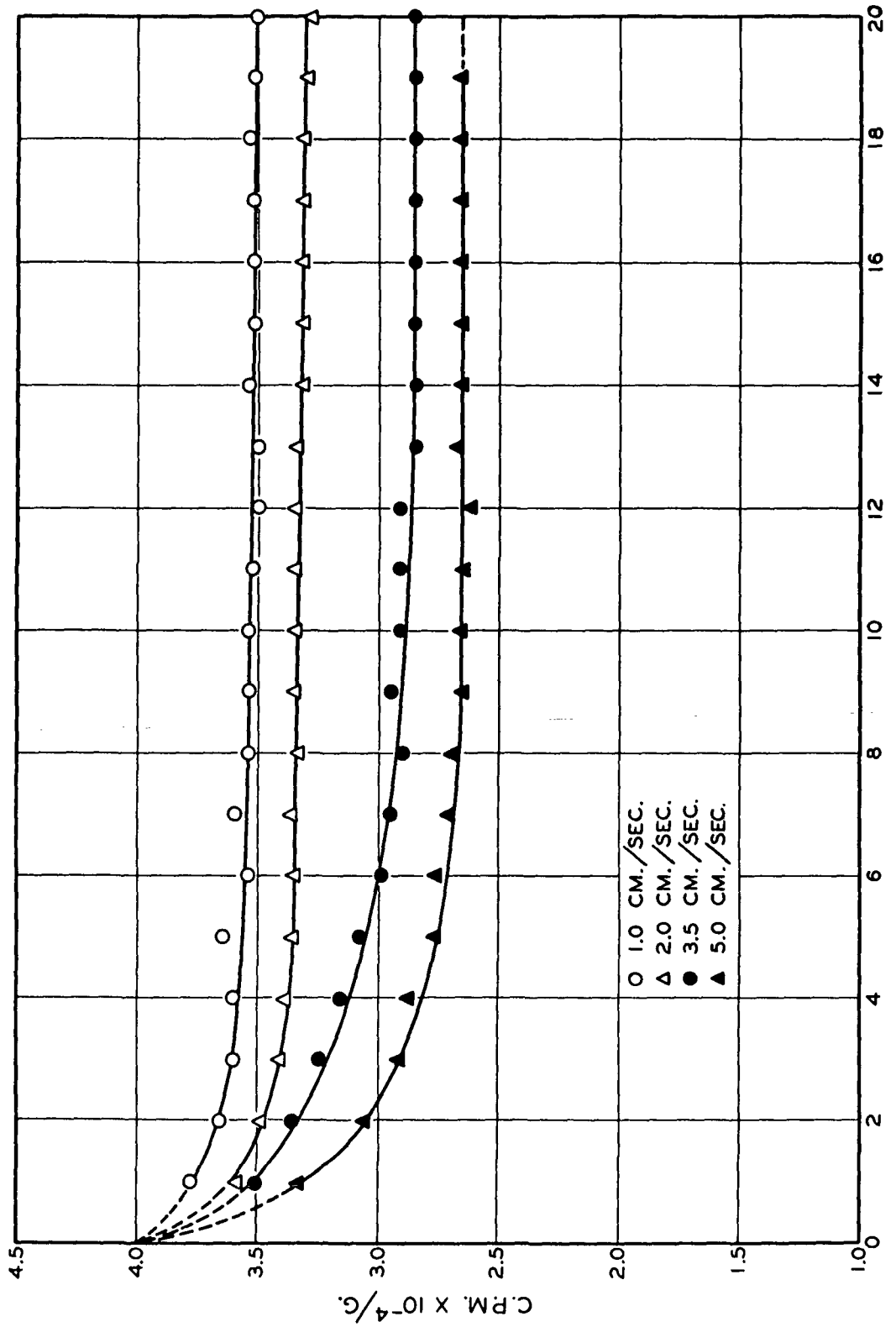

Figure XXIII-7. - Fines Removal by Permeation

Nelson further considered the removal of bound particles in the washing process to be represented by the detachment coefficient $\underline{D_o}$ having the dimensions of reciprocal time. The detachment process was supposed to compete with the reattachment process (described by the collection efficiency $\underline{E}$). In the cumulative-mass co-ordinate system, Equations (VII-31) and (VII-32) for the free and bound particle concentrations become, respectively,

$$\frac{\partial C'}{\partial t'} = E \frac{A_f}{V_f} |U| C - D_o C' \qquad \text{(XXIII-6)}$$

and

$$\frac{\partial C}{\partial t'} = \frac{1 - \epsilon}{\epsilon} \left[\frac{1}{v} |U| \frac{\partial C}{\partial w'} - E \frac{A_f}{V_f} |U| C + D_o C'\right] \qquad \text{(XXIII-7)} .$$

These two equations may be solved numerically together with the viscous flow expression and the compressibility function under specified initial and boundary conditions. The results of computation from the washing experiments are summarized in Table XXIII-3.

TABLE XXIII-3

FINES REMOVAL BY WASHING

$\underline{U}$, cm./sec.	$\underline{A_b}$, c.p.m./g. $\times 10^{-4}$	$\underline{m_b'}$, c.p.m./g. $\times 10^{-4}$	$\underline{t_b}$, sec.	$\underline{E}$,[a] $\times 10^{3}$	$\underline{D_o}$, sec.$^{-1}$ $\times 10^{2}$
1.0	0.5	3.5	102	4.47	1.03
2.0	0.7	3.3	78	2.82	1.04
3.5	1.15	2.85	144	1.94	1.04
5.0	1.35	2.65	92	1.53	1.05

[a] $\underline{E} = 0.00447 \underline{U}^{-2/3}$.

If the collection efficiency were assumed to be zero, Equation (XXIII-6 would reduce to an exponential solution with the value of $\underline{D}_o$ evaluated to be 0.0101 sec.$^{-1}$. Thus, it appears that the more general treatment developed here is being applied to a limiting case, in which reattachment is a comparatively unimportant process.

XXIV. COLLECTION MECHANISMS IN PARTICLE FILTRATIONS

The collection of particles in fiber mats was studied extensively in aerosol filtration. Recently, Han (XXIV-1) made a dimensional analysis of available data and offered suitable correlations for practical uses. The results of the analysis are presented here on account of their close relationship with liquid filtration.

GENERAL CONSIDERATIONS

In the absence of external and imposed forces, gravitational, electrostatic, magnetic, thermal, and chemical, the collision of particles with a fiber arises from three well-known aerodynamic factors. Particles with negligible mass will collide with a fiber as they follow the fluid motion to the neighborhood of the fiber within a distance of their radii. This is called interception. While the fluid must spread around the fiber, approaching particles tend to execute less curved trajectories, depending on their inertia, and head toward the fiber, resulting in impaction. Very small particles exhibit Brownian motion due to the bombardment of the fluid molecules. As they are passing by the fiber, collisions can result from their zigzag motion. This mechanism of collection is often referred to as diffusion.

Diffusion increases with decreasing particle size and fluid velocity, but is independent of particle density. On the contrary, impaction is enhanced by high velocities with large and heavy particles. Interception is favored primarily by increasing particle sizes. Whatever mechanisms may be operative in a fiber mat, retention increases with decreasing mat porosity and fiber diameter as expressed in Equation (VII-3).

The assumption will be made that a definite percentage of particles colliding with fibers results in adhesion. For a given particle-fluid-fiber system, at least the following variables will affect the collection efficiency:

$$E = f(d_p, \rho_p, D, \rho, \mu, U, d_f, \epsilon, \ldots) \qquad \text{(XXIV-1)},$$

where D is the diffusion coefficient or diffusivity of the particles in the fluid. The seven stated variables may be reduced to four dimensionless parameters: the Reynolds number, Re_f, as $\rho d_f U/\mu$; the Schmidt number, Sc, as $\mu/\rho D$; the diameter ratio, R_d, as d_p/d_f; and the impaction number, I, as $R_d^2 R_\rho Re_f/18$. The last parameter containing the density ratio R_ρ, defined as $(\rho_p - \rho)/\rho$, is deduced from the law of motion, the number 18 arising from the Stokes resistance for a sphere in slow motion. Thus, the correlations to be developed will involve one or more of these parameters or their combinations:

$$E = f(Re_f, R_d, I, \epsilon) \qquad \text{(XXIV-2)}.$$

The sources of experimental data chosen for this analysis are listed in Table XXIV-1. In these experiments the particles were believed to be monodispersed.

IMPACTION-INTERCEPTION

In aerosol filtration the particle diameter is often of the order of the mean free path (10^{-5} cm.) of the air molecules. The particles have a tendency to slip between the molecules, resulting in less resistance than indicated by Stokes' law. To account for the higher particle mobility, the Cunningham correction factor is introduced. At ordinary air temperatures and pressures the approximate correction is

TABLE XXIV-1

DATA OF AEROSOL FILTRATIONS

Source	IPC (XXIV-1)		Wong (XXIV-2)	Chen (XXIV-3)	Thomas (XXIV-4)
Particle	aluminum oxide	polystyrene latex	sulfuric acid	dioctyl phthalate	benzene azo naphthol
ρ_p, g./cc.	3.99	1.05	1.39	0.98	1.26
d_p, micron	0.0036-0.0078	0.26-0.8	0.4-1.3	0.15-0.72	0.29
Fiber	dacron	dacron	glass	glass	glass
d_f, micron	17.5	17.5	3.5-9.6	2.5	10.6
Mat	wet formed	wet formed	wet formed	dry formed	
ϵ	0.78-0.91	0.7-0.73	0.9-0.95	0.93-0.98	0.94-0.98
Air					
$\rho \times 10^3$, g./cc.	1.0	1.0	1.1	1.2	1.2
$\mu \times 10^4$, g./(cm.)(sec.)	1.8	1.8	1.9	1.8	1.8
U, cm./sec.	30-450	30-800	20-200	1-50	1-100

$$k^{o} = 1 + 0.16 \times 10^{-4}/d_p \qquad \text{(XXIV-3)}.$$

Theoretical analysis by Davis (III-3) indicated that E is a function of I and Re_f when impaction dominates. Since both parameters contain U, it is desirable to separate I into two factors, R^{o} and Re_f. R^{o} is defined as $(k^{o}/18)(R_d^2 R_\rho)$ and called the inertia number.

The impaction data of IPC were obtained with polystyrene latex particl at high velocities. They are shown in Fig. XXIV-1. There appear three distir guishable regions: a linear region represented by the solid lines, a curved region as an extension toward lower velocities, and an apparently anomalous region consisting of abnormally low data points. The linear region is believed to be representative of impaction. Within the precision of data, the four line corresponding to four particle sizes are parallel to one another with a slope of 3/2. The larger the particle size, the lower is the air velocity for the particles to reach the impaction region. A correlation for impaction may be established as

$$E = \beta(R^{o})(Re_f)^{3/2} = \beta(I)(Re_f)^{1/2} \qquad \text{(XXIV-4)}.$$

The average value of β is 0.24.

The data of IPC were confined to a very narrow porosity range. The effect of porosity on E, however, may be qualitatively deduced. At the same porosity the average pore size of a fiber mat is roughly proportional to the fiber diameter. As the pore size increases, the chance of impaction decreases. With the same fibers the pore size increases with increasing porosity, resulting in more impactional misses. Meanwhile, as the porosity or pore size increases,

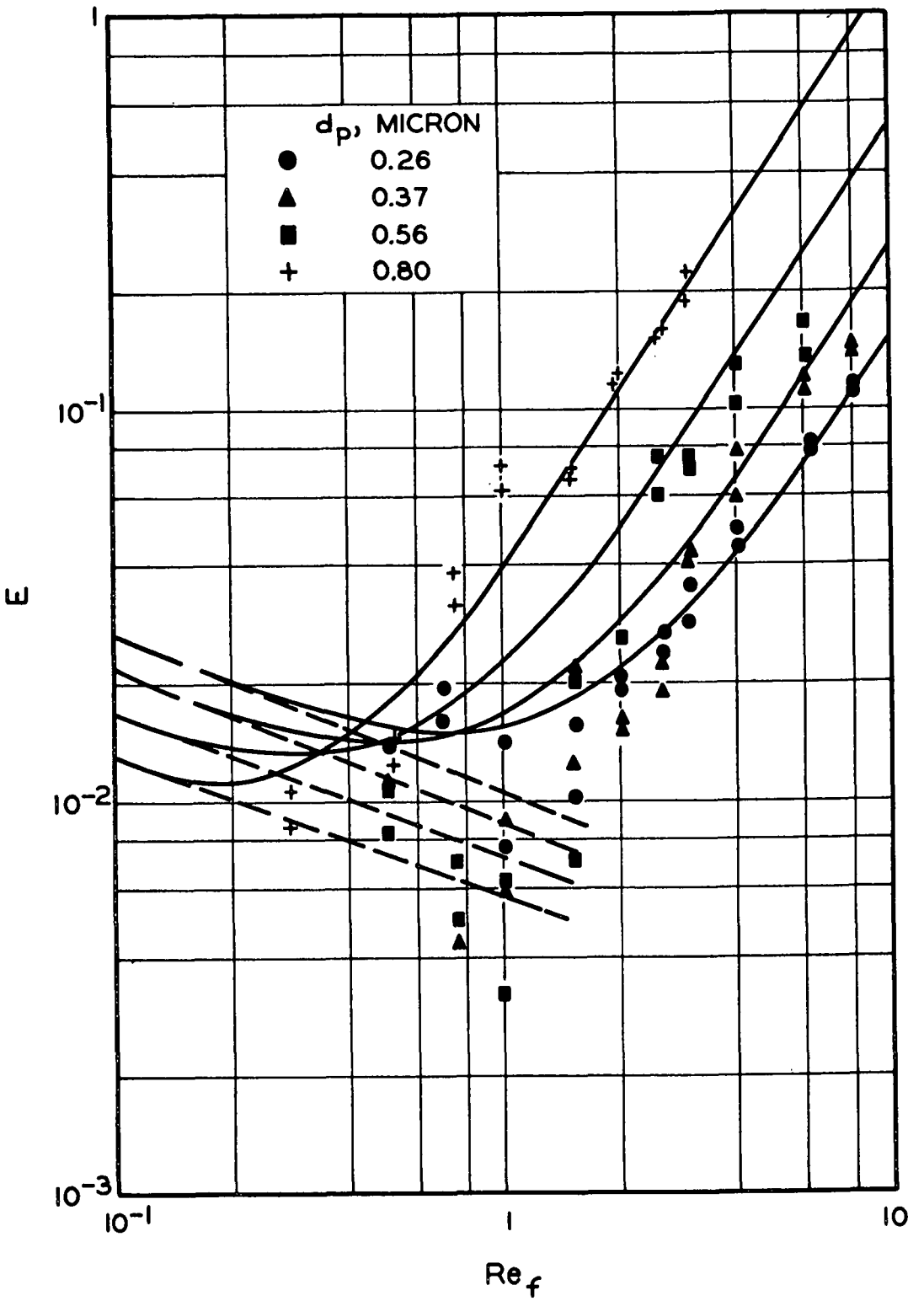

Figure XXIV-1. Impaction Data for Polystyrene Latex Particles

the fluid velocity in the pores decreases at the same approach velocity. This further reduces the chances of impaction.

The data of Wong covered a wider range of $\underline{R}_d$ (0.05-0.3) than those of IPC ($\underline{R}_d$ 0.015-0.045). Wong's results are shown in Fig. XXIV-2 as replotted from his original data. According to Wong, impaction ceases to be effective below a critical impaction number which he suggested to be 0.16. Accepting the existence of critical impaction, we may infer that the horizontal part of the curves represents interception which appears to be independent of the velocity and to be a function of the diameter ratio only. Proceeding with this evidence, we have found that interception also becomes ineffective below the minimum value 0.085 for $\underline{R}_d$:

$$E_b = \gamma(R_d - 0.085) \qquad \text{(XXIV-5)},$$

where γ is 0.4. If this analysis is correct, the previous implication of negligible interception in the IPC impaction data was justifiable.

We now deduct $\underline{E}_b$ from the reported $\underline{E}$ for all Wong's data; the net value presumably represents the collection efficiency due to impaction alone. In this way we have arrived at the same correlation:

$$(E - E_b) N' = \beta (Re_f)^{3/2} \qquad \text{(XXIV-6)}.$$

The value of β for Wong's system is 0.06. The two sets of data are compared in Fig. XXIV-3. They show very similar patterns and have the same degree of scattering.

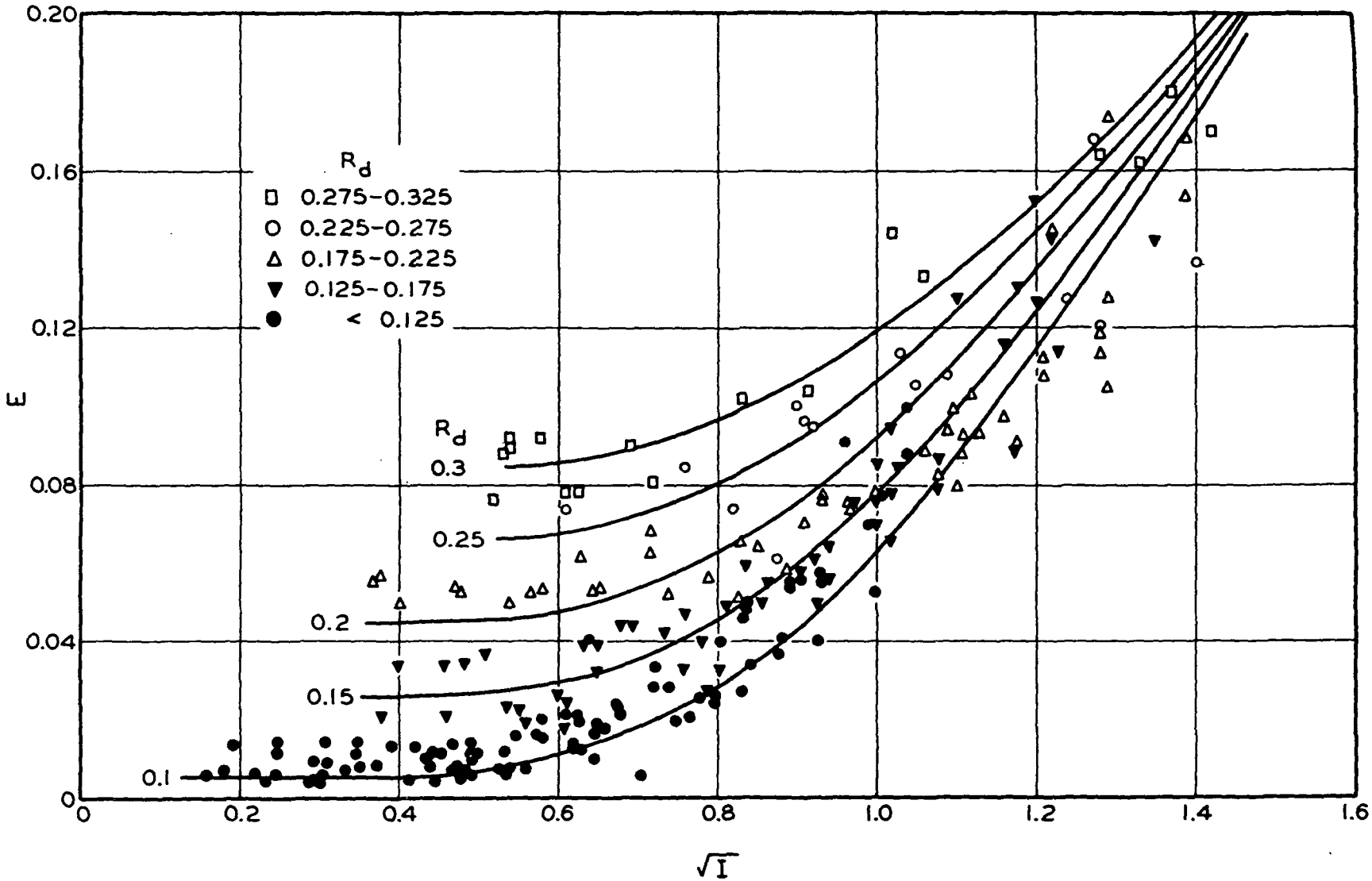

Figure XXIV-2. Impaction Data for Sulfuric Acid Droplets

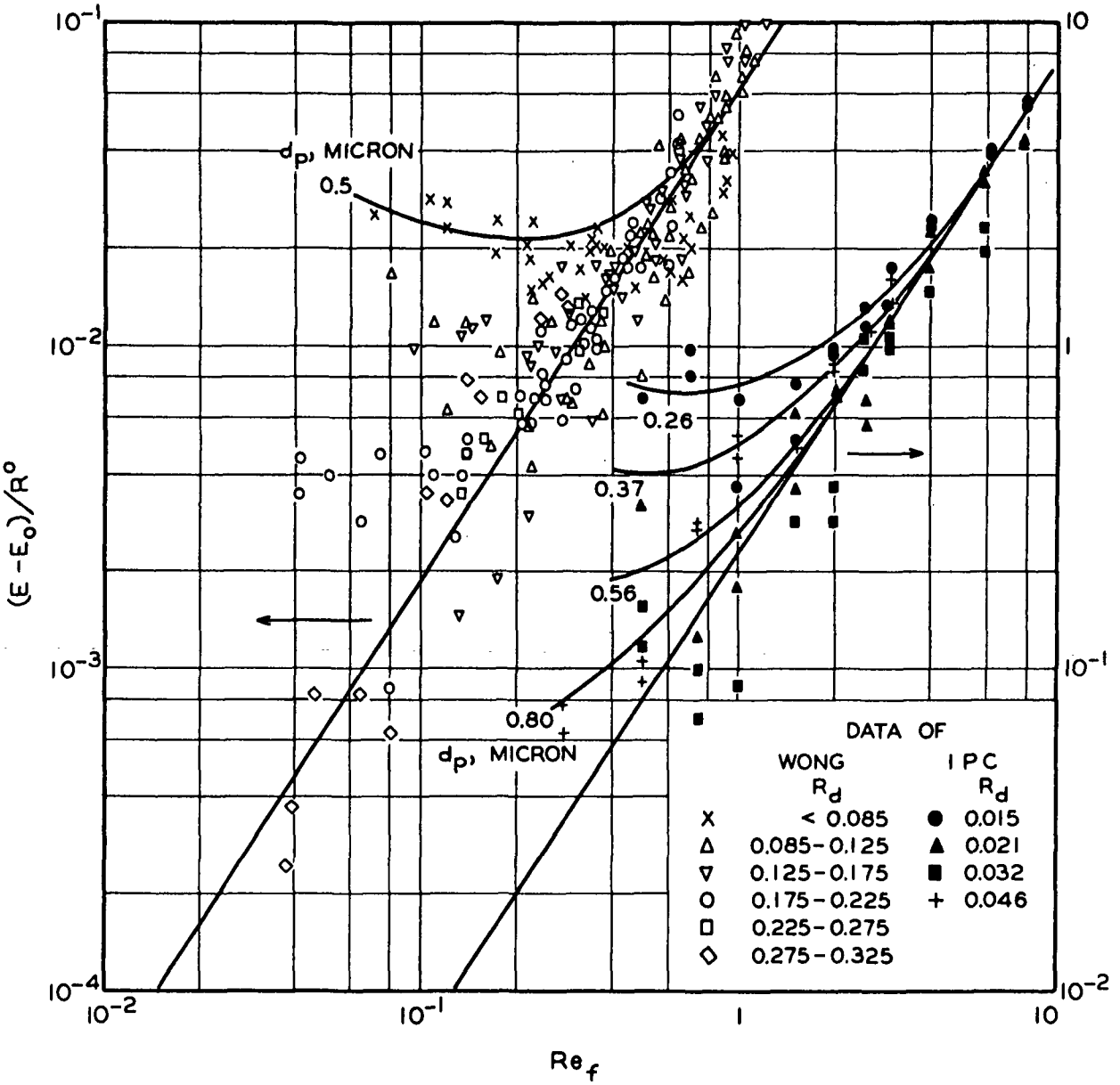

Figure XXIV-3. Comparison of Impaction Data

DIFFUSION-INTERCEPTION

Theoretical analysis of diffusion indicated that $\underline{E}$ is proportional to the diffusion number $(\underline{D}/\underline{d_f U})$ to the power from 1/2 to 2/3. The diffusion number is the reciprocal of the Peclet number, which is the product of the Schmidt number and the Reynolds number.

A part of Chen's data for low $\underline{R_d}$ values may be considered to be diffusion-controlling. By a graphical analysis these data, as shown in Fig. XXIV-4, may be correlated by

$$E = \alpha(Sc)^{-1/2}(Re_f)^{-1/2} \qquad \text{(XXIV-7)},$$

the value of α being 0.8. Additional support for this correlation is obtained from Thomas' data. They show the same slope with α equal to 0.3. It is seen that Thomas' data exhibit increasing deviations at $\underline{Re_f}$ larger than 0.1.

Previous work at IPC dealt with very small particles in transition flow $(0.1 < \underline{Re_f} < 10)$. The IPC data also shown in the same figure may be correlated by

$$E = \alpha(Sc)^{-1/2}(Re_f)^{-2/5} \qquad \text{(XXIV-8)}.$$

The value of α is 0.23. By comparing the three sets of data, it appears that diffusional collection is affected by flow pattern. In creeping flow a dimensional analysis will show that the collection efficiency is dependent on the diffusion number alone. As the Reynolds number increases, fluid inertial effects set in. The change of flow pattern, as discussed before, is gradual, and a very rough criterion for transition is unity $\underline{Re_f}$. It is reasonable to expect that in

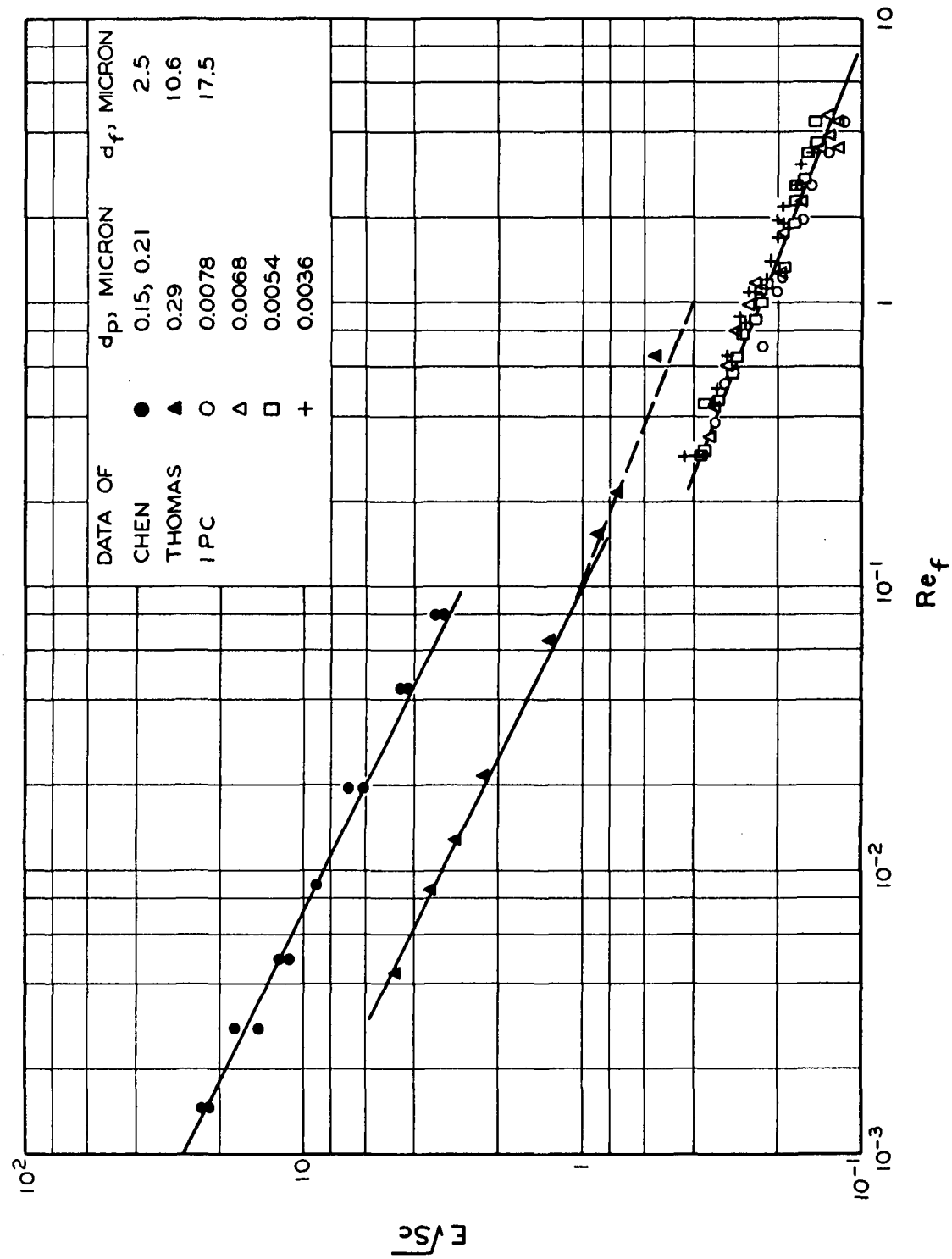
DATA OF
CHEN
THOMAS
I P C
d_p, MICRON
0.15, 0.21
0.29
0.0078
0.0068
0.0054
0.0036
d_f, MICRON
2.5
10.6
17.5
$E\sqrt{Sc}$
Re_f
10^2
10
1
10^{-1}
10^{-2}
10^{-3}
10
1
10^{-1}

transition flow, while the diffusional characteristics of a system remain the same, the dependence on flow should undergo slow changes.

In an analysis (II-3) of Johnson's data (XXIV-5) for water filtration of titanium dioxide particles by nylon fiber mats, the conclusion was reached from both theoretical consideration and experimental evidence (Fig. XXIV-5) that collection efficiency was dependent on the diffusion number to the power 2/3 for $\underline{Re}_f < 1$. The reason for the discrepancy between gas and liquid filtrations is not known. One possibility would be the increasing agglomeration of titanium dioxide particles with increasing velocity in Johnson's experiments.

The effect of interception on diffusion is more complex than in the case of impaction. It is dependent on both $\underline{R}_d$ and $\underline{Re}_f$. The effect of porosity on diffusion is generally minor because of the counteracting factors of decreasing pore size and increasing pore velocity. The IPC data for ϵ between 0.75 and 0.92 are in agreement with this deduction. At very high porosities Chen demonstrated that $\underline{E}$ decreases linearly with increasing ϵ, the maximum effect being about 30% in the porosity range of 0.9-0.98.

DIFFUSION-IMPACTION

In the absence of interception, the two mechanisms are considered to be independent and additive, subject to the limitation of critical impaction. The curved region of the IPC data in Fig. XXIV-1 may be so represented by

$$E = \alpha(Sc)^{-1/2}(Re_f)^{-2/5} + \beta(R^0)(Re_f)^{3/2} \qquad \text{(XXIV-9)}.$$

Taking the derivative of $\underline{E}$ with respect to $\underline{Re}_f$ and setting it to zero, we obtain the minimum point at

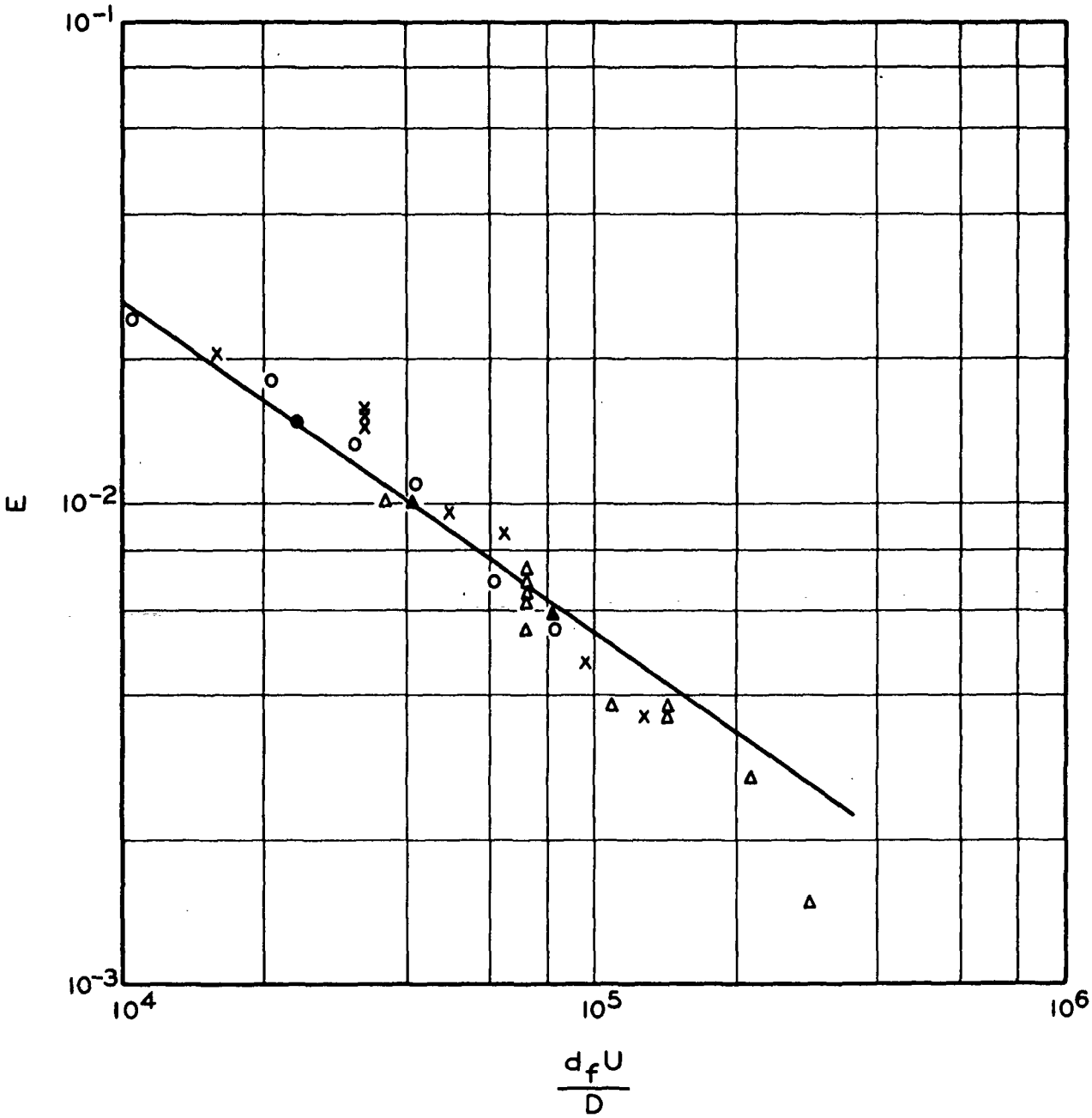

Figure XXIV-5. Diffusion Data for Titanium Dioxide Particles

$$Re_f = \left[\frac{4\alpha(Sc)^{-1/2}}{15\beta R^0}\right]^{10/19} \qquad \text{(XXIV-10)} .$$

Examining the original data, the only apparent minimum is located at $\underline{Re}_f$ 0.75 for the smallest particle size. With the known value of β , α is evaluated to be 3.5. Using this value, all four curves may be reconstructed, as shown in the figure. They appear to be in fair agreement with the trend of the data except the abnormal points.

Obviously, the curves should cross each other because diffusion decreases and impaction increases with increasing particle size; the minimum occurs at progressively lower Reynolds number as the particle size increases. Furthermore, at a certain value of $\underline{Re}_f$, impaction ceases to be effective, and a linear region of pure diffusion will be reached sooner or later. The dashed lines represent such extrapolations.

In a similar manner, Wong's data for $\underline{R}_d$ at 0.08 may be analyzed, using the power 1/2 for $\underline{Re}_f$ in diffusion. At the minimum value of 0.2 for $\underline{Re}_f$, the coefficient α has an estimated value of 2. The curve representing the combined effects of diffusion and impaction is shown in Fig. XXIV-2. For higher $\underline{R}_d$, interception comes into play, and this method of analysis is no longer applicable.

The abnormally low points in the IPC data exist in the neighborhood of unity $\underline{Re}_f$. The scattering is more pronounced with the larger particles. A possible explanation for this anomaly could be that impaction might not become effective in transition flow if diffusion persisted locally in a mat. As pointed out by Fuchs (XXIV-6), transition of aerosol behavior exists in the range of particle sizes between 0.1 and 1 micron. The combination of changing particle

behavior and flow pattern would account for the instability observed. Wong's data show a similar pattern.

ADHESION-DETACHMENT

The coefficients α, β, and γ include all factors not accounted for in the correlations. The major factor should be the degree of adhesion which results from the molecular attraction between particles and fibers on their close encounter in the range where Van der Waals-London forces are operable. Whether a particle will adhere to a fiber (or another particle) or not is dependent on all the forces, molecular, aerodynamic, gravitational, and electrostatic, acting at the site of collision. It is the net force, or rather the energy of interaction, which ultimately determines the fate of the particle. Obviously, different particle-fluid-fiber systems have different degrees of adhesion. Even for apparently the same materials, the nature and treatment of surfaces will result in widely different collection efficiencies under the same filtration conditions.

In Table XXIV-2 the values of α and β are arranged in a descending order. Solid particles appear to have the lowest adhesion. However, when the same fibers are coated with a viscous oil, adhesion is considerably improved. With the same kind of fibers, adhesion of liquid particles can vary widely. It is also interesting to compare the first two sets of data for which both α and β values are available. The ratio of α values is only 1.7 while that of corresponding β values is 4. The much lower adhesion of the liquid particles in the impaction region is probably due to shattering of droplets on impact and re-entrainment of finer particles by air.

TABLE XXIV-2

COMPARISON OF COEFFICIENTS

Air filtration	Diffusion (α)	Impaction (β)
Polystyrene latex-dacron, coated with oil	3.5	0.24
Sulfuric acid-glass	2.0	0.06
Dioctyl phthalate-glass	0.8	
Benzene azo β-naphthol-glass	0.3-0.4	
Aluminum oxide-dacron	0.23	
Water filtration		
Titanium dioxide-nylon	11	
Titanium dioxide-dacron	4.8	

	$\frac{E}{CaCl_2} \times 10^3$	NaCl
Fines-sulfite (1st batch)	70	4
Fines-sulfite (2nd batch)	4	2

With liquid filtrations the situation becomes more complex when colloidal conditions are imposed. The fines prepared from the same pulp in two different batches show a considerable difference. Flocculation of particles could account for a part of the discrepancy.

XXV. EXPERIMENTAL SUPPORT FOR FIBER-RETENTION THEORY

The probability theory of fiber retention was reviewed in Chapter VIII. The experimental evidence for initial retention was supplied by Estridge (III-11), Andersson and Bartok (XXV-1), and Bloom (XXV-2). Abrams (VIII-1) and Han (III-12) dealt with subsequent retention.

INITIAL RETENTION

Estridge considered four idealized cases as follows: (I) parallel wires with uniform spacing and randomly oriented fibers, assuming no friction on contact with a wire, (II) same wires and fibers, assuming no slippage at contact, (III) same wires, with approaching fibers oriented randomly only in the x-y plane, and (IV) square-mesh screens with other conditions the same as in Case I. His predictions are shown in Fig. XXV-1 as solid curves.

For retention experiments he used simple filtration apparatus with means of collecting and weighing the straight rigid nylon fibers of narrow cuts retained on and passed through a grid of very fine wires from an extremely dilute suspension at a slow rate. By making a series of runs with a given fiber-wire combination, a set of retention data was obtained. From a plot of W vs. W_s a smooth curve was constructed and the slope at the origin was taken to be $\bar{P}_i$ for initial retention. The data points are shown in Fig. XXV-1. Their agreement with the curves, in general, is good. Because of the loss of precision in taking the slopes, the data points for parallel wires are not accurate enough to distinguish the three assumed cases. In Estridge's experiments, minor variations in flow rate, pitch-to-diameter ratio, and suspension consistency were found to have no significant effects on the retention results.

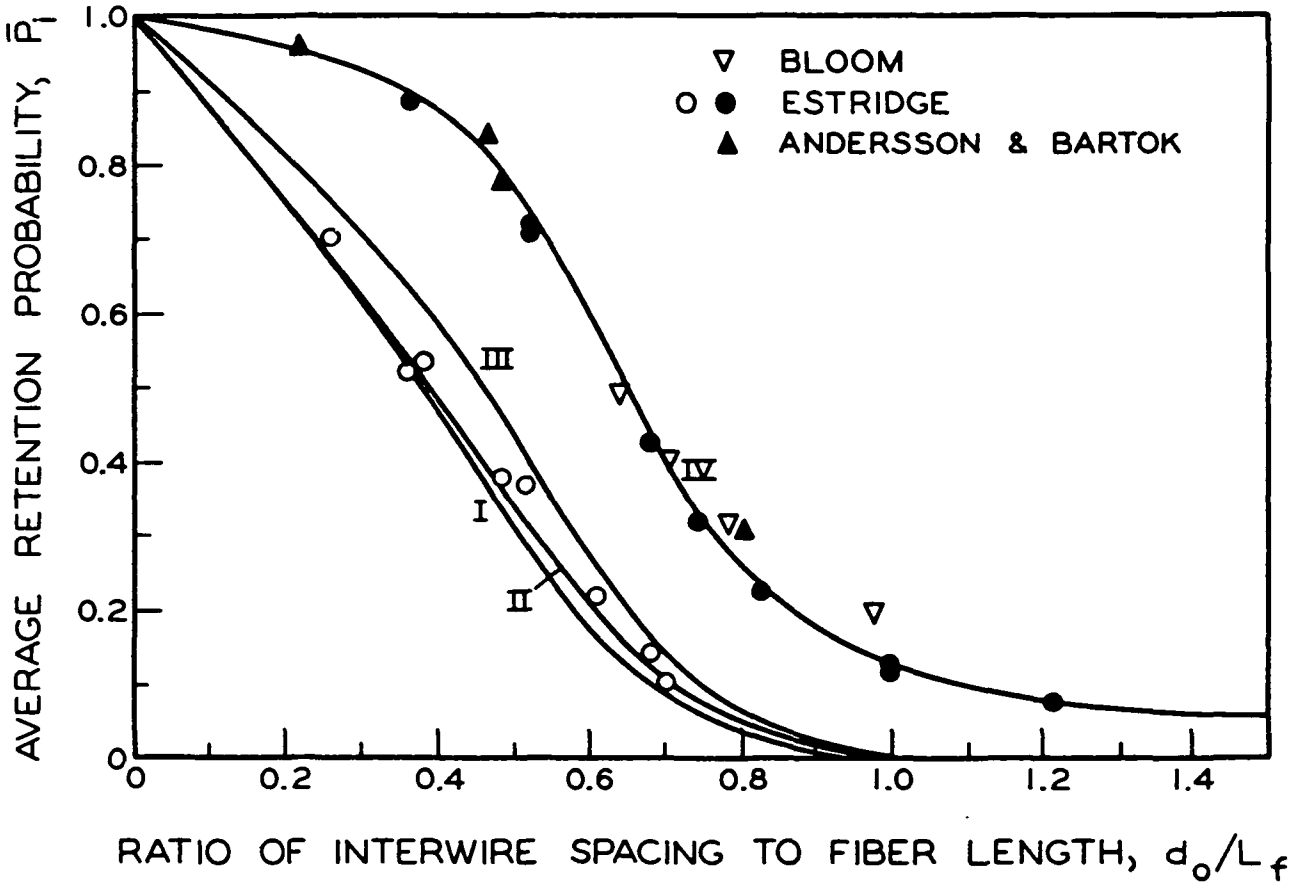

Figure XXV-1. Initial Fiber Retention

Estridge also recalculated the data of Andersson and Bartok for rayon fibers passing through 28-mesh screens in a modified Bauer-McNett classifier, using the net dimension of the screen openings. The results are seen to be in good agreement with Case IV for square meshes.

Bloom experimented with fibers in different length-distributions. He demonstrated that for fibers having the same mass per unit length Estridge's general equation (VIII-6) is valid:

$$R_o = \frac{\Sigma w_{f,i} \bar{P}_i N_i}{\bar{w}_f N_t} \qquad \text{(XXV-1)} .$$

Four different distributions of nylon fibers ($\underline{L}_f$ = 1.5-5.1 mm.) were used with a square-mesh grid ($\underline{d}_o$ = 2.54 mm.). Bloom's results are also included in Fig. XXV-1, the values of fiber length being weight averages.

SUBSEQUENT RETENTION

Abrams modified the filtration apparatus to accommodate the measurement of fiber retention in incremental steps so that a complete set of data could be obtained in a single run. A schematic diagram of his apparatus is illustrated in Fig. XXV-2. Rectangular grids having openings with aspect (length-width) ratios 1, 2, and 3, constructed of 0.013-cm. diameter stainless steel wires and fibers cut from 4.1 and 4.5 x 10^{-3}-cm. diameter nylon filaments were used in the experiments.

Retention data were obtained as before. In addition, photographs of the fiber networks were taken periodically throughout an entire run and were used later to establish the distributions of network distances $\underline{L}_s$. The random scan-line measurements of the network photographs provided frequency distributions as discussed in theory. The average retention probabilities $\underline{\bar{P}}_i$ were then determined by

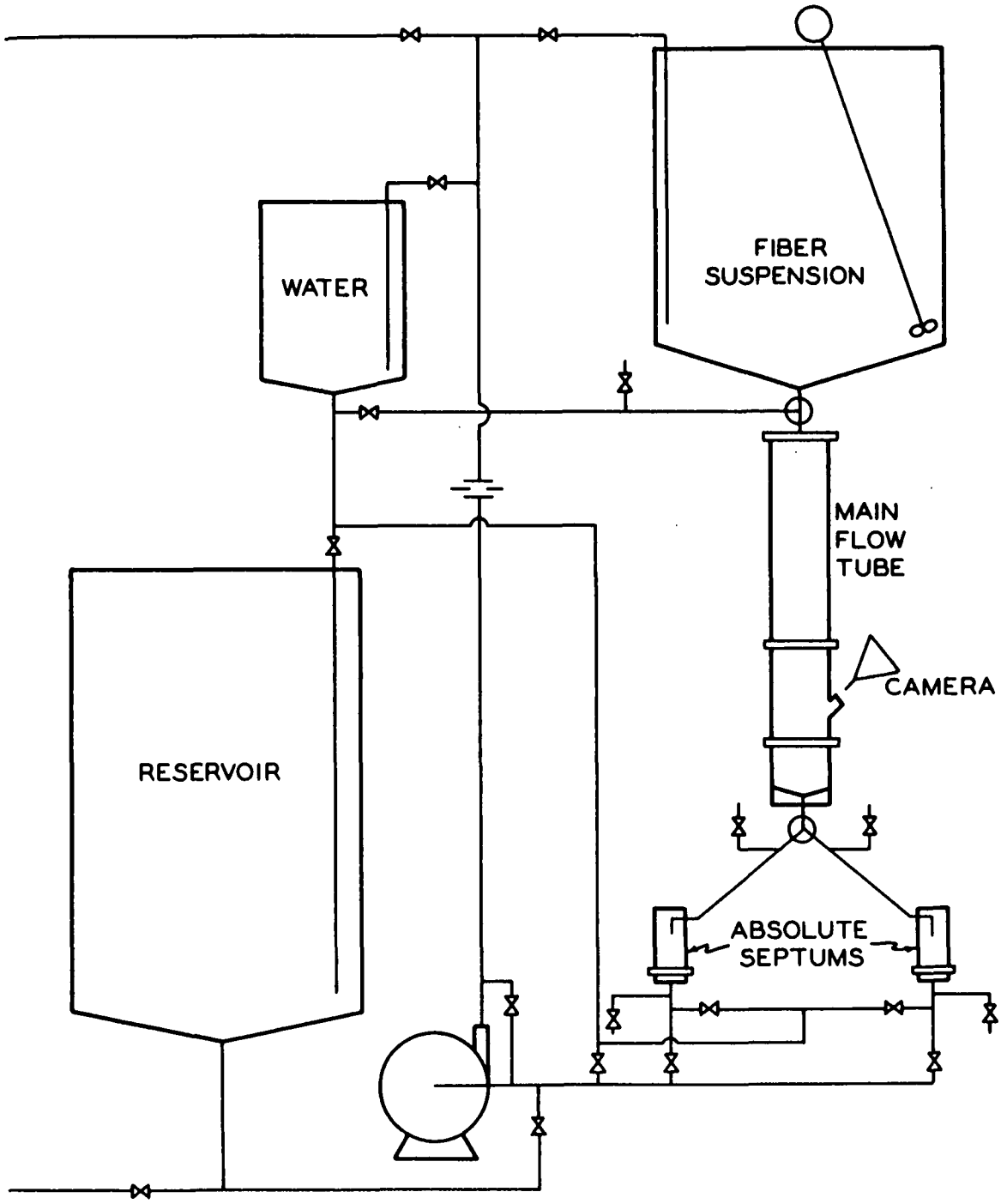

Figure XXV-2. Fiber Retention Apparatus

substituting the estimated distribution functions from the photographs into Equation (VIII-7) and integrating accordingly. The results determined from the retention data and from the theory based on the frequency distribution data are compared in Fig. XXV-3. The discrepancies are very large, the actual retention being lower than the predicted. The two curves, however, are in agreement with each other for initial retention. Abrams attributed the discrepancy in subsequen retention to suspension-network interactions which were not taken into account in the theory.

Because of the inadequacy of the theory, Abrams reverted to the semiempi cal treatment. He evaluated the values of α_0 (VIII-12) from his data, and four that they varied from 0.07 to 0.17, as compared with the theoretical value of 0.3] There was, however, no discernible pattern with respect to fiber length or openin dimensions.

The earlier work of Han on fiber retention was entirely empirical. By intuition he correlated his white water consistency data from sheet-forming experiments in an exponential form. The sheet former was of the rotary suction type covered with conventional wire screens (80 x 57-mesh facing wire and 20-mesh backing wire) and the fibers were classified from a sulfite pulp. His correlati is shown in Fig. XXV-4, in agreement with Equation (III-14). If the line is extrapolated to zero basis weight, the initial white water consistency is 2.7 x 1· or 0.027%. Since the suspension consistency was 0.262%, the initial retention probability would be 0.9. This value appears to be reasonable for a long-fiber stock and the combination screens used. The value of k_0 is 0.045 x 10^4 sq. cm per g., which is smaller than Abrams' lowest value 0.06 x 10^4 corresponding to hi α_0 value 0.1. The agreement is about as good as can be expected.

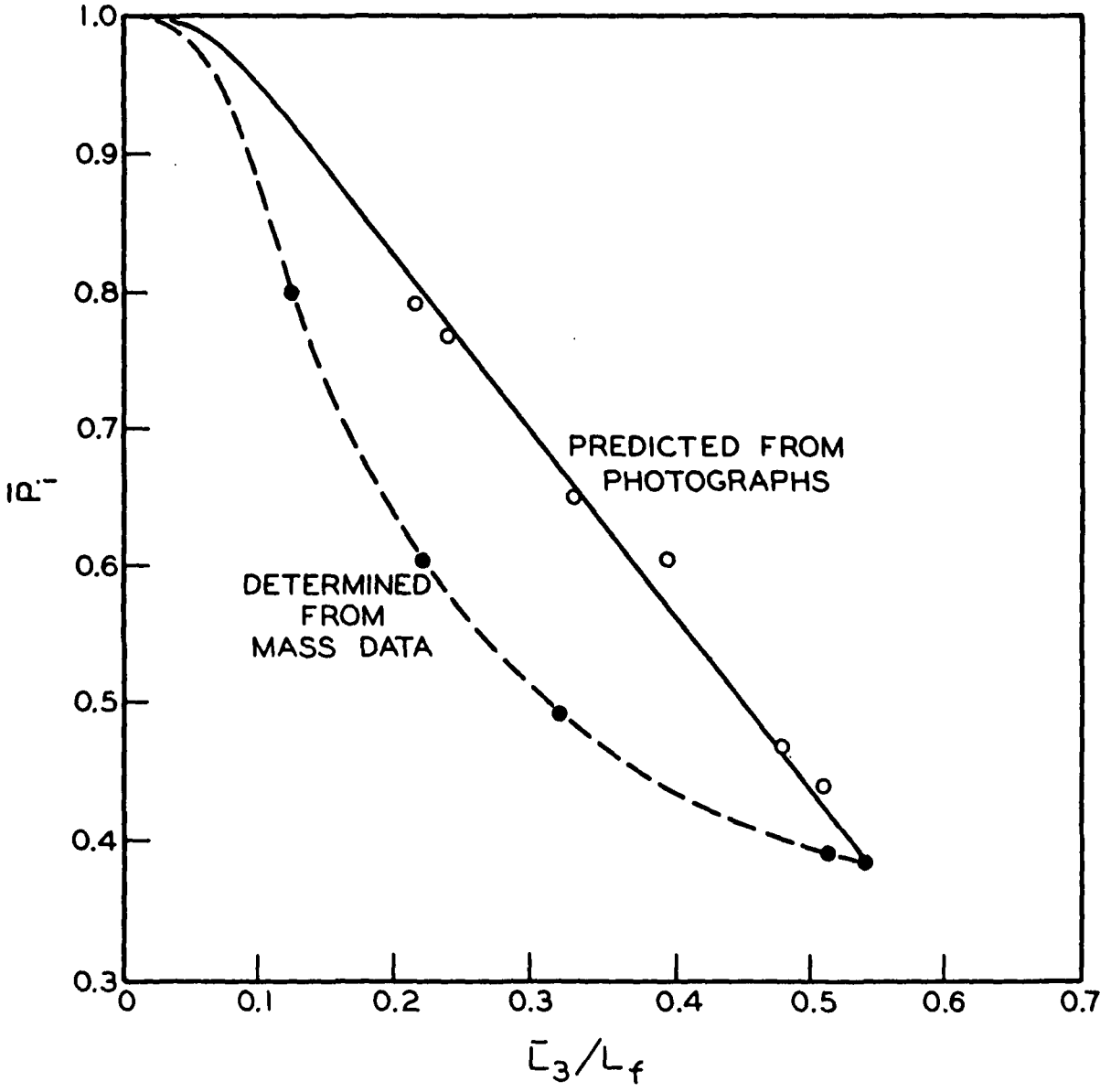

Figure XXV-3. Comparison of Fiber Retention Data with Predictions

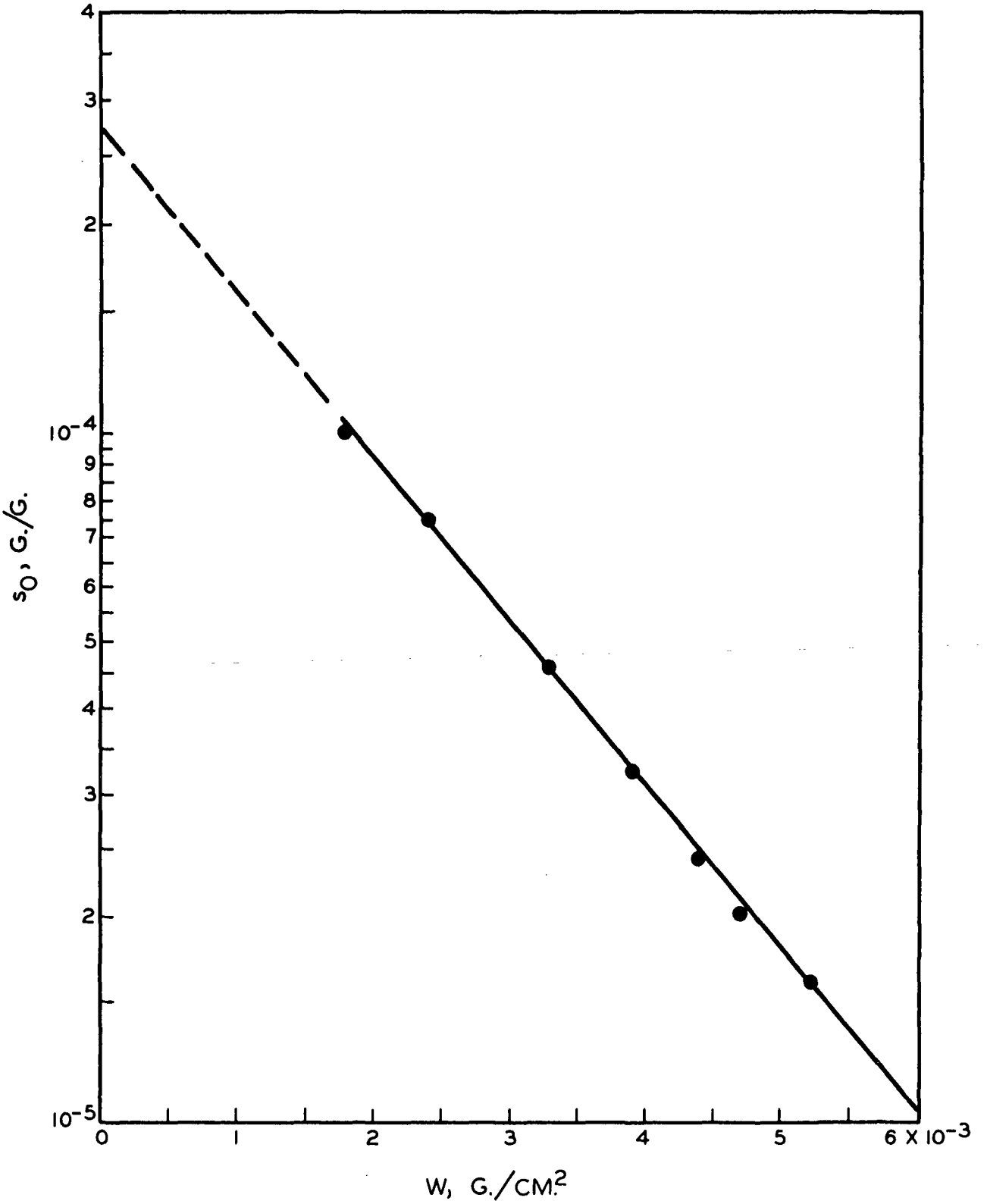

Figure XXV-4. White Water Consistency Correlation

XXVI. HYDRODYNAMIC BEHAVIOR OF CYLINDRICAL FIBERS

The motion, collision, and interaction of fibers in a fluid constitute the dynamic behavior of a fiber suspension. However, observations and interpretations of such phenomena involve considerable difficulties because of the boundary and other effects often associated with experimental conditions. We attempt here to review some studies of the relatively simple phenomena, by which more complex ones may be eventually clarified as our understanding increases.

FIBER SEDIMENTATION

The creeping motion of a finite cylinder, as discussed in Chapter XIV, was studied by Han (XXVI-1) by means of sedimentation in a cylindrical vessel. The results are shown in Fig. XXVI-1. The lower curve represents Oberbeck's solution for a prolate spheroid with its long axis perpendicular to the direction of motion at a constant velocity. The drag force in an infinite fluid is

$$F_\infty = 6\pi\mu U r_o f(\chi) \qquad \text{(XXVI-1)},$$

where, for semiaxis ratios (χ) larger than unity,

$$f(\chi) = \frac{(8/3)}{\frac{\chi}{\chi^2 - 1} + \frac{2\chi^2 - 3}{(\chi^2 - 1)^{3/2}} \ln\left[\chi + \sqrt{\chi^2 - 1}\right]} \qquad \text{(XXVI-2)},$$

r_o being the radius of a spheroid. For $\chi = 1$, $f(\chi) = 1$, and Equation (XXVI-1) reduces to Stokes' formula for a sphere. For $\chi > 10$, F_∞ is the same as Burgers' solution for cylinders:

$$F_\infty = \frac{4\pi\mu U L_f}{\ln\left(2L_f/d_f - 1/2\right)} \qquad \text{(XIV-2)},$$

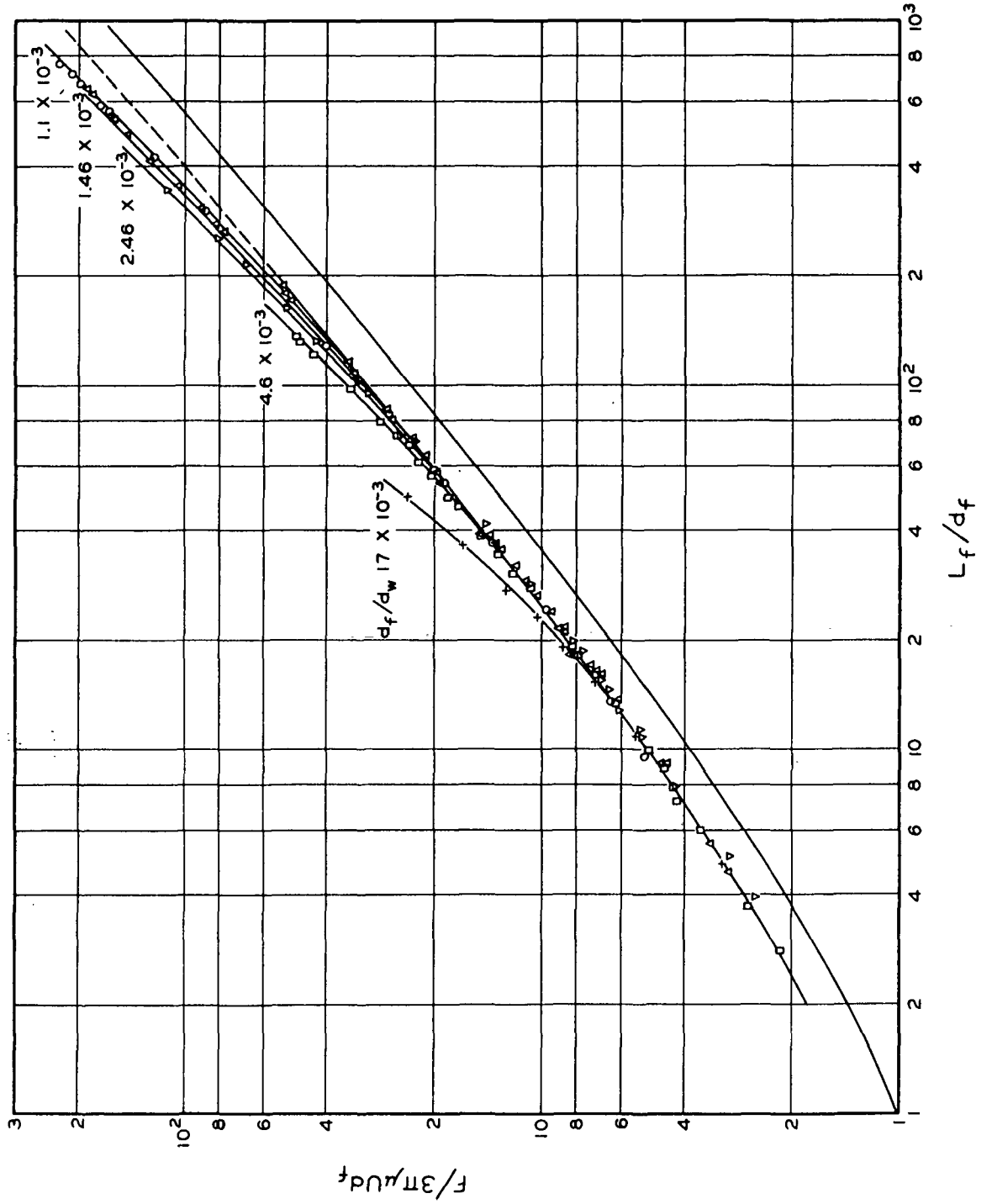
1.1 X 10⁻³
1.46 X 10⁻³
2.46 X 10⁻³
4.6 X 10⁻³
d_f/d_w 17 X 10⁻³
F/3πμUd_f
L_f/d_f
3
2
10²
8
6
4
2
10
8
6
4
2
1
2
4
6
8
10
2
4
6
8
10²
2
4
6
8
10³

where L_f/d_f is the axis ratio.

The experimental data show clearly the wall effect. Using Brenner's correction (XIV-4), the value of k_w was found to be very close to unity. This value agreed with Brenner's theoretical value for parallel walls, rather than that for cylindrical walls. Anyway, after the correction for the wall effect the experimental curves merged into a single one. The corrected drag force within the experimental range was always higher than the theoretical prediction by a constant factor of 4/3. This discrepancy may be attributed to the difference in shape between an ellipsoid of revolution and a cylinder. It is conceivable that as both become infinitely long, their drag forces approach each other and tend to agree with Lamb's solution (XIV-1). With this contention the experimental results are transformed into the drag coefficient as a function of the Reynolds number with the axis ratio as the parameter:

$$C_\infty = \frac{F_\infty}{A_f \rho U^2/2} = \frac{4\pi\mu U d_f f(L_f/d_f)}{L_f d_f \rho U^2/2} = \frac{8\pi f(L_f/d_f)}{(L_f/d_f)Re_f} \qquad \text{(XXVI-3)},$$

where $f(L_f/d_f)$ is the same as $f(\chi)$. Similarly, Lamb's solution may be expressed as

$$C_\infty = \frac{8\pi}{Re_f \ln (7.4/Re_f)} \qquad \text{(XXVI-4)}.$$

The resulting plot is shown in Fig. XXVI-2, in which the data of Jones and Knudsen (XXVI-2) for cylinders with very small axis ratios (1-30) in the Reynolds number range of 10^{-2} to 1 and those of Wieselberger (XXVI-3) for an infinite cylinder at Re_f larger than unity are included. The linear region representing the axis ratios from 5 to 1000 indicate creeping motion. The curve

subst

Equa

re

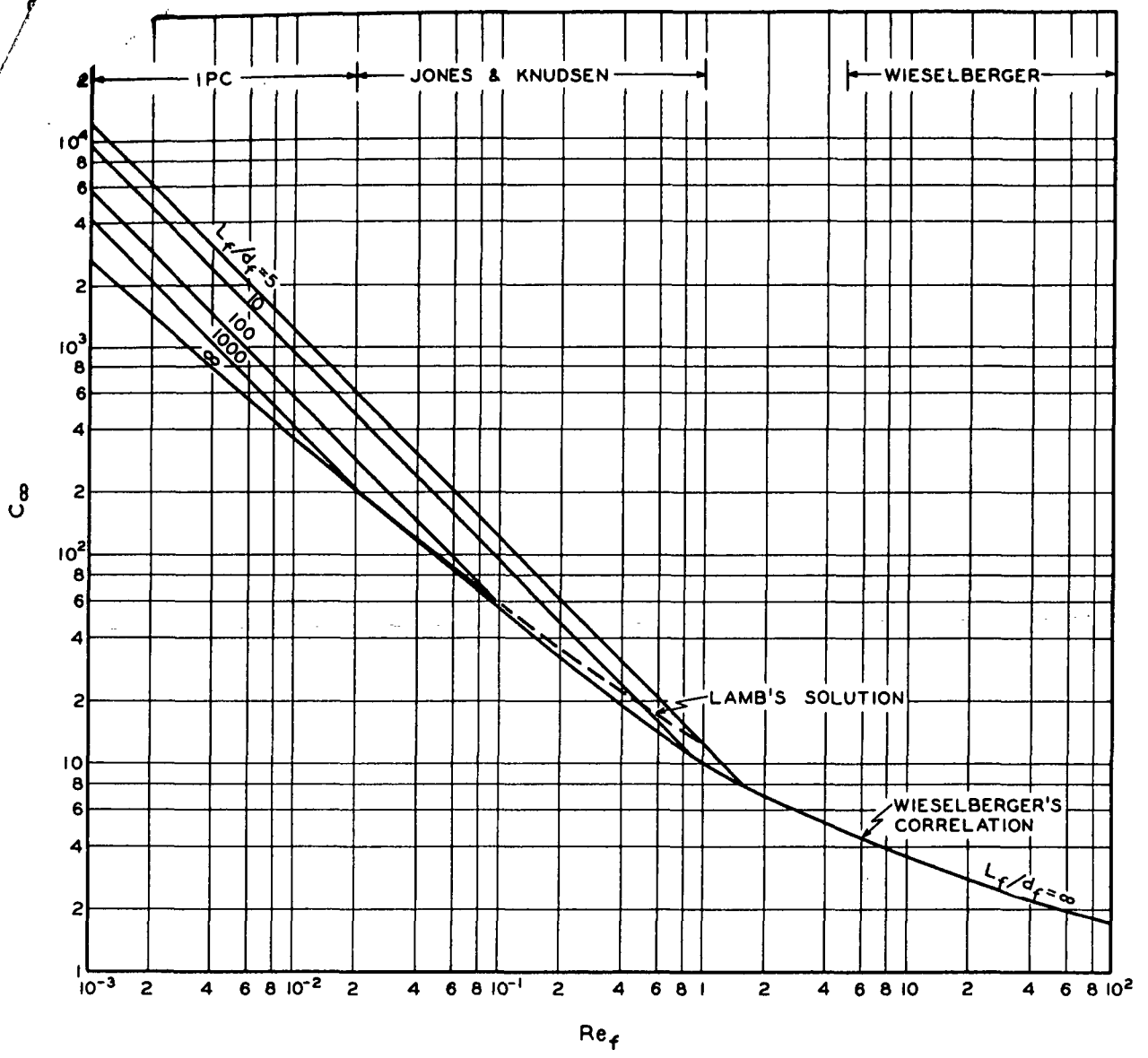

Figure XXVI-2. Correlation of Drag Coefficients for Cylinders

region for an infinite cylinder reveals inertial effects. The lines, when extended to higher Reynolds numbers, sooner or later cross the curve. The intersections occur at

$$Re_f = \exp[2 - \frac{L_f/d_f}{f(L_f/d_f)}] \qquad \text{(XXVI-5)} .$$

The extension of the lines would begin to curve because of inertial effects. Wieselberger measured the drag force on cylinders at Re_f from 5 and upward. He found that the drag coefficient was also dependent on the axis ratio, but to a much milder extent and in the opposite direction. Thus, if the lines were extended beyond the curve, they would cross one another in order to reach Wieselberger's region of high Reynolds numbers.

Han also found that curved cylinders moving concave-downward deviate approximately from Tchen's solution (XIV-4) by the same factor of 4/3 as straight cylinders. Tchen's solution for this case is

$$F_\infty = 2\pi\mu U r \psi f_\infty \qquad \text{(XIV-3)} ,$$

$$f_\infty = \tfrac{1}{2}[(f_r + f_t) + (f_r - f_t)\frac{\sin 2\psi}{2\psi}] ,$$

radial

$$f_r = \frac{4}{\ln (L_f/d_f + e_r)} ,$$

$$e_r = \ln \frac{2\tan(\psi/4)}{(\psi/4)} + 3\frac{\sin\psi}{\psi} - \frac{5}{2} ,$$

tangential

$$f_t = \frac{2}{\ln (L_f/d_f) + e_t} ,$$

$$e_t = \ln \frac{2\tan(\psi/4)}{(\psi/4)} + \frac{3}{2}\frac{\sin\psi}{\psi} - 2 \qquad \text{(XXVI-6)} .$$

The sedimentation results of curved cylinders with radii of curvature 0.61 , 0.94 , and 1.45 are compared with Tchen's solution in Fig. XXVI-3. It is seen that for both experimental results and theoretical predictions the effect of curvature is significant only above the axis ratio 10^2.

SUSPENSION VISCOSITY

Mason (XXVI-4) initiated the study of fiber suspensions in Couette flow. Myers (XXVI-5) constructed a concentric-cylinder viscometer with an air bearing for the inner rotating cylinder in order to measure very low torques. His apparatus is shown in Fig. XXVI-4. The same apparatus was used by Blakeney (XXVI-6) to obtain viscosity data for straight rigid nylon fibers at an axis ratio 20, dispersed in tetrachloroethane--paraffin oil solution ($\rho = 1.14$) at very low volume concentrations. The apparent viscosity was determined from the slope of a linear plot of the measured torque vs. angular velocity in accordance with the well-known equation:

$$\mu_a = \left(\frac{1 - r_i^2/r_o^2}{4\pi h r_i^2}\right) \frac{T}{\omega} \qquad \text{(XXVI-7)} .$$

The apparent viscosity was then corrected for end effects by calibration curves.

Blakeney also took photographs of the fiber suspensions for the purpose of determining the fiber orientation factor $\overline{\sin^4\theta \sin^2 2\psi}$ in Burgers' expression (XIV-7). His final results are shown in Fig. XXVI-5. In the low concentration range up to 0.4×10^{-2} there is a linear region in agreement with Burgers' theory:

$$\frac{\mu_s}{\mu} = 1 + \alpha^o C \qquad \text{(XIV-6)} .$$

The experimental value of α^o as determined from the slope of the line is 1.98, as compared with the value 1.95 determined from Burgers' theory with the

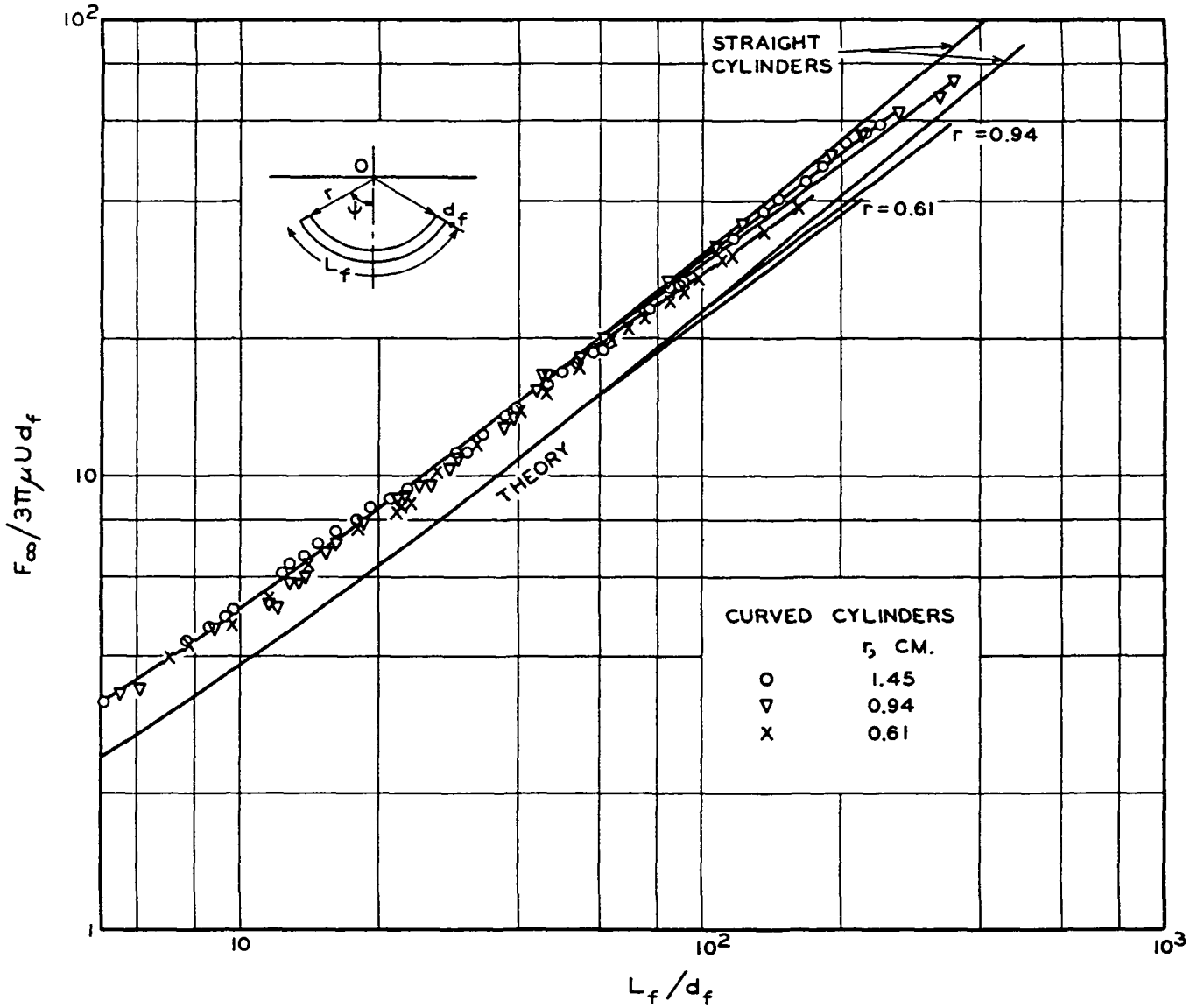

Figure XXVI-3. Sedimentation of Curved Cylinders

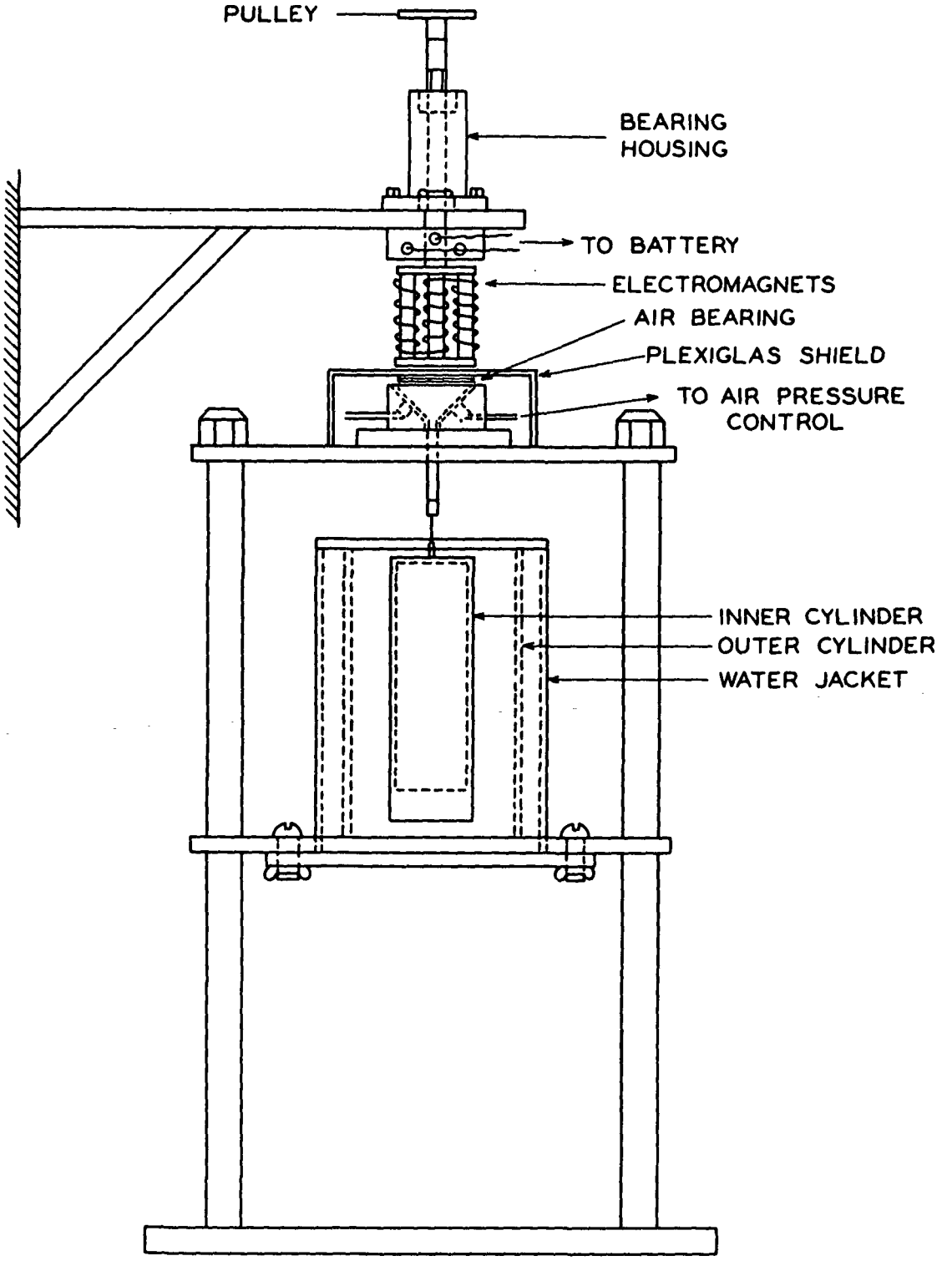

Figure XXVI-4. Couette Viscometer

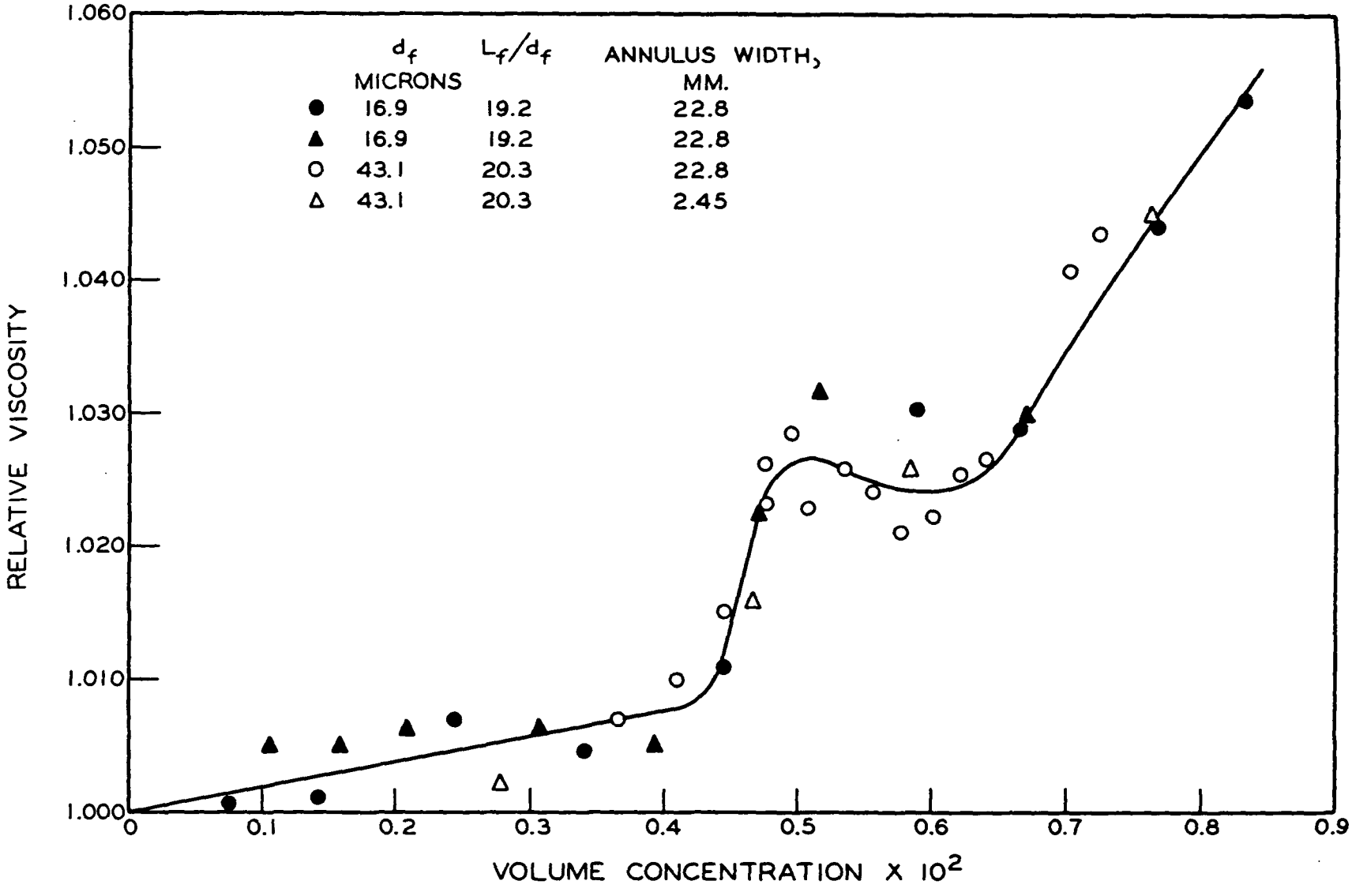

Figure XXVI-5. Viscosity of Fiber Suspensions

photographically evaluated average orientation factor 0.0563. According to Burgers, the orientation factor may vary from $(4/\pi)(d_f/L_f)$ for completely random orientations to $2(d_f/L_f)$ for random orientations in the x-y plane only. At the axis ratio 20, his values would be from 0.064 to 0.1. Again, there seems to be some minor defect in Burgers' theory, probably in his accounting for the orientation factor based on Jeffrey's analysis of ellipsoids (XIV-7).

The curved part is of particular interest in the behavior of fiber suspensions. First of all, in spite of the higher concentrations the system still exhibits the Newtonian behavior. Secondly, the deviation from the linear relationship begins at the concentration 0.42×10^{-2}. This value happens to be close to Mason's "critical concentration," $(3/2)/(L_f/d_f)^2$, at which the hydrodynamic interaction of fibers is supposed to become appreciable. Thirdly, the orientation factor determined from the photographs changes significantly with the concentration, as shown in Table XXVI-1.

TABLE XXVI-1

EVALUATION OF THE ORIENTATION FACTOR

C	$\overline{\sin^4\theta \sin^2 2\varphi}$
0.106-0.424	0.0563 (av.)
0.504	0.0881
0.557	0.0665
0.663	0.0575

With the fiber interactions and the change of fiber orientations in mind, Blakeney proposed the empirical correlation for the curved region:

$$\frac{\mu_s}{\mu} = 1 + \alpha^o C + \beta^o (\alpha^o C)^2 \qquad \text{(XIV-8)},$$

for which β^o was evaluated to be 468 from his data. The fit was fair over the inflection part and poor at higher concentrations.

In Blakeney's experiments the wall effect was negligible. Both Myers and Blakeney found the pronounced effect of curved fibers on viscosity (fiber rotation) in the linear region, in contrast to the linear motion of a curved fiber. For a slight curvature (176^o) at the same axis ratio 20, the apparent viscosity increased by as much as 30% at the critical concentration. Blakeney also coincidentally observed the effect of flocculation. When a low torque was applied to a certain dispersed suspension at the beginning of one experiment, the fibers immediately began to form flocs (not a uniform network), which continued to grow until an apparently stable size was reached at the fixed shear field. The growth of the flocs caused a decrease in the angular velocity and an increase in the apparent viscosity. As the torque was increased the flocs were breaking down slowly until a smaller stable size was attained. The general behavior of a flocculated suspension was of the Ostwald-Philippoff type which consists of three regions: two Newtonian regions joined by a non-Newtonian region. With fiber suspensions the first Newtonian region is usually indistinguishable experimentally because very low angular velocities are required. At a given concentration flocculation could increase the viscosity considerably, depending on the state of flocculation. For example, an effect as much as 60% was observed at concentration 0.1×10^{-2} for nylon fibers in glycerine-water.

SUSPENSION FLOW

Flow of fiber suspensions in a tube or pipe has been investigated by several workers, among whom Daily (XXVI-7) has presented some interesting data. Their work is briefly reviewed here.

The general behavior of fiber suspensions in pipe flow may be divided into three regimes: (1) Plug flow in which a cohesive fiber network moves as a whole at velocity U in the central part of the pipe, leaving a clear-water annulus next to the pipe wall. The flow is laminar in the annulus. An increase of velocity reduces the annulus thickness. In this regime the pressure gradient is approximately proportional to $U^{1/4}$. (2) Mixed flow in which the laminar flow becomes unstable and fibers are entrained in the annulus layer. Further increase of velocity produces more mixing until the plug completely disintegrates. In this regime the pressure gradient becomes approximately proportional to $U^{1.65}$. (3) Turbulent flow which manifests a lower friction than that of pure water at the same velocity. In this regime, the pressure gradient is approximately proportional to U^2.

It is a common practice to present pipe flow data in terms of friction factor and Reynolds number. Such a plot for nylon fibers is shown in Fig. XXVI-6, based on Daily's data. The major features of the flow have been outlined above. Further interpretation, however, is difficult not only because of the non-Newtonian behavior of the probably flocculated suspensions but also due to the lack of adequate understanding of turbulent flow in general. For instance, Daily (XXVI-8) later showed that suspensions of rigid spheres always resulted in higher friction losses than water, even in the turbulent regime.

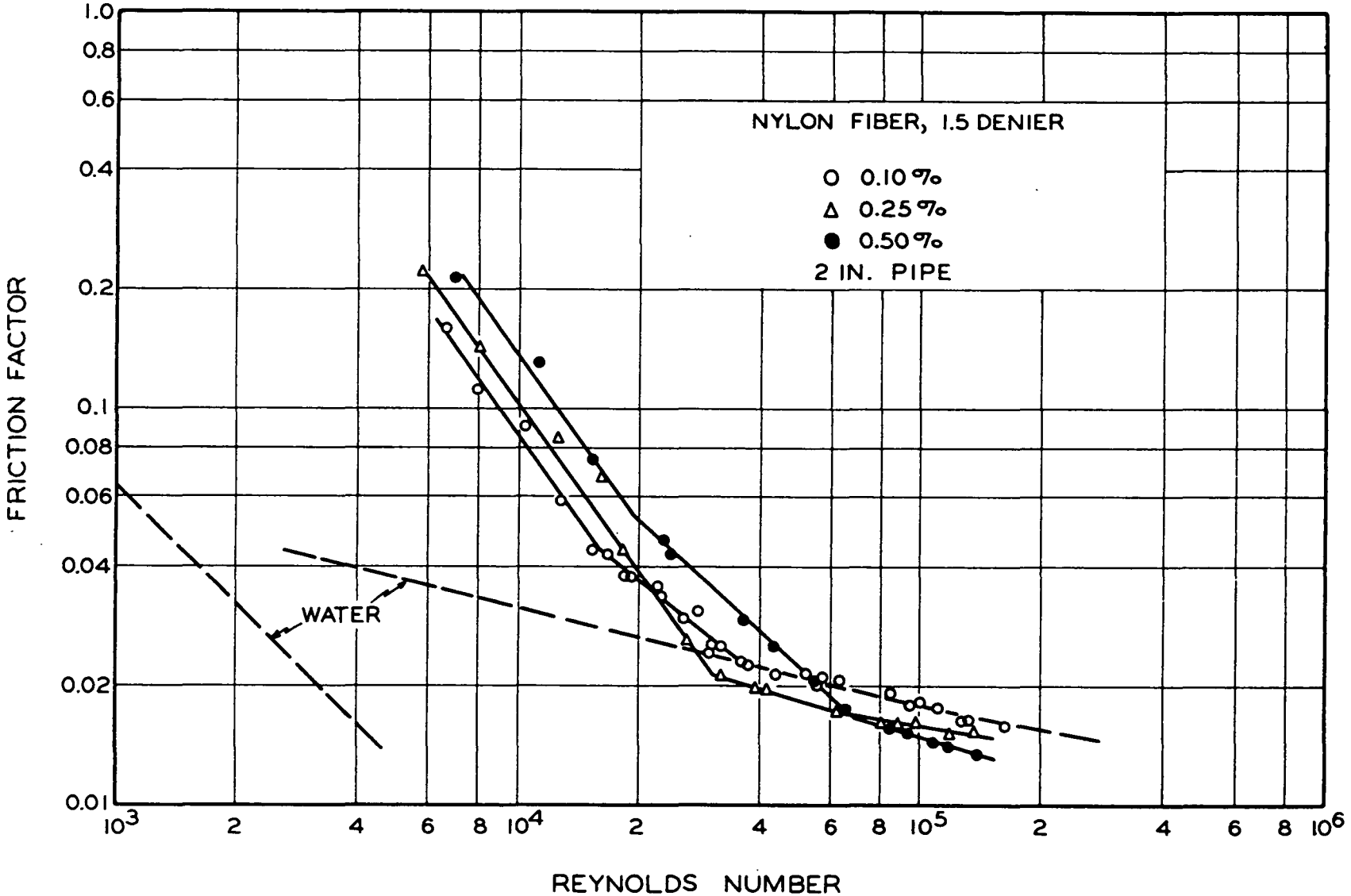

Figure XXVI-6. Correlation of Pipe Flow

"If blind faith in mathematical analysis is so apt to result in erroneous conclusions, one is inclined to repeat the question asked by engineers of past centuries: why waste time with theories when experimental evidence is invariably required? Those engineers themselves unwittingly provided the answer by accumulating field and laboratory data out of all proportion to the new knowledge thereby obtained."

(Rouse, Hunter, Ed. Advanced mechanics of fluids. Chap. I. p. 3. New York, John Wiley & Sons, Inc., 1959.)

PART THREE

APPLICATIONS AND APPROXIMATIONS

XXVII. DYNAMIC DRAINAGE IN PRESSURE-SUCTION FORMERS

Applications of the filtration theory to continuous formers have demonstrated its usefulness and clarified some misconceptions concerning their operations. The pressure-suction formers are more amenable to analysis than others, and will therefore be discussed first. They are usually classified into three types: rotary, horizontal, and inclined. The general features of their operation, however, are very similar.

ROTARY FORMERS

The drainage experiments with a rotary former reported by Han (III-12) were most detailed at that time. The forming unit was essentially a suction roll with a short roof over the forming area (Fig. XXVII-1). The centrifugally cast bronze roll was 10 in. in diameter with drilled and countersunk holes in its shell. Inside the roll was fitted with a suction box covering an effective forming area 6 in. on the circumference and 2 in. wide in the cross direction. The suction box was provided with a movable partition to divide drainage into two parts for the purpose of incremental flow measurements. The Plexiglas roof was molded to a parabolic curve in conformance with the simple filtration theory (Chapter IX). Six pressure taps were located along the roof and connected to individual manometers through an air purge system. The roll was covered with a 20 x 20-mesh backing wire and an 80 x 57-mesh facing wire. Air nozzles were used for removing the wet web and water showers for cleaning the wires and filling the drainage holes. A flow diagram of the complete apparatus is shown in Fig. XXVII-2. In making a run the roll was set at a desired speed and a supply of fresh water to the system was initiated. The heavy stock was then delivered to the suction line of the fan pump, through which the diluted stock was sent to the forming section. Vacuum and water

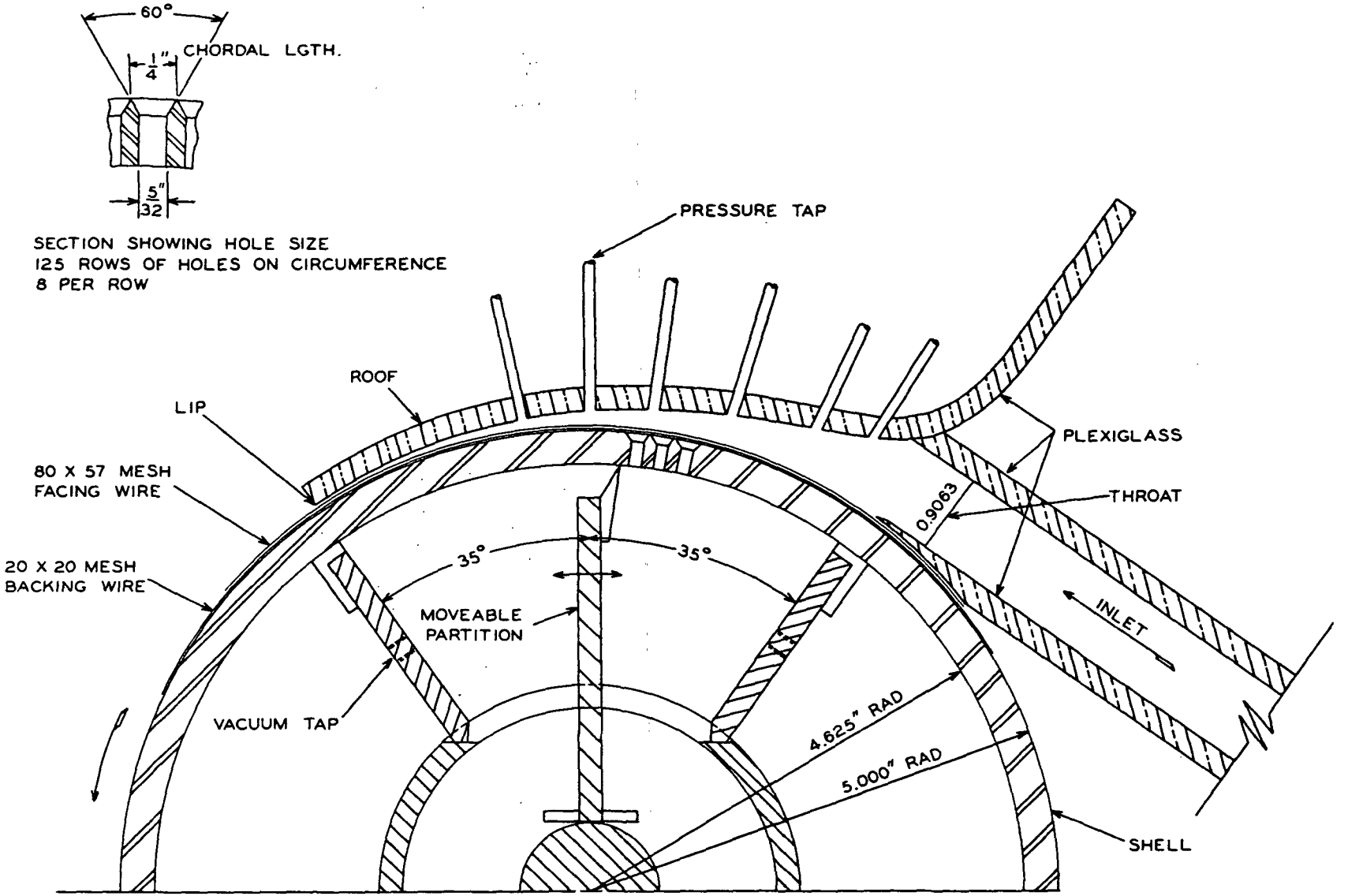

Figure XXVII-1. Suction Forming Unit

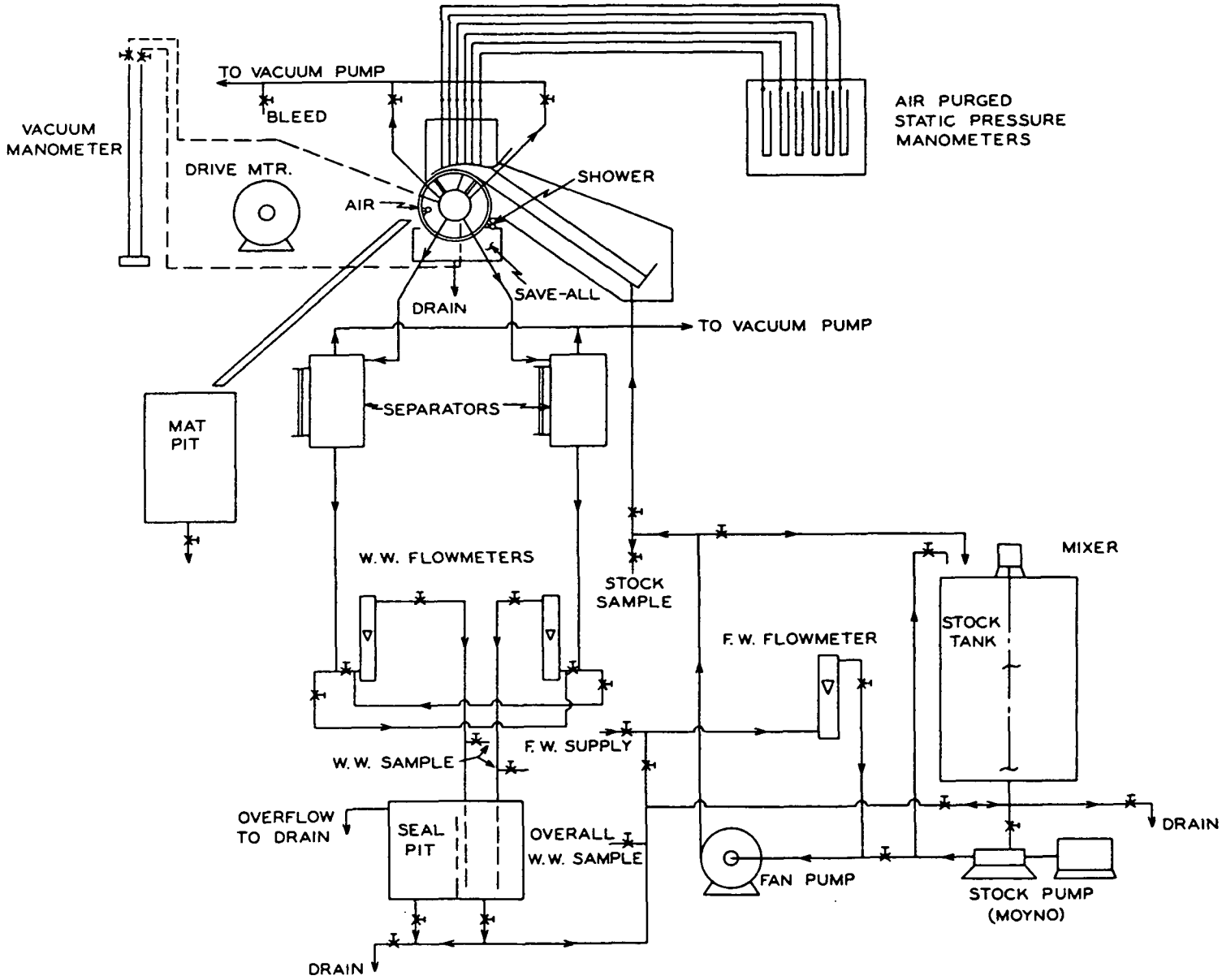

Figure XXVII-2. Flow Diagram for Suction Former

flow were adjusted until the roof was completely filled, with a very small amount of the free slurry emerging with the web from the lip of the roof. The white water was drained to the saveall and discarded. When the over-all operation reached a steady state, various measurements and samples were taken at each partition setting in the vacuum box until the entire forming zone had been scanned. A sulfite pulp refined to a Canadian standard freeness of 600 was used as the original stock. The results of one complete run are summarized in Table XXVII-1.

In the table the pressure drop was obtained from the measured values of hydrostatic head and suction. The total Bernoulli head (gravity, velocity, and static) along the roof was found to be nearly constant. The drainage velocity $\underline{U}_0$ was determined graphically from the slope of the drainage curve ($\underline{q}_0$ vs. $\underline{x}$). The local white water consistency was calculated from the relationship:

$$s_0 = \bar{s} + q_0(d\bar{s}/dq_0) \qquad \text{(XXVII-1)}.$$

The basis weight was then derived by integrating the fiber balance:

$$U_w dW = \frac{\rho(s - s_0)}{1 - s\bar{m}}\, dq_0 \qquad \text{(XXVII-2)},$$

where the web moisture $\underline{\bar{m}}$ was determined from a wet mat density test. Finally, the total drainage resistance was evaluated from the simplified Darcy's law:

$$U_0 = \frac{\Delta p_t}{\mu R_t} \qquad \text{(XXVII-3)}.$$

In the analysis of drainage the total resistance was plotted against the basis weight. The result showed an initial curved region, followed by a linear region. If the wire resistance was assumed to be constant, then the

TABLE XXVII-1

DRAINAGE RESULTS

Forming length (L_w) = 15.6 cm., forming width = 5.08 cm.
Wire speed (U_w) = 45.5 cm./sec.
Inlet consistency (s) = 0.0062 g./g., viscosity (μ) = 0.012 g./(sec.)(cm.), density (ρ) = 1.0 g./cc.
Web moisture ($\bar{m}$) = 30 g./g.

Forming length, x, cm.	0	0.5	1	2	4	6	8	10	12	15.6
Roof height, H, cm.	2.3	1.95	1.68	1.29	0.85	0.58	0.41	0.32	0.25	0.15
Pressure drop, $\Delta p_t/\rho g$, cm. H_2O	17.1	16.9	16.6	15.9	14.3	12.7	11.3	10.3	10.3	10.3
Drainage, q_0, cc./(sec.)(cm.)	0	2.16	3.15	4.13	5.51	6.40	7.18	7.78	8.36	9.25
U_0, cm./sec.	98	25	14.5	9.5	6.1	4.7	3.6	3.0	2.7	-
White water consistency, g./g.										
$\bar{s}_0 \times 10^4$	-	-	1.6	1.43	1.20	1.06	0.95	0.89	0.83	0.76
$s_0 \times 10^4$	2.7	1.4	1.0	0.75	0.45	0.32	0.24	0.20	0.16	0.13
Basis weight, $W \times 10^3$, g./sq. cm.	0	1.2	1.8	2.4	3.3	3.9	4.4	4.7	5.2	5.6
Resistance, $R_t \times 10^{-5}$, 1/cm.	0.14	0.55	0.93	1.3	1.9	2.2	2.5	2.8	3.1	-

derivative of the total resistance with respect to the basis weight would be the average specific filtration resistance $\bar{R}$. The value so obtained in the linear region was 0.68×10^8 cm./g. at the pressure drop 10 cm. water, as compared with 0.65×10^8 determined by a constant-rate filtration test on a sample of the exit web. The curved region could be correlated by a quadratic equation:

$$R_t = R_w + \bar{R}_i W + \frac{\bar{R}_f - \bar{R}_i}{2W_f} W^2 \qquad \text{(XXVII-4)}$$

where R_w is the wire resistance, $\bar{R}_i$ the initial web resistance, and $\bar{R}_f$ the final web resistance at W_f. R_w may be estimated from the screen resistance data (Chapter XVIII). $\bar{R}_i$ and $\bar{R}_f$ may be measured by filtration tests. With an existing former the couch sample will yield $\bar{R}_f$ directly. If the fines are then removed from the couch sample by classification and another filtration test is made on the classified sample the result will be close to $\bar{R}_i$.

With these approximations the drainage equation for a thin web may be written as

$$\frac{L_w \rho (s - \bar{s}_0) \overline{\Delta p}_t}{U_w \mu (1 - s\bar{m})} = \left(2R_w + \frac{2\bar{R}_i + \bar{R}_f}{3} W_f\right) \frac{W_f}{2} \qquad \text{(XXVII-5)}$$

For high basis weights R_w may be neglected and both $\bar{R}_i$ and $\bar{R}_f$ assumed to be constant at $\bar{R}$. Equation (XXVII-5) then reduces to Equation (IX-47), in which t is the forming time and equal to L_w/U_w.

In operating a suction former it is desirable to match the stock and wire velocities for the purpose of minimizing the shearing action between the free slurry and the formed web. The clearance of the roof, which determines the average velocity of the free slurry, is consequently a function of the drainage. The

throat or slice opening at the inlet of the roof is fixed by the desired basis weight at a given stock consistency:

$$H_o = \frac{q_o}{U_w} \cong \frac{W_f(1 - s\bar{m})}{\rho(s - \bar{s}_o)} \qquad \text{(XXVII-6)} ,$$

where q_o is the volumetric flow rate of the inlet stock per unit width. The roof curve may be related to the drainage by

$$\frac{H}{H_o} = 1 - \frac{q_0}{q_o} \qquad \text{(XXVII-7)} .$$

Three runs were carried out in which the web from the preceding one was redispersed and used as the stock for the next. This series of experiments was designed to ascertain the effect of fiber loss on drainage pattern. Neglecting the initial drainage, the results could be correlated by a power function:

$$\left(\frac{q_0}{q_{0,f}}\right)^n = \frac{x}{L_w} \qquad \text{(XXVII-8)} .$$

The value of n increases with increasing fiber loss as shown in Fig. XXVII-3. In the rare case of complete retention, the above equation becomes parabolic with $n = 2$, as indicated by Equation (IX-20). Taking the fiber loss into consideration, the roof contour may be approximated by

$$\frac{H}{H_o} \cong 1 - \left(\frac{x}{L_w}\right)^{1/n} \qquad \text{(XXVII-9)} .$$

For a more rigorous treatment, Equation (IX-45) based on the exponential nature of fiber loss should be used.

Very recently, Amneus (XXVII-1) extended the drainage analysis for rotary formers to the transition flow. He contended that the exponential concept of fiber

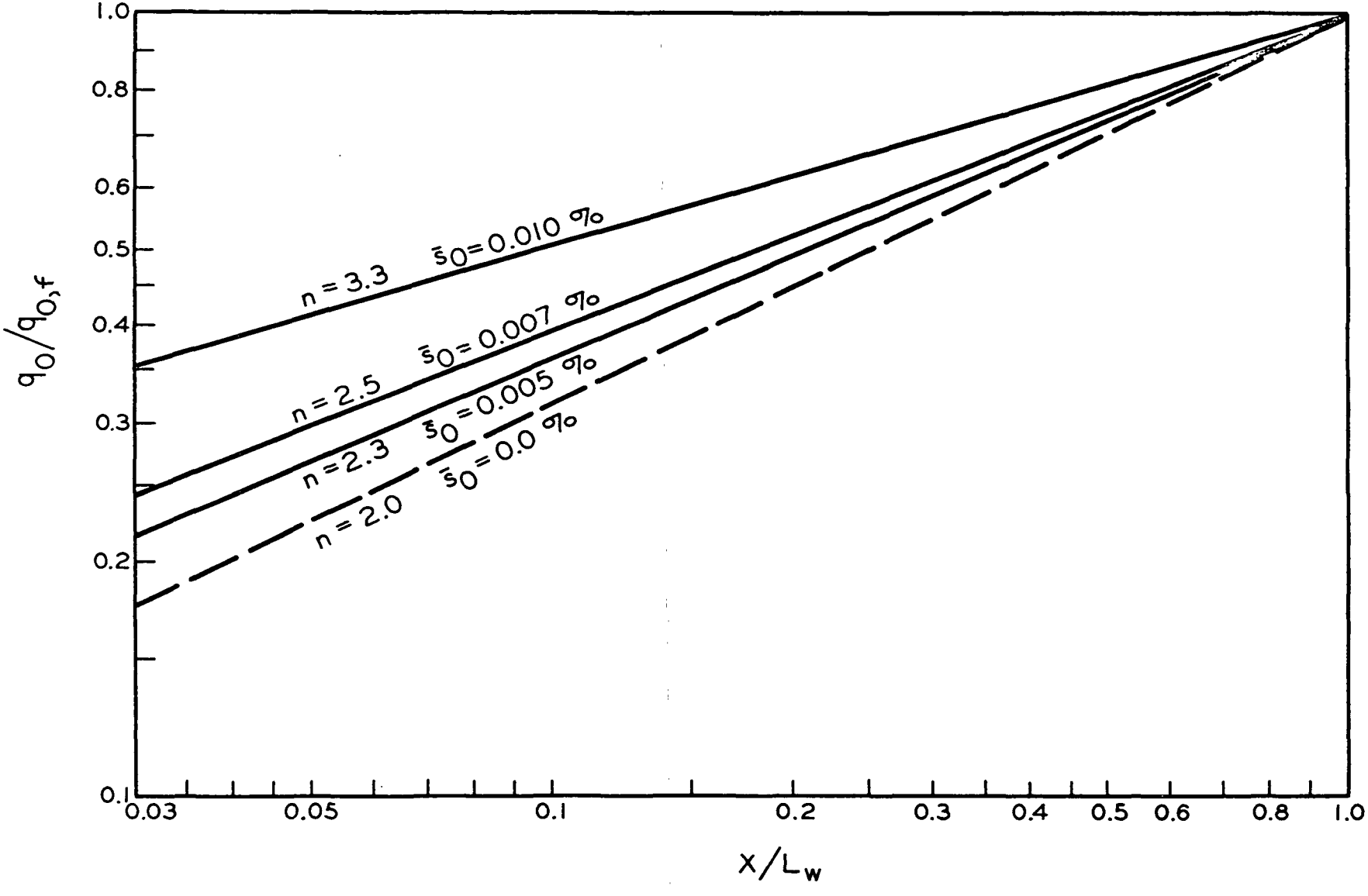

Figure XXVII-3. Effect of Fiber Loss on Drainage

retention is similar to the "blocking" concept of cake filtration early suggested by Hermans and Bredeé (XXVII-2):

$$\frac{A_e}{A_{e,w}} = \exp(-K_e W) \qquad \text{(XXVII-10)} ,$$

where A_e is the effective flow area for drainage through the web-wire combination, $A_{e,w}$ that through the wire alone, and K_e is supposed to be a constant. He further assumed that the inertial term of the transition flow equation may be related to the effective flow area by

$$\Delta p_t = \frac{\beta' S_0 L}{\epsilon^3} \rho U_0^2 = \frac{\beta' \rho}{A_e} U_0^2 \qquad \text{(XXVII-11)} .$$

Combining the two equations at constant drainage the result is

$$\frac{\Delta p_t}{\Delta p_w} = \exp(K_e W) \qquad \text{(XXVII-12)} ,$$

in which Δp_t is the pressure drop across the web-wire combination and Δp_w that across the bare wire. It is implied that β' is the same for wire and web. K_e may be evaluated experimentally. When complete fiber retention is reached, the pressure drop becomes nearly a parabolic function of the basis weight ($\Delta p_t \propto W^{1.9}$) according to his results of a simple constant-rate drainage test.

With these approximations Amneus proceeded to design the roof contour for a specific furnish-wire combination, basis weight, and operating speed in a manner similar to that for the previous case. He showed good agreement in drainage measured on the pilot former so designed and by the drainage tester. A general agreement was also obtained from a production former.

HORIZONTAL FORMERS

The IPC web former designed by Heller (XXVII-3) consists of a horizontal wire supported by a flat suction box. A schematic diagram of the entire system is shown in Fig. XXVII-4, followed by two photographic views (Fig. XXVII-5 and XXVII-6).

The results of a comprehensive study with this former by Ingmanson and Chang (XXVII-4) are reviewed here. A classified sulfite pulp was used in these experiments with an 80 x 72-mesh semitwill wire. The resistance of the wire was determined by permeation. The compressibility constants were found to be 0.00286 for $\underline{M}$ and 0.346 for $\underline{N}$. The dependence of specific surface $\underline{S_w}$ and volume $\underline{v}$ on pressure was evaluated by the method outlined in Chapter XIX from filtration and dynamic drainage data. The mat moisture $\underline{\bar{m}}$ was determined from the average mat density at known pressure drops.

Two series of runs were made. Each series consisted of several runs at various constant pressure drops across the web. In each subseries the wire and slice velocities were kept constant while the white water consistency in the wire pit was varied. The wire velocity ranged from 5 to 22 cm./sec., the basis weight from 11 to 220 g./sq. m., the total pressure drop from 10 to 70 cm. of water, and the inlet consistency from 0.04 to 0.5%.

For the analysis of drainage data, the construction of a correction diagram was helpful. Assuming a pressure drop across the bare wire, the corresponding filtrate velocity was obtained from the wire resistance data. The pressure drop across the web was taken to be the difference between the measured over-all value and the assumed wire value. The basis weight was calculated from the flow expression (IX-23), and the filtrate volume by the fiber balance (IX-36).

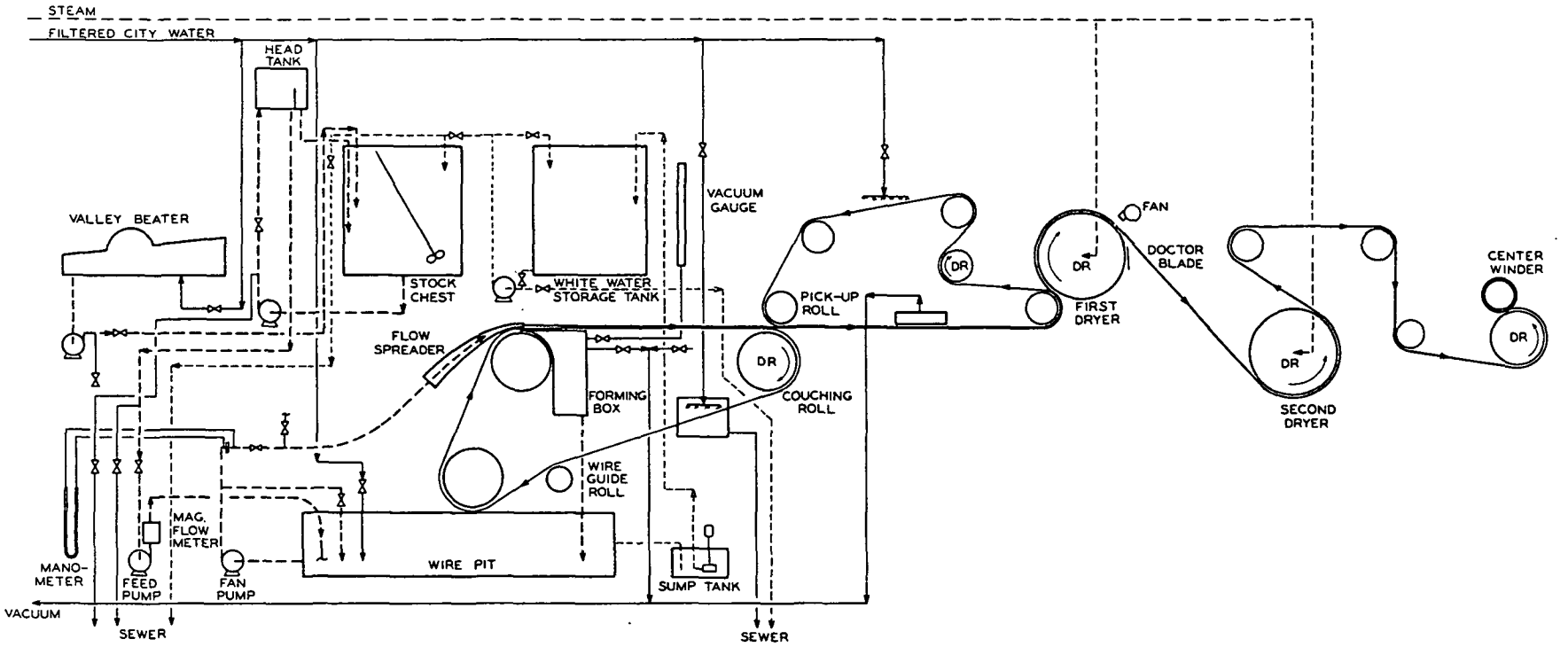

Figure XXVII-4. IPC Web Former

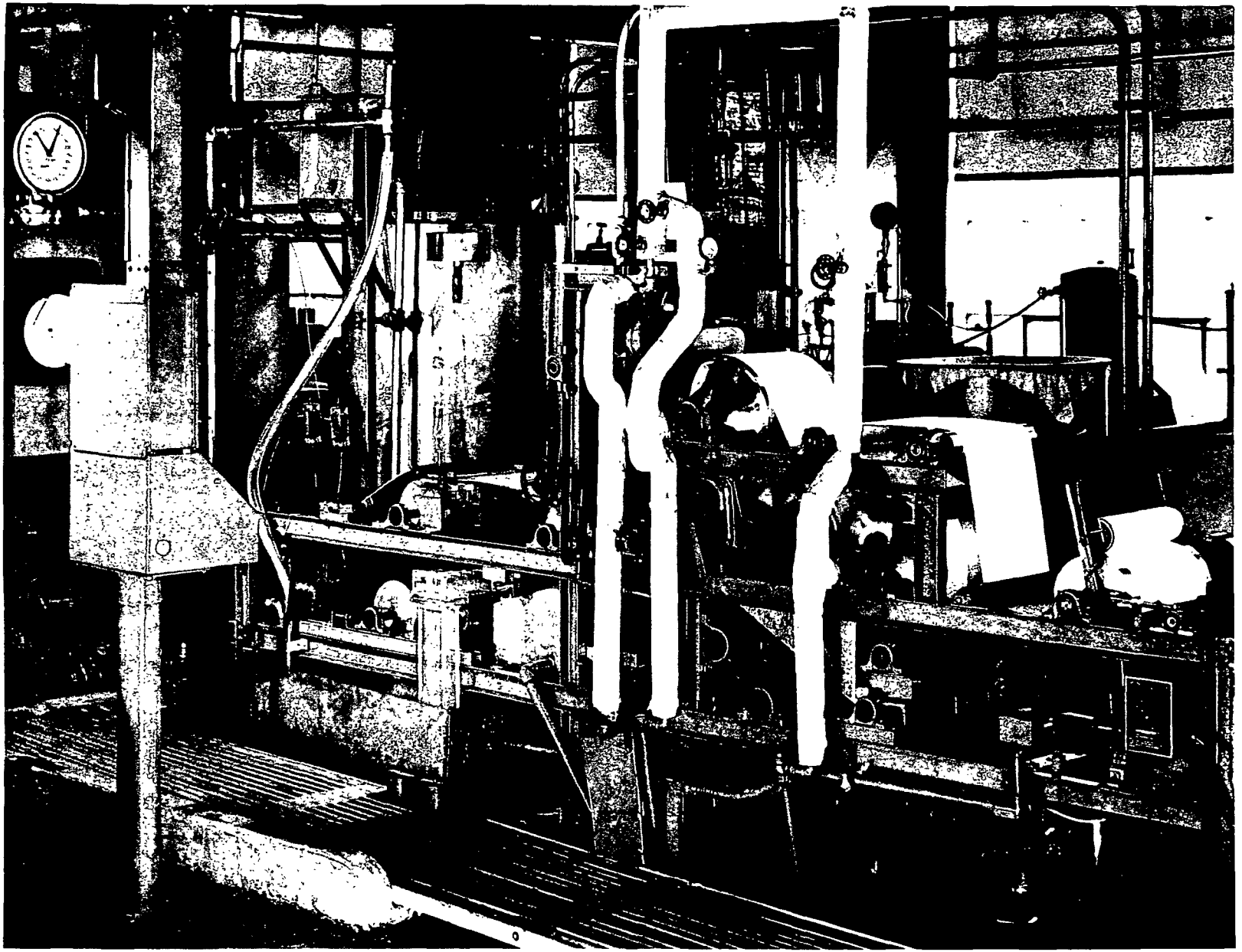

Figure XXVII-5. Front View of IPC Web Former

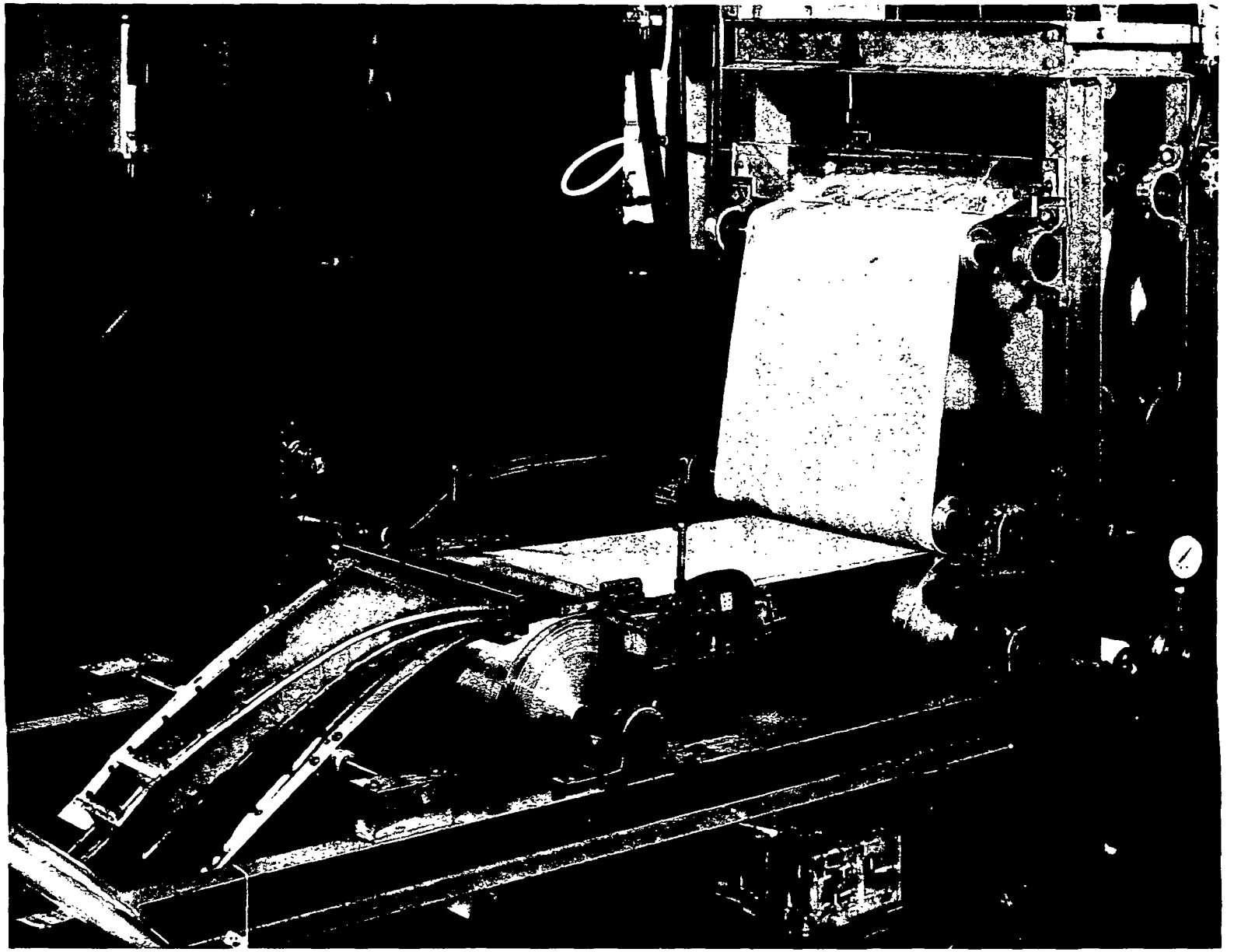

Figure XXVII-6. Web Forming Section

A filtration curve, (dt/dV_0) vs. V_0, was plotted and the area under the curve yielded the forming time if the filtration process was carried out batchwise. For a continuous former the forming length is simply the product of the wire speed and the forming time. Finally, correction for the effects of high consistency on drainage rate and fiber balance were incorporated by

$$\left[\Delta p_t - \Delta p_w\right] = \left[\bar{R}\mu U_0 J_u + \bar{R}'\rho U_0^2 J_u^2\right]\left[\frac{\rho(s - \bar{s}_0)}{1 - s\bar{m}} V_0 J_m\right] \qquad \text{(XXVII-13)} .$$

The correction factors J_u and J_m were derived from the previous graphical analysis of high-consistency filtrations (Chapter XXII). Their definitions are

$$J_u = \bar{U}_r/U_0 \cong \frac{W_e}{W} \qquad \text{(XXVII-14)}$$

and

$$J_m = \frac{1 - s\bar{m}_e}{1 - s\bar{m}} \qquad \text{(XXVII-15)} .$$

In both definitions the subscript e refers to equilibrium filtration at very low consistencies. It is to be noted from Fig. XXII-3 that the mat moisture lines are not exactly parallel, and consequently J_m is slightly pressure dependent. The deviation, however, is not large, the maximum being 6% at 1% consistency. The correction diagram so constructed is illustrated in Fig. XXVII-7.

The corrected results reveal the relative importance of wire, viscous, and inertial resistances in sheet forming. (The effect of fiber-wire interaction on drainage in these experiments was found to be negligible.) As an example, the pressure drops due to wire (Δp_w), viscous (Δp_v) and inertial (Δp_i) resistances as a function of the basis weight are depicted in Fig. XXVII-8. Based on this

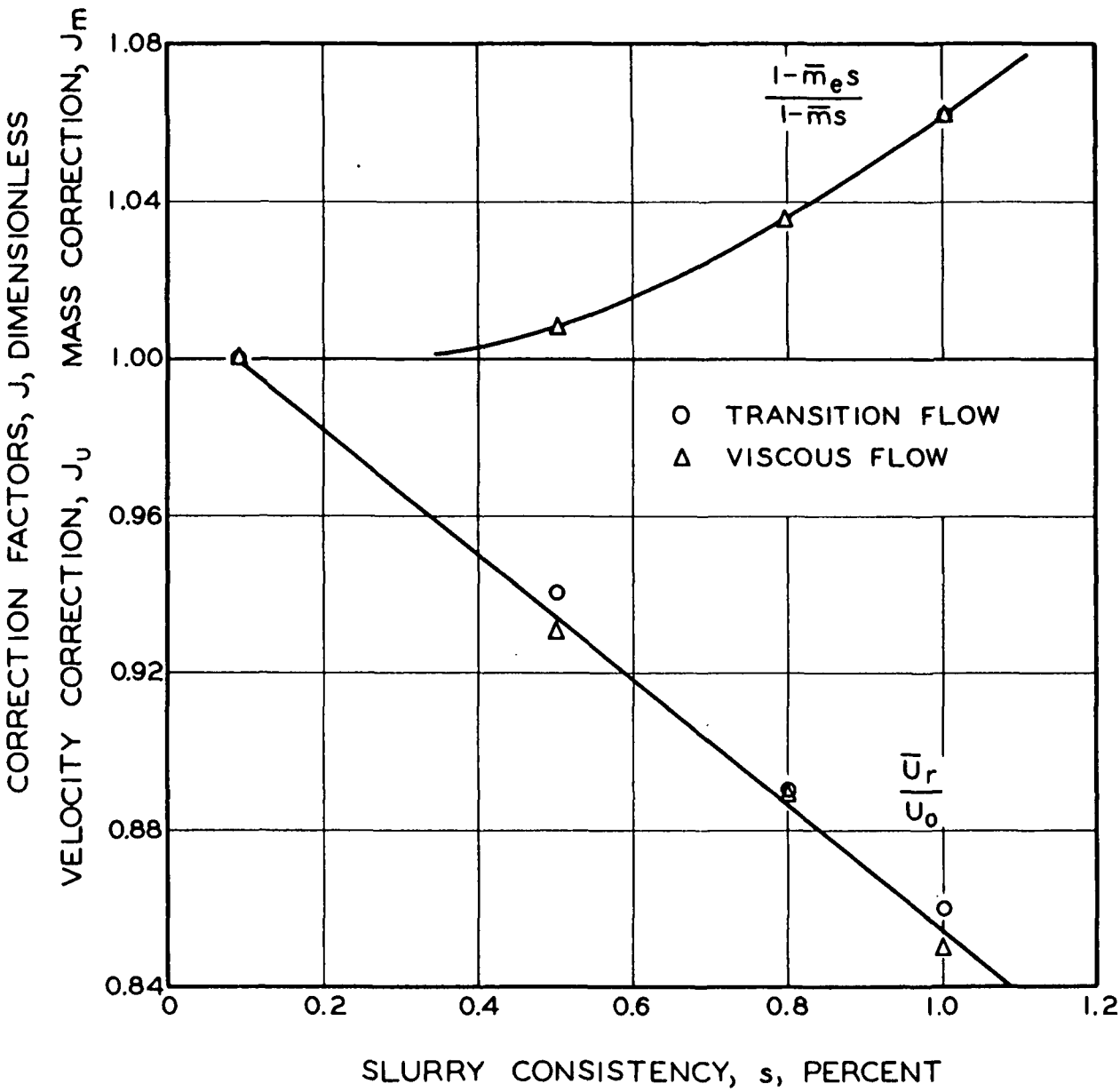

Figure XXVII-7. Correction Diagram

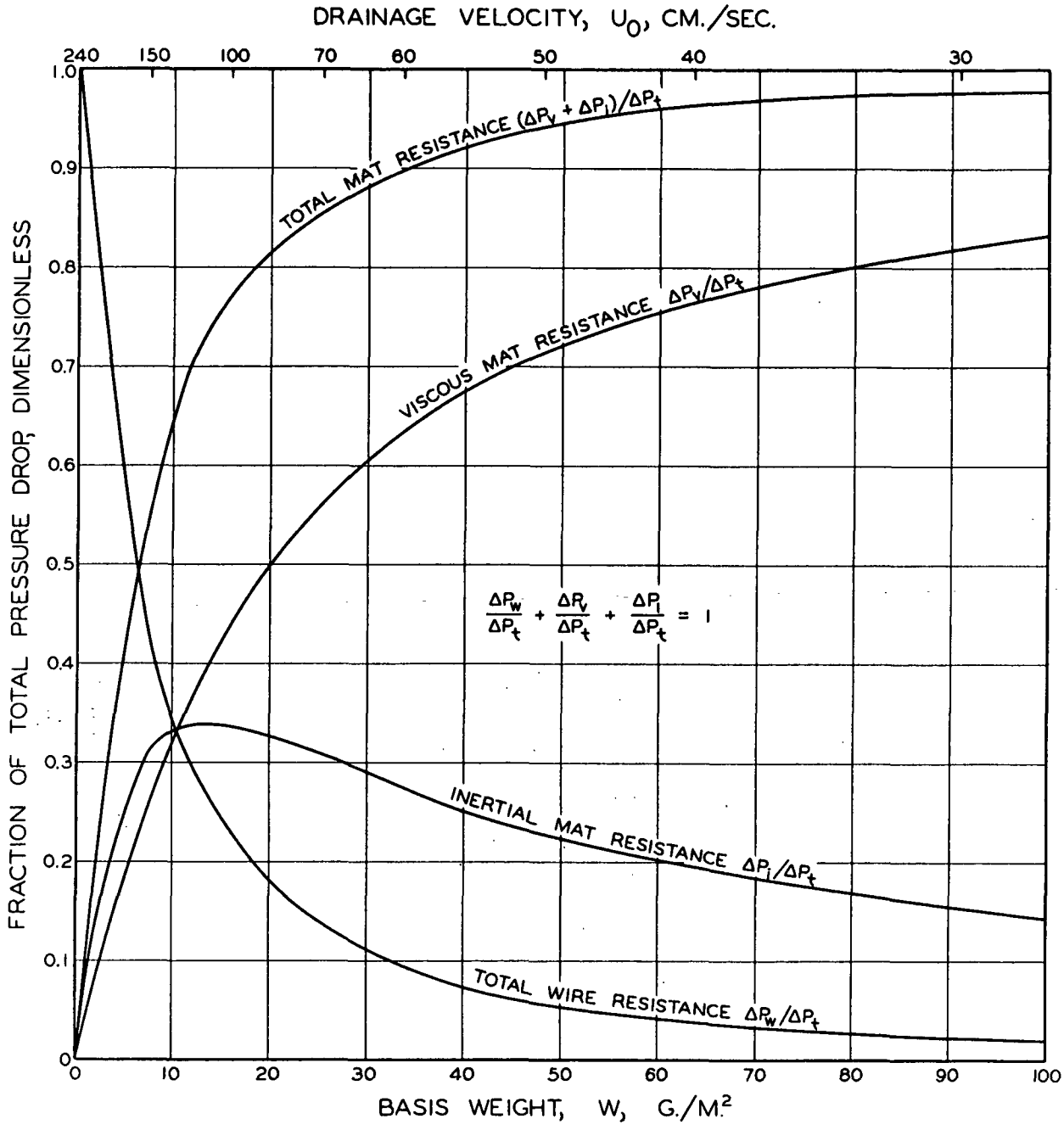

Figure XXVII-8. Distribution of Resistances

diagram the analysis of Han for viscous resistance $\bar{R}$ at high basis weights is justifiable, while Amneus' analysis of rapid drainage, assumed to be in inertial and wire resistances only, appears to be fortuitous because at very low basis weights the omission of viscous resistance was possibly compensated by that due to fiber-wire interaction.

The forming length measured at the IPC web former in Ingmanson and Chang's experiments ranged from 0.4 to 4 cm. The deviations from the predicted values were almost always negative (actual length shorter than calculated length), the largest discrepancy occurring at very short forming lengths which were especially difficult to measure precisely. The average of 29 runs was -24%. The majority of runs was within -20%.

Treating web forming as a constant-pressure process, they further analyzed the drainage data in accordance with Equation (IX-32). The pressure drop across a thick web was determined from Fig. XXVII-8, and the values of $\underline{W}^*$ and $\underline{K}^*$ were then calculated from the known system specifications. The calculated results are shown in Fig. XXVII-9 for two different run conditions. The actual two data points are also included for comparison. The agreement is satisfactory in view of the imprecise measurement of the forming time. It is interesting to note that the limiting slopes of these curves shift toward the lower time scale as the value of the filtration parameter $\underline{K}^*$ decreases.

Some of the web formation showed apparent flocculation. A crude test was initiated to ascertain its effect on drainage. About a hundred samples of ca. 0.5 cm. were punched out of a sheet. Of these samples, half were from the thick spots and half from the thin spots. By measuring the basis weight and area of each sample, calculating the weighted average flow for the flocculated sheet, and comparing the result with the actual drainage, the discrepancy was found to be

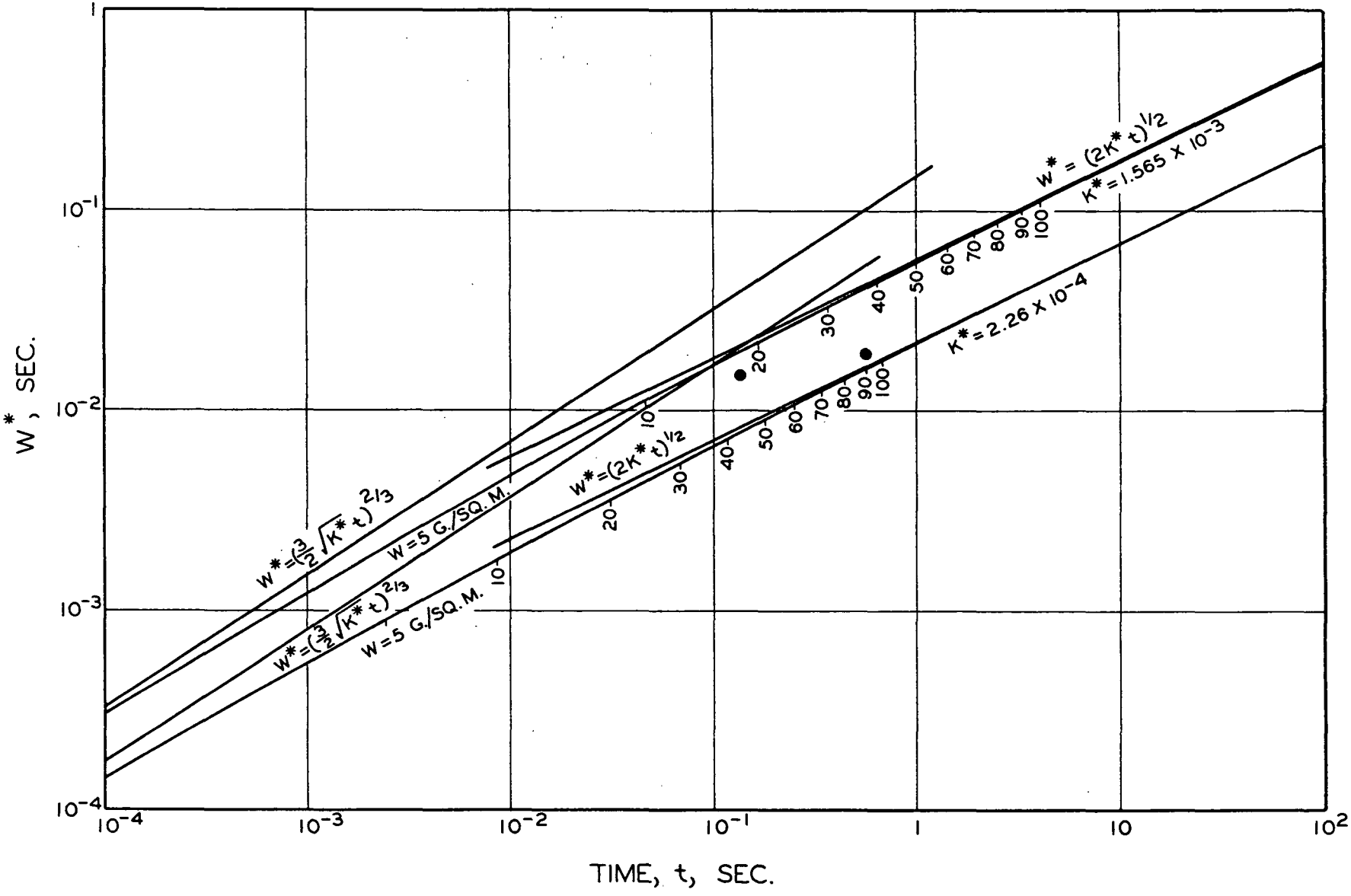
1
10^{-1}
10^{-2}
10^{-3}
10^{-4}
W^*, SEC.
10^{-4}
10^{-3}
10^{-2}
10^{-1}
1
10
10^2
TIME, t, SEC.
$W^* = (2K^* t)^{1/2}$
$K^* = 1.565 \times 10^{-3}$
$K^* = 2.26 \times 10^{-4}$
$W^* = (\frac{3}{2}\sqrt{K^* t})^{2/3}$
W = 5 G./SQ. M.
$W^* = (\frac{3}{2}\sqrt{K^* t})^{2/3}$
W = 5 G./SQ. M.
$W^* = (2K^* t)^{1/2}$
10
20
30
40
50
60
70
80
90
100

only about 4%. Thus, it appears that flocculation had only a very minor effect on drainage under the experimental conditions. Improved formation was achieved by adding 0.5% locust bean gum, based on the dry fiber weight, to the same stock which had shown flocculation.

Another interesting series of experiments was made with regard to fiber orientations. In these runs dyed dacron fibers were introduced to the stock. The samples were examined microscopically, and the fiber orientation results are illustrated in Fig. XXVII-10, which consists of four runs under different forming conditions. The tensile strength of these samples was also measured in both machine and cross directions. The results are summarized in Table XXVII-2.

TABLE XXVII-2

FIBER ORIENTATION AND TENSILE RATIO

Curve in Fig. XXVII-10	Tensile, lb./in.			Orientation Parameters			Zero-span Tensile,[a] lb./in.		
	M.D.	C.D.	M.D./C.D.	α	β	β/α	M.D.	C.D.	M.D./C.D.
1	11.4	19.8	0.58	0.307	0.037	0.120	39.2	36.5	1.08
2	46.0	30.6	1.50	0.290	0.090	0.309	37.8	31.8	1.19
3	2.9	2.6	1.12	0.363	0.142	-0.390	33.7	44.8	0.75
4	5.0	5.9	0.85	0.271	0.151	0.556	35.9	26.8	1.35

[a] Corrected to 45 lb./(25 x 40 in.-500).

There is no apparent correlation between fiber orientation and sheet tensile, contrary to the common belief. Zero-span tensile, however, is related to fiber orientations, and consequently a better indication of sheet "squareness." According to Van den Akker (XXVII-5), the angular distribution function may be expressed by

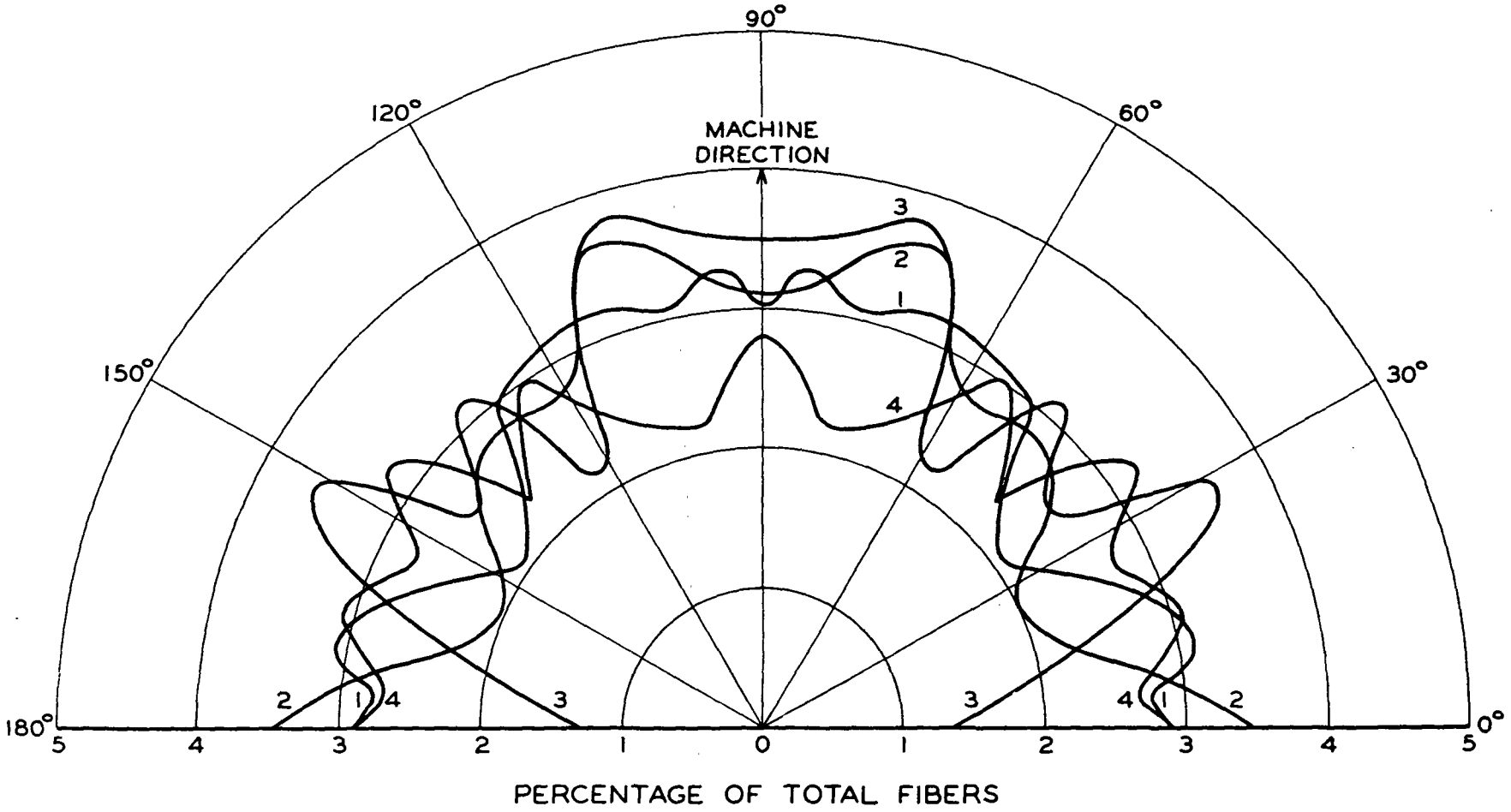

Figure XXVII-10. Fiber Orientation Diagram

$$P(\theta) = \alpha + \beta \sin^6\theta \qquad \text{(XXVII-16)},$$

where θ is the fiber angle with respect to the cross direction, and α and β are two orientation parameters. The values of α and β are evaluated, respectively, from the zero-span tensile ratio (M.D./C.D.), R_θ, by

$$\alpha = \frac{21 - R_\theta}{\pi(9R_\theta + 11)} \qquad \text{(XXVII-17)}$$

and

$$\beta = \frac{32(R_\theta - 1)}{\pi(9R_\theta + 11)} \qquad \text{(XXVII-18)}.$$

The ratio β/α may be used as an indication of "squareness." If this ratio is positive, the sheet has a preferred orientation in the machine direction; if negative, orientation is toward the cross direction. A square sheet would have a zero value of β/α. The results of calculations appear to be in general agreement with the shapes of the curves as numbered.

For a very free but easily flocculated stock such as one of synthetic fibers with large axis ratios, very low consistencies are often necessary to achieve satisfactory formation. In such cases the slice opening necessary to match the stock and wire velocities would be impractical on a horizontal wire. For example, if the stock consistency is given at 0.05% and the basis weight is desired at 120 g./sq. m., the slice opening has to be 24 cm. With narrower openings, the higher slice jet velocity would tend to shear the weak web on the slower wire, resulting in stock rolling and poor formation. One solution for these extreme cases is to use an inclined wire at very low speeds. The high-velocity jet would impinge the wire at an angle and thus reduce the severity of disturbances. Since

shear is dependent on velocity difference, rather than velocity ratio, the inclined wire device would have the same difficulty at high speeds.

The specific filtration resistance of synthetic fibers (nylon and orlon) is of the order of 10^6 cm./g., as compared with 10^8-10^9 for wood fibers. Since they are also less compressible, the increase in resistance is only 20-30% with a tenfold increase in pressure drop. At such low resistances, gravity drainage on an inclined wire under a deep pond is feasible at very low speeds. The approximate drainage equation based on viscous flow is

$$\frac{sL_w^2 \rho g \sin\theta}{\mu U_w} = \bar{R}W^2 + R_w W \qquad \text{(XXVII-19)},$$

where θ is the angle of inclination of the wire to the horizontal plane. The following data from an experimental former may be used as an illustration (XXVII-5):

Fiber	1/4-in. orlon
s	0.0005 g./cc.
W	0.0122 g./sq. cm.
μ	0.013 g./(cm.)(sec.)
U_w	1.1 cm./sec.
θ	30°
$\bar{R}$	2×10^6 cm./g.
R_w	1×10^4 1/cm.

The forming length calculated from Equation (XXVII-19) is 5.7 cm., as compared with the actual length 5.1 cm.

In the 1950's both rotary and horizontal suction formers were experimented with in a comparatively crude manner. As far as drainage was concerned, the results always indicated higher rates than predicted by viscous flow at the same pressure drop. Some data (XXVII-6) in terms of filtration resistance are compiled in Table XXVII-3 to indicate the discrepancies.

TABLE XXVII-3

COMPARISON OF DRAINAGE

	C.S. Freeness	$\overline{\Delta p}$, cm. H_2O	$\overline{R} \times 10^{-8}$, cm./g. Machine	Lab.	Ratio
Rotary Former					
Book	300	62	6.3	11	0.58
Book	300	160	11	17	0.65
Book	295	105	7.4	13	0.57
Book	325	48	4.0	7.4	0.54
Book	360	125	9	12	0.75
Kraft	590	48	1.2	1.9	0.63
Tissue	640	17	0.51	8.1	0.63
Tissue	640	41	0.94	1.1	0.82
Horizontal Former					
News	160	7.3	3.2	6.3	0.52
News	160	15	5.3	8.1	0.65
News	180	15	5.2	7.5	0.69
				Av. ca.	0.65

With all the refinements described before in connection with the IPC web former, the improvement in drainage predictions appears to be only moderate. There remains an overprediction of forming time of about 20-25%. We believe this discrepancy to be largely due to the difference in compression conditions. In the laboratory filtration test the mat is subjected to a macroscopically uniform pressure drop over its entire area except around the circumference due to wall effects. On a former the web is exposed to continuously varying pressure drops in the machine direction. Thus, the individual fibers in the web are experiencing different degrees of compression at the same instant. As a result, the portion of the web at a higher pressure drop tends to transmit the compressive stresses to the adjacent portion at a lower pressure drop. In other words, the highly compacted fibers are supported by their less stressed neighboring fibers and so on. The net effect of this nonuniform compression would be a tendency for the web to be less compacted than under the laboratory uniform load condition.

The extent to which this nonuniform compression effect takes place will depend on the ability of the fibers to support one another, which is related to fiber orientation, interfiber friction, and basis weight. The maximum effect may be expected to be for long fibers, oriented only in the plane of the web, with high friction and large basis weight in a short forming zone, such as table roll nip. If this interpretation is correct, the drainage resistance would be smaller on a machine because of the more porous web structure.

XXVIII. THE PUZZLE OF FOURDRINIER DRAINAGE

The application of the table-roll suction theory to drainage on fourdriniers, as attempted by Ingmanson (XXVIII-1, XXVIII-2), showed very large deviations from laboratory filtration results. The filtration resistance on table rolls was found to be smaller than that determined from a laboratory test by an order of magnitude. This puzzle has remained unsolved to date.

DATA ANALYSIS

Two commercial machines, one making bond paper and another making board, were dealt with. The operating conditions are summarized in Table XXVIII-1.

TABLE XXVIII-1

OPERATING CONDITIONS OF TWO FOURDRINIERS

	Bond Machine	Board Machine
Furnish	50% cotton linters, 50% sulfite	50% kraft, 50% groundwood
Headbox consistency, %	0.555	1.21
White water consistency, %	0.119	0.112
Temperature, °F.	90	90
Wire mesh	70 x 56	60 x 38
Wire speed, ft./min.	343	243
No. and diam. of table rolls	39 (4-1/2 in.)	37 (6-3/8 in.)
Basis weight	15.7 lb./(17 x 22 in.-500)	130 lb./3000 sq. ft.

The measured drainage and white water consistency at the table rolls of the bond machine are shown in Fig. XXVIII-1 and XXVIII-2, respectively. The total resistance of the web-wire combination at each table roll was calculated from Taylor's formula (XV-13):

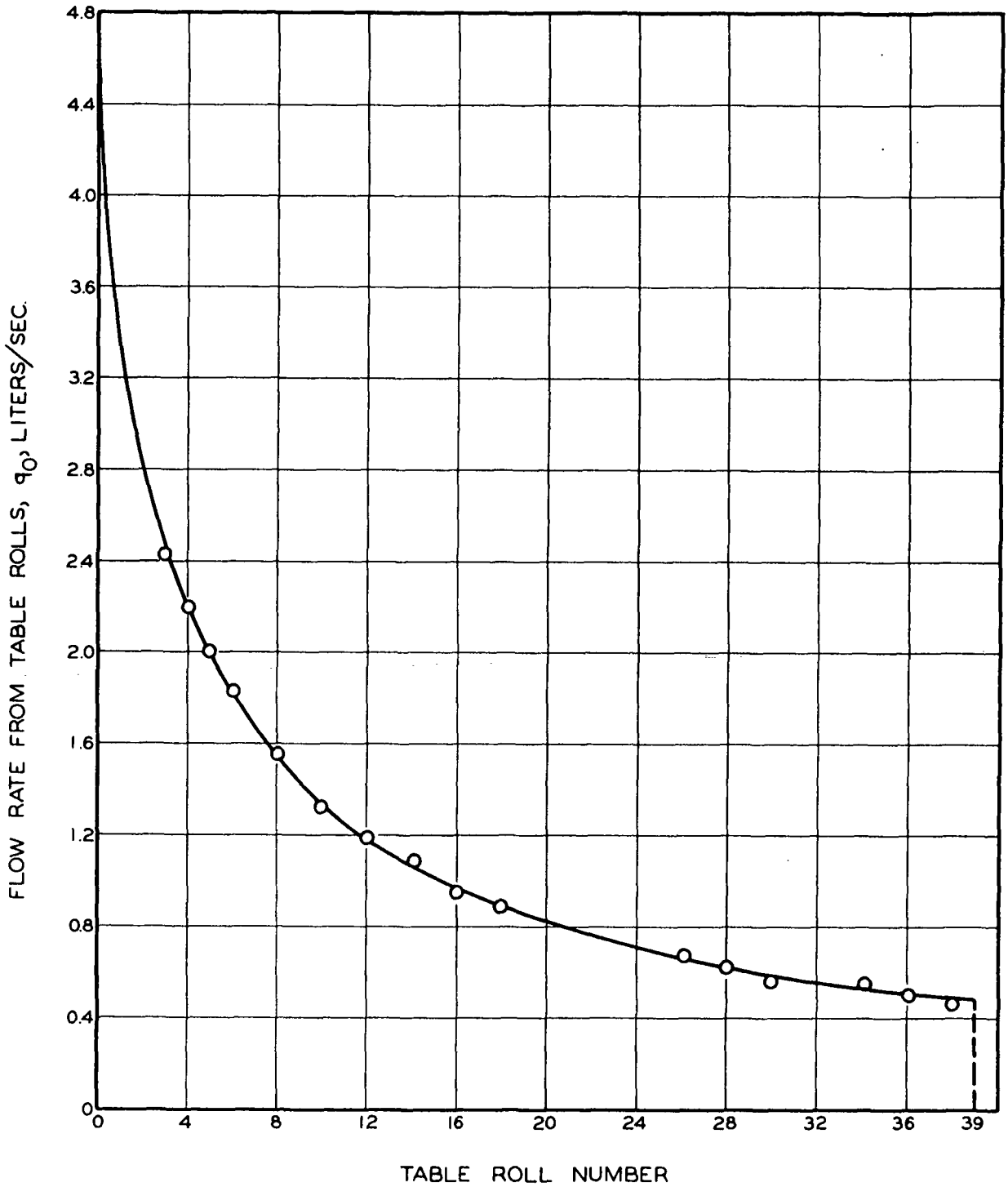

Figure XXVIII-1. Drainage on a Bond Machine

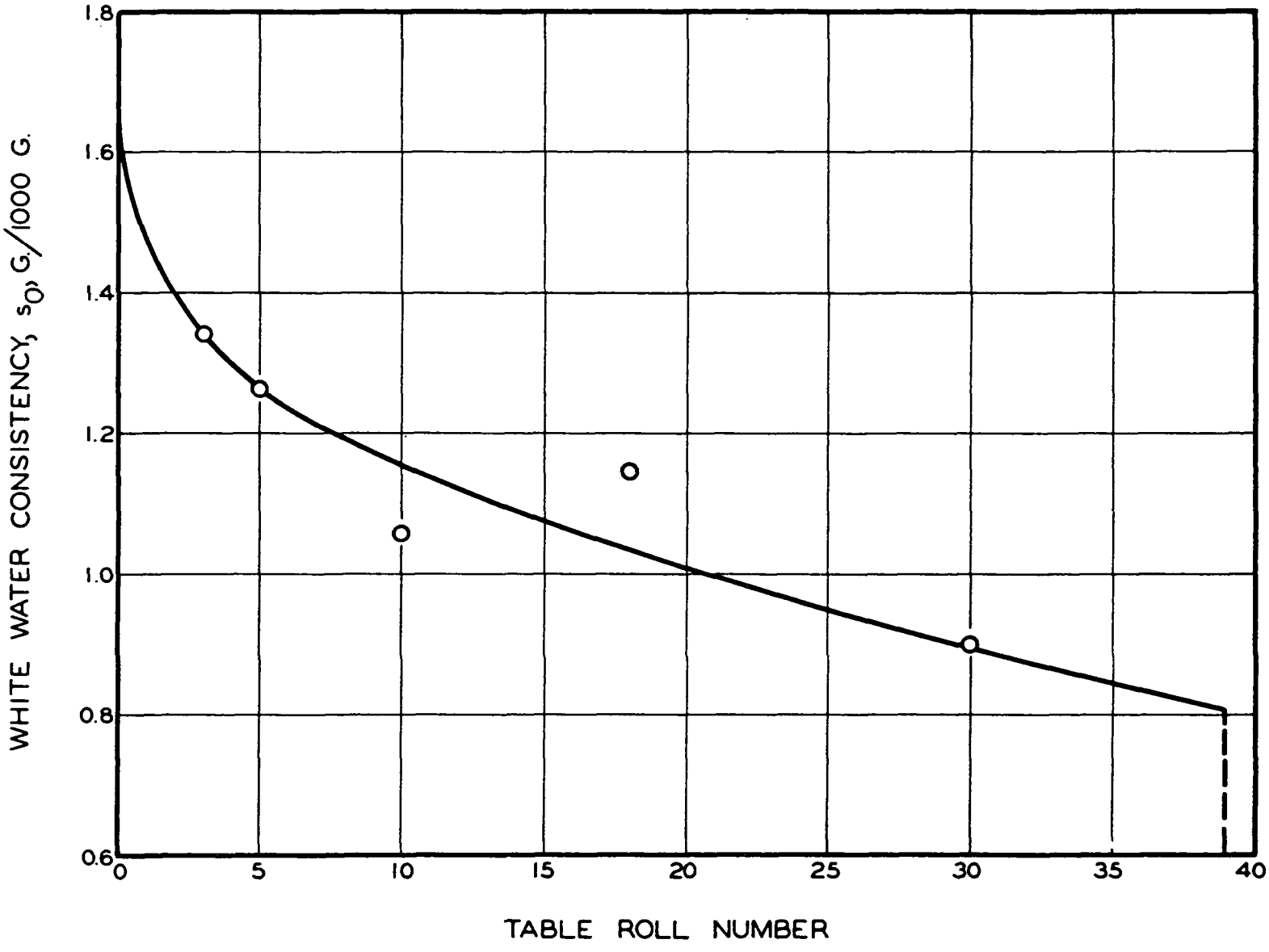

Figure XXVIII-2. White Water Consistency on a Bond Machine

$$R_t = \left[\frac{0.295 r_o \rho^2 U_w^3}{\mu^2 q_o}\right]^{1/2} = 6.75 \times 10^6 / q_o^{1/2} \qquad \text{(XXVIII-1)},$$

where $\underline{R_t}$ is in units of cm.$^{-1}$. The average basis weight increase was calculated from

$$\Delta \bar{W} = \left(\frac{s - \bar{s}_o}{1 - s\bar{m}}\right) \frac{\rho q_o}{U_w} \qquad \text{(XXVIII-2)}.$$

Using the value 77 for $\underline{\bar{m}}$ from trial and error, the values of $\underline{R_t}$ were calculated as a function of $\underline{\bar{W}_n}$. By assuming a constant wire resistance, the slope of the $\underline{R_t}$ vs. $\underline{\bar{W}_n}$ curve was taken to be the average specific filtration resistance which is shown in Fig. XXVIII-3. It is seen that $\underline{\bar{R}}$ increases linearly with the basis weight. This increase was attributed to the increasing retention of fines and filler in the web, as evidenced by the correlation in Fig. XXVIII-4.

The value of $\underline{\bar{R}}$ at the final basis weight was 0.5×10^8 cm./g. To check this value, a web sample was taken at the couch roll and measured for specific filtration resistances in a laboratory test. It was found that the machine value of $\underline{\bar{R}}$ corresponded to a pressure drop of 0.5 cm. of water based on the laboratory results. According to Taylor's theory, the maximum suction of this machine would be 15.4 cm. of water, and the pressure drop across the web would be about 10 cm. of water after deducting the wire resistance. The discrepancy in terms of pressure drop was alarmingly a factor of 20! Accepting the theoretical suction, the lowest value of $\underline{\bar{R}}$ would be about 5×10^{-8} by the laboratory test, which is ten times the machine figure.

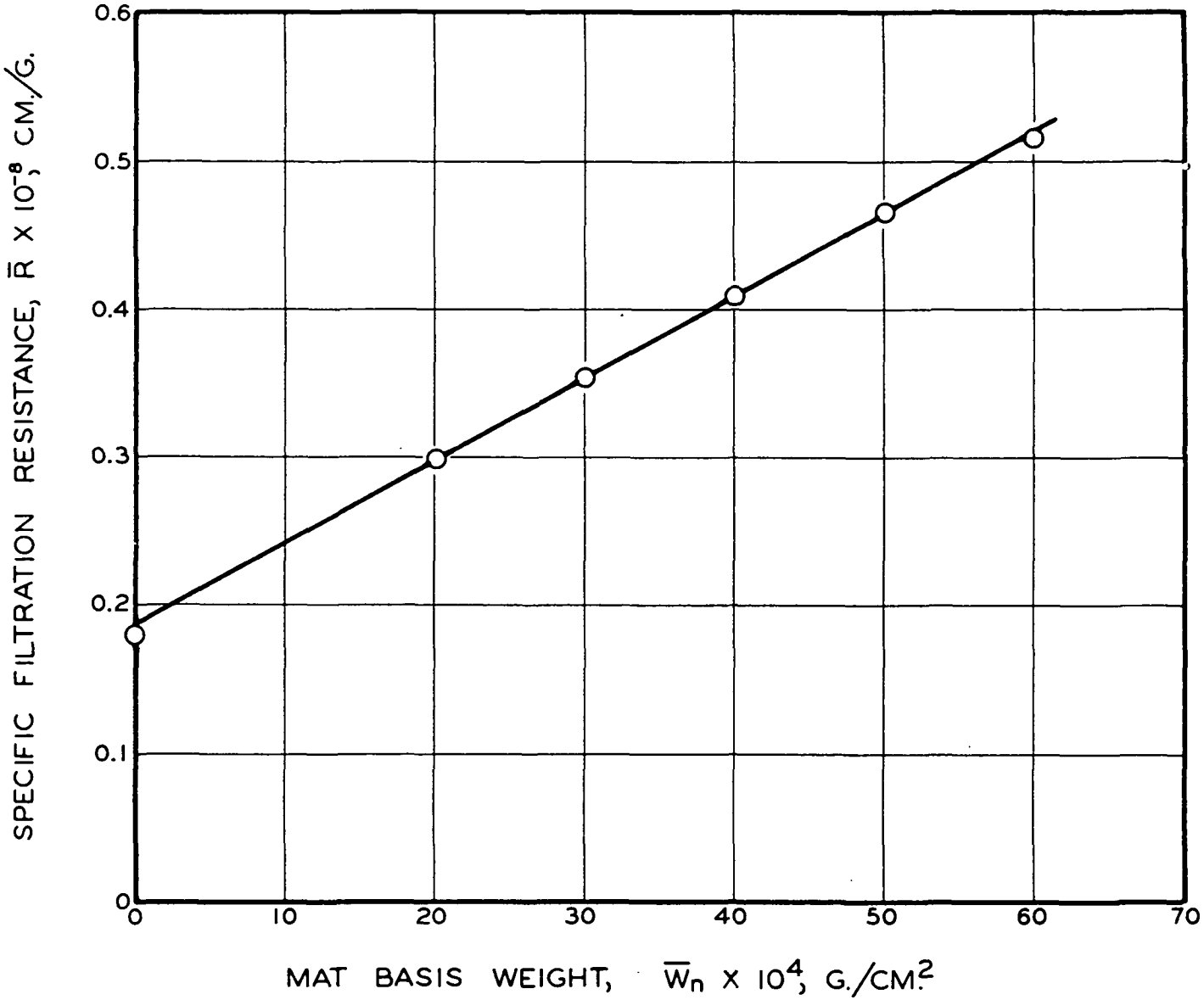

Figure XXVIII-3. Drainage Resistance on a Bond Machine

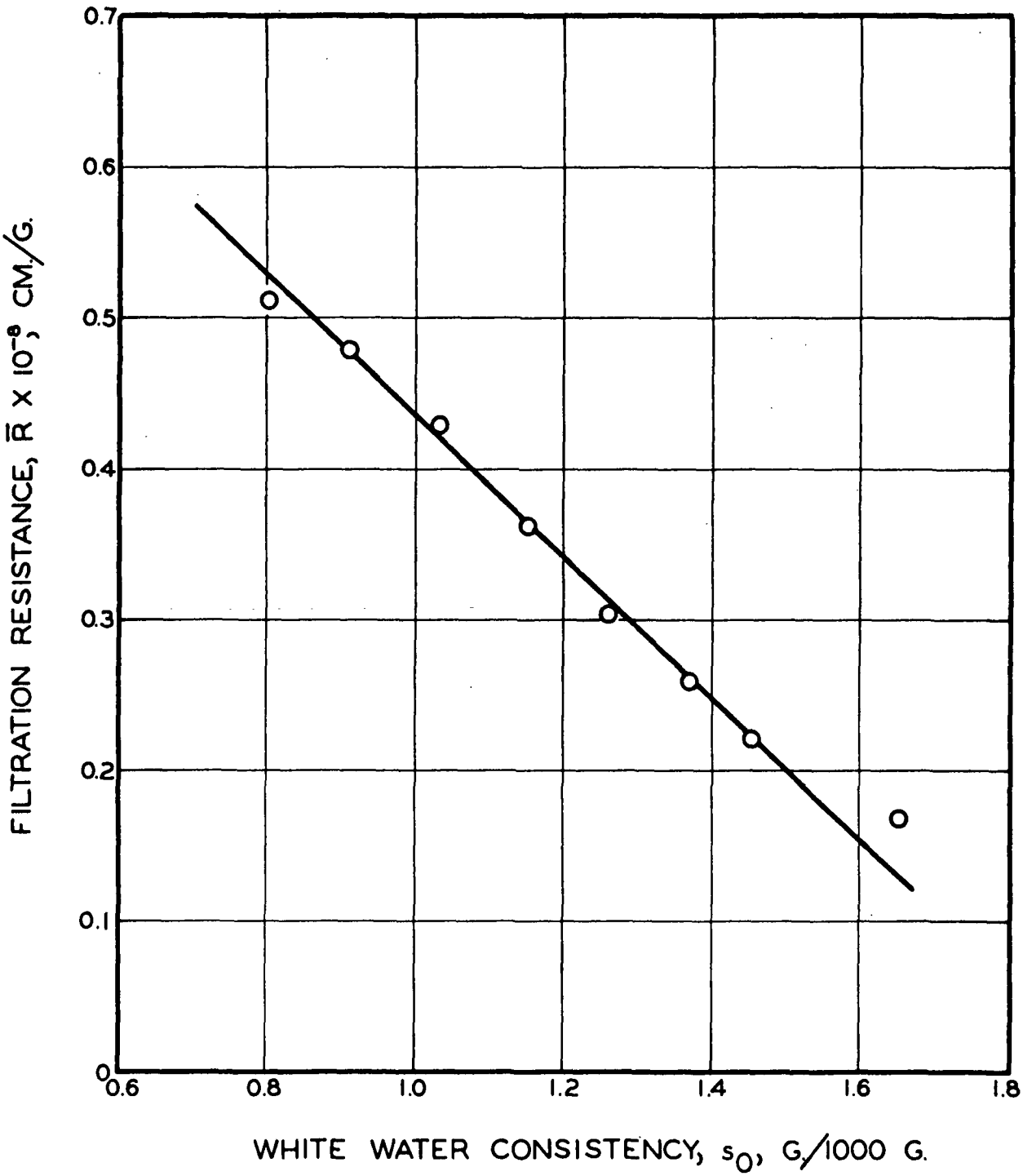

Figure XXVIII-4. Effect of Fines and Filler Retention on Resistance

APPROXIMATE APPLICATION

In spite of the unresolved discrepancy, Taylor's theory and laboratory filtration test have been utilized for the estimate of wire length under a given set of conditions. From the linear relationship between specific resistance and basis weight, the total resistance is assumed to be quadratic:

$$R_t = R_w + \bar{R}_i \bar{W} + \frac{\bar{R}_f - \bar{R}_i}{2W_f} \bar{W}^2 \qquad \text{(XXVIII-3)},$$

which is the same as Equation (XXVII-4). Combining Equations (XXVIII-1) and (XXVIII-2), we have

$$\Delta \bar{W} = \frac{0.295 r_o \rho^3 U_w^2}{\mu^2 R_t^2} \left[\frac{s - \bar{s}_{0,n}}{1 - s\bar{m}} \right]$$

$$= \frac{\bar{K}_t}{R_t^2} \qquad \text{(XXVIII-4)}.$$

If the average basis weight is treated as a continuous function of the table roll number, the derivative of $\bar{W}$ with respect to roll number is closely $\Delta \bar{W}$. Upon integration we have

$$\bar{K}_t N = \left(\frac{\bar{R}_f - \bar{R}_i}{2W_f} \right) \frac{\bar{W}^5}{5} + \bar{R}_i \left(\frac{\bar{R}_f - \bar{R}_i}{2W_f} \right) \frac{\bar{W}^4}{2}$$

$$+ \left[\frac{2}{3} \left(\frac{\bar{R}_f - \bar{R}_i}{2W_f} \right) R_w + \frac{1}{3} \bar{R}_i \right] \bar{W}^3 + R_w \bar{R}_i \bar{W}^2 + R_w^2 \bar{W}$$

(XXVIII-5),

in which N is the total number of table rolls.

This approximation was applied to the board machine. With the laboratory-determined values of $\bar{R}_f$ for the couch sample, $\bar{R}_i$ for the sample after removal of fines, and $\bar{m}$ for both samples as functions of pressure drop, an effective pressure drop across the web was arrived at by trial and error:

$$\Delta p_e = \frac{1}{20} \left(\frac{1}{2} \rho U_w^2\right) \frac{R_t - R_w}{R_t} \qquad \text{(XXVIII-6)},$$

where the fraction 1/20 accounts for the previously mentioned discrepancy. Equation (XXVIII-5) was then solved for the roll number from the known values of R_w, $\bar{R}_i$ and $\bar{R}_f$ at Δp_e. The result of calculations showed N to be 34 under the known conditions. The actual number was 37. By this approximation we have estimated wire length for commercial machines to operate at higher speeds.

COMPUTER PROGRAMMING

On the basis of the filtration theories and laws (Chapters II and III), Schoeffler and Sullivan (XXVIII-3) proceeded to apply the mathematical models to computer programming for data processing of fourdrinier drainage. In addition to the continuity conditions, flow expressions, compressibility functions, and retention relationships, they incorporate other empirical parameters to account for machine conditions.

The fourdrinier is divided into three sections: (1) from the slice to the first table roll, (2) from the first to last table rolls, and (3) from the end of the table-roll section to the wet line over the suction boxes. In the first section it is assumed that the drainage is due to gravity alone. Over the table-roll section the effect of the table rolls is taken to be the average suction being proportional to the square of the wire speed. Over the suction boxes the average applied vacuum is used.

Solutions of the set of equations were carried out on a digital computer. Each partial differential equation is reduced to a finite difference equation. A satisfactory "grid" size was found to result if the web was divided into 100-200 "layers" in the drainage direction and about a quarter of these in the machine direction. The boundary conditions are specified to be

$$H = H_o - \int_o^t U_o dt \qquad \text{(XXVIII-7)},$$

$$W = \frac{1}{v} \int_o^L (1 - \epsilon) dz \qquad \text{(XXVIII-8)},$$

$$p_f(L,t) = 0, \quad p_f(0,t) = -\Delta p \qquad \text{(XXVIII-9)},$$

$$\epsilon(L,t) = \epsilon_o, \quad U_s(L,t) = U_o \qquad \text{(XXVIII-10)}.$$

At each time, a value of web thickness and drainage volume is assumed. The equations are then solved, starting at the web face from the boundary conditions. When the solution reaches the wire, the pressure drop must equal the known value, the drainage must equal the suspension flow, and the basis weight must satisfy the fiber retention, or the iterative process be repeated. In the machine direction the solution starts at $\underline{t} = 0$ and proceeds until the free slurry vanishes at the wet line. The information so obtained is sufficient to calculate drainage, white water consistency, average web density, etc. at various points of interest along the wire.

Several years ago we were of the opinion that the simple filtration model was not then quite adequate for the purpose of data processing to a useful extent. In fact, we considered that an indiscriminate use of such sophisticated and powerful tools as digital and analog computers on paper machines would yield

little to justify their costs. Unfortunately, the premature attempts and failures have dampened some enthusiasm for ultimate automatic control of paper machines. We believe that our present refined models could be the basis for rational applications in operation analysis of a paper machine, and with the improvement of instrumentation the day of profitable automation for papermaking may not be too far away.

XXIX. SIMPLIFIED DESIGN OF TWO-WIRE FORMERS

Two-wire formers have received much attention since the original version of Inverform for boardmaking. Recently, Gustafson and Parker (XXIX-1) presented some results of their experiments with a new device for forming book paper, which consists essentially of a horizontal, converging forming zone with a special inlet for improved formation. An analysis of drainage design by Ingmanson (XXIX-2) for such a former is presented here, which may contribute to its further development.

DESIGN PROCEDURE

The general design calls for forming a web between two horizontal, converging wires travelling at a high speed from a high-consistency stock with incomplete retention. A schematic diagram of the forming zone is shown in Fig. XXIX-1, which is purposely exaggerated in its z scale. It is assumed that a free jet of the stock enters the forming zone at the same horizontal wire velocity U_w. The wire convergence is to be so designed as to maintain a constant pressure in the free slurry while it drains equally through both wires. As the wires converge upon the entering jet, by virtue of its incompressibility, the drainage velocity U_0 will be taken to correspond to the vertical wire velocity along the entire forming zone. Under the prescribed velocity conditions,

$$U_0 = U_w \frac{dz}{dx} \qquad \text{(XXIX-1)} .$$

By knowing U_0 as a function of x, the symmetrical contour of the wires is thereby fixed. The basis weight of the web increases as drainage is forced through the wires. If atmospheric pressure is maintained outside the wires, a hydrostatic pressure will develop in the free slurry. This internal pressure may be kept constant by proper wire convergence.

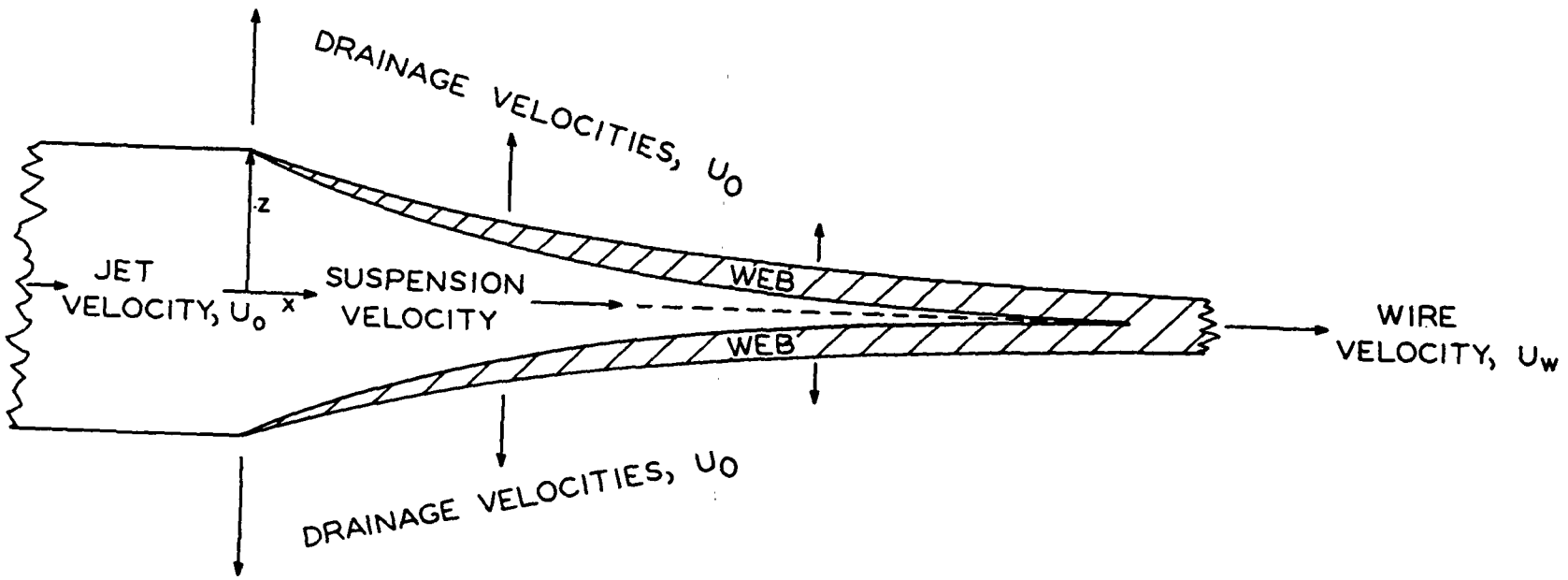

Figure XXIX-1. Horizontal Converging Two-Wire Forming Zone

The specific case under consideration is a 40-g./sq. m. book paper formed at 2150 f.p.m. from a stock at 1% consistency. The forming conditions are summarized in Table XXIX-1, which correspond closely to those of Gustafson and Parker.

TABLE XXIX-1

FORMING CONDITIONS

Furnish	Raw stock for coating
$\underline{S_v}$, sq. cm./cc.	7200
$\underline{v}$, cc./g.	2.80
$\underline{M}$, c.g.s. units	0.00207
$\underline{N}$	0.375
$\underline{R_b}$	0.5
$\underline{k_b}$, sq. cm./g.	500
Wires	64 x 51-mesh twill
Thickness, cm.	0.0551
Surface per unit volume of screen, sq. cm./cc.	58.4
Porosity	0.661
Operating conditions	Symmetrical, horizontal, two-wire
$\underline{\Delta p_t}/\rho g$, in. of water	10
$\underline{s}$, g./g.	0.01
$\underline{T}$, °C.	25
$\underline{U_w}$, f.p.m.	2150
$\underline{W}$, g./sq. m.	40

As has been shown before (Chapter XVII), a filtration curve of (dt/dV_0) vs. V_0 is constructed, from which the forming time is obtained for the specified basis weight and converted to the forming length at the given horizontal wire speed. The results of calculations after correction for high consistency are shown in Fig. XXIX-2. It is seen that U_0 varies from 100 to 5 cm./sec. over the basis weight range from 0 to 20 g./sq. m. on each wire. In this region of flow the inertial effect occupies a significant part of the total pressure drop. At unity basis weight, the inertial resistance term is about 20%, while at 20 it has decreased to 2%. At the same basis weights, the wire resistance accounts for 60% and 1% of Δp_t, respectively. For viscous flow only, with negligible wire resistance and complete fiber retention, the filtration curve becomes linear.

Next, U_0 is determined as a function of x by graphical integration of the filtration curve. The slope (dz/dx) is evaluated from Equation (XXIX-1). The resulting contour of the wires is shown in Fig. XXIX-3 as z vs. x. This completes the drainage design.

OPERATING FEATURES

The entrance height of the forming zone is fixed by the jet thickness which is calculated from the over-all fiber balance, allowing for incomplete retention. In this particular case, the retention is 67%, in close agreement with the experimental value of 69%. The forming length as designed is 22 cm. The internal pressure is 10 in. of water above the external pressure.

For practical operation the wires will be supported by suction boxes. Then the internal pressure may be kept at a desired value such as atmospheric pressure. The vacuum in the curved suction boxes may be easily equalized to give symmetrical drainage, resulting in the shortest forming length. High internal

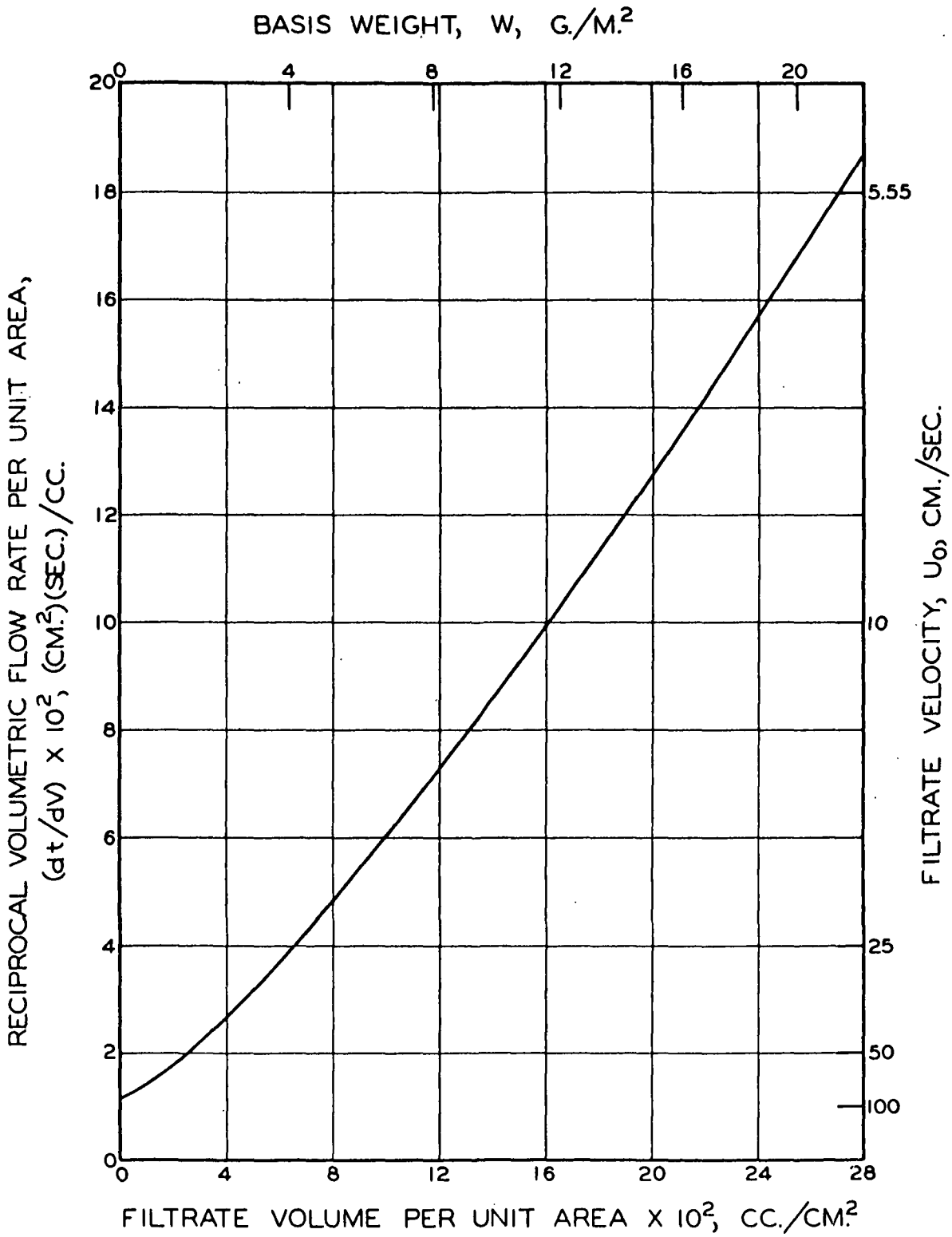

Figure XXIX-2. Drainage Curve

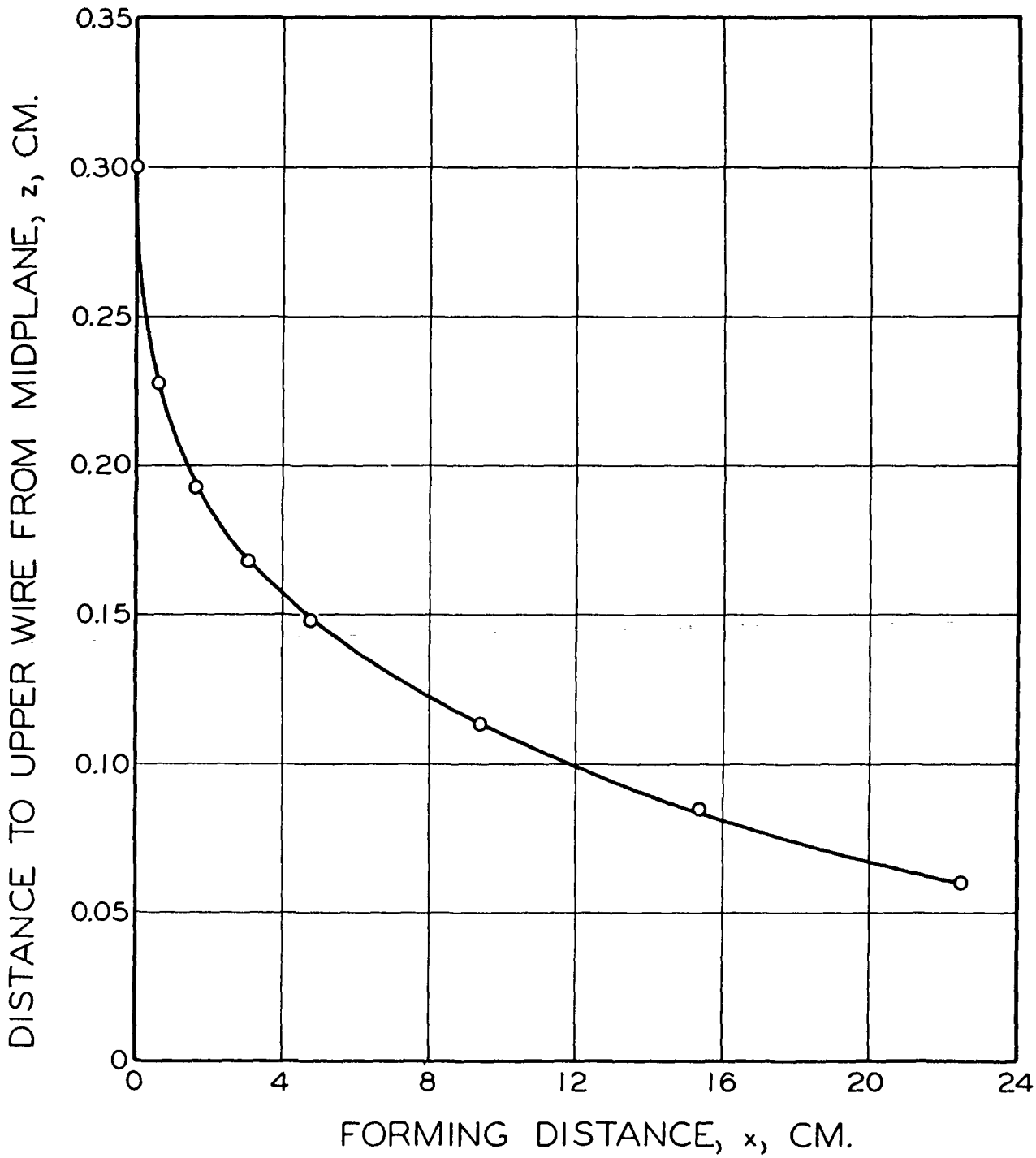

Figure XXIX-3. Wire Contour

pressures should be avoided because they will cause difficulty in sealing as well as Bernoulli's effect in slowing the jet velocity.

If two straight wires with constant slope were used, the drainage velocity would remain essentially constant, and the internal pressure would increase exponentially at constant external pressure. For a final pressure drop, say, 10 in. of water, the forming length required would be roughly double that at constant pressure. This result is also in general agreement with the experimental observations.

XXX. MISCELLANEOUS ILLUSTRATIONS OF HYDRODYNAMIC EVALUATION

Hydrodynamic evaluation of pulps as presented in Chapter XIX has been used in research and practice. We conclude this review by relating a number of such applications to illustrate its power as well as limitations. For certain reasons, references to the actual cases are omitted, and they should not be quote in any manner.

PULP EVALUATION

Sheet Strength

The correlations of hydrodynamic properties of wood pulps with handshee tensile have been well established. Figures XXX-1 and XXX-2 show the correspondence of sheet tensile with specific surface and specific volume, respectively, f a bleached sulfite pulp, whole and classified. The implications of such correlations are quite clear. The increase of surface area by refining contributes to tensile at a decreasing rate, while the increase in swollen volume is almost linear with tensile within the practical range. Conventional refining unravels fiber surfaces but also creates fines, some of which do not assist in bonding to a significant extent. Swelling, however, enhances fiber conformability in wet pressing, and therefore improves bonding.

Surface Unravelling

Classified unbleached sulfite fibers were stirred in a British disintegrator for the purpose of unravelling the fiber surfaces. The original and resultin fibers were analyzed by filtration tests and checked against sheet tensile, as follows.

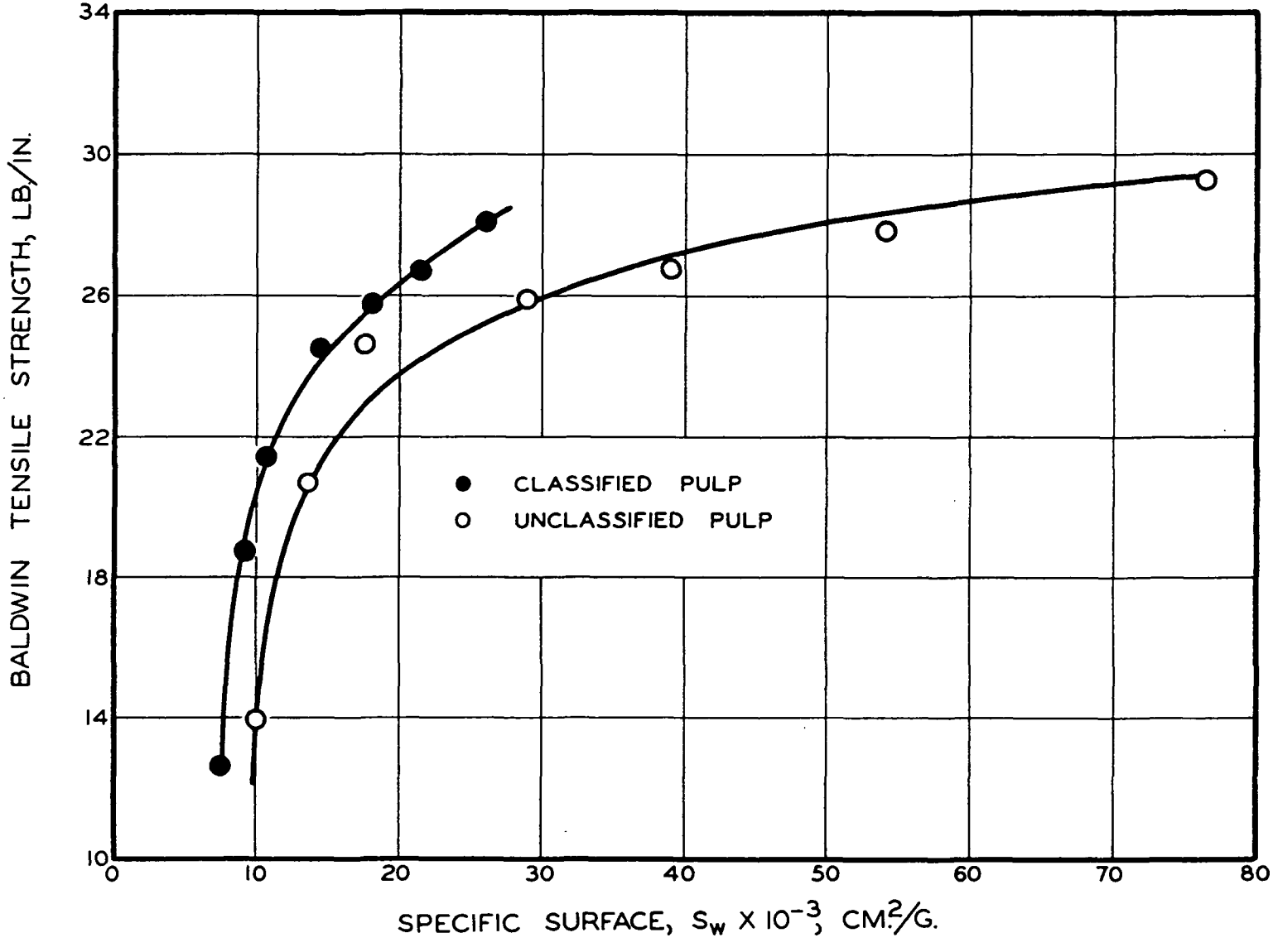

Figure XXX-1. Correlation of Handsheet Tensile with Specific Surface

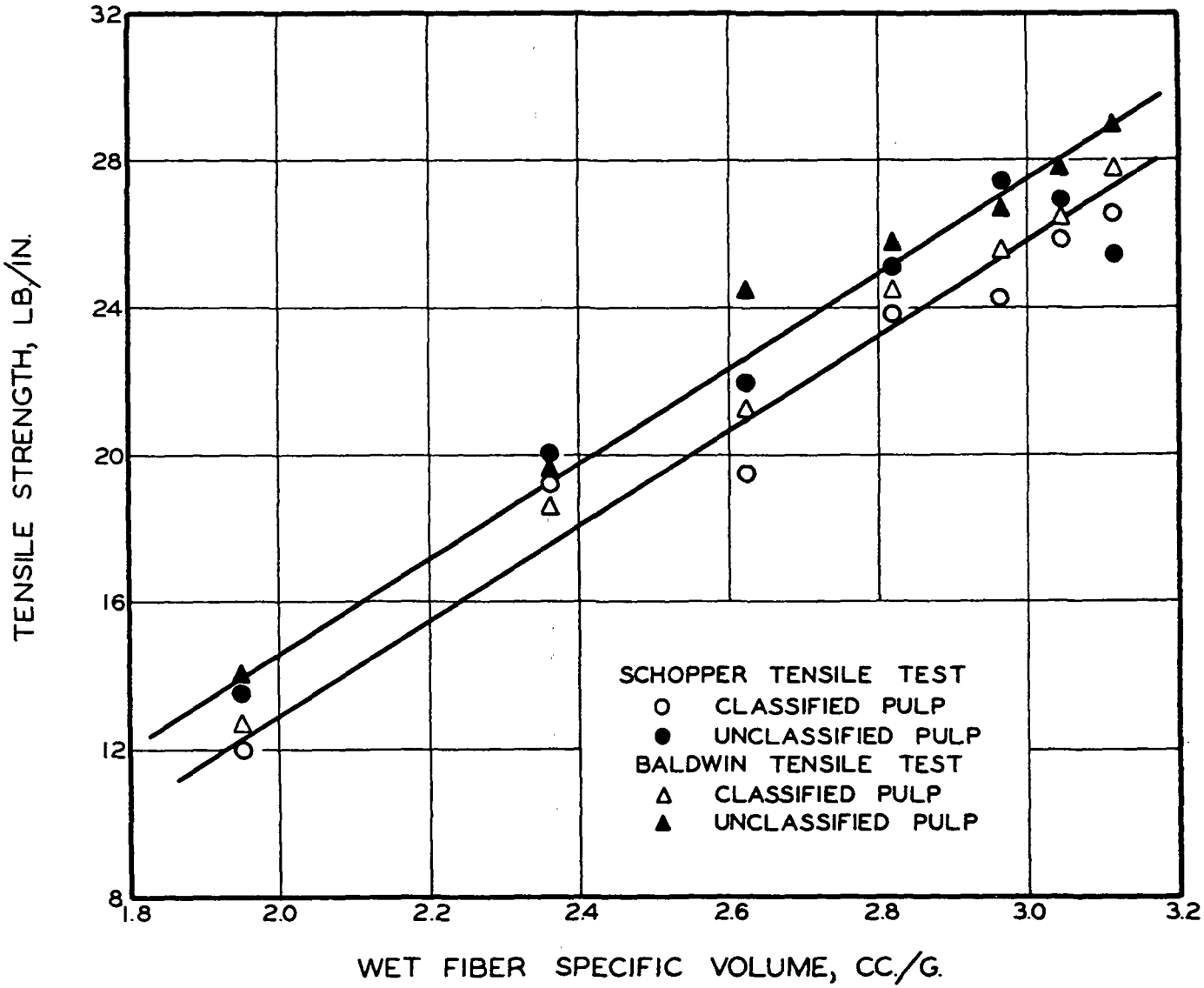

Figure XXX-2. Correlation of Handsheet Tensile with Specific Volume

Fibers	Original	15,000 Counts	300,000 Counts
$\underline{S}_w$, sq. cm./g.	10,780	38,400	70,800
$\underline{v}$, cc./g.	0.96	3.21	3.88
Tensile, lb./in.	29.9	42.7	14.4

Most of the newly created surface areas were due to the unravelled primary and outer secondary wall fragments which comprised only about 3% of the classified fiber mass and contributed considerably to bonding. However, the additional surfaces created by prolonged unravelling appeared to be detrimental to bonding, in spite of the increase in swelling.

Hemicellulose Sorption

Additives such as locust bean gum are often adsorbed on fiber surfaces to enhance bonding. The rate of sorption is dependent on specific surface as demonstrated below with the sorption of partially methylated gum on sulfite fibers.

$\underline{S}_w$, sq. cm./g.	Initial Rate x 10^5, $sec.^{-1}$
9,260	14.8
11,780	16.1
15,610	17.9
29,900	26.5

These data indicate a linear relationship. However, for different pulps and refining conditions the accessibility of the hydrodynamic surfaces for sorption should also be taken into consideration.

Cellulose Modification

Sodium carboxymethylation of cotton linters was found to increase swollen volume and bonding without significant effect on surface area.

Degree of Substitution	$\underline{S}_w$, sq. cm./g.	$\underline{v}$, cc./g.	Relative Bonding
0.002 (control)	20,250	1.48	1
0.019	19,600	2.14	1.5
0.040	22,800	2.32	2

Decrystallization of highly purified cotton cellulose by aqueous ethylamine was found to increase specific volume and decrease specific surface. A corresponding decrease in fiber strength was also noted.

Crystallinity index	70.1	69.4	62.8	56.0	52.1
$\underline{v}$, g./cc.	2.40	2.38	3.02	3.08	3.00
$\underline{S}_w$, sq. cm./g.	4100	3920	3520	3350	3240
Zero-span tensile, kg./sq. m.	24.8	24.7	21.0	20.9	20.2

Hypochlorite Bleaching

Hypochlorite bleaching of neutral sulfite semichemical aspen pulp indicated that the specific volume of the bleached pulps was linear with their residual Klason lignin content. The specific surface increased mildly. The strength of handsheets improved considerably.

High-Consistency Refining

Conventional refining of pulps does not alter the mat compressibility to a significant extent because of the counterbalancing effects of fiber-length

reduction and fines production. High-consistency refining showed an increase of compressibility by 15% for a kraft pulp over conventional refining, although the compressibility was practically independent of the level of refining just as in conventional refining. In the compacting pressure range of 10-100 cm. of water the values of $\underline{N}$ remained the same for both cases.

At the same freeness level, high-consistency refining indicated about the same degree of fiber swelling as, but considerably lower surface area than, conventional refining.

	Unrefined	Conventionally Refined		High-Consistency Refined	
		High Freeness	Low Freeness	High Freeness	Low Freeness
$\underline{S_w}$, sq. cm./g.	7,800	18,700	37,600	14,600	20,800
$\underline{v}$, cc./g.	2.60	3.00	3.27	2.93	3.16
$\underline{c}$, g./cc., at 50 cm. water	0.118	0.118	0.118	0.130	0.130

Microscopic examination of high-consistency refined pulps showed little fiber-length reduction, near absence of fines, and gentle peeling of the outer secondary walls. All these factors tended to contribute to tear, tensile, and burst.

MACHINE OPERATION

Wet Breaks

A mill substituted a foreign pulp for its own pulp on one paper machine and encountered less frequent wet breaks at the couch roll. All conventional methods (freeness, beating curves, and handsheet tests) failed to reveal significant differences in the two pulps. By filtration tests samples of the two pulps

showed close filtration resistances. However, in conjunction with compressibility tests, it was found that the foreign pulp had a significantly higher specific volume, 2.5 cc./g. as compared with 1.8 for the original pulp. By further refining of the original pulp the machine runnability was improved as expected.

Furnish Adjustment

A fourdrinier machine developed occasional difficulties in producing satisfactory corrugating medium. Samples from the stuffbox and the reel under good and poor conditions were submitted for analysis. The results are summarized as follows:

Board sample	Good	Poor
Basis weight, lb./1000 sq. ft.	32.4	27.0
Caliper x 10^3	11.6	10.3
Apparent density	2.8	2.6
Burst, pt./100 lb.	179	146
Tensile, lb./(in.)(100 lb.), M.D.	154	133
C.D.	75	59
Thwing formation	4.5	4.8
Stock sample		
C.S. freeness	285	360
$\underline{S}_w$, sq. cm./g.	36,300	31,100
$\underline{v}$, cc./g.	2.77	2.41
Repulped board sample		
$\underline{S}_w$, sq. cm./g	25,350	28,900
$\underline{v}$, cc./g.	1.85	1.78

The 20% larger burst and tensile of the good board was attributed primarily to the 15% greater specific volume, indicating some differences in pulping and refining between the good and poor pulps. The reverse of specific surface in the corresponding repulped samples was also noted. This was thought to be due to a greater loss of fines from the white water system when the machine was making good board. By classifying the stock and repulped board samples and considering the fraction through 150-mesh screen as fines, it was estimated that 7.6% and 4.5% of the inlet stocks were lost from the white water system for good and poor board, respectively, in agreement with the filtration data. By adjusting pulping and refining to increase the specific volume of the poor pulp and reducing the fines retention in the poor board, the problem was eventually solved.

Ply Difference

Difficulties were experienced in maintaining drying rate and burst of jute linerboard on a cylinder machine. Samples of the furnishes and board were taken for examination.

Machine	Operation	Sample	$\underline{S}_w$, sq. cm./g.	$\underline{v}$, cc./g.
A	normal	filler	39,350	1.92
		top liner	54,800	2.14
		wet web	39,700	1.98
B	good	filler	36,300	1.95
		top liner	42,400	2.18
		wet web	41,400	1.60
B	poor	filler	42,900	1.91
		top liner	45,300	2.38
		wet web	40,200	1.70

As the filtration resistance of the three web samples showed only 5% variations, the rate of water removal at the wet end should be about the same in spite of the different furnishes. The good and poor board from Machine B should also have nearly the same strength. By repulping these web samples the following test results on handsheets were obtained:

	Good Web	Poor Web
Basis weight, lb./1000 sq. ft.	13.5	13.6
Caliper, points	4.7	4.8
Burst, pt./100 lb.	42	48
Tensile, lb./in.	12.6	13.6

It turned out that the "poor" web was somewhat better than the "good" web, in conformance with the filtration results. Therefore, the difficulties were not in the wet end, nor with the furnishes.

Temperature Increase

A special twin-cylinder machine was manufacturing insulation board. It was desired to increase the production by raising the stock temperature. Wet samples of two grades of board were tested for filtration resistance at two temperatures. Board B was made from the same stock as Board A, except for the addition of 22% resin.

$\Delta p/\rho g$, cm. H_2O	$\bar{R} \times 10^{-8}$, cm./g. 25°C. Board A	25°C. Board B	48°C. Board A	48°C. Board B
50	1.26	1.16	1.65	1.40
60	1.35	1.25	1.79	1.53
70	1.44	1.33	1.92	1.65
80	1.53	1.42	2.04	1.75
90	1.61	1.51	2.16	1.87

It was concluded that at 25°C. the increase in production with Board B over Board A was 9% by area. By raising the stock temperature the production of A would gain 1% per °C. and that of B, 1-1/2% per °C. These predictions were confirmed in actual operations. The compressibility tests on the same samples indicated a 25% increase in apparent density of Board B over A. The hydrodynamic properties were evaluated to be as follows:

	S_w, sq. cm./g.	v, cc./g.
Board A	11,900	2.45
Board B	9,650	2.31

As Board B contained resin, a part of the fines in the stock would be agglomerated through adhesion, accounting for its lower specific surface. Furthermore, there would be more uniform distribution of fines in the board. Fines agglomeration and adhesion to the fibers would be enhanced at higher temperatures due to the presence of the resin. These factors could contribute to a 50% better temperature effect on drainage than Board A, as revealed by the filtration results.

Suction Capacity

The fourdrinier machine was making mimeo at 470 f.p.m. The problem was concerned with suction box capacity. A web sample was taken at the couch roll and tested for permeability with moisture-saturated air. The equilibrium permeability data are shown in Fig. XXX-3. The volumetric flow rate is directly proportional to the pressure drop up to 12 in. mercury, indicating absence of slip, negligible compressibility, and little inertial effects.

Since the contact time of the web with the boxes was very short, about 0.1 sec., the desired air resistance should be in the initial period of unsteady-state permeation, which is shown in Fig. XXX-4. The zero-time flow ($\underline{A}$ = 49.5 sq. cm.) was considered to correspond to the machine condition. This value was used to estimate air flow through a suction box area of 820 sq. in. at a vacuum of 6 in. of mercury. The flow rate would be 12 cu. ft./min. of free air at 70°F. and 1 atm. If the same area were used on the intended new Rotabelt to be operated at 20 in. of mercury, the flow rate would be 50 cu. ft./min. of free air. It was concluded that the original specifications of 500 cu. ft./min. for the Rotabelt contained an unreasonably large safety factor.

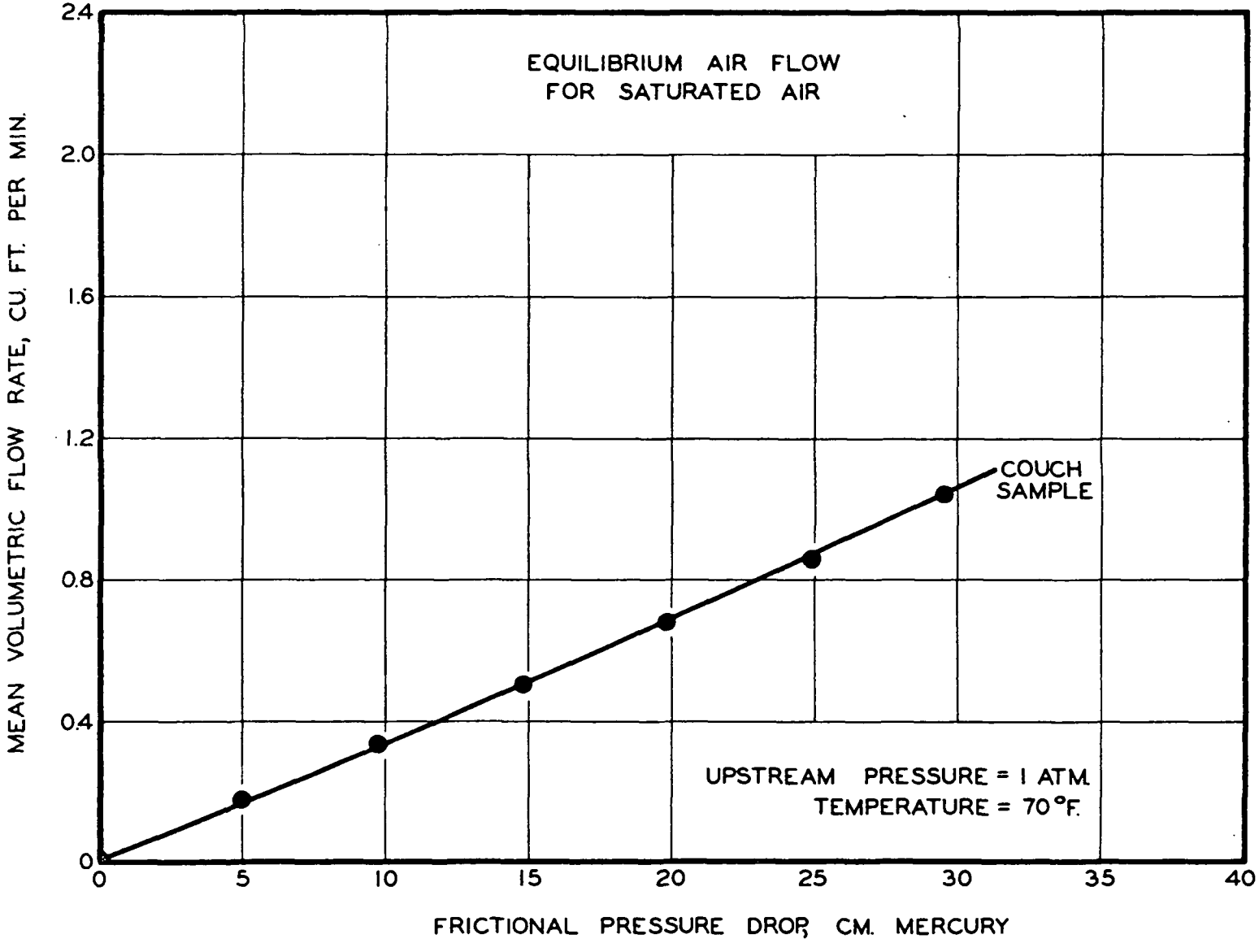

Figure XXX-3. Air Permeability of a Web Sample

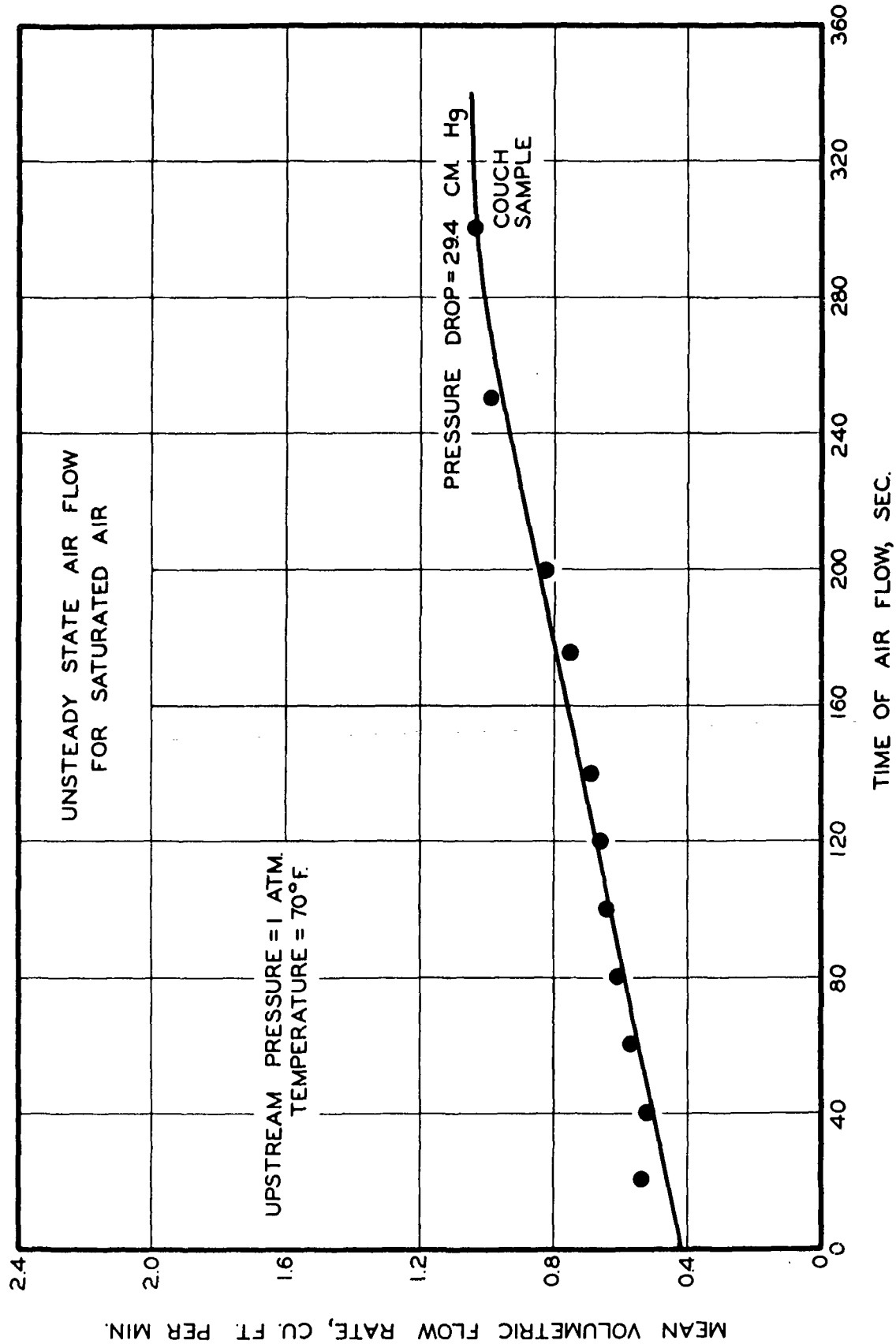

Figure XXX-4. Air Permeability of a Web Sample

NOMENCLATURE

Capitals:

$\underline{A}$ = area

$\underline{B}$ = numerical coefficients

$\underline{C}$ = free particle concentration; volume or number concentration

$\underline{C}'$ = bound particle concentration

$\underline{D}$ = diffusivity; width; coefficient

$\underline{E}$ = collection efficiency; energy; modulus of elasticity

$\underline{F}$ = drag force

$\underline{G}$ = velocity gradient

$\underline{H}$ = height; location

$\underline{I}$ = porosity correction factor; impaction number; moment of inertia; constant

$\underline{J}$ = correction factor; location

$\underline{K}$ = attenuation coefficient; permeability; constant

$\underline{K}'$ = attenuation factor

$\underline{L}$ = length; thickness

$\underline{M}$ = compressibility coefficient

$\underline{M}'$ = numerical coefficient

$\underline{N}$ = number; compressibility power

$\underline{N}'$ = numerical constant

$\underline{P}$ = probability; pressure variable

$\underline{R}$ = viscous filtration resistance; retention fraction; distance; ratio

$\underline{R}'$ = inertial filtration resistance

$\underline{Re}$ = Reynolds number

$\underline{Re}'$ = Reynolds number for porous media

$\underline{S}$ = specific surface; arc length; correlation function

Sc = Schmidt number

T = temperature; torque

U = superficial velocity

U' = mat face velocity

V = volume

W = mass of fibers

X = x distance variable

Y = mat density variable

Z = complex variable

Lower case:

a = viscous resistance

a' = constant

b = inertial resistance

b' = inertial resistance constant

c = mat density

d = diameter; distance of separation

d' = distance of separation

e = angular factor

f = friction factor

f' = friction factor for porous media; friction coefficient

g = gravitational constant

h = distance; constant

j = j type

k = Kozeny factor; coefficient; constant

k' = constant

m = mass ratio of free particles to fibers; mat moisture

m' = mass of bound particles to fibers

$\underline{n}$ = number; power

$\underline{p}$ = pressure

$\underline{p}'$ = pressure

$\underline{q}$ = volumetric flow rate per unit width

$\underline{r}$ = $\underline{r}$ co-ordinate; radius

$\underline{s}$ = consistency

$\underline{s}'$ = consistency coefficient

$\underline{t}$ = time co-ordinate

$\underline{t}'$ = time variable

$\underline{u}$ = velocity

$\underline{v}$ = specific volume

$\underline{w}$ = mass co-ordinate; mass

$\underline{w}'$ = mass variable

$\underline{x}$ = $\underline{x}$ co-ordinate

$\underline{y}$ = $\underline{y}$ co-ordinate

$\underline{z}$ = $\underline{z}$ co-ordinate

Greek symbols:

α = pore shape factor; diffusion correlation coefficient; fiber orientation parameter; constant

α' = viscous resistance coefficient

β = pore shape factor; impaction correlation coefficient; fiber orientation parameter; constant

β' = inertial resistance coefficient

γ = interception correlation coefficient; compressibility power

δ = length of a vector

ϵ = porosity

ζ = unspecified function

η = distance variable

θ = θ co-ordinate; angle

$\varkappa$ = correction factor

λ = thickness variable

μ = viscosity

ξ = mat density variable

ρ = density

σ = stress

τ = time variable

φ = φ co-ordinate; angle; potential function

χ = semiaxis ratio

ψ = stream function

ω = solid fractions; angular velocity

Subscripts:

$\underline{a}$ = atmospheric; apparent

$\underline{av}$ = average

$\underline{c}$ = contact; center

$\underline{d}$ = diameter

$\underline{e}$ = equilibrium; effective

$\underline{f}$ = fiber; final

$\underline{h}$ = distance

$\underline{i}$ = ith type; initial; inside

$\underline{L}$ = mat face

o = origin; reference to zero; outside; per unit volume of system; Darcy; fiber retention

$\underline{p}$ = particle

$\underline{R}$ = table roll

$\underline{r}$ = relative; $\underline{r}$ direction

$\underline{s}$ = suspension; segment

$\underline{t}$ = total; tangential

$\underline{v}$ = per unit volume of fiber

$\underline{w}$ = wire; per unit mass of fiber; wall

$\underline{x}$ = $\underline{x}$ direction

$\underline{y}$ = $\underline{y}$ direction

$\underline{z}$ = $\underline{z}$ direction

0 = origin; filtrate

1,2,3... = number

∞ = infinite

ρ = density

Miscellaneous:

$\bar{\ }$ = average

$\vec{\ }$ = vector

^{o}, * = explained in text

$|\ |$ = positive magnitude

$\cdot$ = dot product

$\underline{x}$ = cross product

∇ = del

∇^2 = Laplacian

erf = error function

e or exp = exponential function

$f(\ )$ = function

$g(\ )$ = function

$\int$ = integral

ln = natural logarithm

log = common logarithm

sgn = sign

Σ = summation

LITERATURE CITED

II- 1. Nelson, R. W., Tappi 47, no. 12:752(1964).

II- 2. Ingmanson, W. L., Tappi 47, no. 12:742(1964).

II- 3. Han, S. T., Tappi 47, no. 12:782(1964).

II- 4. Hisey, R. W. An investigation of the mechanism of the dewatering of compressible beds. Doctor's Dissertation. Appleton, Wis., The Institute of Paper Chemistry, 1955; Tappi 39, no. 10:690(1956).

II- 5. Meyer, H., Tappi 45, no. 4:296(1962).

III- 1. Darcy, H. Les fontaines publiques de la ville de Dijon. Paris, Victor Dalmint, 1856.

III- 2. Carman, P. C., Trans. Inst. Chem. Engrs. (London) 15:150(1937).

III- 3. Davis, C. N., Proc. Inst. Mech. Engrs. (London) B 1:185(1952).

III- 4. Carroll, C. W. Private communication, 1965.

III- 5. Forchheimer, Ph., Z. Ver. deut. Ing. 45:1782(1901).

III- 6. Ergun, S., Chem. Eng. Progr. 48:89(1952).

III- 7. Qviller, O., Papir-J. 26, no. 23:312(Dec. 15, 1938).

III- 8. Campbell, W. B., Pulp Paper Mag. Can. 48, no. 3:103(1947).

III- 9. Ingmanson, W. L., and Whitney, R. P., Tappi 37, no. 11:523(1954).

III-10. Wilder, H. D. The compression creep properties of wet pulp mats. Doctor's Dissertation. Appleton, Wis., The Institute of Paper Chemistry, 1959; Tappi 43, no. 8:715(1960).

III-11. Estridge, R. The initial retention of fibers by wire grids. Doctor's Dissertation. Appleton, Wis., The Institute of Paper Chemistry, 1961.

III-12. Han, S. T., Tappi 45, no. 4:292(1962).

IV- 1. Irmay, S., Trans. Am. Geo. Union 39, no. 4:702(1958).

IV- 2. Rouse, H. Advanced mechanics of fluids. New York, John Wiley & Sons, 1959.

V- 1. Emersleben, O., Phys. Z. 26:601(1925).

V- 2. Happel, J., A.I.Ch.E. Journal 5, no. 2:174(1959).

V- 3. Han, S. T. Unpublished work. Appleton, Wis., The Institute of Paper Chemistry, 1965.

VI- 1. Onogi, S., and Sasaguri, K., Tappi 44, no. 12:874(1961).

VI- 2. Van Wyk, C. M., J. Textile Inst. 37:T-285(1946).

VIII- 1. Abrams, R. W. The retention of fibers from dilute suspensions. Doctor's Dissertation. Appleton, Wis., The Institute of Paper Chemistry, 1964; Tappi 47, no. 12:773(1964).

IX- 1. Ingmanson, W. L. An investigation of the mechanism of water removal from pulp slurries. Doctor's Dissertation. Appleton, Wis., The Institute of Paper Chemistry, 1951; Tappi 35, no. 10:439(1952).

IX- 2. Whitney, R. P., Ingmanson, W. L., and Han, S. T., Tappi 38, no. 3:157 (1955).

IX- 3. Han, S. T., and Ingmanson, W. L. Unpublished work. Appleton, Wis., The Institute of Paper Chemistry, 1962.

X- 1. Meyer, H. Unpublished work. Appleton, Wis., The Institute of Paper Chemistry, 1965.

X- 2. Emmons, H. W. The continuum properties of fiber suspensions. Paper presented at the 20th TAPPI Engineering Conference, Minneapolis, Minn., 1965.

XI- 1. Nelson, R. W. Unpublished work. Appleton, Wis., The Institute of Paper Chemistry, 1965.

XII- 1. Chalkeley, J. W., Cornfield, J., and Park, H., Science 110:295(1949).

XII- 2. Debye, P., Anderson, H. R., Jr., and Brumberger, H., J. Appl. Phys. 28, no. 6:679(1957).

XII- 3. Prager, S., Phys. of Fluids 4, no. 12:1477(1961).

XII- 4. Weissberg, H. L., and Prager, S., Phys. of Fluids 5, no. 11:1390(1962).

XII- 5. Parker, J. D. An investigation of the permeability to water of partially saturated beds of glass fibers. Doctor's Dissertation. Appleton, Wis., The Institute of Paper Chemistry, 1958.

XII- 6. Fatt, I. The network model in the study of porous media. Doctor's Dissertation. Los Angeles, University of Southern California, 1955.

XII- 7. Rose, W., Illinois State Geolog. Survey Circular 237, 1957.

XII- 8. Kallmes, O., and Corte, H., Tappi 43, no. 9:737(1960).

XII- 9. Nelson, R. W. Unpublished work. Appleton, Wis., The Institute of Paper Chemistry, 1965.

XIII- 1. Meyer, H. Unpublished work. Appleton, Wis., The Institute of Paper Chemistry, 1964.

XIV- 1. Lamb, H. Hydrodynamics. 6th ed. New York, Dover, 1945.

XIV- 2. Burgers, J. M. Second report on viscosity and plasticity. Chap. III. On the motion of small particles of elongated form suspended in a viscous fluid. New York, Nordemann, 1938.

XIV- 3. Oberbeck, A. In Lamb's Hydrodynamics. 6th ed. New York, Dover, 1945.

XIV- 4. Tchen, C. M., J. Appl. Phys. 25, no. 4:463(1954).

XIV- 5. Brenner, H. J., Fluid Mech. 12:35(1962).

XIV- 6. Happel, J. Hydrodynamics of dilute systems of particles. In Summary Report 1960-1965, Pioneering Research Program. Appleton, Wis., The Institute of Paper Chemistry, 1965.

XIV- 7. Jeffrey, G. B., Proc. Roy. Soc. (London) A102:161(1923).

XIV- 8. Blakeney, W. R. The viscosity of fiber suspensions. Doctor's Dissertation. Appleton, Wis., The Institute of Paper Chemistry, 1965.

XIV- 9. Mason, S. G., Tappi 37, no. 11:494(1954).

XIV-10. Derjaguin, B. V., Nature 138:330(1936).

XIV-11. Bikerman, J. J. Surface chemistry for industrial research. New York, Academic Press, 1948.

XIV-12. Hamaker, H. C., Rec. Trav. Chim. 55:1015(1936).

XIV-13. Mossman, C. E., and Mason, S. G., Can. J. Chem. 37:1153(1959).

XIV-14. Perry, J. F. Unpublished work. Appleton, Wis., The Institute of Paper Chemistry, 1965.

XIV-15. Meyer, H. Unpublished work. Appleton, Wis., The Institute of Paper Chemistry, 1965.

XV- 1. Wrist, P. E., Pulp Paper Mag. Can. 55:115(1954).

XV- 2. Taylor, G. I., Pulp Paper Mag. Can. 57:267(1956).

XV- 3. Meyer, H., Tappi 47, no. 2:114(1964).

XV- 4. Miller, G. F., Proc. Roy. Soc. 236:529(1926).

XV- 5. Bergström, J., Svensk Papperstid. 60:1(1957).

XVI- 1. Meyer, H. Unpublished work. Appleton, Wis., The Institute of Paper Chemistry, 1965.

XVII- 1. Jones, R. L. An investigation of the effect of fiber structural properties on the compression response of fibrous beds. Doctor's Dissertation. Appleton, Wis., The Institute of Paper Chemistry, 1962; Tappi 46, no. 1:20(1963).

XVII- 2. Elias, T. C. An investigation of the compression response of ideal unbonded fibrous structures by direct observation. Doctor's Dissertation. Appleton, Wis., The Institute of Paper Chemistry, 1965.

XVII- 3. Wrist, P. E., Tappi 44, no. 1:181A(1961).

XVII- 4. Chang, N. L. Unpublished work. Appleton, Wis., The Institute of Paper Chemistry, 1965.

XVII- 5. Han, S. T. Unpublished work. Appleton, Wis., The Institute of Paper Chemistry, 1965.

XVIII- 1. Ingmanson, W. L., Andrews, B. D., and Johnson, R. C., Tappi 42, no. 10: 840(1959).

XVIII- 2. Ingmanson, W. L., and Andrews, B. D., Tappi 46, no. 3:150(1963).

XVIII- 3. Carman, P. C. Flow of gases through porous media. New York, Academic Press, 1956.

XVIII- 4. Robertson, A. F., Textile Res. J. 20:838(1950).

XVIII- 5. Wieghardt, K. E. G., The Aeronautical Quarterly IV:186(1953).

XVIII- 6. Cornell, W. G., A.S.M.E. Transactions, Paper 57-F-19(1951).

XVIII- 7. Grootenhuis, P., Proc. Inst. Mech. Engrs. (London) 168, no. 34:837 (1954).

XVIII- 8. Ingmanson, W. L., Han, S. T., Wilder, H. D., and Myers, W. T., Jr., Tappi 44, no. 1:47(1961).

XIX- 1. Robertson, A. A., and Mason, S. G., Pulp Paper Mag. Can. 50, no. 13: 103(1949).

XIX- 2. Ingmanson, W. L., and Andrews, B. D. Unpublished work. Appleton, Wis., The Institute of Paper Chemistry, 1964.

XIX- 3. Bliesner, W. C. A study of the porous structure of fibrous sheets using permeability techniques. Doctor's Dissertation. Appleton, Wis., The Institute of Paper Chemistry, 1963; Tappi 47, no. 7:392-400(1964).

XIX- 4. Van den Akker, J. A. In Bolam's The formation and structure of paper. Vol. I. p. 205. London, Eng., Tech. Sect. Brit. Paper & Board Makers' Assoc., 1962.

XIX- 5. Labrecque, R. P. Ph.D. thesis in progress. Appleton, Wis., The Institute of Paper Chemistry, 1965.

XIX- 6. Meyer, H. Unpublished work. Appleton, Wis., The Institute of Paper Chemistry, 1964.

XIX- 7. Andrews, B. D. Unpublished work. Appleton, Wis., The Institute of Paper Chemistry, 1964.

XX- 1. White, L. R. Unpublished work. Appleton, Wis., The Institute of Paper Chemistry, 1963.

XX- 2. Andrews, B. D. Unpublished work. Appleton, Wis., The Institute of Paper Chemistry, 1964.

XX- 3. Ingmanson, W. L. Unpublished work. Appleton, Wis., The Institute of Paper Chemistry, 1964.

XXI- 1. Andrews, B. D. Unpublished work. Appleton, Wis., The Institute of Paper Chemistry, 1965.

XXI- 2. Meyer, H. Unpublished work. Appleton, Wis., The Institute of Paper Chemistry, 1965.

XXII- 1. Ingmanson, W. L. Unpublished work. Appleton, Wis., The Institute of Paper Chemistry, 1965.

XXIII- 1. Han, S. T., and Chang, N. L. Unpublished work. Appleton, Wis., The Institute of Paper Chemistry, 1965.

XXIII- 2. Nelson, R. W. Unpublished work. Appleton, Wis., The Institute of Paper Chemistry, 1965.

XXIV- 1. Han, S. T. Unpublished work. Appleton, Wis., The Institute of Paper Chemistry, 1964.

XXIV- 2. Wong, J. B. Collection of aerosols by fiber mats. Doctor's Dissertation. Urbana, Ill., University of Illinois, 1954.

XXIV- 3. Chen, C. Y. Filtration of aerosols by fibrous media. Eng. Exp. Station Annual Report to U.S. Army Chemical Corps. Urbana, Ill., University of Illinois, 1954.

XXIV- 4. Thomas, D. G. Doctor's Dissertation. Columbus, O., Ohio State University, 1953.

XXIV- 5. Johnson, R. C. A study of particle retention in relation to the structure of a fibrous mat. Doctor's Dissertation. Appleton, Wis., The Institute of Paper Chemistry, 1962; Tappi 46, no. 5:304(1963).

XXIV- 6. Fuchs, N. A. The mechanics of aerosols. New York, Macmillan Co., 1964.

XXV- 1. Anderson, O., and Bartok, W., Svensk Papperstid. 58, no. 10:367(1955).

XXV- 2. Bloom, G. R. Unpublished work. Appleton, Wis., The Institute of Paper Chemistry, 1964.

XXVI- 1. Han, S. T. Unpublished work. Appleton, Wis., The Institute of Paper Chemistry, 1961.

XXVI- 2. Jones, A. M., and Knudsen, J. G., A.I.Ch.E. Journal 7, no. 1:20(1961).

XXVI- 3. Wieselberger, C. Ergebnisse der aerodynamischen Versuchsanstalt 2 (1923).

XXVI- 4. Mason, S. G., Pulp Paper Mag. Can. 51, no. 5:93(1950).

XXVI- 5. Myers, W. T., Jr. The rheology of synthetic fiber suspensions. Doctor's Dissertation. Appleton, Wis., The Institute of Paper Chemistry, 1962.

XXVI- 6. Blakeney, W. R. The viscosity of fiber suspensions. Doctor's Dissertation. Appleton, Wis., The Institute of Paper Chemistry, 1965.

XXVI- 7. Daily, J. W., and Bugliarello, G., Tappi 44, no. 7:497-512(1961).

XXVI- 8. Daily, J. W. Study of turbulent transfer mechanics of fluid suspensions of solid particles. In Summary report 1960-1965, Pioneering Research Program. Appleton, Wis., The Institute of Paper Chemistry, 1965.

XXVII- 1. Amneus, J. S. A new pulp drainage model, its application and verification. Paper presented at 20th TAPPI Engineering Conference, Minneapolis, Minn., Sept. 12-16, 1965.

XXVII- 2. Hermans, P. H., and Bredée, H. L., Rec. trav. chim. 54:680(1935).

XXVII- 3. Heller, H. H. Unpublished work. Appleton, Wis., The Institute of Paper Chemistry, 1964.

XXVII- 4. Ingmanson, W. L., and Chang, N. L. Unpublished work. Appleton, Wis., The Institute of Paper Chemistry, 1965.

XXVII- 5. Van den Akker, J. A. Unpublished work. Appleton, Wis., The Institute of Paper Chemistry, 1963.

XXVII- 6. Han, S. T. Unpublished work. Appleton, Wis., The Institute of Paper Chemistry, 1958.

XXVIII- 1. Ingmanson, W. L., Tappi 40, no. 12:936(1957).

XXVIII- 2. Ingmanson, W. L., Tappi 42, no. 6:449(1959).

XXVIII- 3. Schoeffler, J. D., and Sullivan, P. R. A model of sheet formation and drainage on a fourdrinier. Paper presented at 20th TAPPI Engineering Conference, Minneapolis, Minn., Sept. 12-16, 1965.

XXIX- 1. Gustafson, D., and Parker, J., Svensk Papperstid. 67, no. 14:545(1964).

XXIX- 2. Ingmanson, W. L. Unpublished work. Appleton, Wis., The Institute of Paper Chemistry, 1965.

This review was prepared by S. T. Han with the close co-operation of his associates, W. L. Ingmanson, H. Meyer, R. W. Nelson, B. D. Andrews, and N. L. Chang. While its contents have been critically examined, the author remains solely responsible for any errors of commission or omission, as well as possible obscurity or even incomprehensibility. No apology, however, is offered for the extensive use of mathematics. In view of the previous fruitful effort in the sheet-forming research, we hopefully anticipate continued generation of results, through diligence and understanding, useful to the paper industry which the Institute is dedicated to serve. If the reader finds some use of this review, the author and his colleagues will feel amply rewarded for the many hours devoted to its preparation.

THE INSTITUTE OF PAPER CHEMISTRY
Appleton, Wisconsin
November 30, 1965